Maria João Narciso Furtado de Melo Pereira
Licenciada em Conservação e Restauro

CHINESE COINS IN COPPER BASED ALLOYS: ELEMENTAL AND MICROSTRUCTURAL CHARACTERIZATION

Dissertação para obtenção do Grau de Doutor em
Conservação e Restauro, especialidade Ciências da Conservação

Orientador: Maria de Fátima Araújo, Investigadora Principal,
IST/ITN, Instituto Superior Técnico
Universidade Técnica de Lisboa
Co-orientador: Rui Jorge Cordeiro Silva, Professor Auxiliar,
Faculdade de Ciências e Tecnologia,
Universidade Nova de Lisboa

Júri:

Presidente: Prof. Doutor Fernando Jorge da Silva Pina
Arguentes: Prof. Doutor Luís Filipe Malheiros de Freitas Ferreira
Prof. Doutor António José Estevão Grande Candeias
Vogais: Profª Doutora Márcia Vilarigues
Prof. Doutor António Manuel Monge Soares

FACULDADE DE CIÊNCIAS E TECNOLOGIA
UNIVERSIDADE NOVA DE LISBOA

Março 2013

Chinese Coins In Copper Based Alloys:
Elemental And Microstructural Characterization

Lisboa, Setembro de 2012

Dedication & Acknowledgements

To my family, especially my parents, who have always motivated me to work hard and pursue an education; and to my husband that also always supported and encouraged me. To my daughter, so she can one day read about the work that accompanied her mother during her first childhood and understand what was shown and discussed in the many conferences that she attended since such a young age.

I would like to especially thank my supervisors, Maria de Fátima Araújo (*IST/ITN, Instituto Superior Técnico, Universidade Técnica de Lisboa*) and Rui Silva (*Faculdade de Ciências e Tecnologia, Universidade Nova de Lisboa*: FCT-UNL), for believing in me, for giving me the opportunity to develop this work and for the valuable and intense brainstorming sessions.

My gratitude also goes to the Museum of the Macao Scientific and Cultural Centre, represented by its Director, Luis Filipe Sousa Barreto, that not only allowed the study of the numismatic collection held by the Centre, but also encouraged and promoted the developed work, among other things, through partial funding to attend the BUMA VII Conference in 2009; and by inviting me to perform a public lecture on the subject at the CCCM in 2011.

I also would like to thank several individuals that positively contributed to the completion of the work this dissertation contains:

My colleagues, Pedro Valério and Elin Figueiredo, for the initial training they patiently gave me, for the interesting work discussions and for their moral support. For their support towards the end of the work, I could not forget to mention the colleagues Filipa Pereira and Filipa Lopes. And also to the rest of my IST-ITN colleagues, that shared this academic and also personal walk with me: my marriage, pregnancy and raising of my daughter.

My colleagues at the Structural Materials Group of CENIMAT/I3N (FCT-UNL), in the person of Francisco Manuel Braz Fernandes, for the dedication in preparing practical work, in paper reviewing and in results discussions. To the rest of the colleagues at CENIMAT/I3N, I am grateful for having felt welcome in spite we come from different areas of interest.

My colleagues at the Conservation and Restoration Department (FCT-UNL), especially to Márcia Vilarigues and Ana Maria Martins, for the technical and logistic support given.

To António Candeias, Isabel Ribeiro and Mª José Oliveira from IMC laboratories, for the use of their equipment and technical support given throughout this research.

To Luís Filipe F. R. Thomaz (Instituto de Estudo Orientais, Universidade Católica Portuguesa) and to Augusto Mouta (private collector), for the interesting discussions and ideas relatively to the History of the Chinese numismatics.

I also am in debt to the following persons for their support: Helen Wang (British Museum, U.K.), Quanyu Wang (British Museum, U.K.), Han Rubin (Institute of Historical Metallurgy & Materials – UST, China), Elisabetta Colla (CCCM, Portugal), R.M.Pillai (NIIST, India), Weirong Zhou (Beijing Numismatic Museum, China), Michael Wayman (Univ. Alberta, Canada) and João André Carriço.

Finally, I am thankful for the following financial supports:

- PhD grant (ref. SFRH/BD/29736/2006) awarded by the *Portuguese Foundation for Science and Technology* (FCT-MCTES) during the period of 2007-2011;
- International Conference Attending grant awarded by *Fundação Calouste Gulbenkian* to attend the conference Eurocorr in 2010;
- CENIMAT/I3N funding by FCT-MCTES to attend the conference TOFA in 2010.

Sumário

A colecção de moedas chinesas vazadas pertencentes ao Museu do CCCM em Lisboa (Portugal) foi disponibilizada para estudos analíticos e metalográficos. Tal investigação no Ocidente não é frequente neste tipo de artefacto, conquanto o número considerável de objectos semelhantes que integram museus e colecções privadas, na Europa e América do Norte.

Primeiramente foi feita uma caracterização elementar por espectrometria FRXDE em 380 moedas em liga de cobre, que revelou diferentes tipos de ligas (cobres, bronzes e latões) com teores variáveis de elementos de liga e elementos vestigiais. Nas moedas de bronze, um dos principais constituintes foi o chumbo, que por vezes apresentava um teor consideravelmente variável entre os dois lados da mesma moeda. As moedas de latão apresentavam consideráveis teores de zinco (<63 %p), e frequentemente foi detectada a presença de chumbo, estanho, antimónio, ferro e arsénio.

A observação microestrutural do interior das 109 moedas através de técnicas metalográficas permitiu confirmar a coerência da tecnologia de produção (vazamento em moldes de areia), e estabelecer um paralelo entre os teores elementares (obtidos por micro-FRX) e as fases metálicas (observadas por MO e MEV, e analisadas por EDS-MEV e micro-DRX), recorrendo ao estudo de diagramas de fases em condições de equilíbrio.

A comparação entre a susceptibilidade à corrosão de fases metálicas nas moedas de bronze mostrou uma corrosão transglobular preferencial de glóbulos ricos em chumbo; e também que os produtos resultantes da corrosão do chumbo e/ou do estanho são frequentemente depositados na superfície destas moedas. Quanto às moedas em latão, verificou-se que o processo de corrosão mais comum era a deszincificação, e também que a presença de alguns elementos menores influenciava em grande medida a susceptibilidade à corrosão, prejudicando (p.e., o Fe) ou melhorando (p.e. o Sn, o Sb e o As) a resistência à corrosão das fases em que estes elementos mais se concentram.

Os resultados obtidos são uma mais valia para a caracterização de ligas semelhantes, nomeadamente através da correlação entre os seus teores elementares e os micro-constituintes observados. O conhecimento das susceptibilidades à corrosão nas fases metálicas do bronze e do latão pode contribuir para um melhorado diagnóstico macroscópico de peças semelhantes ao nível da conservação dos objectos.

Por último, todos os resultados obtidos durante este estudo suportam a autenticidade das peças.

Termos-chave

Arqueometalurgia, moedas, China, ligas de cobre, microestruturas multifásicas

Abstract

The Chinese cast coin collection from the CCCM's Museum in Lisbon (Portugal) was accessible for analytical and metallographic characterization. In spite of the considerable number of similar items that populate museums and private collectors in Europe and North America, studies carried out in the western world are very scarce.

Firstly, elemental characterization by EDXRF spectrometry was performed on 380 copper-based coins, revealing different types of alloys (coppers, bronzes and brasses) with variable alloy elemental composition. In bronze coins one of the main constituents was lead, which sometimes presented considerable content variations between the obverse and reverse of the same coin. Brass coins were found to be rich in zinc (<63 wt.%), but often presented traces or small contents of lead, tin, antimony, iron and arsenic.

Metallographic techniques used in the study of 109 coins microstructures could confirm the production process consistency (sand casting), and establish a parallel between the elemental contents (obtained by micro-EDXRF) and the present metallic phases (observed by OM and SEM, and analyzed by SEM-EDS and micro-XRD), resorting to equilibrium phase diagrams.

A comparison between the corrosion susceptibility of metallic phases in bronze coins showed preferential transglobular corrosion of lead-rich globules, and also that lead and/or tin corrosion by-products are often deposited at the surface of these coins. When considering brass coins, the most common corrosion process was dezincification. Also, the presence of some minor elements was found to greatly influence the corrosion susceptibility, demoting (e.g., Fe) or promoting (e.g., Sn, Sb and As) the corrosion resistance of the phases in which these elements are in higher concentration.

The obtained results are an added value to the characterization of similar alloys, namely through the co-relation between their elemental contents and the current micro-constituents. Also, the corrosion susceptibilities in bronze and brass metallic phases can contribute to an improved macroscopic diagnose for conservation purposes in similar items.

All the results obtained during this study support the coins authenticity.

Keywords

Arqueometallurgy, cash coins, China, copper-based alloys, multiphase microstructures

"(...) si tous les groups sociaux et économiques, les producteurs, les commerçants, l'État, acceptent le signe monétaire pour la valeur communément définie, il n'y a pas de raison de ne pas utiliser dans ce but un morceau de bamboo, une feuille de papier ou une pièce de plomb."

François Thierry,
in
La Fiduciarité Idéale à l'épreuve des Coûts de Production : Quelques Éléments Sur La Contradiction Fondamentale de la Monnaie en Chine, 2003.

Index of Contents

GENERAL INTRODUCTION 1

1. Chinese Coinage – Brief history 2
1.1. The functions of Chinese money 2
1.2. Metallic money 2
1.3. Original, counterfeit and false coins 5
1.4. Diversity of Chinese Currency 6

2. Production Technology 8
2.1. Ores, Metals and Alloys in cash coin casting 11
2.1.1. Copper (Cu) 11
2.1.2. Tin (Sn) 12
2.1.3. Lead (Pb) 12
2.1.4. Zinc (Zn) 13
2.1.5. Antimony (Sb) 15
2.1.6. Other metals 16
2.3. Metallurgical characteristics 16

CHAPTER 1 - MATERIALS AND METHODS 17

1.1. Coin selection at CCCM 17

1.2. Methodology and Instrumentation 18
1.2.1 Macro-Energy Dispersive X-Ray Spectrometry 20
1.2.2 Metallographic Preparation 23
1.2.3 Micro-Energy Dispersive X-Ray Spectrometry 25
1.2.4 Optical Microscopy 27
1.2.5 Scanning Electron Microscopy with Micro X-Ray Analysis 28
1.2.6 Micro X-Ray Diffraction 29
1.2.7 Digital Radiography (X-ray imaging) 29

1.3. Protection and Chromatic Reintegration of Artefacts 30

CHAPTER 2 – ANALYTICAL AND MICROSTRUCTURAL RESULTS 31

2.1. Elemental Characterization 31
2.1.1. Preliminary alloy characterization 31
2.1.2. Alloy characterization in clean areas of the selected coins 32

2.2. Microstructural characterization 36
2.2.1. Solidification structure 36
2.2.2. Thermo-mechanical processes 37
2.2.3. Microstructural phases 38
2.2.3.1. Common bronze microstructures (Cu-Sn) 38
2.2.1.2. Common brass microstructures (Cu-Zn) 39

2.3. Bronzes 41
2.3.1. Southern Song dynasty coins (1174 – 1265 AD) 41
2.3.1.1. Chun Xi Yuan Bao coins (1174 – 1189 AD) 41
2.3.1.2. Qing Yuan Tong Bao coins (1195 – 1200 AD) 43
2.3.1.3. Jia Ding Tong Bao coins (1208 – 1224 AD) 45
2.3.1.4. Shao Ding Tong Bao coins (1228 – 1233 AD) 46
2.3.1.5. Chun You Yuan Bao coins (1241 – 1252 AD) 48
2.3.1.6. Jing Ding Yuan Bao coin (1260 – 1264AD) 49
2.3.1.7. Xian Chun Yuan Bao coins (1265 – 1274 AD) 49

2.3.2 Other dynasties bronze coins 51
2.3.2.1. Eastern Han dynasty (25-220 AD) 51
2.3.2.2. Tang dynasty (618-906 AD) 52
2.3.2.3. Qing dynasty (1644-1912 AD) 53

2.4. Brasses 55
2.4.1. Ming dynasty coins (1368-1644 AD) 55
2.4.1.1. Wan Li Tong Bao (1573 – 1620 AD) 56
2.4.1.2. Tai Chang Tong Bao (1620 AD) 57
2.4.1.3. Tian Qi Tong Bao (1621 – 1627 AD) 58
2.4.1.4. Chong Zhen Tong Bao (1628 – 1644 AD) 59
2.4.2. Qing dynasty coins (1644 – 1912 AD) 63
2.4.2.1. Kang Xi Tong Bao (1662-1722 AD) 64
2.4.2.2. Qian Long Tong Bao (1736 – 1795 AD) 65
2.4.2.3. Jia Qing Tong Bao (1796 – 1820AD) 67

2.5. Copper coins 70

2.6. General Remarks 72

CHAPTER 3 – DISCUSSION 73

3.1. Effects of the presence of other elements in copper alloys 73
3.1.1. Microstructural influence of Pb 74
3.1.2. Microstructural influence of Sn 77
3.1.2.1. Microstructural influence of Sb 80
3.1.4. Microstructural influence of Fe 84
3.1.4.1. Microstructural influence of Fe and As 85
3.1.5. Microstructural influence of As 87
3.1.6. Microstructural influence of S 87

3.2. General Remarks 89

CHAPTER 4 - CONSIDERATIONS ON CORROSION 91

4.1. Coppers 91

4.2. Bronzes 92
4.2.1. Sn effect 92
4.2.2. Pb effect 93
4.3.2. Fe effect 96

4.3. Brasses 96
4.3.1. Sn or Sb effect 97
4.3.2. Fe-As effect 99
4.3.3. Pb effect on corrosion 99

4.4. General Remarks 100

GENERAL CONCLUSIONS 103

REFERENCES 107

APPENDIX 118

APPENDIX I – Glossary 118

Appendix II – Chinese Chronology **122**

Appendix III – Polishing and clean area representativeness **124**

Appendix IV – Elements and compounds chemical and physical properties **127**

Appendix V - Cu-Zn Diffusion Couple **130**

Appendix VI - Comparing macro-EDXRF and micro-EDXRF **131**

Appendix VII – Coin data: information and analysis **132**

Appendix VIII - Digital X-Radiography of selected coins and Pb content (macro-EDXRF) **166**

Index of Figures

Fig. A. Coin #2133: Xiao Ban Liang, Western Han dynasty, 206 BC, CCCM Museum……..3
Fig. B. Coin #2298: Song Yuan Tong Bao and character distribution……..4.
Fig. C. Bas-relief depicting several stages of the millenary coin casting process……..10
Fig. D. Schematics showing the relationship between alloy type and composition for copper alloys……11
Fig. 1.1 Distribution of selected coins by dynasties……17
Fig.1.2 Coins from various periods of the Southern Song, Ming and Qing dynasties……..18
Fig. 1.3 Coin distribution per reign in Southern Song, Ming and Qing dynasties in the studied collection……...20
Fig. 1.4 (a) KEVEX 771 spectrometer at QAA Lab; (b) KEVEX rotating sample tray; (c) coins fitted on the sample holders; (d) detail of custom made sample holder……..21
Fig. 1.5 Simplified block diagram of a EDXRF spectrometer ……..21
Fig. 1.6 Schematics of the main procedures and analyses performed on the coins……24
Fig. 1.7 (a) Coin resin mounting; (b) embedded coin after polishing; (c) in sample holder; (d) Si-C polishing……24
Fig. 1.8 Finishing stages of the polishing process……..25
Fig. 1.9 ARTtax Spectrometer and cleaned coin edge area to be analysed……25.
Fig. 1.10 (a) Optical microscope Leica DMI 5000 M: (b) resin mounted; (c) sample-holder……...27
Fig. 1.11 SEM-EDS equipment: sample holder with mounted and un-mounted coins and SEM chamber……..28
Fig. 1.12 XRD equipment Bruker AXS D8 chamber, chamber plate and area selection for analysis……29
Fig. 1.13 Art-X-ray radiation source and target table; output system……..30
Fig. 2.1 Alloy type distribution along the Chinese dynasties represented in the CCCM collection……31
Fig. 2.2 Lead, tin and zinc contents (wt.%) obtained by macro-EDXRF on the surface of the studied coins……...32
Fig. 2.3 Main elements obtained by EDXRF on the surface and polished areas……..33
Fig. 2.4 Bronze (a) and brass (b) coins superficial elemental enrichment or depletion……34
Fig. 2.5 (a) Bronze coins according to Sn/Fe distribution for the various studied periods. (b) Brass coins according to a Pb/Fe distribution for the various studied periods……...35
Fig. 2.6 Columnar solidification microstructures: a) Coin #2766 presenting a dendritic growth; b) Coin #2774 presenting a granular structure……..36
Fig. 2.7 Coin imprint defects: (a) Coin #2608: excess metal globule (b) Coin #2630: feeding fault……...37
Fig. 2.8 File marks in coins (a) #2829 and (b) #2997. Slip bands in coins (c) #2645 and (d) #2661……..37
Fig. 2.9 Coins (a) #2767; (b) #2777; (c) X; (d) #2774 (all BF-OM, etched)……....38
Fig. 2.10 Partial metastable phase diagram for the Cu-Sn system. On the left, coin #2209 (~2 wt.% Sn). On the right, coin #2242 (~15 wt% Sn). Both micrographs in BF-OM, etched.....39
Fig. 2.11 Cu-rich corner of the Cu-Zn equilibrium phase diagram and examples in the selected coins……39
Fig. 2.12 Obverse and reverse of Chun Xi Yuan Bao coins (ref.: #2416; #2419; #2421; #2427; #2433)……..41
Fig. 2.13 Details of microstructures in the Chun Xi coins……..42
Fig. 2.14 Coin #2416: (a) BF-OM; (b) BSE-SEM. EDS spectra of (c) spot #1 (lower Sn content); (d) spot #2 (higher Sn content); e) spot #4 (Cu-Fe-S inclusion); f) spot #5 (Fe-rich phase)……43
Fig. 2.15 Obverse and reverse of Qing Yuan coins (ref.:#2471; #2479; #2495; #2498; #2500; #2501; #2503; #2504)……43
Fig. 2.16 Details of microstructures in the Qing Yuan coins (all in BF-OM, non-etched)……..44
Fig. 2.17 Obverse and reverse of Jia Ding coins (ref.: #2519; #2522; #2525; #2528; #2534; #2544)……..45
Fig. 2.18 Detail of coin #2544 in: (a) BF-OM and (b) BSE-SEM. (c) clean edge area (d) SEM-EDS spectra collected from (b)……..46
Fig. 2.19 Details of microstructures in the Jia Ding coins (all in BF-OM, non-etched)……..46
Fig. 2.20 Obverse and reverse of Shao Ding coins (ref.: #2558; #2563; #2564; #2568; #2571)……47
Fig. 2.21 Details of microstructures in the Shao Ding coins (all BF-OM non-etched, except #2563, PL-OM)…….47

Fig. 2.22 Obverse and reverse of Chun You coins (ref.: #2578; #2581; #2582; #2585; #2588)……48
Fig. 2.23 Details of microstructures in the Chun You coins (all in BF-OM, non-etched)……..49
Fig. 2.24 Coin from the Jing Ding reign (ref.: #2616): obverse, reverse & clean area (BF-OM, non-etched)……..49
Fig. 2.25 Coins from the Xian Chun reign (ref.: #2614; #2615; #2617; #2619; #2621; #2623; #2624; #2625; #2626; #2631)……..50
Fig. 2.26 Details of microstructures in the Xian Chun coins in BF-OM (all in BF-OM, non-etched)……...51
Fig. 2.27 Obverse and reverse images of coin #2209, BF-OM cleaned edge area and detail (non-etched)……52
Fig. 2.28 Obverse and reverse image of coin #2242, BF-OM cleaned edge area and a detail……..52
Fig. 2.29 Obverse and reverse images of coins #2704 and #2977; BF-OM cleaned edge areas and details…….53
Fig. 2.30 Elemental contents of coins #2704 and #2977, from the surface and from a cleaned edge area……..54
Fig. 2.31 Administrative regions of the Ming Empire……..55
Fig. 2.32 Wan Li Tong Bao coins (ref.:#2650; #2653): obverse and reverse; BF-OM clean areas and detail…….56
Fig. 2.33 Tai Chang Tong Bao coins (ref.:#2659): obverse and reverse; BF-OM clean area and detail……..57
Fig. 2.34 Tian Qi Tong Bao coins (ref.: #2632; #2635; #2636; #2639; #2642; #2645)……58
Fig. 2.35 Details of microstructures in the Tian Qi coins (all in BF-OM, #2632 & #2635 etched)……...59
Fig. 2.36 Chong Zhen Tong Bao coins (ref.: #2661; #2662; #2663; #2664; #2666; #2667; #2670; #2671; #3271; #3272; #3273; #3274; #3275; #3276; #3277; #3278; X)……...60
Fig. 2.37 Details of microstructures in the Chong Zhen coins……..62
Fig. 2.38 Map of China's Provinces during the Qing dynasty……...63
Fig. 2.39 Kang Xi Tong Bao coins (ref.: #2710; #2723; #2728; #2733; #2736; #2737)……...64
Fig. 2.40 Details of microstructures in the Kang Xi coins (in BF-OM, etched coins are signalled)……65
Fig. 2.41 Qian Long Tong Bao coins (ref.: #2758; #2761; #2762; #2763; #2764; #2766; #2767; #2770; #2772; #2773; #2774; #2775; #2776)……65
Fig. 2.42 Details of microstructures of the Qian Long coins (in BF-OM, etched)……...67
Fig. 2.43 Jia Qing Tong Bao coins (ref.: #2777; #2782; #2783; #2785; #2786; #2787; #2788; #2789; #2790; #2791; #2792; #2793; #2794; #2796; #2799; #2802)……68
Fig.2.44 Details of microstructures of the Jia Qing coins (in BF-OM, etched coins are signalled)……69
Fig. 2.45 Copper-rich coins from the Qing Dynasty (ref.: #2771; #2779; #2797; #2818; #2820; #2826; #2924; #2950; #Y; #2970; #2989; #2993; #3010)……70
Fig. 2.46 OM images of the cleaned sections and details of the copper-rich coins #2771, #2779 and #2797. Detail of coin #2779 in SEM-BSE: inclusions consist of Cu and S (spectra of spot #1)……71
Fig. 3.1 Cu-Pb equilibrium phase diagram. Examples of a hypo and a hypermonotectic alloy. ……75
Fig. 3.2 Coin #2544 (55 wt.% Pb): (a) detail of a Pb globule (BF-OM); (b) detail of (a) (BF-OM); (c) BSE-SEM of (b); (d), (e), (f): EDS spots in (c)……76
Fig. 3.3 Pb average content of 20 high-leaded coins: image and chemical analysis……77
Fig. 3.4 OM microstructures of brass coins and their elemental compositions……78
Fig. 3.5 Partial isothermal section (450 ºC) of the Cu-Sn-Zn phase diagram, and microstructural examples of selected coins: #2642, α+□; #2770, α+β+□; and #2767, β+□……79
Fig. 3.6 Micro-XRD diffractograms (relative intensities versus two-theta angles for Cu(Kα) radiation) obtained for the diffusion couple Cu-Zn (grey line); coin # 2767 (blue line) and coin #2710 (green line)……80
Fig. 3.7 Microstructural observation of coins #2790 (etched) and #2733 (non-etched) in OM-BF and in BSE-SEM. Spectra of spot #1 and spot #2 in SEM-EDS……81
Fig. 3.8 (a) Isothermal section of the ternary diagram Cu-Sn-Sb at 400 ºC; (b) partial binary Cu-Sn diagram; (c) partial binary Cu-Sb diagram, adapted from……81
Fig. 3.9 Micro XRD of coins #3271 and #2666: antimony rich phase in orange colour……82
Fig. 3.10 Observed and predicted phases using the partial isothermal section of the Cu-Sn-Zn phase diagram (450 ºC) for the studied brass coins……83

Fig. 3.11 Representation by reigns of the studied brass coins on the partial isothermal section of the Cu-Sn-Zn phase diagram (450 ºC): (a) Ming dynasty coins; (b) Qing dynasty coins. 83
Fig. 3.12 Partial Cu-Fe phase diagram. Ferrite (α-Fe) in coin #2427 and #2544 84
Fig. 3.13 Bronze coins Fe phase constitution on a partial Cu-Fe-Sn ternary diagram (isothermal section at 900ºC) 85
Fig. 3.14 Coin #2782 (~1.5Fe wt.%; ~2.7As wt.%): SEM mapping of a region. 85
Fig. 3.15 On the left: micro-XRD of coin #2785. On the right, OM images of coin #2785. 86
Fig. 3.16 Bronze coin distribution in a partial isothermal section of Cu-Fe-As phase diagram at 25 ºC 86
Fig. 3.17 Partial Cu-As phase diagram. OM of coin #2519. Micro-XRD of same coin. 87
Fig.3.18 – Coin #2779: (a) Detail of polished microstructure in OM-BF (non-etched); (b) SEM image of a different area (BSE); (c) detail of corroded area, in OM-BF (etched). 88
Fig. 3.19 - Coin # 2209: (a) detail of polished microstructure in OM-BF; (b) SEM image in BSE mode; (c) EDS spectra of the large grey globule; (d) micro-XRD of the area 88
Fig. 4.1 On the left, OM images of the polished rim in coin #2771. On the right, micro-XRD of coin #2771 92
Fig. 4.2 Elemental mapping of clean areas in coins (a) 2421 and (b) 2427 93
Fig. 4.3 Polished rim area of coin #2544: the Pb-rich phase is corroded. 93
Fig. 4.4 Coin #2421 (~40 wt.% Pb) transglobular corrosion. Pb corrosion products. 94
Fig. 4.5 BSE-SEM images of coins a) #2416 and b) #M117 (superficial areas) 94
Fig. 4.7 micro-XRD of a corroded Pb-rich globule in coin #2522 95
Fig. 4.8 Fracture area of coin #2582 (SEM-EDS). 96
Fig. 4.9 Corroded regions in bronze coins (BF-OM): ferrite (grey phase) seems to be unaltered. 96
Fig. 4.10 Polished rim area of coin #2761 (37 wt.%; α+β): Cu redeposition due to a dezincification process 97
Fig. 4.11 Etched microstructures of brass coins (a) 2762 (39.1wt.% Zn); (b) 2723 (51.6 wt.% Zn) 97
Fig. 4.12 Microstructures of leaded tin brass coins: (a) #2767 (41.3%Zn); (b) #3271 (29.9%Zn) 98
Fig. 4.13 (a) Brass coins phase constitution in a partial isothermal section of Cu-Zn-Sn phase diagram (450ºC). (b) Microstructure of coin #2671 98
Fig. 4.14 Detail of OM-BF etched of coin #2770. 99
Fig. 4.15 Microstructure of coin #2785 and SEM-EDS X-ray mapping. 100
Fig. III.1.1 Schematics used to explain the calculations of the analysed depth in polishing. 124
Fig. III.1.2 OM observation of two distinct abraded areas from the edge of coin #2792. 124
Fig. III.1.3 Coin #M177: edge and radial cut microstructures (OM-BF, Etched). 125
Fig. III.1.4 Coins #2666 and #3271. Clean areas from the edge and from the reverse of each coin. 125
Fig. III.1.5 Micro-EDXRF results of the two main elements of 4 coins in 2 distinct cleaned areas. 126
Fig. III.2.1 Schematics of the sample holder developed 126
Fig. IV.1 Cu-Ni equilibrium diagram 128
Fig. IV.2 X-ray diffractograms for brass gamma phase (Cu5Zn8) and bronze delta phase (Cu41Sn11) 128
Fig. IV.3 X-ray diffractograms for bronze epsilon phase (Cu3Sn) and Cu-Sb delta phase (Cu4Sb) 129
Fig. V.1 Cross-section of the Cu-Zn diffusion couple in O.M. 130
Fig. V.2 Micro-XRD of a spot of the Cu-Zn diffusion couple 130
Fig. VI.1 EDXRF vs micro-EDXRF results (wt.%) obtained from the surface of 14 selected coins. 131
Fig. VI.2 Coins #2782 and #2704 (obverses).. 131

Index of Tables

Table A. Correspondence of weight units and their common names. 8
Table 1.1 Experimental methodology applied to study the selected coins 19
Table 1.2 Chronological timeline indicating the represented dynasties in the CCCM coin collection 20
Table 1.3 EDXRF analysis of Phosphor Bronze 364 to calculate the accuracy in the bronze analysis. 22
Table 1.4 EDXRF analysis of Brass C30.25 to calculate the accuracy in brass analysis 22
Table 1.5 EDXRF analyses of Leaded Bronze C50.01, to test precision. 23
Table 1.6 EDXRF analysis of Free-Cutting Brass C1103 to test brass calibration precision. 23
Table 1.7 Quantification limits for macro-EDXRF analysis (wt.%). 23
Table 1.8 Micro-EDXRF analysis of Leaded Bronze C50.04 to calculate the accuracy of the method. 26
Table 1.9 Micro-EDXRF analysis of Free-Cutting Brass C1104 to calculate the accuracy of the method. 26
Table 1.10 Micro-EDXRF analysis of Leaded Bronze C50.04 to test method precision 26
Table 1.11 Micro-EDXRF analysis of Free-Cutting Brass C1104 to test the precision of the method. 27
Table 1.12 Quantification limits for micro-EDXRF analysis (wt.%). 27
Table 2.1 EDXRF results and microstructural observation of the Chun Xi coins 42
Table 2.2 EDXRF results and microstructural observation of the Qing Yuan coins 44
Table 2.3 EDXRF results and microstructural observation of the Jia Ding coins. 45
Table 2.4 EDXRF results and microstructural observation of the Shao Ding coins. 47
Table 2.5 EDXRF results and microstructural observation of the Chun You coins. 48
Table 2.6 EDXRF results and microstructural observation of the Jing Ding coin. 49
Table 2.7 EDXRF results and microstructural observation of the Xian Chun coins. 50
Table 2.8 EDXRF results and microstructural observation of the Xiao Wu Zhu coin. 52
Table 2.9 EDXRF results and microstructural observation of the Kai Yuan Tong Bao coin 53
Table 2.10 EDXRF results and microstructural observation of the Jing Ding coin. 53
Table 2.11 EDXRF results and microstructural observation of the Wan Li coins. 57
Table 2.12 EDXRF results and microstructural observation of the Tai Chang coin. 57
Table 2.13 EDXRF results and microstructural observation of the Tian Qi coins. 59
Table 2.14 EDXRF results and microstructural observation of the Chong Zhen coins. 61
Table 2.15 EDXRF results and microstructural observation of the Kang Xi coins. 64
Table 2.16 EDXRF results and microstructural observation of the Qian Long coins. 66
Table 2.17 EDXRF results and microstructural observation of the Jia Qing coins. 68
Table 2.18 EDXRF results and microstructural observation of the copper coins. 71
Table 3.1. Elements present in the 109 cleaned and analysed coins 74
Table 3.2 Crystallographic data of gamma and delta phases Cu-Zn and Cu-Sn systems 79
Table 3.3. Crystallographic data of delta phase in Cu-Sb and Cu-Sn systems 82
Table II.1. Main Chinese Dynasties. 122
Table II.2. Chronological table of the reigns present in the studied coins 123
Table III.1.1 Micro-EDXRF analysis of 2 distinct cleaned areas of the edge of coin #2792 125
Table III.1.2 Micro-EDXRF analysis of cleaned areas of the edge and radius of coin #M117 125
Table III.1.3 Micro-EDXRF analysis of cleaned areas of the edge and reverse rim of coins 2666 and 3271 126
Table IV.1 Chemical and physical characteristics of the alloying elements 127
Table IV.2 Optical observation of metallic phases and inclusions in copper-based alloys 128
Table V.1 SEM-EDS of diffusion couple Cu-Zn 130
Table VII.1 Coin attributed data, physical measurements and EDXRF 132
Table VII.2 Macro-EDXRF (surface) and micro-EDXRF (cleaned sections) of 109 selected coins 137
Table VII.3 Micro-EDXRF and OM images of the cleaned sections 139

Symbols and Notations

BF – Bright field illumination in OM
BM – British Museum
BNF – British Non-Ferrous Metals Technology Centre
BSE – Backscattered Electron imaging mode of SEM
CENIMAT – Centro de Investigação de Materiais (DCM/FCT-UNL)
CCCM – Centro Científico e Cultural de Macau
CNM – China Numismatic Museum
DCR – Departamento de Conservação e Restauro (FCT-UNL)
DF – Dark field illumination in OM
EDXRF – Energy Dispersive X-ray Fluorescence Spectrometry
fcc – Face-centered cubic system (crystallographic arrangement of atoms)
FCT-UNL – Faculdade de Ciências e Tecnologia da Universidade Nova de Lisboa
FEPA - Federation of European Producers of Abrasives
IMC-MC – Instituto dos Museus e da Conservação – Ministério da Cultura
ITN/IST – Instituto Tecnológico e Nuclear/Instituto Superior Técnico
NBS – National Bureau of Standards
OM – Optical Microscopy
PL – Polarized light in OM
QAA – Química Analítica e Ambiental
SEM-EDS – Scanning Electron Microscopy with X-Ray Microanalysis
XRD – X-ray Diffraction
ZAF – Z (atomic number), A (absorption), F (fluorescence matrix effects)

α-Cu – Alpha Cu-rich phase from several systems: Cu-Sn; Cu-Zn; Cu-Fe
(Pb) – Alpha Pb-rich phase from the Cu-Pb system
F_1 – Primary iron-rich phase, possibly α-Fe (ferrite) from the Cu-Fe system
F_2 - Fe,As-rich phase, possibly Fe_2As (iron arsenide) from the Fe-As system
C_1 – Cu-S inclusion, possibly Cu_2S (chalcocite) from the Cu-S system
B_1 – Cu,Fe,S-rich phase, possibly Cu_5SFe_4 (bornite) from the Cu-Fe-S system
D_1 – Cu,As-rich phase, possibly Cu_3As (domeykite) from the Cu-As system
G1 – Cu,Sn-rich phase, possibly γ-brass from the Cu-Zn system or δ-bronze from the Cu-Sn system
G2 – Cu,Sb-rich phase, possibly γ-brass from the Cu-Zn system or δ-bronze from the Cu-Sn system
∅ - diameter

General Introduction[1]

In recent times, there is a pressing need to understand the cultural heritage materials that have come to be gathered/ collected, in order to conserve them based on scientific grounds, beyond the obvious contribution towards the evolution and disclosure of the knowledge about people and their civilizations.

In Portugal, concerning ancient metal artefacts, studies have been consistently increasing in the last years, especially developed by the team constituted by researchers from the Environmental and Analytical Chemistry group (QAA, from ITN/IST), and from Departamento de Ciência dos Materiais and Departamento de Conservação e Restauro (from FCT-UNL), mainly in Portuguese archaeological metallic artefacts from known excavations [Araújo *et al.*, 2010].

China is a vast and populous country with an ancient history and a civilization that bloomed in literature, arts, technology and industry early on. As trading and commerce were always very important within and outside its territory, money became consequently necessary and indispensable. Cash coins are part of the Chinese metallic money history and were abundantly used for a period of about 2000 years, not only in China but in trading regions throughout East Asia [Zhou, 2004]. They are known as *qian* in mandarin (i.e., money); *cash* in English (from the French term *caisse*) and in Portuguese as *sapecas*, supposedly from the Malayan term *sapaku*, that means “one-cent”, due to the strings of one-hundred coins made after production to ease their transport and distribution [Dalgado, 1982].

Several catalogues have been published by Western researchers, including a thorough description and images or rubbings of Chinese cash coins [Schjoth, 1965; Petrie, 1964; Cresswell, 1979; Lockhart, 1975; Coole *et al.*, 1967; Coole, 1981], and also of cash coins produced outside the Chinese territory in nearby regions, or exported there from China – like Japan, Vietnam, Philippines, India and Arabia – where the production technology had a small to great success [Gosen, 1963; Mandel, 1972; Cribb, 1996a; Cribb and Potts, 1996b; Thierry, 2003]. Considering material characterization, although there are some chemical characterization studies on Chinese coins (see refs. in section 2.3), it became evident there were not many studies involving the microstructural features of these artifacts, especially published in western languages. So when the opportunity to access a collection of Chinese coins acquired at Macau, an ex-Portuguese Special Administrative Region arose, it was seized in order to characterize their composition, structure and production techniques.

Next, a brief overview of the Chinese coinage history and production follows[2].

[1] Part of the results presented in this chapter was presented as an oral communication: M.J.Furtado. *Moedas Imperiais Chinesas da colecção do Museu do Centro Científico e Cultural de Macau*. Lisbon (Portugal), August 2011 and published with the same title and author in Numismática, 114, (38/4), see [Furtado, 2011].

[2] A table of the main Chinese dynasties and a table of the main Chinese reigns in the studied coins can be found in Appendix II to help the reader with chronologic issues.

1. Chinese Coinage – Brief history

1.1. The functions of Chinese money

While in Minor and Central Asia coins had an intrinsic value determined by the weight and purity of the precious metals used; in China, by contrast, money had an eminently fiduciary character from the start [Thierry, 2001]. Its value relied on trust between economic agents and the issuer, but mostly by quantitative coinage control. Chinese metallic money, in general, was thus conditioned by its singular function, promoting transactions, independently of the intrinsic value of the material it was made of, as Thierry [2001] describes:

> *"En Chine, l'État n'est pas là pour garantir la qualité de la monnaie, il est là pour en garantir la circulation et la circulation est liée au bon rapport entre la valeur des biens et des services et la valeur d'échange de la monnaie, pas à sa valeur intrinsèque".*

> *"(...) la monnaie chinoise classique s'apparente plus à ce que les Occidentalistes appellent «monnaie de nécessité» (...): faible valeur intrinsèque, circulation fondée sur la confiance, monopole d'État non-impératif, et souplesse d'adaptation aux conditions locales".*

Currencies with a high intrinsic value (gold, jade, silver, tortoise shell, etc.) were in fact collector objects, or financially were used as collateral or in high transactions. Von Glahn [1996] states that, during the Ming dynasty, the *"high-value silver served as the principal instrument of exchange in wholesale commerce and long-distance trade, while bronze coin constituted the primary currency of petty retail marketing"* and also that *"Grain rotted; animals sickened or aged; but metallic money retained its value immune from the ravages of time. (...) money enabled the transfer of value across time as well as space"*. Putting high intrinsic value coins into circulation would have led to hoarding, which would have prevented them from serving their function [von Glahn, 1996; Caestecker, 2010].

1.2. Metallic money

Chinese coinage history dates back as early as 1500 BC: after the widespread use of cowry shells in commercial trades, the production of cowry-like coins began by using materials such as stone, bone and clay [Thierry, 1992]. Later, during the 7th century BC, cast metal was added to the raw materials used to produce cowry-like coins [Eagleton and Williams, 1997]. Although other forms of payment subsided for many years – silk, cattle, rice, silver ingots, paper money, among others [Wagel, 1915; von Glahn, 1996; Huang, 1974] – metallic coins were used for more than 2500 years as the means of payment in small, everyday transactions.

After man-made cowries, the political gaps gave rise, broadly, to different kinds of metallic money. Until the Qin dynasty (3rd century BC), China was made of a feudal system consisting of various states that depended on the king and periodically fought internal wars for leadership. Each provincial lord was responsible for controlling currency, so each form of money evolved very

differently, although they were exchanged throughout the various states [Hartill, 2005; Thierry, 2001]. Agricultural regions cast tool-coins such as spades or knives, which little by little, were miniaturized to serve as money (probably since the 8th century BC). Other regions adopted circular coins with a hole in the centre: the "ring coin" (*huan qian*) or "round money" (*yuan qian*) that appeared as early as the 4th century BC, during the Warring States period [Coole, 1981; Thierry, 1992; Hartill, 2005]. Its typology consisted of a round shaped disk with a concentric round hole, with or without characters in one or both faces. There are various theories that try to explain the shape of this coin and the most accepted ones are:

1) the shape emulates *bi* disks, decorative pieces made out of jade and used since the Neolithic as amulets or in funerary rites of high social status individualities [Teng, 2000];

2) according to Peng [1965], the proportion between the diameters of the coin and its orifice are different to that of *bi* disks, so the author suggests the inspiration for this coin came from another utensil of general use in ancient China: spinning whorls, a common object in textile production.

Either way, the round coin was the predecessor of the cash coin (*qian*): a round coin with a concentric square hole. It started out with no rim and a flat reverse. It was around the reign of Duke Xiao (361-338 BC) of the Qin state that the first official circular coins with square holes in the centre were issued, called *Ban Liang* (half-liang, a weighing unit) [Yang, 1952; Hartill, 2005], although it was only widely spread during the Qin dynasty, by its first emperor Shi Huang. He adopted the round coin as the official form of currency in China (206 AD), over all other typologies [von Glahn, 1996]. This coin required a reduced amount of metal, its symmetrical shape rendered the production more expedite and its size made transportation and use more convenient. All the above made the production of round coins quite cost-effective. As private minting was allowed at the time, this coin exists in different sizes and calligraphies (example in Fig. A).

Fig. A. Coin #2133: *Xiao Ban Liang*, Western Han dynasty, 206 BC, CCCM Museum.

During the following dynasties, a change in policies drove the monetary system to a set of reforms that introduced some innovations in cash coins. For example, under emperor Wu Di, of the Western Han dynasty, the use of cash coin was already well established, a monetary reform uniformed the coin typology (e.g., introducing an inner and outer rim and another attempt to establish a fixed weight for the coins) issuing *Wu Zhu* coins (i.e., 5 Zhu, which is a weighing unit). The emperor tried to restrict its production to the central government, severely punishing counterfeiters. Golas [1999] refers that by then, the *"minting of bronze coins consumed by far the largest part of the copper mined in China."*

The *Ban Liang* coins and the *Wu Zhu* coins were failed attempts to give the coins an intrinsic value relating it with a nominal weight. This collided with the Confucionist philosophy that established a fiduciary value to coins [Thierry, 2001]. Both systems worked, in reality, in a fiduciary mode, with significant shifts in the coins actual weight, therefore, their denomination was in fact false.

Later (621 AD), the first emperor of the Tang dynasty, Gao Zu, returned the cash coin its fiduciary value, where the coins value was independent of its weight, size or composition [Thierry, 2001]. He also instituted – among others – an important monetary reform: the use of a new script. Up to this moment, the characters used in cash coins were in seal script, in spite of clerical, standard and running scripts have existed since the Han dynasty [Ouyang and Wang, 2008]. From the Tang onwards, the coin obverse starts having four characters, situated on the main cardinal points, read top-bottom-right-left [Thierry, 2003; Hartill, 2005]: two characters indicating the reign title of issue (the name of the reign or the name of the emperor) and two relating to the coins function (see Fig. B). The main characters used for function until the end of cash coinage production were: *Tong Bao* (circulating currency), *Zhong Bao* (heavy currency) or *Yuan Bao* (primary currency). Coins (the object designated as *qian*; or *wen,* when designating quantity) now have a denomination that is independent of its intrinsic value, having a fluctuating value, established by the market. Sets of markings (crescent, point, *et cetera*) were also added to refer to mints, years or special editions, but little is still known about them [Hartill, 2005]. Tang dynasty was also the time when Chinese currency was exported throughout Asia and afterwards, its system replicated in those regions, e.g. in Japan [Saitou *et al.*, 1998].

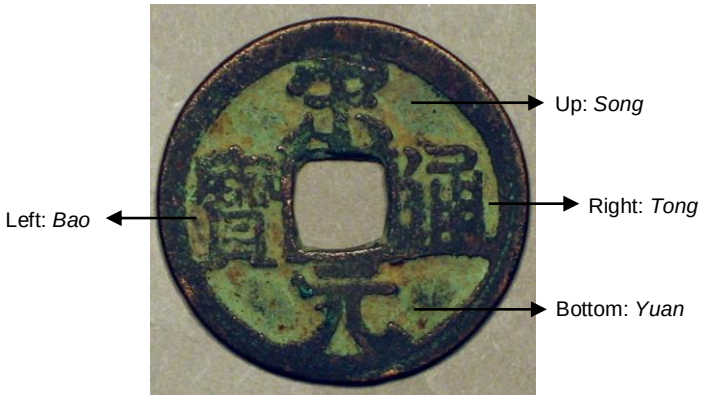

Fig. B. Coin #2298: *Song Yuan Tong Bao* and character distribution.

Gorny [2003] states that during the following dynasty, Song, "*The varieties in calligraphy style, position of the writing relative to the rims, dimensions and styles of the inner and outer rims, and the size of the center holes, all these methods were used to denote mint location, workshop or furnace, and casting period (more than one per year)*". This is supported by Hartill [2005], that refers a particular set of coins during the Northern Song dynasty in which *"two or three calligraphic different styles on coins of the same period title which are otherwise identical in size of hole, width of rim, thickness, size and position of the characters and alloy".* He assumes that these differences can be due to the craftsmen of different mints, but *"no attributions have yet been proposed"*.

Ming dynasty coinage was marked by a change in composition with the introduction of zinc, and the alloy altered from bronzes to brasses [Gu, 1667]. Another change happened during Emperor Chong Zhen, with the re-establishment of characters on the coins reverse, possibly indicating its minting place [Hartill, 2005], resuming Tang dynasty's Emperor Wuzong two-reign period (845-46 AD) in which this was performed [Thierry, 2003; Hartill, 2005]. The characters on the reverse and/or the different types of calligraphic styles served to distinguish between mints, until the end of the Qing dynasty [Burger, 1976].

1.3. Original, counterfeit and forgeries

Craddock [2009] distinguishes between two different fraudulent reproduction of coins: a) counterfeits or "*coins which are copies of current coins made with the intention of passing them into circulation and obtaining no more than their face value*"; and b) forgeries or "*copies of coins that are valued, usually far above their face value, and collected for their own sake, and prized for their beauty, historic interest or just plain rarity*".

Cash coins were used in everyday transactions and their use channelled large tons of metal. Although their composition eventually started to be established by the central government[3] yearly, in reality there were many periods in which each province or private minter was allowed to establish its own composition; and there are compositional differences even within the same mints, so one might hypothesise that the values ordered by the central government were mostly guidelines to be followed or adopted only by the main Boards.

Generally, when private minting is discussed, the composition is usually inferior to that of official coinage, due to the obtainable profit margin [von Glahn, 1996], but this depended on many factors. So the idea that a qualitative analysis of a counterfeit coin is nearly always essential to distinguish it from an official coin [Scott-Dodd, 1939] it is not universally valid for Chinese cash coins: there is an expected variation of compositional values.

The prominent reason for counterfeiting (i.e., issuing cash coins when there was an official proscription to do so) was profit, which was facilitated by the simultaneous circulation of different coins with different denominations and weights. This allied to the fact that most mints just worked some months per year, left the qualified personnel available to fabricate coins during the rest of the time [Burguer, 1976]. Song [1637], in late 17th century, referred to "*the disadvantage of coins is that*

[3] The responsible entities for cash minting were the Board of Works and the Board of Revenue (corresponding to Ministries of Public Work and Finance, respectively). Hartill [2005], p.445:

> *"The Board of Revenue mint* [bao quan] *(…) was used for the Provincial Coinage Service established in each province in 1368, superseding the previous Jiangxi Coinage Service [huo quan ju]. It was responsible for the production of coins in accordance with the orders of the central government following designs issued by the Board of Works. From 1380, coinage was specifically made the responsibility of the Board of Works, whereas the production and circulation of paper money was assigned to the Board of Revenue. From 1622, (…)* [it was] *established in Peking to increase the amount of cash available for defence against the Manchus.(…)*
> *The Board of Works mint (…) attached to the Board of Works (…). It was known as the Bao Yuan. (…) From 1421 to the end of the Ming there was another Bao yuan at Nanking (…). After 1625, the Board of Revenue became the chief agency for coinage matters. (…)"*

they can be easily minted illegally, which is harmful to the people. That is why in all parts of the empire circulation of coins is frequently stopped."

Sometimes, however, private coinage minting was encouraged by the official government as a way to overcome coin shortage, or otherwise, when downsizing was necessary, this money was bought by officials or received as tax, so it would not circulate. The prohibition or encouragement of private minting occurred several times during Imperial China [von Glahn, 1996; Peng, 1965; Wagel, 1915]. Most rulers, in fact, cared more on the number of coins produced than on their composition, in order to keep transaction fluidity [Thierry, 2001]:

> *"Durant toute l'histoire de l'empire chinois, le monopole d'émission n'est pas considéré come un donné absolue ou comme une prérogative intangible de l'État. Si les autorités ne sont pas à même d'assurer l'approvisionnement de la société en moyens de paiement, elles peuvent trouver intérêt à faire partager le coût du travail à la société ou même de le transférer aux entrepreneurs privés. À de très nombreuses reprises les autorités ont d'elles-mêmes donné la liberté de fonte, soit à la population (...), soit à des entités administratives."*

For example, with the rise of copper price, coins started to be cast in bronze (probably using scrap metal from other metallurgy products), lead, iron or later, in brass alloys to reduce the amount of copper needed. Although in Western civilization this was cause for crisis (due to the devaluation of the intrinsic value of the coin), in China this type of operation allowed fluidifying and rebooting monetary circulation.

Burger [1976] refers that during the Qing dynasty there were some eras and provinces where private coinage surpassed the official coinage. From the 19th century onwards, it was so generalized that the detection of counterfeit coins was hardly noticeable: a way to distinguish them was measuring their inner diameter: if using a regular coin as a mould to reproduce others, the resulting coins would be lighter and smaller. That is why heavier coins were collected to replicate new coins. However, melting coins and/or casting fakes during this dynasty was frequently punishable with death and even cutting or filing coins had the punishment of 100 whiplashes with a stick.

1.4. Diversity of Chinese Currency

There was never true uniformity in Chinese currency, because even after the introduction of coinage, payments still included the use of material assets, as well as the circulation of contemporary and former ancient coins[4] and also the diverse quality of coins. Guaranteed that the stringed coins looked uniform as a set, all coins were possible to use and it would be impossible to read their individual inscriptions [Thierry, 2001]:

[4] During times of coin shortness, "*(…) the populace simply resorted to using the coins minted by previous dynasties*" [Huang, 1974].

"Les chinois ont toujours et régulièrement utilisé les monnaies des dynasties antérieures tant qu'elles avaient l'aspect qui convenait. Les dépôts monétaires découverts en Chine montrent clairement que de tout temps l'usage des monnaies antérieures est une réalité économique, et cela jusqu'au début de la République (…) elle tend à s'abstraire du temps et du lieu.
(…)
À partir du moment où le signe monétaire est accepté par tous, acheteurs, vendeurs et l'État, pour la même valeur d'échange, la circulation se fait sans problèmes."

Thierry [1992] explains that, in China, bronze coins worked as credits and their value was set by the Government, regardless of their weight or metal value. Wagel [1915] exposes this situation differently:

"(…). We do not know if, at any period in the history of this country, there was any fixity as regards money. All that we know is that trade in this country, both internal and external, has always been double faced; business between one province and another, between even two districts in the same province, has had to be take count of not only the value of commodities but also the value of money. (…) The value of money or the tael *is regulated by the weight as well as purity and local custom."*

During the Ming dynasty the denomination system of Chinese cash coinage depended on the rate value for silver. Huang [1974] reports on this influence:

"*In the fourteenth century (…) it was decreed that 1,000 standard coins were to be worth 1 tael of silver. After 1500, partly due to the rise in the price of copper, the rate was revised to 700 and sometimes 800 coins per tael of silver. The actual rates in private transactions varied considerably from this norm, depending on local copper prices and the quality of the coins.*"

This dependence increased during the Qing dynasty, undoubtedly due to the foreign potencies influence [Thierry, 2001]:

"Plus tard encore, les empereurs manchous de la dynastie Qing (1644-1911), les Portugais de Macao, les Hollandais et les Espagnols de Taïwan et de Luçon et les Anglais de Hong Kong seront autant de barbares qui tenteront d'imposer à la Chine l'usage monétaire des métaux précieux et qui parviendront à lui imposer celui de l'argent".

The denominations for fixed weights of silver were the candareen *(fen)* and the tael (*liang*, the Chinese ounce), see correspondences in Table A. The lowest weight measure was the actual coin, *cash* (in English); in mandarin *qian*, *wen or li* (the last one in later dynasties). It corresponded to 1/10th tael of silver [Huang, 1974; US Congress, 1901] but this value could greatly fluctuate. In

theory, at least each coin should be equivalent to 1-cash, but according to its weight, or simply by government attribution, cash coins could have the denominations 1-cash; 2-cash, 3- or 4-cash (rare); 5-cash; 10-cash; 50-cash and 100-cash.

Burger [1976] and Hartill [2005] suggest different weighing standards from the presented in Table 1, and Peng [1965] states that the weighing equivalent units could have changed throughout the years.

Table A. Correspondence of weight units and their common names (adapted from Huang, 1974; US Congress, 1901).

10 cash (*qian/wen/li*)	1 candareen (*fen*)
10 candareen (*fen*)	1 mace
10 mace	1 tael (*liang*) (~16 g [Hartill, 2005])

2. Production Technology[5]

Cash coin production did not suffer many changes throughout the 2000 years of its continuous use. Up until the first striking machines – imported from Birmingham (U.K.) – started producing in 1889, the mass production process was handmade using casting moulds [Thierry, 1992].

There were basically three types of coin casting methods throughout Chinese history: hemmed clay casting, stack clay casting and sand casting with master coins [Xian, 2004]. The first method used one or two piece moulds; the second method used 2-piece moulds but overlapped in such a way that several layers of moulds could serve simultaneously. The last method involved imprinting the positive image (model) on a two-part sand-filled mould: the sand could be re-used several times.

The first moulds were generally one-piece, sculpted from a portion of *terracotta* or stone, where the metal alloy was poured into. There was even a period during the Qin dynasty when wooden models were used, but because they were rapidly consumed, their use was abandoned [Burger, 1976].

The final product was a coin with a decorated obverse (from the characters incised on the mould) and a flat reverse [Thierry, 1992]. There are very few remains of clay moulds, because they are easily perishable. Also, the shapes and inscriptions were carved on the mould, so there were much more variations from coin to coin: this implied more time to complete each mould and, as they could break or crumble, they had to be frequently replaced. Since late Zhou dynasty, stone or bronze models were used to produce clay moulds [Barbieri-Low, 2007; Burger, 1976]. Later, during the Han dynasty, there was a production standardization using plaster and also bronze models to produce the clay moulds in a more expedite mode [Hartill, 2005]. This reduced the dissimilarities between coins of the same mint. From ~600 AD onwards (Tang dynasty) the adopted moulds were made from a sifted mixture of sand, ground baked clay and charcoal, filling a wooden frame. Sand moulds belong to the type of aggregate moulds [Campbell, 2003]. In China, due to its abundance

[5] Part of the results presented in this section was previously published: M.J.Furtado - *Moedas Imperiais Chinesas da colecção do Museu do Centro Científico e Cultural de Macau*. Numismática, 112, December 2011.

and its small grain size, loess was the prominent material used [Golas, 1999]. In a study concerning the archaeological find of a minting site in the Xi'an region in China [Xian, 2004], casting remains of several ages were found. The author describes the region as abundant in loess, which was necessary for coin casting, and located near a river, where charcoal could be easily transported by water, to serve as fuel. The city was near the Han dynasty capital, so government control was executable. Several relics were uncovered, like clay moulds for coin-casting. Accompanying these pieces there was a lot of charcoal ashes, among which copper residues were found.

In a XVII century treatise [Song, 1637], the contemporary coin casting technology was described in detail and it is considered to have been a current practice for centuries before this document was written: coin models[6] – excellent quality issues of the coins to reproduce – were imprinted on one of the halves of the sand mould. The other half was placed directly on it to perform the reverse imprint. After the impression, the mould halves were separated and the models removed. A sprue system was made to connect the impressions to a main pouring opening and both halves were assembled. This caused the casting product to be a *money-tree* or *cash-tree* (*qian-shu* in mandarin) consisting of several coins attached by sprue to a central axis [Burger, 1976]. Several wooden frames were joined together and became ready to receive the molten alloy [Thierry, 1992]. Copper was melted in a crucible made of extremely fine powdered material described as "crushed dry earth and brick fragments mixed with charcoal powder". It was known this step would help in the alloy melting process because the carbon in the charcoal acts as a reducing agent avoiding significant copper oxidation [Campbell, 2003].

Song [1637] writes that to make the melt, copper was melted in a crucible made of earth and crushed bricks (7 parts) and charcoal (3 parts), ~25 cm deep and 8 cm in diameter. Each crucible could sustain up to 6 Kg of metal. Once the copper had melted (1083 ºC) zinc was slowly added to the crucible, and the mixture kept in the furnace to homogenize. It could then be poured into the mould (see Fig. C for a depiction of the process). This seems to imply that the Chinese were already familiar with the zinc speltering process.
Although post-casting work was performed on bronzes as early as 200 BC [Li *et al.*, 2011], until the Han dynasty, the coins were not polished by norm: some have uneven rims and sprue remains [Thierry, 1992]. After that period, the coins underwent a thorough sequence of post-production: after cooling, the coin tree was removed from the mould and the coins were separated from the sprue. The coins were stacked by the central hole on a wooden stick and any sprue remains on the

[6] Positive moulds were called *mother-cash* or *seed coin* (*mu qian* in mandarin) up until the 17th century. They were individually sculpted out of a soft material (wood, bone, ivory, *et cetera*) or alloy (pure tin, copper or brass), possessed a very high quality in detail and could be used hundreds of times before having to be replaced. But the fact they were crafted one by one, meant there would be differences among them. After the 17th century, these coins were named *ancestor coins* or *master cash* (*zu qian* in mandarin) and were used as moulds to cast the *mother-cash* that were then shipped to the province mints. This saved some time and effort, as well as uniformed the production [Thierry, 1992]. This author also refers that sometimes the cast coins were used as mother coins – especially during a crisis or in private minting –, which lead to an inferior quality final product.

edges were removed by filing. As new-made coins are usually covered with copper oxide - looking blackish -, most of the times surface polishing was performed to give the coins a shiny finishing.

Fig. C. *Bas-relief* depicting several stages of the millenary coin casting process (China Numismatic Museum, Beijing). From [Bavarian, 2005].

They were put in a cylinder with plant straw and agitated for 1 hour by two workers in order to become shiny and smooth [Burger, 1976]. Burger also cites an official document dated from 1741 that also includes a job description for someone to file the "eye", i.e., the hole of the coin [Burger, 1976]. Hartill [2005] cites the following record, concerning a coin mint, from the Guangxi Gazetteer:

> *"As well as buildings for the furnaces, administration and security, there was room for the temple of the furnace god, and a shrine for the local gods. Each furnace had one foreman, one man to stoke the fire, one man to pour the molten metal, one man of all work, one man to tend the sand, one man to brush the ashes, one man to turn the coins on the lathe, one man to polish the coins, one man to attend to their edges, and one man to work the treadle."*

During the Ming dynasty, Huang [1974] states that:

> *"After the coins were cast, a great amount of work was involved in trimming and polishing the edges. (...) up to one-third of the metal had to be filed off in order to produce top-quality coins.(...) Coins were fixed in position for trimming by stringing them on a square rod, of which the two ends were clamped tight."*

In order to facilitate trimming, which after the 16th century was said to have become more of a hand-trimming work in order to save manufacturing costs, Huang [1974] adds that the workers mixed more tin and lead in the alloy. The lead addition hindered the quality of government-cast coins, which in its turn encouraged counterfeiting. Huang [1974] also concluded that it was the lack of adequate financing rather than lack of technological skill that forced down manufacturing standards.

2.1. Ores, Metals and Alloys in cash coin casting

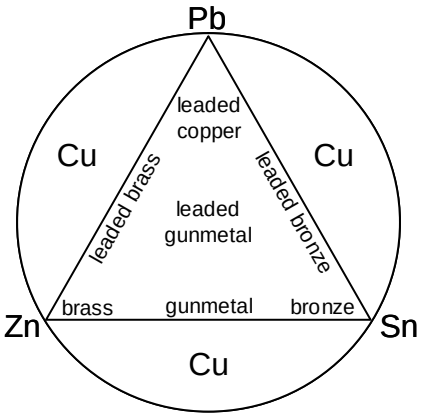

Fig. D. Schematics showing the relationship between alloy type and composition for copper alloys (adapted from [Bayley, 1998]).

The Chinese Empire was rich in many ore deposits and found a way to explore them for casting purposes [Golas, 1999; Chen, 1991]. The main metallic deposits allowed the extraction of the following metals: gold, silver, iron and the ones most used in copper cash coinage[7]: copper (*hong-tong* or *tong* in mandarin), tin (*xi* or *bai-xi*), lead (*woyuan* [Zhou, 2007], *qian*, *hei-qian* or *hei-xi*) and zinc (*woyuan*, *yan* or *yuan* [Zhou, 2007], *xin*, *bai-qian*, *qian*, *bai-xi*, *wo-qian* or *shui-xi*). Figure D presents schematics of the major alloys containing these elements. Chinese coins in other based alloys were also produced: as gold, silver, iron and lead [Yang, 1952]. The author refers to gold and silver coins being used as gifts or toys but not in small commercial transactions. Iron and lead were used in areas/times where copper was too expensive.

2.1.1. Copper (Cu)

The minerals used to obtain copper were malachite, azurite, tenorite, cuprite, chrysocolla, brochantite, chalcanthite, bournonite, enargite, tetrahedrite, chalcopyrite, chalcosite and bornite [Golas, 1999] so it is no surprise to observe any of these as corrosion products in copper cash coins.

During the Han dynasty, according to Golas [1999]:

> *"As early as the 1st century, some 100,000 convict workers were said to be employed in the production of copper and iron and, between 188 BC and ~5 AD, the government minted an average of 220 million coins per year. In following dynasties, the government found itself repeatedly trying to devise policies to close the gap between available supplies of copper and the often large amounts needed by its mints in order to maintain a copper-based currency."*

[7] *Pinyin* denominations obtained from [Burger, 1976; Zhou [2007]. It is clear that some denominations have the same pinyin name - although the characters may be different – which causes some confusion when deciphering ancient treatises to identify the metals used thoughout Chinese History.

Throughout the years, the value of metallic copper and copper cash coins fluctuated due to the availability of the mineral and the government policies [Golas, 1999]. Copper shortage and copper imports are frequently mentioned. The re-use of copper from melted down coins and objects was also a common practice, especially when mining production was unavailable:

> *"(...) even after the [Yuan] Mongols re-established minting in 1309 AD, only small numbers of coins were produced, mostly it would seem using copper from melted down coins and objects rather than from new mining production".*

Copper was also imported from Japan [Glamann, 1953] due to the large amounts of this metal required to cast coins.

2.1.2. Tin (Sn)

Tin was extracted mainly from cassiterite ore (nearly 80% content), and as its melting point is quite low (232 ºC) it is expected that its use in metallurgy was discovered early on. According to Golas [1999], cassiterite in China is very rich in iron, which remained present in the metal smelted from this ore. It was mostly used in the 1st millennium for tinning purposes. Later, it became very important due to its combination with copper (especially in contents above ~10 wt%), to produce an alloy superior to copper in hardness and fluidity: bronze. Its main uses were to produce weaponry and ritual objects (as the Shang and Zhou dynasty bronze vases).

2.1.3. Lead (Pb)

Lead was an available and abundant raw material in the Chinese territory [Golas, 1999]. It has physical properties that benefit casting, and therefore was an economically and technically favourable metal for casting coins.

As in the Roman Empire, lead was often mistaken with tin by the early Chinese. Golas [1999] refers three main tin producing sites in a Han chronicle (*Hsu Han Shu*) in which one was probably producing lead. The two metals had a similar appearance, low melting point and hardness. However their weight and colour distinguished them: tin, lighter, was called "white tin" (*bai xi*) and lead, heavier, was called "black tin" (*hei xi*). Golas [1999] adds "The adulteration may sometimes have been unintentional, resulting from simple misidentification." And however sceptic about this when concerning miners – because cerussite (a colourless to grey lead carbonate) was hardly confused with cassiterite (a white to brown tin oxide), – the confusion between galena (a black lead sulphide) and cassiterite could in fact existed among miners because of their similar physical properties.

Golas indicates 8 wt% as the borderline for intentional Pb addition and that it was probably in late Shang dynasty that its usefulness in bronze alloys was recognized. Lead was used in large scale in Chinese coin casting during the imperial period [Vogel, 1987]. Pan *et al.* [2007] suggests Pb was used according to the artefact function: it was in some cases to increase the objects weight (due to

Pb higher density), due to its abundance in China [Golas, 1999] and consequent lower price when compared with other metals but also because of its physical properties that helped during the casting process: lead addition improved melt fluidity and lowered the alloys melting point [Cowell *et al.*, 2005a].

2.1.4. Zinc (Zn)

While, according to Craddock [1998], copper, tin and lead were effortlessly found in their metallic form, and their alloys formed by mixing and stirring, brass could not be made in this way because zinc ore was only available in Nature as zinc oxide, carbonate or sulphide. There is little evidence on zinc ore extraction in China before the 18th century AD; however, its use dates back as early as the 1st millennium BC [Golas, 1999]. Its main mining ores were smithsonite, calamite, zincite, willemite and franklinite. Its use to make brass can then be through two distinct processes, cementation – in which the zinc ore is used – or speltering – in which metallic zinc from a refined ore is used.

Zinc has a boiling temperature of 915 ºC subliming by the temperature required to reduce its oxide to metal (from 915 ºC to 1000 ºC) [Craddock, 1995], so a more complex system of smelting is necessary to capture the gaseous zinc and cool it down to the metallic form. As such, procedures for producing metallic zinc appeared only quite late in China, as elsewhere in the world (Craddock [1998], Zhou [2007]). The traditional Chinese zinc smelting process was still being used until the 1990's with little modification [Petersen, 1990]. Zhou [2007] states that:

> *"The production of zinc for making brass coinage began in the Wanly period of the Ming dynasty (16th century), and developed from the existing cementation process. It followed naturally from the development of the Chinese brass industry. Although this technology emerged relatively late, it was unlike zinc production technology used elsewhere and thus there is no reason to believe that it came from outside China."*

Craddock supports this hypothesis stating that the first good account of zinc production in China is in the *Tian Gong Kai Wu* ("The workings of heaven revealed"), a 17th century Chinese technology treatise [Song, 1637], and it is clearly distinct from the Indian process, so it seems it was not influenced by previous or exogenous cultures.

Long before the smelting process was established, brass objects were produced. While ancient sources suggested it was via smelting a copper-zinc ore (natural brass), this is very uncommon and the most common acception is the cementation process allowed the production of accidental brass through the use of zinc-rich ore, around the 2nd millennium BC in China [Golas, 1999; Li and Han, 1992] and even earlier in India [Craddock, 1998; Deshpande, 1996; Scott, 1991]; and by the end of the first millennium in Greek civilization [Craddock, 1995]; however, the use of metallic zinc

to cast cash coins isn't reported until the Ming dynasty (around 1520 AD[8]), and analytical data by several authors [Zhou and Fan, 1993; Zhao *et al.*, 1986; Bowman *et al.*, 2005; Dai and Zhou, 1992] supports this hypothesis. Craddock [2008] infers, about a zinc retort found in the Yangliusi excavations:

> *"Brass, the alloy of copper and zinc, only became popular in China from the 16th century, when it was adopted for the cash coinage, and it is assumed that the production of zinc on an industrial scale dates from that period. The radiocarbon dates from the Yangliusi site range from the 15th to early 17th century, and thus, supports this dating."*

With a melting temperature of 1000 ºC, a brass alloy could have up to 28 wt.% Zn [Craddock, 1995].
Craddock [1995] adds that *"Through the sixteenth century brass replaced bronze as the usual metal for coinage, and the zinc content rose way over 30 per cent, suggesting that the alloys was made by spelter*ing copper and zinc metals."

Golas [1999] refers that zinc and lead are produced by the same geological conditions; and these two metals are frequently found together, which can be an explanation for the name confusion between them. Zhou [2007] refers to the mandarin names of zinc and lead (both its names in *hanyu pinyin* are *woyuan* but the Chinese characters are different) which may have caused some degree of confusion. Steinhoff and Bandari [2007] refers that this element, similarly to lead, also improves casting properties, which may be, in part why Pb use decreased and zinc use increased since the time it could be refined and used in coinage.

Several studies concerning the chemical analysis of cash coins have been performed, especially in the Far East (China and Japan) since the beginning of the 20th century [Yoshimasa, 1911; Mabuchi *et al.*, 1978; Mabuchi *et al.*, 1979; Notsu and Mabuchi, 1979; Dai, 1985; Wang *et al.*, 1995; Dai and Zhou, 1992; Cowell *et al.*, 2005a; Sano *et al.*, 1983; Lin *et al.*, 1994], and were published usually in Japanese or Chinese Mandarin - languages that are not universal for the westerner scientist, - which make it difficult to access the information within. Even one of Zhou Weirong's[9] latest books, *Chinese Coins: Alloy Composition and Metallurgical Research* [2004] is written in Chinese Mandarin, and there are no translations available.
Although written sources [Song, 1637; Peng, 1965] indicate strict imperial recipes for cash coin alloying, in practice the analytical results obtained from different sources [Bowman *et al.*, 2005; Dai and Zhou, 1992; Lei *et al.*, 2003] show there is a great elemental dispersion within coins of the same reign. This may be related to several factors, as lack of regulation enforcement, raw material

[8] Craddock [1995] refers an earlier date suggested by Cowell and by Bowman: *"The first brass coinage seems to have been in the Hong Zhi period in the year AD 1505, and contemporary accounts note that they were made from copper and new 'tin', that is zinc."*
[9] Zhou Weirong is one of the leading researchers in Chinese coinage. He works at the CNM, Beijing.

availability and metal recycling[10]. Composition was often changed to prevent forgeries [Hartill, 2005] but, as explained earlier, often more importance was given to quantity than quality in coin production.

Until 1715 AD, *tong* meant only "alloying metal" [Burger, 1976]. As noted above, until the early 16th century, the customary alloy was bronze (Cu-Sn) with some impurities (e.g., Fe) and sometimes high percentages of Pb. Later, Zn started to replace Sn and Pb in cash coins [Cowell *et al.*, 2005a] and by mid-16th century brass was instituted as official alloy [Zhou and Fan, 1993]. This was probably due to tin scarceness and the consequent increase in its price. Zinc was a viable, cheaper alternative. There is some controversy as which method (cementation or speltering) was used to produce the first brass coins [Cowell *et al.*, 2005b], but there is written source from the first half of the 17th century that states the production metallic zinc was well established in China [Song, 1637] and even earlier in India so we will assume the brass coins in this study were obtained by speltered zinc.

According to Song [1637], in the 17th century the casting alloy was composed of 6 to 7 parts copper, and 4 to 3 parts zinc. He also admits to an overestimation of the Zn content due to its sublimation and consequent loss – about ¼ of the total amount of Zn – during the melting process (Zn has a boiling point of ~907 ºC while Cu has a melting point of ~1083 ºC), which could mean Zn would approximately range between 22.5 and 28 wt.%.

Song also writes about the quality of the coins: thicker and heavier are considered better than thinner and lighter coins. He refers that as zinc was cheaper than copper, sometimes forgers used twice the amount of zinc than copper but this rendered the coin with an inferior quality. In his opinion, during the Ming dynasty, "*only (...) coins minted (...) in Peking and (...) in Kwangtung are of high quality (...).*", which shows composition was not the same in every province.

2.1.5. Antimony (Sb)

Antimony rich ores were mainly found in China in the Nanning, Ssucheng, Taiping and Xilin districts of the Hunan province [Wang, 1919]. This metal occurs in nature as Kermesite ($2Sb_2S_3 \cdot Sb_2O_3$), Cervantite (Sb_2O_4), Valentinite or Senarmontite (Sb_2O_3). Associated with lack of alloy refining [Cowell *et al.*, 2005a] (there is reference to Sb decrease in coinage during the time copper was imported from Japan [Cowell *et al.*, 2005b]), it appears to be an intentional element in Chinese coinage, as Zhou [2004] seems to indicate in his reaseach. Several studies in Chinese coinage refer to this element in elemental analysis as Wang [2005] and He *et al.* [2011].

[10] According to Thierry [1992] recycling was a common practice in China, especially in periods of Cu deficiency. And it was not limited to copper, but other metals were also used: lead, tin, iron or zinc. Walker [1980] notes that in the West (up to the Iron Age), iron contents up to 20 wt.% were considered as impurities from Cu ores and/or deliberately added (as iron oxides) into the furnace as flux. Sometimes, scrap metal was recycled, which caused compositional and physical properties variations in alloys. This was highly probable to occur in China, especially when dealing with coinage, because no special properties were required.

2.1.6. Other metals

Frequently metals like nickel, iron and arsenic are found in contents reaching 1-2 wt.%. They are commonly found to be associated with minerals used to extract copper [Earl and Adriaens, 2000], and therefore will not be considered as intencionally added. This indicates the manufacturers could not detect or prevent this contamination and/or where not concerned about its presence.

2.3. Metallurgical characteristics

While there are many studies regarding cash coin composition, not much work has been done from the microstructural characterization point of view. Research concerning the coins metallography have been published [Wu, 1929; Shen, 1929; Shigeshi, 1959; Wayman and Wang, 2005], but while the first three - in Chinese Mandarin – in Prof. Zhou Weirong's opinion lack consistency [Wang, 2005], the latter – in English - concerns Fe-based coins. So there is a need for the transmission of knowledge between different languages, as well as proceed with further investigation on the subject, because microstructurally there is still much to be done concerning Cu-based cash coins.

Chapter 1 - Materials and Methods

1.1. Coin selection at CCCM

Nowadays there are already some large cash coin collections in the West. In Europe, museums like the British Museum (London), the Musée Guimet (Paris), the Kulturhistorisk Museum (Oslo) and some museums across Germany [Heidemann, 2004] possess some of the most important coin collections. Madrid has two notable collections at the *Museo Arqueológico Nacional de Madrid* and at the Cerralbo Museum [Serra, 2005; Serra, 2006]. In Portugal there is a coin collection with over 1000 pieces of Chinese numismatics at the Museum of the Macau Scientific and Cultural Centre (CCCM) that ranges from the Neolithic to the People's Republic of China.

The studied coins belong precisely to that collection. They were acquired in specialized shops at Macau (China), in 1998, through an art-collector and connoisseur (Mr. António Sapage) to integrate the CCCM Museum collection. The information about the coins was limited to what was written on their individual card containers: the coins attributed name and date, as well as its inventory number and sometimes additional information on the coin type, the *hanyu pinyin* of the reverse inscriptions, or the name of the mint and its province were written on it. The numismatic collection has several coin typologies, but cash coins are the majority – 522 pieces – ranging from 206 B.C. to the late 19th century. From these, 380 coins are Cu-based and were targeted for this research (see Fig.1.1). Among them, 14 were recovered from an archaeological site (St. Paul's College, Macao) and their production reign is unknown.

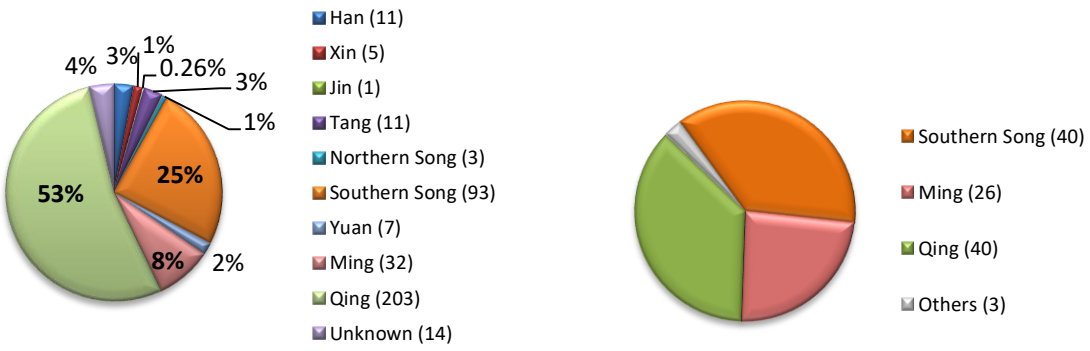

Fig. 1.1 Distribution of selected coins by dynasties: on the left, the 380 coins; on the right 109 coins selected for edge polishing to access clean metal.

As the authenticity of the collection was an issue and the presence of several alloys (bronze and brass [Furtado, 2004]) was another because the collection was initially classified as "bronze", sets of coins were chosen from several reigns of the Southern Song, Ming and Qing dynasties because of their abundance in the collection and possible presence of different alloys. Two other coins from earlier dynasties – Han, Tang – were chosen because of their physical appearance (one due to the shiny finishing patina and the other because of the coin sharp angles and calligraphy detail perfection) to inquire about the possibility of forgery. One of the St. Paul's coins was chosen because it was broken in half, allowing access to radial and tangential cross-sections and comparison between them.

Considering the larger groups – from the Southern Song, Ming and Qing dynasties – coins were chosen from different reigns (see Fig. 1.2), generally with a 1-cash but also in 2, 5 or 10-cash. In the three dynasties, similar coins (same designation and size) were chosen from several periods and in Ming and Qing dynasties, singular coins were also targeted for specific questions.

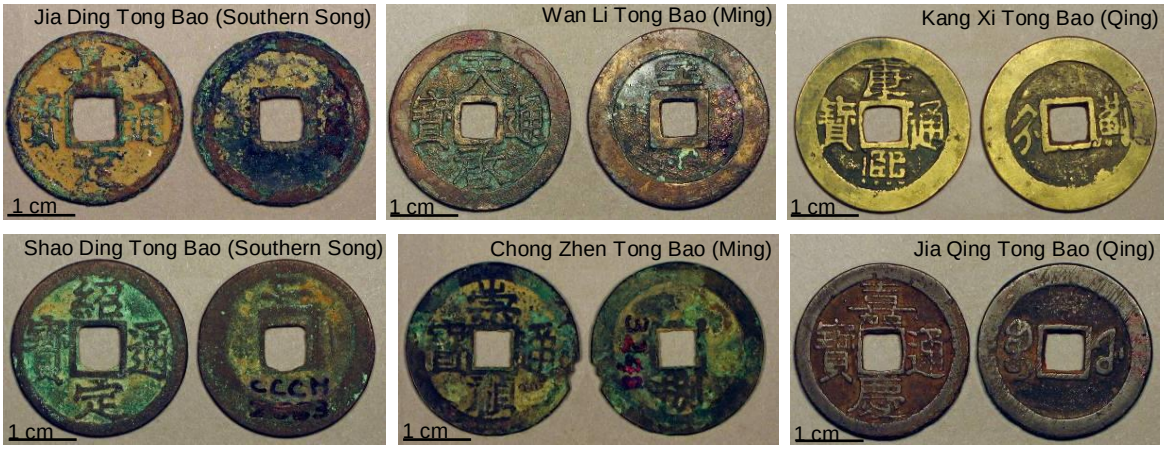

Fig.1.2 Coins (obverses and reverses) from various periods of the Southern Song, Ming and Qing dynasties. From left to right and top to bottom: #2522, #2563, #2642, #3278, #2728 and #2787.

1.2. Methodology and Instrumentation

The 20th century technological developments provided tools to research into the chemical and physical properties of matter. Several analytical techniques are currently applied in the fields of art, archaeology and history [Ciliberto *et al.*, 2000; Pollard *et al.*, 2007] helping disciplines like conservation science. Looking at artefacts from within, and not only from the aesthetics point of view, can bring forward very important data to the knowledge of their production, corrosion and conservation aspects.

Concerning cultural heritage, sampling and interventions that could cause some destruction are condemned, so techniques that are non-invasive and non-destructive have to be favoured. While some techniques require little to no sampling, when dealing with metallic artefacts from excavations or that were exposed to different environments having formed a patina, access to their interior is generally necessary and inevitable to obtain trustworthy information [Denker *et al.*, 2005; Figueiredo *et al.*, 2007a].

Regarding numismatic artefacts, the use of X-ray based analytical techniques is widely spread. Energy Dispersive X-ray Fluorescence (EDXRF) and Particle Induced X-ray Emission (PIXE) have been used for several decades [Araújo *et al.*, 1993; Cabral *et al.*, 1979; Cabral, 1995; Cabral *et al.*, 1998; Guerra, 2008; Giumlia-Mair, 2005; Lutz and Pernicka, 1996]; as well as Energy Dispersive Spectroscopy - Scanning Electron Microscopy (SEM-EDS) [Lei *et al.*, 2003; Lei *et al.*, 2004; Ingo *et al.*, 2006; Figueiredo *et al.*, 2010]. All giving expedite and simultaneous data on the various alloying elements in a physically non-invasive manner.

SEM and Optical Microscopy (OM) observations are the main techniques when dealing with metallurgical research [Mei and Rehren, 2009; Scott, 2010; Ingo *et al.*, 2002], being useful in characterizing the microstructural features as well as the alteration layers common in archaeological artefactes. While the mentioned X-ray techniques require specific and expensive equipment, the OM requires specific but less costly equipment, being quite accessible to perform given the right conditions [Rovira and Gómez Ramos, 2003; Scott, 1991]. Although these are non-destructive techniques, they often require partial cleaning in order to remove alteration layers, sometimes very different from the original alloy [Figueiredo *et al.*, 2007a] and access the artefacts interior, so they can be entitled micro-invasive.

The methodology applied in the present work was designed, therefore, to go from the non-invasive to milli-invasive analyses, when needed and with specific objectives, in order to minimize coin intrusion and acquire complementary relevant information. Firstly, photographic records from the obverses and reverses of the 380 coins were obtained over a Colorama Stormgrey canvas and Philips Classictone illumination (60 W) with a Nikon Coolpix 5.2MP, in macro autofocus mode. All coins were weighted with a Kern 440-51N scale and their diameter measured with a stainless-steel vernier calliper. The methodology schematic is described in Table 1.1. Preliminary macro-EDXRF elemental assessment was performed in all the selected coins (n=380) of both the obverse and reverse.

Table 1.1 Experimental methodology applied to study the selected coins

<table>
<tr><th>1st - Global examination</th><th>2nd - Elemental characterization</th><th>2nd - Microstructural characterization</th><th>3rd - Compositional characterization</th></tr>
<tr><td>(no preparation required)</td><td colspan="3">(cleaning of small area required)</td></tr>
<tr><td>Macro-EDXRF
{preliminary alloy composition, ~3 cm ∅}
(all 380 coins)</td><td>Micro-EDXRF
{determination of alloy composition, spot <100 μm ∅}
(109 coins)</td><td>OM
{microstructural observation, 2mm^2 clean elliptical area}
(109 coins)</td><td rowspan="2">Micro-XRD
{identification of crystalline chemical compounds, spot ~1.2 mm^2}
(10 coins)</td></tr>
<tr><td>Digital X-ray
{alloy homogeneity/ casting defects}
(35 coins)</td><td colspan="2">SEM-EDS
{microstructural and elemental characterization, spot ~3μm ∅}
(28 coins)</td></tr>
</table>

From this initial group of Cu-based coins (n=380), 109 coins were selected from 5 different dynasties to perform microstructural observation and elemental analysis after a metallographic assessment (see Table 1.2).

The coin selection was chosen from 3 main sets of coins from the Southern Song (1174-1265 AD, 40 coins), Ming (1576-1628 AD, 26 coins) and Qing (1662-1821 AD, 40 coins) dynasties (see Fig. 1.3). Two coins were chosen from the Eastern Han and Tang dynasties, respectively.

Table 1.2 Chronological timeline indicating the represented dynasties in the CCCM copper-based cash coin collection and the number of coins from certain dynasties selected for the analyses performed (*RSP – Ruins of St. Paul, in Macau)

	Western Han Dynasty (206BC-9AD)	Xin Dynasty (9-25AD)	Eastern Han Dynasty (25-220AD)	Tang Dynasty (≈618-907 AD)	Song Dynasty (≈960-1279 AD)	Yuan Rebels (1271-1368 AD)	Ming Dynasty (≈1368-1644 AD)	Qing Dynasty (1662-1910 AD)	Unknown (Archaeological finds of RSP*)
EDXRF (all 380 coins)	10 coins	5 coins	1 coin	7 coins	96 coins	3 coins	35 coins	208 coins	15 coins
Micro-EDXRF & OM (109 coins)			1 coin	1 coin	40 coins		26 coins	40 coins	1 coin
SEM-EDS (28 coins)			1 coin		5 coins		4 coins	17 coins	1 coin
Micro-XRD (10 coins)			1 coin		2 coins		2 coins	5 coins	
Digital X-ray (35 coins)	1 coin	1 coin			18 coins	1 coin	4 coins	10 coins	

When observing their microstructures, in coins where the identification of metallic phases, inclusions or their corrosion products were uncertain, SEM-EDS and micro-XRD (micro X-ray diffraction) were used to clarify them. Digital radiography (digital X-ray) was performed in a set of high leaded coins to evaluate alloy homogeneity.

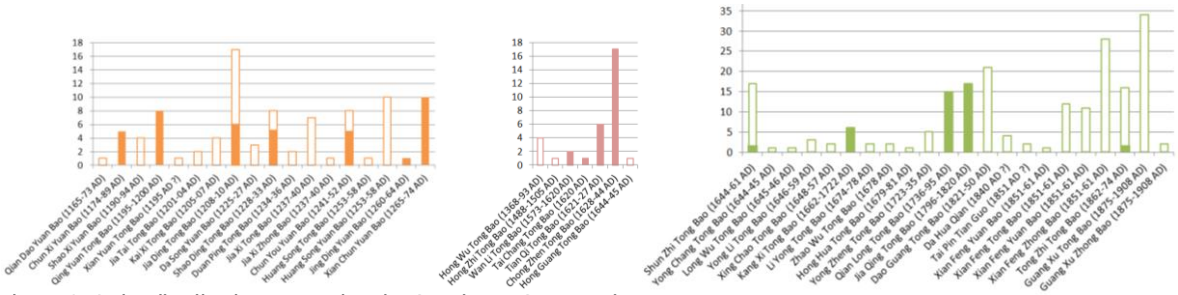

Fig. 1.3 Coin distribution per reign in Southern Song, Ming and Qing dynasties (in orange, pink and green color, respectively) in the studied collection. The empty bars represent the coins selected from these 3 dynasties belonging to the inital 380 coins. Full colored bars represent the number of selected coins from these 3 sets for metallographic and analytical examination (106 coins). The XX axis displays the coin names; and the first production year is mentioned between brackets.

1.2.1 Macro-Energy Dispersive X-Ray Spectrometry

Surface composition was obtained using an EDXRF spectrometer KEVEX EDX-771 Analyst System (at QAA, ITN), Fig. 1.4.

Both faces of the coins were analysed with no previous superficial preparation. This allowed a rapid assessment of the alloy types present (elemental alloying metals) and superficial minor elements (mostly from superficial corroded layers). The coins were placed inside the measuring chamber using a 16-slot rotating tray (for most coins) or a plane fixed tray (for larger coins). Some coins fitted the sample holders but for the smaller ones, special sample holders were especially adapted in order to carry out the analyses.

Fig. 1.4 (a) KEVEX 771 spectrometer at QAA Lab; (b) KEVEX rotating sample tray; (c) coins fitted on the sample holders; (d) detail of custom made sample holder.

Primary radiation originates from a rhodium anode X-ray tube with the maximum cathode potential of 60 kV, maximum current intensity of 3.3 mA (~200 W). The primary beam crosses a 125 μm thick beryllium window into the measuring chamber. The sample holder has a useful diameter experimentally determined to be ~2 cm ∅ (3.14 cm^2), when using the rotating sample holder (Fig. 1.5 b).

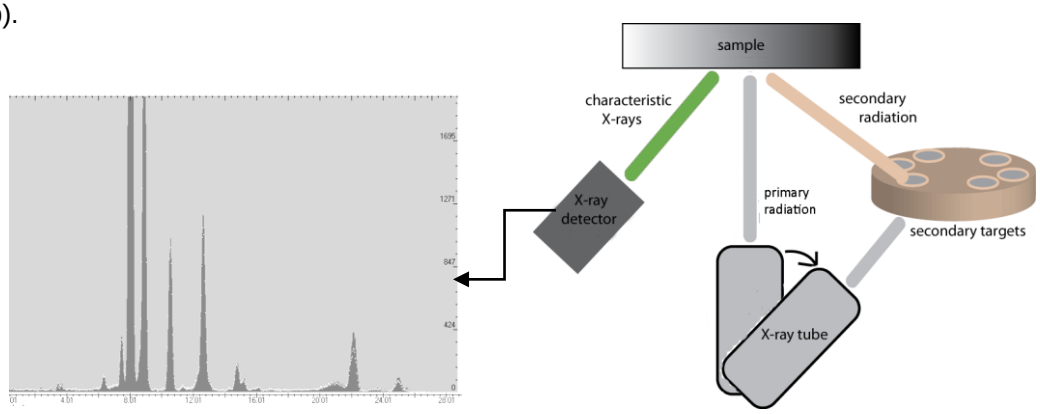

Fig. 1.5 Simplified block diagram of a EDXRF spectrometer (adapted from Jenkins, 1995).

The primary photon beam can be optimized using the secondary target geometry (see Fig.1.5), selecting one of the available targets (Gd, Ag, Zr, Ge, Fe or Ti). Each coin was analysed using two conditions: two different targets were used to produce incident monochromatic secondary radiations: silver (35 kV tube voltage; 0.2 mA current intensity) and gadolinium (57 kV tube voltage; 1 mA current intensity). The first is more efficient for detecting the characteristic X-ray peaks of K lines in metallic elements like iron, nickel, copper, zinc, arsenic and the L lines of Pb; and the other for the K lines of elements like tin and antimony. Spectra were collected during 300 seconds. The Si(Li) liquid nitrogen cooled detector has a resolution of 175 eV at 5.9 keV (Mn-Kα) and allows the detection of elements with an atomic number ≥12 (Mg).

The measured characteristic X-ray peaks intensity calculated by a Gaussian deconvolution process is converted to elemental concentrations using the EXACT software (Energy-dispersive X-ray Analysis Computation Technique), which is based on the fundamental parameter method but using a minimum set of standards. Calibration is performed using a single calibration coeficient for each element, determined by measuring a certified reference material of similar composition [Araújo *et al.*, 2003].

As the selected coins are composed of different alloys (mostly bronzes and brasses), two calibrations were developed. For each one, a single calibration coefficient was calculated for every element. For bronze coins, the certified reference material used was the Leaded Bronze C50.01 from the British Non-Ferrous Metals Technology Centre (BNF, in the UK), whilst for brass coins, the Free-Cutting Brass C1103 Standard Reference Material from the National Bureau of Standards (NBS, in the USA) was chosen.

In order to determine the accuracy of the method, similar certified reference materials were tested as "unknown", using the equation (1.1), see tables 1.3 and 1.4. In bronzes, for major elements excluding Pb the accuracy is better than 1 wt.%. Lead, due to its immiscibility in Cu-based alloys, has a slightly lower accuracy, but still below 10 wt.% for bronzes and 5 wt.% for brasses.

$$\text{Accuracy (\%)} = \frac{|(\text{certified content}) - (\text{obtained content})|}{(\text{certified content})} \times 100 \quad \text{(Eq. 1.1)}$$

In the case of minor elements, the accuracy is lower. For Ni and Zn in bronzes, this is justifiable due to the strong peak overlapping and to the high Cu K line intensity.

Table 1.3 EDXRF analysis of Phosphor Bronze 364 (from BCS, UK) using the bronze calibration to calculate the accuracy of the method (n=10).

wt.%	Cu	Sn	Pb	Sb
Certified	80.60	9.30	9.20	0.18
Obtained	79.81	9.40	10.0	0.16
Accuracy* (%)	1	1	9	11

* calculated according to Eq. 1.1

Table 1.4 EDXRF analysis of Brass C30.25 (from BNF, UK) using the brass calibration to calculate the accuracy of the method for the main elements (n=10).

wt.%	Cu	Zn	Pb
Certified	57.29	37.95	4.78
Obtained	57.05	37.79	5.03
Accuracy* (%)	<1	<1	5

* calculated according to Eq. 1.1

Regarding the precision of the analytical procedure, a repeatedly analysed similar certified material was tested to check the contents precision (Tables 1.5 and 1.6.). The results are very reproducible, especially for major elements.

Table 1.5 EDXRF analyses of Leaded Bronze C50.01 (from BNF, UK), to test method precision.

	Cu	Sn	Pb	Ni	Fe	Sb
Certified content (wt.%)	76.1	9.4	11.3	1.4	0.27	0.57
Average content [$\mu=\sum\mu_i/n$] (n=5) (wt.%)	77.0	9.2	11.1	1.6	0.27	0.55
RDS [(STD/μ)x100] (%)	0.4	2.6	1.3	11.3	11.5	3.5

Table 1.6 EDXRF analysis of Free-Cutting Brass C1103 (from NBS, UK), to test method precision.

	Cu	Zn	Ni	Fe	Sn	Pb
Certified content (wt.%)	59.27	35.72	0.15	0.3	0.9	3.73
Average content [$\mu=\sum\mu_i/n$] (n=9) (wt.%)	61.22	34.86	0.08	0.23	0.88	2.74
RDS [(STD/μ)x100] (%)	0.1	0.3	8.3	4.8	3.0	3.6

The quantification limits, calculated according to the International Unit of Pure and Applied Chemistry [IUPAC, 1978], were considered to be 10/3 of the detection limits[11], and are presented in Table 1.7.

For nickel and zinc (the later only in bronzes), the calculated values are usually under the quantification limit because they are present in small contents and due to spectral interferences. The energy of their K lines ($K\beta_{Ni}$=8.2 keV and $K\alpha_{Zn}$=8.6 keV, respectively) is very close to Cu K lines ($K\alpha$= 8.04 keV and $K\beta$=8.9 keV), a major element in these alloys.

Table 1.7 Quantification limits for macro-EDXRF analysis (wt.%).

Calibration	Ni	Fe	Zn	As	Sn	Pb
Bronzes	0.10	0.05	0.20	(0.15)	-	0.15
Brasses	0.10	0.07	-	(0.11)	0.10	0.11

In both alloys, due to the interference between the Pb Lα line (10.55 keV) and As Kα line (10.54 keV), the quantification limit of As was considered to be equal to the Pb limit (0.15 in bronzes and 0.11 in brasses).

1.2.2 Metallographic Preparation

In order to obtain valuable information about the original alloy composition and microstructural features of the selected coins [Wayman, 2000], it was required to access a freshly clean metallic zone.

[11] Detection limit was calculated for a 99,6% trust level as 3x(peak background)$^{1/2}$/sensitivity

Some authors refer in particular cases the possibility of sampling (usually in fragmented artefacts, bars, *et cetera*) to obtain a clean cross-section [Valério *et al.*, 2010a; Figueiredo *et al.*, 2010; Silva *et al.*, 2008], others - when concerning coins – partially or completely polish one of the faces [Denker *et al.*, 2005; Lei *et al.*, 2003] or remove sections [Ingo *et al.*, 2006]. Unless fragments are available, these procedures can damage the objects integrity and its aesthetic comprehension, which is highly unwanted when dealing with cultural heritage objects. Therefore a minimum invasive methodology was required, in the manner of a small abrasion of the surface, allowing insight of the alloy but still respecting the object and permitting its general fruition after the work is done (Fig. 1.6).

Three recent studies involving coins, 2 of them on Chinese cash coins [Calliari *et al.*, 1999; Wayman, 2000; Wang, 2005], referred the analyses performed were done on a clean area of the coin edge. This minimal intervention was discussed with the Museum responsible, who agreed it to be reasonable.

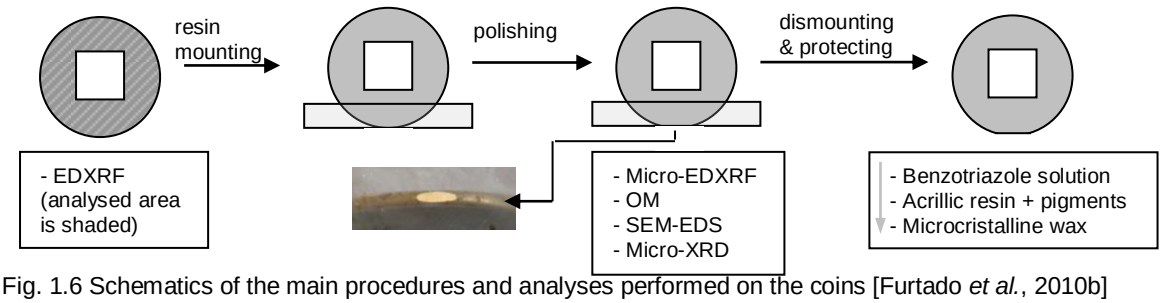

Fig. 1.6 Schematics of the main procedures and analyses performed on the coins [Furtado *et al.*, 2010b]

The representativeness of the abraded edge area was experimentally confirmed by comparing the micro-EDXRF results and OM observation obtained from small clean areas of the edge, of a radial cross-section and from the reverse of several coins. These results allied with the theoretical calculations on the solidification line depth (see all in Appendix III).

As microstructural observation requires a polished surface, in order to obtain a stable plane to polish, the first samples to be observed were embedded in epoxy resin (*Epoxicure*, from *Buehler*), a reversible procedure (see Fig. 1.7). In time, a sample holder in epoxy resin was especially developed in order to avoid having to embed the coins in resin, making the polishing process more expedite and less expensive (see Appendix III – Fig. III.2.1.).

Fig. 1.7 (a) Coin resin mounting; (b) embedded coin after polishing; (c) coin in sample holder; (d) Si-C paper polishing of an embedded coin

Independently of being embedded in resin or fixed in a holder, the coins were polished using a set of silicon carbide sand papers up to P4000 grit size (ISO/FEPA), and then using a diamond paste from 3 to 1 micron on a polishing cloth or cotton swab, by means of a polishing machine or a hand-held rotary power tool (coupled with a flexible cord), respectively (see Fig. 1.8). This permitted to obtain a clean average area of ~3mm^2, suitable for microscopic observation (OM or SEM), as well as spot analyses, like micro-EDXRF, SEM-EDS or micro-XRD.

Fig. 1.8 Finishing stages of the polishing process: with a polishing machine or a hand-held rotary tool. Etching in un-mounted coins was performed with the aid of a pipette.

1.2.3 Micro-Energy Dispersive X-Ray Spectrometry

Bulk alloy composition of 109 coins was obtained through micro-EDXRF analysis, performed with an ArtTAX Pro Spectrometer (at DCR, FCT-UNL, Fig. 1.9) on a freshly cleaned small edge area of each coin, to make sure there was no influence of top alteration layers. In 14 coins, several spectra were also acquired from diverse spots along their un-prepared surface (see Appendix VI).

This equipment has a molybdenum anode X-ray tube with a set of polycapillary lenses that create a primary X-ray beam microspot of about 70 μm ∅. The position of the analysed area is controlled by an integrated CCD camera that shows a magnified image of the region under investigation, illuminated by a set of white LEDs for image optimization. A three beam-crossing diodes (a cross target seen on camera and a red laser diode) allow the exact positioning of the beam on the sample via a motor-driven stage that moves along the X, Y or Z axis.

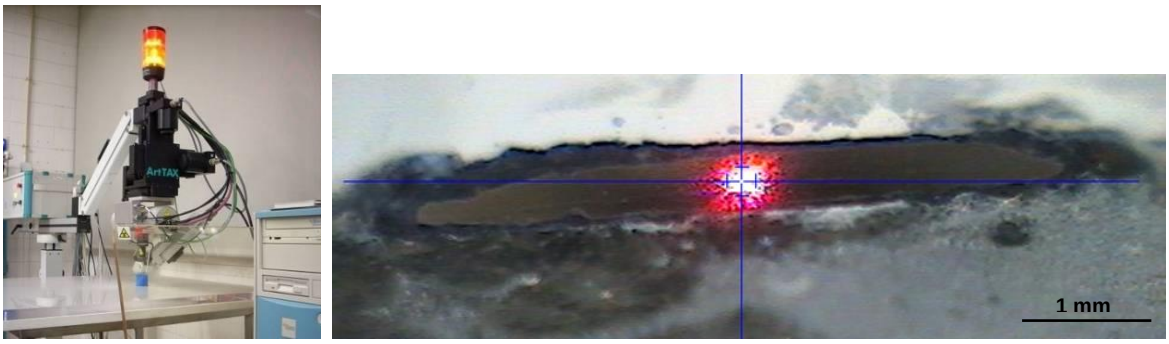

Fig. 1.9 ARTtax Spectrometer and cleaned coin edge area to be analysed.

The characteristic X-rays emitted by the sample constituents are detected with an electro-thermally cooled silicon drift detector (XFlash) with a 8 micron beryllium window, and has a 160 eV resolution

in a 5mm^2 area for Mn (Kα) radiation [Bronk *et al.*, 2001]. The analysing conditions were 40 kV tube voltage, 0.5 mA current intensity and 250 s live time. Three to five different spots per cleaned area on each coin were analysed and the average result considered.

Elemental composition was determined with the WinAxil software [Canberra, 2003], using the fundamental parameter method and experimental calibration factors obtained using certified reference materials: Leaded Bronze C50.01 from BNF, for bronzes and Free-Cutting Brass C1103 from NBS, for brasses. The accuracy of this analytical technique was tested with two other certified reference materials (Leaded Bronze C50.04 from BNF, for bronzes and Free-Cutting Brass C1104 from NBS, for brasses) and the results are shown in Tables 1.8 and 1.9.

Table 1.8 Micro-EDXRF analysis of Leaded Bronze C50.04 (from BNF, UK) using the bronze calibration to calculate the accuracy of the method.

wt.%	Cu	Sn	Pb	Ni	Fe	Zn	As
Certified	76.75	11.10	9.13	1.29	0.11	0.91	0.12
Obtained ± 1σ*	77.87±0.88	10.57±0.16	8.57±0.81	1.31±0.01	0.13±0.03	0.71±0.01	-
Accuracy**	1.5	4.8	6.1	1.6	18.2	21.9	-

* 1σ = one standard deviation; ** calculated according to equation (1.1); the obtained value is an average of 3 analysed spots

For major elements, in bronzes, the accuracy is better than 6%; while in brasses, the accuracy is better than 1% (except for Pb, ~10% due to this element immiscibility in Cu alloys). In both alloys, for minor elements, the calculated accuracy is lower due to the strong matrix effects including peak overlapping (e.g., for As-Kα and Pb-Lα; Cu and Zn K-lines; and Sb and Sn L-lines).

Table 1.9 Micro-EDXRF analysis of Free-Cutting Brass C1104 (from NBS, USA) using the brass calibration to calculate the accuracy of the method.

wt.%	Cu	Zn	Pb	Fe	Sn
Certified	61.33	35.31	2.77	0.088	0.43
Obtained ± 1σ*	60.87±0.20	35.37±0.16	3.07±0.24	0.08±0.1	0.53±0.09
Accuracy (%)	0.8	0.2	10.8	9.1	23.3

* 1σ = one standard deviation; ** calculated according to equation (1.1)

Concerning micro-EDXRF precision, a repeatedly analysed similar certified material was tested to check elemental reproducibility (Tables 1.10 and 1.11). The results are very reproducible, especially for major elements.

Table 1.10 Micro-EDXRF analysis of Leaded Bronze C50.04 (from BNF, UK) to test the precision of the method.

	Cu	Sn	Pb	Ni	Fe	Zn	As	Sb
Certified content (wt.%)	76.75	11.10	9.13	1.29	0.11	0.91	0.12	0.40
Average content [$\mu=\sum\mu_i/n$] (n=4) (wt.%)	77.58	10.53	9.00	1.27	0.13	0.69	0.18	0.43
RDS [(STD/μ)x100] (%)	2.8	6.0	17.5	2.0	22.0	2.2	12.8	20.9

Table 1.11 Micro-EDXRF analysis of Free-Cutting Brass C1104 (from NBS, USA) to test the precision of the method.

	Cu	Zn	Fe	Sn	Pb
Certified content (wt.%)	61.33	35.31	0.088	0.43*	2.77
Average content [$\mu=\sum\mu_i/n$] (n=5) (wt.%)	61.32	34.87	0.090	0.70	3.06
RDS [(STD/μ)x100] (%)	1.7	1.6	7.5	17.5	24.9

* under the quantification limit

The quantification limits, calculated according to the International Unit of Pure and Applied Chemistry [IUPAC, 1978], were considered to be 10/3 of the detection limits[12], and are presented in Table 1.12. The interferences are identical to the refered in the macro-EDXRF section.

Table 1.12 Quantification limits for micro-EDXRF analysis (wt.%).

Calibration	Ni	Fe	Zn	As	Sn	Sb	Pb
Bronzes	(0.10)	0.05	(0.35)	(0.10)	0.50	0.50	0.10
Brasses	(0.10)	0.05	-	(0.10)	0.50	0.50	0.10

1.2.4 Optical Microscopy

This technique requires a fresh and well polished surface, allowing a good distinction between phases with different colours, in non-etched or etched conditions, as well as the visualization of features like grains, inclusions, pores, thermo-mechanical evidences and corrosion alterations. The available objective magnification powers are 5x, 10x, 20x, 50x and 100x and there is also an intermediate lens that permits an increased factor magnification of 1.5x and 2x on each objective.

The optical microscope used was a Leica DMI 5000 M (CENIMAT/I3N, FCT-UNL) that has the ability, due to its inverse lenses system, to observe large artefacts placed on the microscope stage, directly above the objectives without sampling (see Fig.1.10). The microscope allows the capture of images with a coupled Leica digital camera through the use of software (LAS V2.6) that within its many functions permits the collection of images from a selected field at different depths, integrating all the focused parts into one multi-focused image, which is very useful because most surfaces

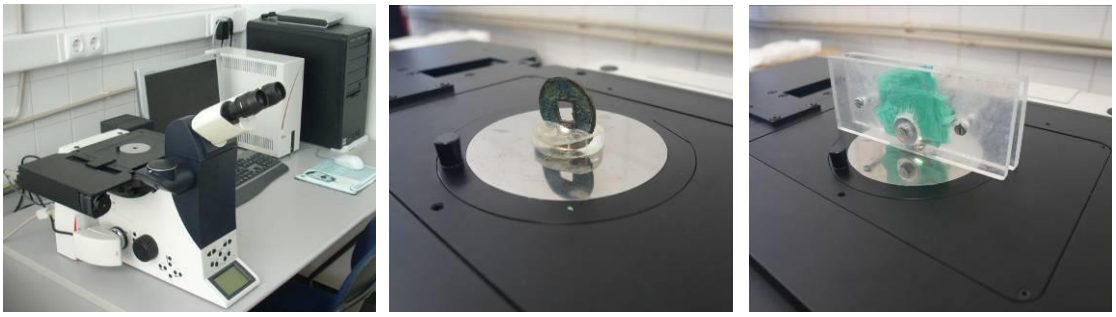

Fig. 1.10 (a) Optical microscope Leica DMI 5000 M sample observation: (b) resin mounted; (c) in sample-holder

when magnified show significant roughness. It is also able to obtain images in matrix arrangements, and juxtaposing them in order to obtain a wider field image.

[12] Detection limits were calculated as 3x(peak background)$^{1/2}$/sensitivity

This equipment has a lighting system for bright field (BF), dark field (DF), cross-polarized light (PL) and differential interference contrast (DIC) observation modes. These different image contrast modes are helpful in the identification of particular microstructural features. While BF lighting permitted common microstructural observations, DF and DIC lighting enhanced protuberance and depression contrasts on the surface, like pores or polishing imperfections. PL lighting and also DF – at some extent – can improve the visualization and identification of certain phases by revealing its different characteristic colours (see Appendix IV – Table IV.2.).

After metallographic preparation, the selected coins (109 in total) were observed in both unetched and etched conditions. Several etching solutions [Voort, 1984] were initially made and tested on commercial brass and bronze samples, and it was found that the best results were obtained using an aqueous ferric chloride solution. Etching evidences coring effects, grain boundaries and other heterogeneities developed during the objects manufacture [Scott, 2010; Voort, 2004].

1.2.5 Scanning Electron Microscopy with Micro X-Ray Analysis

The equipment used at CENIMAT/I3N (FCT-UNL) was a scanning electron microscope Zeiss DSM 962 with a secondary electrons (SE) and backscattered electrons (BSE) imaging modes (Fig.1.11). The system also has an energy dispersive spectrometer (EDS) detector: an Oxford Instruments INCAx-sight with an ultra-thin window.

The coins were small enough to fit the SEM chamber, which made sampling unnecessary. The observed coins underwent different preparations to achieve optimal conditions: while the first samples – resin embedded – were sputtered with gold or partially covered with carbon or copper tape to prevent peripheral charging effects from accumulating on its surface, the later coins – non-mounted – were simply fixed to the sample holder with some carbon or copper tape to achieve contact, which facilitated the SEM-EDS operations without the need to totally cover it.

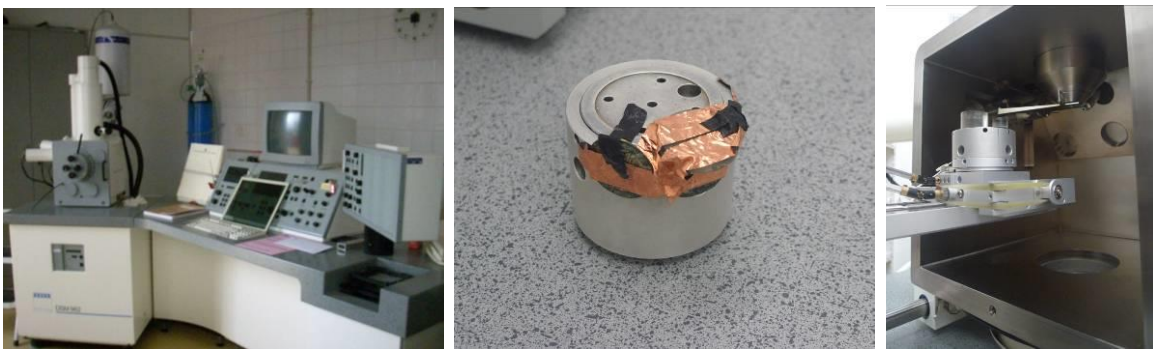

Fig. 1.11 SEM-EDS equipment: sample holder with mounted and un-mounted coins and SEM chamber

Experimental conditions were 20 KeV, ~3 A and 70 μA of accelerating voltage, filament current and emission current, respectively. The working distance was 25 mm. EDS semi-quantifications were

performed for 60 seconds lifetime acquisitions and using an automatic ZAF correction procedure. EDS gain calibration was adjusted with a pure cobalt sample.

Due to its higher atomic number contrast, BSE was the image mode preferentially used. The contrast between elements is higher the more their atomic numbers are apart. On the other hand, SEM-EDS allows both spot analysis and elemental X-ray mapping. SEM-EDS can detect elements with Z>5. This method, allowing the observation of elemental micro-distributions and also assessing the elemental contents of the present phases, is a valuable aid in the identification of uncommon phases in the analysed coins.

1.2.6 Micro X-Ray Diffraction

This analysis technique allows the identification of several compounds simultaneously, from both metallic and corroded areas, however, due to its relatively large spot (~1mm^2 ∅), it is not possible to analyse individually small grain phases, that usually have overlapping peaks and make diffractogram interpretation harder.

Micro X-ray diffraction analyses were made with a Bruker AXS D8 Discover diffractometer (at IMC-MC), as seen in Fig. 1.12. The model possesses a copper anode X-ray tube that produces an incident parallel monochromatic beam (Cu Kα; λ=1.54 Å). Its intensity is enhanced by a Goebel mirror prior to reaching the sample. The beam positioning is controlled by an automated laser-video alignment system that allows visualization and selection of the analysed area, using a motor that moves along the X, Y or Z axis. The diffracted beams are collected with a HI-STAR area detector and processed using a GADDS software system. The analytical conditions were: a ∅1 mm slit collimator (calculated irradiated circular area of ~1.2 mm^2), an angular variation of 12º-105º, 40 kV tube voltage, 40 mA current intensity. Acquisition times varied between 15 to 60 minutes, according to the samples.
This technique was used to aid in the identification of less common crystalline metallic phases and inclusions.

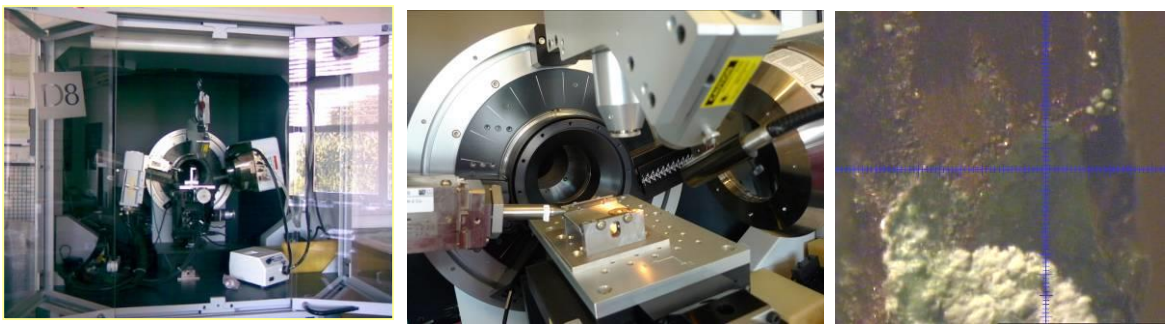

Fig. 1.12 XRD equipment Bruker AXS D8 chamber, chamber plate and area selection for analysis.

1.2.7 Digital Radiography (X-ray imaging)

Digital radiography is a fast imaging technique especially useful to observe metalwork features according to its morphology and densities (e.g., when an archaeological sample has a very heterogeneous and voluminous corrosion layer, when dealing with objects composed of several parts or simply to see defects and heterogeneities in the alloy or other production processing details). Choosing the intensity and energy of the X-ray beam or the correct exposure time depends on the degree to which the X-rays are able to traverse materials, which is a function of the thickness, density and the chemical elements under examination, as well as the X-rays absorption properties of the individual constituents under examination (attenuation increases with the increase of atomic number and its concentration). In this study, it was particularly useful to examine Pb distribution across the whole object volume (in the case of cash coins, many coins at once, too). This technique was also useful to detect casting defects caused by the mould-casting process. Coins have an excellent typology for this analysis because of its thinness between two parallel and flat surfaces: the ambiguities that could result of the superimposed features of the two-dimensional image are almost inexistent [Fell, 1995].

An ArtXRay Digital X-ray System, SEZ series from NTB GmbH (at DCR-FCT-UNL) was used to obtain the digital radiographies of selected coins (see Fig.1.13). The analytical conditions used were 90 kV of voltage; 5 mA of current intensity; with a focus-detector distance of ~0.20 m and integration time 150 ms (true time of ~30 minutes). The *iX-Pect* software was used for image processing purposes.

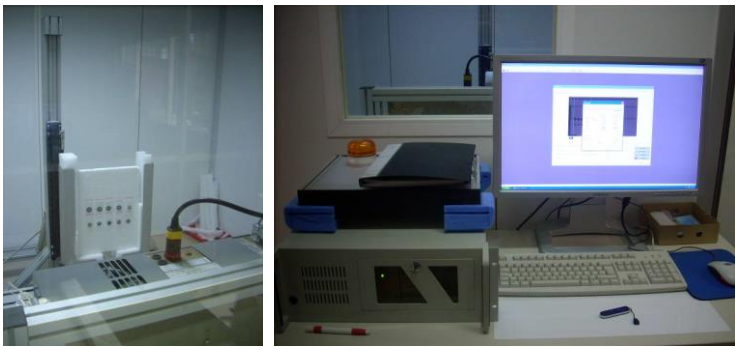

Fig. 1.13 Art-X-ray radiation source and target table; output system

1.3. Protection and Chromatic Reintegration of Artefacts

The mounted coins were removed from the epoxy resin by heating to 100 ºC in a laboratory incubator until the resin softens enough to allow tensioning it until it breaks. The coins are easily separated and sometimes only a “watermark” line is visible (from the resin height on the coin) which can be removed with a cotton swab and acetone. The polished areas were then covered with an ethanol solution of 3% in weight benzotriazole (BTA), which is a known corrosion inhibitor for Cu-alloys [Combarieu *et al.*, 1998; Faltermeier, 1998; Loeper-Atia and Robbiola, 1998]. Chromatic reintegration of these areas was performed by brush-painting with inorganic pigments (ocres, greens, etc) in a 5% in weight acetone:toluene solution of Paraloid B72. The covered surfaces were then protected with a coat of microcrystalline wax paste dissolved in White Spirit [Walker, 1980].

Chapter 2 – Analytical and Microstructural Results

2.1. Elemental Characterization

Elemental EDXRF analysis was performed directly on the coins surfaces by conventional macro-EDXRF and on cleaned metallic areas by micro-EDXRF. The results are discussed in the following subsections.

2.1.1. Preliminary alloy characterization

Preliminary alloy characterization was done by macro-EDXRF on the obverse and reverse of the 380 Cu-based coins without any surface preparation, as described in Chapter 1 (section 1.2.1). The results are presented in Appendix VII (Table VII.1). This allowed dividing the studied alloys into three main groups: bronzes (Cu-Sn alloys), brasses (Cu-Zn alloys) and a few almost pure coppers, as seen in Fig. 2.1. In the studied collection, until the 16th century, all coins are leaded bronzes but after that date, they are mostly brass coins with a decreasing number of bronze coins. In the last dynasty (Qing), besides brasses, there are also thirteen 99% "pure" Cu coins, not found in the studied coins from previous dynasties. In total, 62% of the studied coins are brasses, 35% are bronzes and 3% are almost pure copper.

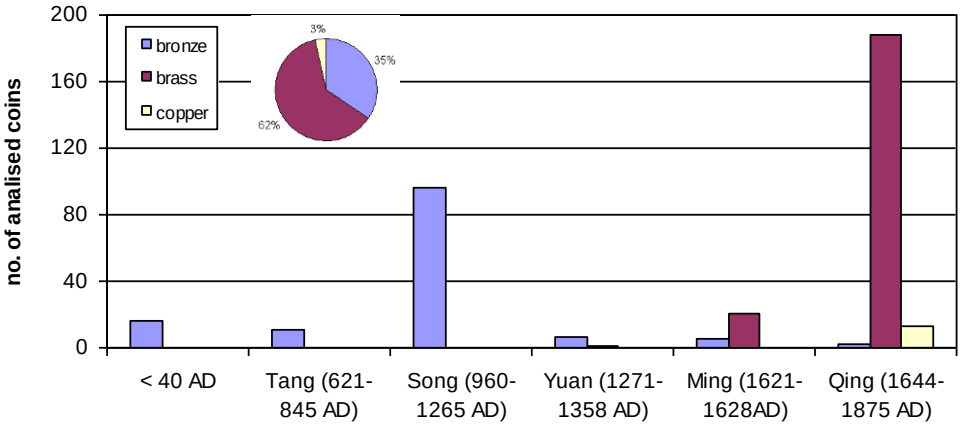

Fig. 2.1 Alloy type distribution along the Chinese dynasties represented in the CCCM collection (macro EDXRF). The circular graphic shows the alloy type distribution among the 380 analysed coins.

Besides the main alloying elements - copper, tin or zinc - lead was found to be a major element in many coins. Minor elements are generally iron, niquel, arsenic, antimony and sometimes bismuth. Zinc is present in bronze coins as a trace element while in brasses is common the occurrence of tin and antimony. Aluminium, silicon, cobalt and selenium were sometimes detected on the surface and can probably be related to contaminations from the environmental conditions where some of the coins were preserved in (burial conditions). As such, these elements were not considered as alloy components.

In Fig. 2.2 the macro-EDXRF elemental values for Zn, Sn and Pb are plotted against the successive historical periods of the studied coins. It is clear that Zn was only present in cash coins in relevant amounts since the 16th century onwards. Lead was more prominent in the alloy

composition until this period, reaching the highest contents during the 12th and 13th century. Tin was used in variable but still significant amounts also until the 16th century, but was still incorporated in the alloy in the following centuries. Further discussion ahead will deal with the results obtained from the clean edge areas with micro-EDXRF in selected periods.

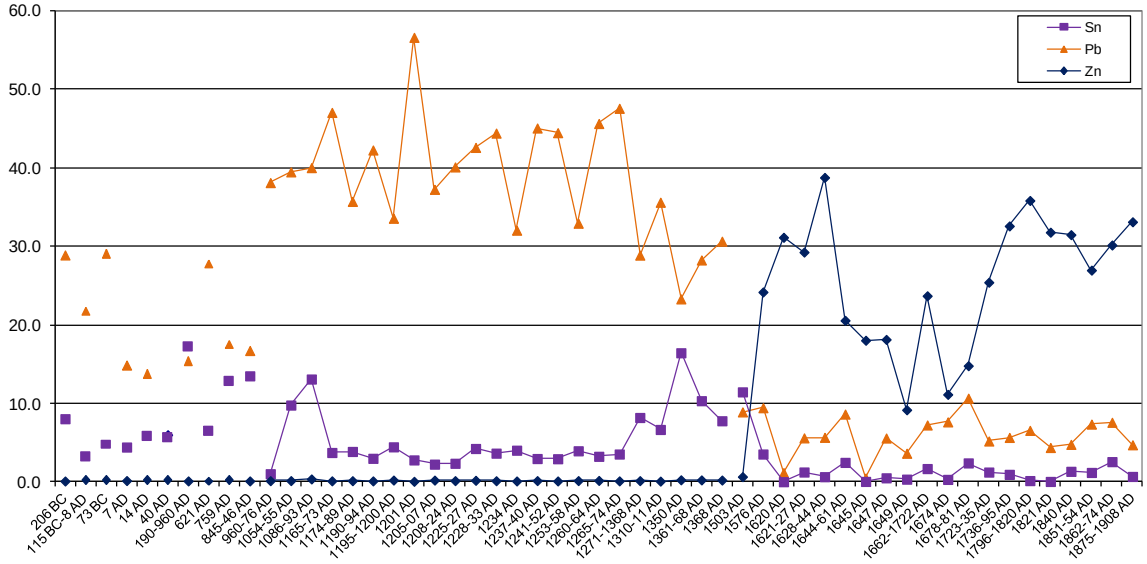

Fig. 2.2 Lead, tin and zinc contents (wt.%) obtained by macro-EDXRF on the surface of the studied coins (n=380 coins, average values from the various chronological periods studied). Single markers are due to chronological gaps in the available coin collection.

Still considering macro-EDXRF, although some of the older coins possess alteration layers visible to the naked eye, the elemental values obtained from the obverse and reverse sides are quite similar. Only Pb presents a higher discrepancy between these values in some coins, like #2627 $Pb_{obverse}$= 48.1 wt.% and $Pb_{reverse}$= 26.9 wt.%; or #2274, $Pb_{obverse}$= 35.1 wt.% and $Pb_{reverse}$= 21.3 wt.%. This is probably due to heterogeneities in the superficial corrosion layer, or to the irregular Pb distribution throughout the coin, as will be discussed in Chapter 3, section 3.1.1. This is why analysis and observation of an area free from superficial alteration is very important.

2.1.2. Alloy characterization in clean areas of the selected coins

From the initial 380 coins, 109 coins were chosen to perform micro-EDXRF analysis on a clean edge area, prepared as explained in Chapter 1 (section 1.2.2). Due to the large amount of available coins attributable to many dynasties and reigns within a time span of about 2000 years, the coin selection to perform microstructural observation and elemental analysis was chosen from 3 main groups of alloys: bronzes, brasses and coppers from reigns with several identical coins (same name, same cash value and same size). The obtained results are compared with the macro-EDXRF results in Fig. 2.3.

Concerning the cleaned alloy results from micro-EDXRF analysis – not influenced by the corrosion layers and closer to the original alloy contents –, tin contents are always below ~5 wt.%, except in

two coins (#2242 and #2977), dated of the 7th and 19th century, reaching 15 and 10 wt.%, respectively. After the 17th century, the Sn content suffered a clear decrease to lower amounts (<1.5 wt.%). Pb seems to have been used in very high amounts (>10 wt.%) during the 12th to 13th century, returning to lower values from the 16th century onwards.

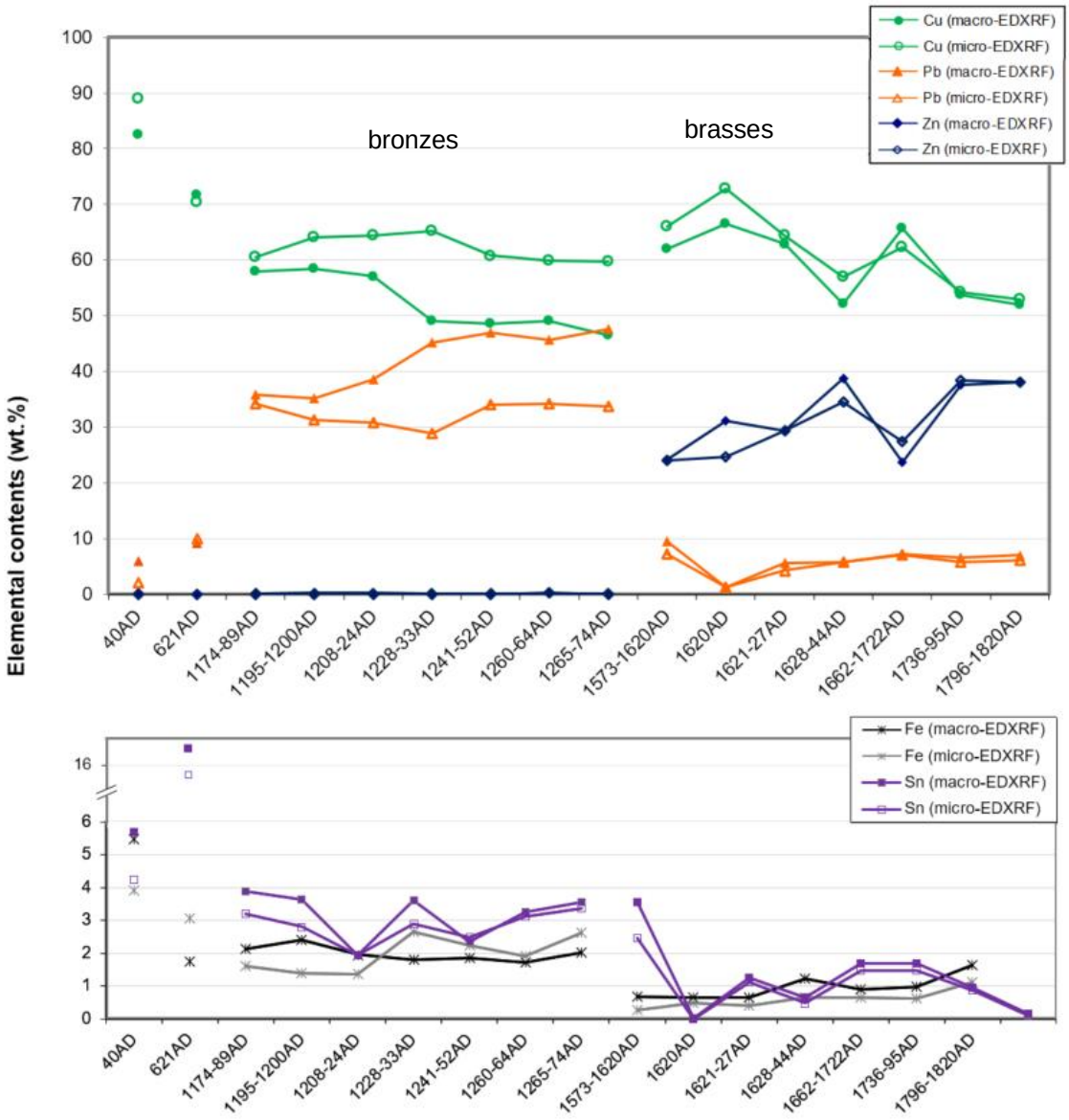

Fig. 2.3 Main elements obtained by EDXRF on the surface and polished areas, by macro and micro-EDXRF, respectively (n=103 coins[13], average values from the various chronological periods studied). Single markers are due to chronological gaps in the available coin collection.

When comparing the elemental composition obtained without removing the corrosion layer (macro-EDXRF results) with that obtained from cleaned areas (micro-EDXRF), the outer layers can be assessed for an “enrichment” or “depletion” of the analysed elements. This depends on (1) elemental corrosion susceptibility of the alloy; and (2) elemental leaching of the corresponding corrosion products in the environment (according to their solubility). Both in bronzes and in brasses

[13] N=103 coins comes from the total of 109 coins that were subjected to micro-EDXRF, from which 6 coins, considered exceptions were removed: 2 bronze coins from the Qing dynasty, 3 coins with 99 wt.%Cu and 1 archaeological (unknown date).

most of the coins suffer from superficial enrichment in Pb, Sn, or Zn, with consequent Cu depletion (the later more evident in coins earlier than 1621 AD, bronze coins with high amounts of Pb).

Concerning the main elements along the several time periods studied, it is visible that the largest differences between surface and metal contents occur for Pb in bronze coins during the 12th to 13th century, when this element was used in higher amounts to produce the coins. These are due to a superficial corrosion layer enrichment of this element in ancient bronze alloys (Fig. 2.3), that could be explained by (1) a Pb preferential corrosion and leaching, relatively to Cu, with reprecipitation of corrosion products in outer corrosion layers; or (2) a lower solubility of Pb corrosion products that reprecipitated in the outer layers in certain conditions, comparatively to Cu corrosion products. In both situations, (1) and (2), the outer layers would be richer in Pb. Comparing the surface and cleaned metal contents according to the alloy type, bronze coins present a higher Pb content at the surface in more than half of the coins, while brass coins have almost the same amount of coins with Pb enrichment or Pb depletion (Fig. 2.4).

Regarding Sn in bronze coins, the values obtained over the non-cleaned surfaces and on the cleaned metal areas are mostly similar (see Fig. 2.3), except in two cases where Sn content was over 5 wt.% and even higher at the surface (coins #2704 and #2977). Whether bronzes or brasses, Sn corrosion products (tin oxides) are relatively insoluble which leads to a corrosion layer Sn enrichment.

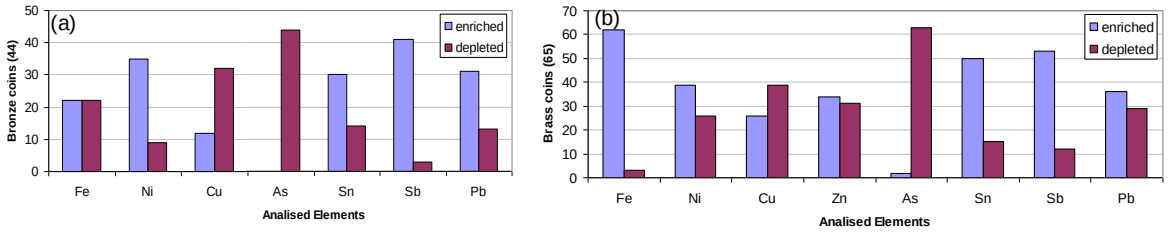

Fig. 2.4 Bronze (a) and brass (b) coins superficial elemental enrichment or depletion (comparing EDXRF from the surface and from the clean edge area).

Zinc can be considered a minor element in the analysed bronze coins until the 16th century, hardly being detected (Fig. 2.3). Regarding brass issues - Fig. 2.4(b) -, the number of coins with Zn enrichment is almost the same as the ones suffering from Zn depletion (Fig. 2.4(b)): in this type of alloys, Zn contents are much higher than in bronze issues and there seems to be a tendency for Zn superficial enrichment when Sn contents decrease (issues minted in 1620 AD and 1628 AD, Fig. 2.3). This Zn enrichment can be explained by the protective effect Sn seems to have in Zn-rich phases: Sn delays the Zn-rich phase corrosion, causing this element not to leach towards the surface. When Sn is absent, Zn gets leached and part of its salts can precipitate on the surface.

Concerning the minor element Fe, it appears from Fig. 2.3 that Fe contents were higher in bronze issues (up to 4 wt.%) and lower in the first brass issues with a erratic rise over time, but in average, under 1 wt.%. This heterogeneity can signify Fe was an impurity in the alloy (from raw material or

scrap metal or from a stage of the production process), as described in General Introduction. Plus, it indicates the manufacturers could not detect or prevent/control this contamination and/or were not concerned about its presence.

Ni is a common element in both bronzes and brasses; however its low content renders its quantification difficult. However according to the Cu-Ni phase diagram, these two elements have complete miscibility both in the liquid and solid state so there should not be any particular Ni-rich phase to observe in the microstructures.
Arsenic is present in some coins, in variable amounts. Its determination by EDXRF is also difficult when considering high leaded coins due to the overlap of characteristic X-ray lines: K_{α}[As]= 10.5 KeV and L_{α}[Pb]= 10.5 KeV, as reported in Chapter 1.

Sano and Tominaga [1982] correlated Fe and Sn for bronze coins, and Fe and Ni for brass coins to be able to have an alloy fingerprint during a certain period. Plotting Fe-Sn for bronzes and Fe-Pb for brasses – because Ni values were sometimes below the quantification limits – (see Fig. 2.5), according to their minting periods, it was possible to infer the composition consistency in each studied period. Considering Fe was an ore impurity, the results show that Sn values in bronze coins within each reign during the late 12th to mid-13th century, were more stable during the 1242-52 AD reign (variation of about ~1 wt% while other reigns present ranges of over 3 to 5 wt%). However, this might be related to the coins originating from different mints (the coins provenance is unknown), which can have different compositions as stated in General Introduction, or changes in composition during the various years within the same reign. When plotting Pb and Fe contents for brasses, it is noticeable that in spite the Fe contents are relatively lower than in bronze issues, their range is wider within reigns (up to 2 wt%); and the same happens to Pb, attesting to the lack of control over composition regarding these two elements. This makes difficult the task of grouping coins based on their composition.

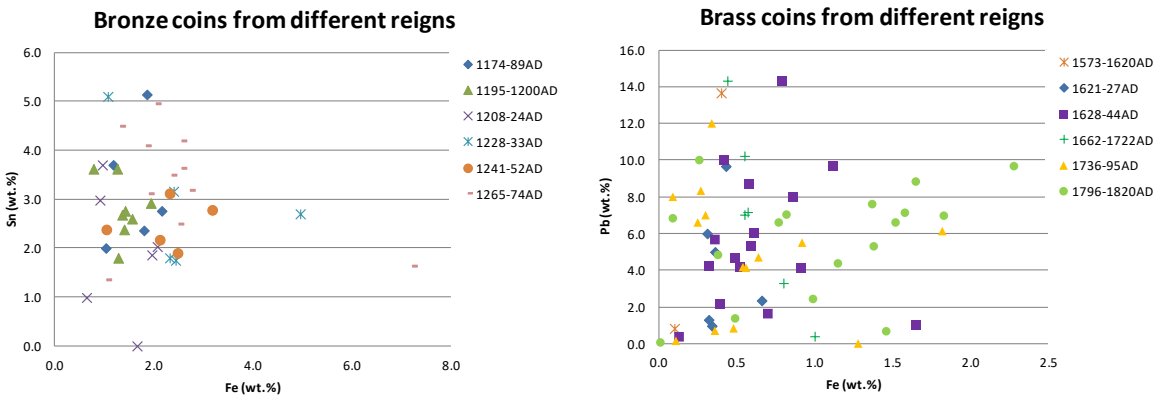

Fig. 2.5 (a) Bronze coins according to Sn/Fe distribution for the various studied periods. (b) Brass coins according to a Pb/Fe distribution for the various studied periods.

2.2. Microstructural characterization

The microstructural observation of the 109 coins was performed through OM and SEM after metallographic preparation (described in Chapter 1). Interpretation of these structures was based on microscopic observation and elemental composition obtained from the clean edge area.

2.2.1. Solidification structure

Taking into account the production processes involved in their manufacture, these coins have typical as-cast microstructures. The Chinese coin sand mould casting technique described in General Introduction causes the coins to cool gradually - mainly due to the specific heat of the sand mould constituents, that absorb and contain the transferred heat from the melt - but not too slowly, because of their small size and reduced thickness. As solidification occurs, the crystal growth of cast alloys can be dentritic or cellular (see Fig. 2.6) and this depends on the alloy composition and the casting conditions (mould material and pouring temperature) that will affect the constitutional supercooling [Campbell, 2003; Wang and Ottaway, 2004]. This non-equilibrium condition promotes the growth of a cored structure, as solute segregation occurs during solidification [Campbell, 2003].

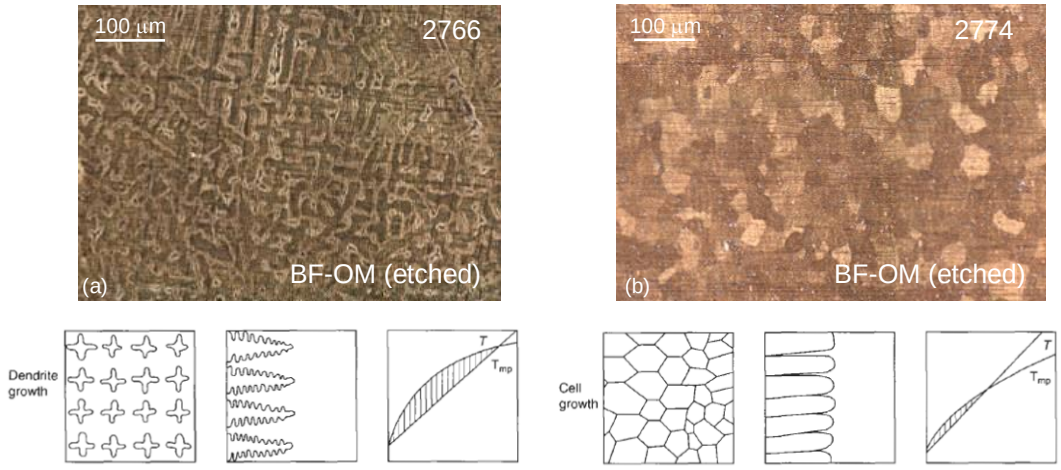

Fig. 2.6 Columnar solidification microstructures: a) Coin #2766 presenting a dendritic growth; b) Coin #2774 presenting a granular structure. Below each microstructure, schematics that take into account the constitutional supercooling condition in the grain morphology developed [adapted from Campbell, 2003].

The grain size ranges from 5 to 100 μm, and minor phases are somewhat difficult to identify, even in higher OM magnifications (1000x). The small grains confer extra toughness and a reduced porosity usually dispersed in interdendritic regions [Campbell, 2003].

The metal recycling and/or poor control of the coins composition, as reported by various sources [Thierry, 1993; Hartill, 2005], generally increments the number of the main metallic phases, promoting the formation of secondary phases (less significant), due to the presence of other elements in minor (e.g. S, Fe, Sb, As) or major contents (e.g., Pb). As-cast alloys naturally present porosities, but the recycling of corroded metals, as well as pouring in a moist environment can worsen the situation. Brass melts, however, are said to be protected from this situation if Zn flaring is performed, due to the constant Zn vaporization during pouring, which transports other gases

away from the metal surface [Campbell, 2003]. This procedure was known by the Chinese craftsmen at least since the 17th century and was even reported in the Chinese technology treatise *Tian Gong Kai Wu* [Song, 1637].

The production methodology of these coins promotes the appearance of several casting defects, as feeding faults or asynchronies between impressions of both sides, as can be seen in Fig.2.7.

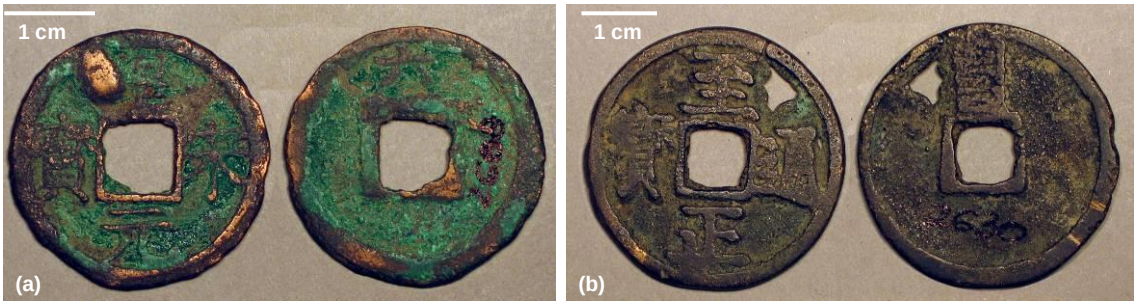

Fig. 2.7 (a) Coin #2608: excess metal globule from imperfect mould imprint (obverse) and non-concentric rim (reverse). (b) Coin #2630: feeding fault that crosses the coin through and through.

2.2.2. Thermo-mechanical processes

The presence of parallel scratches - see Fig. 2.8, (a) and (b) -, especially in peripheral areas (coin edge and rim) may be attributed to the deformation caused by filing off sprue remainings after casting in post-production work [Wang and Ottaway, 2004]. Microstructurally, evidence of slip bands, characteristic of plastic deformed FCC structures like in α-Cu phase, appear in a few coins - see arrows in Fig. 2.8, (c) and (d) - and may be due to the prior described deformations inflicted on the surface. The microstructures in the great majority of the studied coins do not evidence an intense thermo-mechanical work as an overall distribution of slip bands, distorted grains or

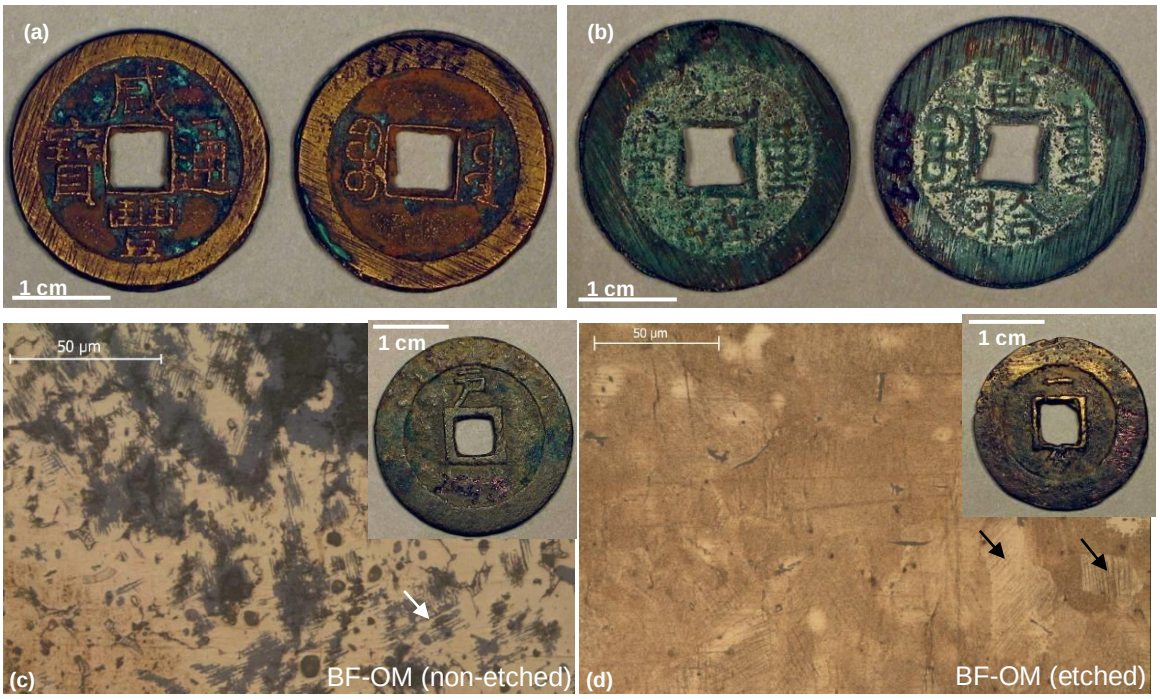

Fig. 2.8 File marks visible on the obverse and reverse rims of coins (a) #2829 and (b) #2997. Slip bands along different directions of the microstructures in coins (c) #2645 and (d) #2661.

recrystallized grains (twinned polygonal grains) [Scott, 1991]. Slip bands would only be evident in the case of superficial plastic deformation without subsequent annealing. Moreover, annealing after mechanical work should result in a recrystallized structure.

There are, however, a few coins that present what appears to be a recrystalized structure (polygonal grains without annealing twins), in Fig. 2.8(d) and Fig. 2.9. This can be consequence of a slower cooling rate (for example, using well-insulated casting moulds), a later unintentional heating that allowed the grains to anneal into a more stable configuration [Scott, 1991], or of an alloy system with a narrow solidification temperature range (i.e., very similar values between liquidus and solidus temperatures): experiments with β-brass production [Wang and Ottaway, 2004] showed this phase tends to solidify with a polygonal tendency.

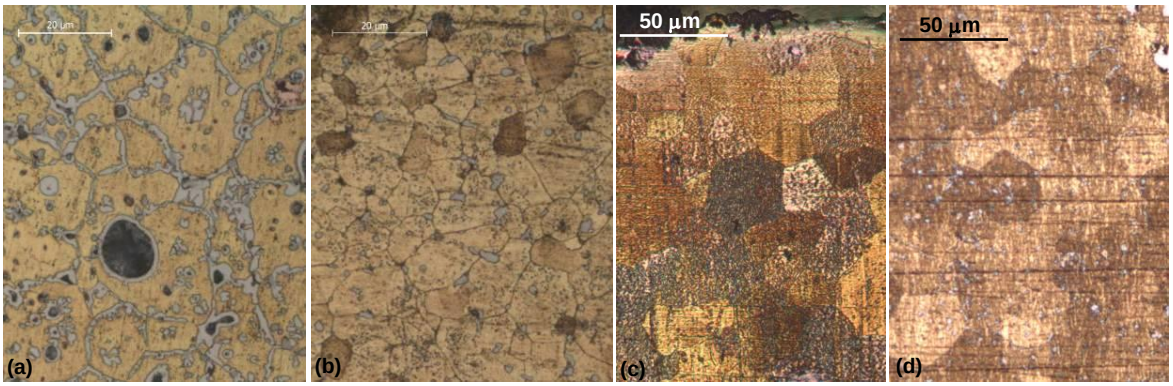

Fig. 2.9 Coins (a) #2767; (b) #2777; (c) X; (d) #2774 (all BF-OM, etched). Pseudo-polygonal grains visible: (a) and (b) have a β+γ structure, while (c) and (d) have an all-beta phase structure.

2.2.3. Microstructural phases

Copper-based alloys with a high Cu content (95 wt.%) usually present only an α-Cu metallic phase, that will be mainly referred to just as α.

2.2.3.1. Common bronze microstructures (Cu-Sn)

Typical bronze phases are α and δ-Cu,Sn (which for the sake of simplicity, will subsequently be referred to as δ). In these coins, the elemental compositions normally produce α phase structures but, for Sn contents above ~7 wt.%, in non-equilibrium cooling conditions, some α+δ eutectoid can be formed (see Fig. 2.10, coin #2242). The primary α phase in both cases presents characteristics of a clear as-cast alloy, with a dendritic grain structure and evidence of coring. The main optical characteristics of these phases can be consulted in Appendix IV (see Table IV.2).

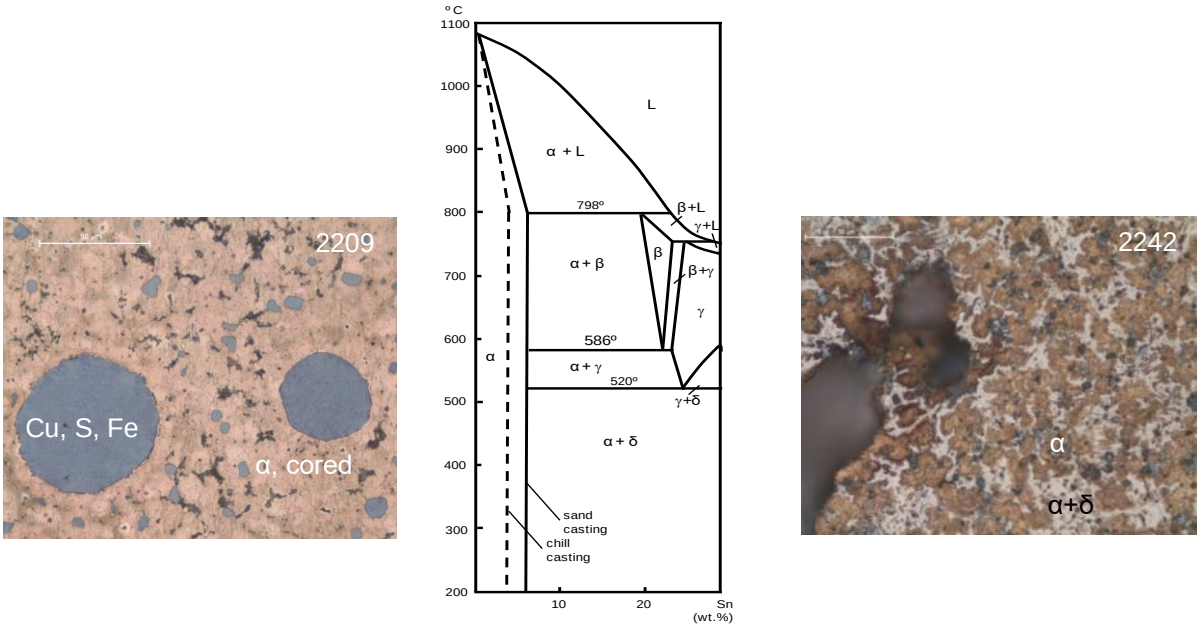

Fig. 2.10 Partial metastable phase diagram for the Cu-Sn system (adapted from [CTIF, 1967]). On the left, the microstructure of coin #2209 (~2 wt.% Sn) exhibiting a dendritic cored α phase matrix (grey features are Cu-S, Cu-Pb or Cu-Fe). On the right, the microstructure of coin #2242 (~15 wt% Sn): observation of a dendritic cored α matrix with an intergranular α+δ eutectoid. Both micrographs in BF-OM, etched).

2.2.1.2. Common brass microstructures (Cu-Zn)

Common brass phases are α, β-Cu,Zn and γ-Cu,Zn (for the sake of simplicity, the two former phases will be referred just as β and γ, respectively). A diffusion couple Cu-Zn was produced in laboratory (see Appendix V) to characterize, in terms of microscopic observations and microanalysis, the possible phases characteristic of this binary system (based on the equilibrium binary Cu-Zn diagram in Fig. 2.11): α, β, γ, ε and (Zn).

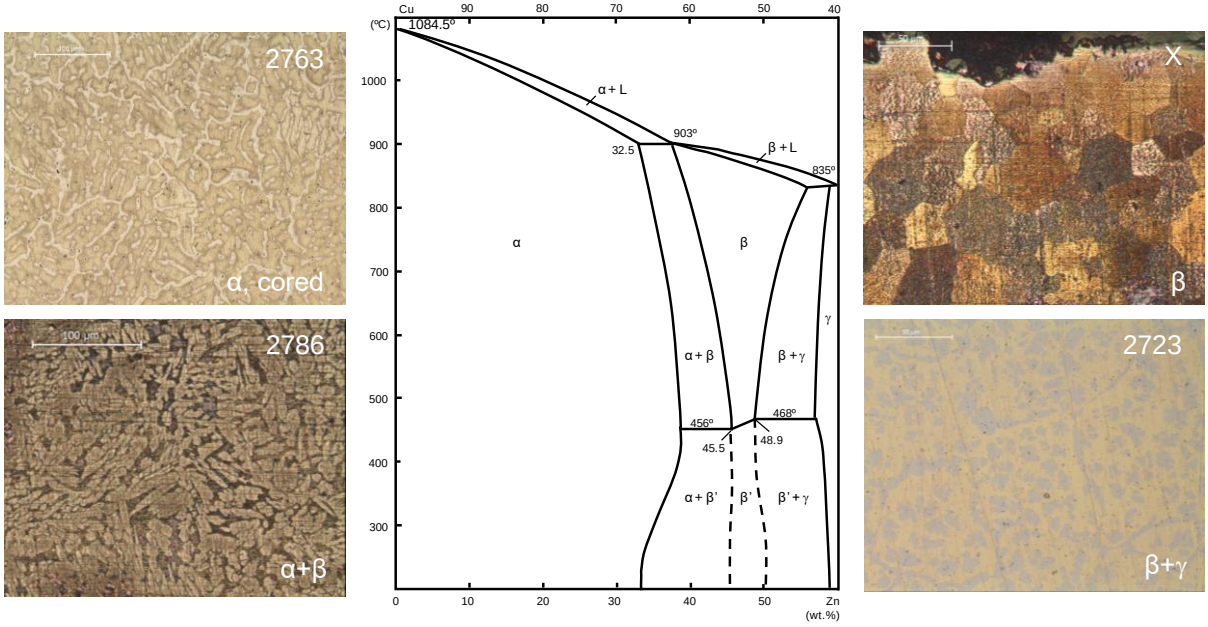

Fig. 2.11 Cu-rich corner of the equilibrium phase diagram for the Cu-Zn system (adapted from [CDA, 1992]) and examples from microstructures of the observed coins (all etched, except for #2723).

Concerning the selected coins, the brass pieces also present typical as-cast structures and the observed phases range from α to β+γ, depending on the various contents of the Cu-Zn equilibrium diagram (Fig. 2.11). A table summarizing the main optical characteristics of these phases can be consulted in Appendix IV (see Table IV.2).

Primary phases present coring effects, which are more visible after etching, especially in coarse monophasic structures. In brasses, α and β phases have very similar colours under the OM (yellow in BF illumination), but etching helped to distinguish between them. They are also difficult to distinguish in BSE-SEM imaging due to its average atomic number proximity (they have very similar compositions). Otherwise, γ phase with a light grey colour and an interdendritic location, is easily identifiable in OM and better discerned in BSE-SEM than α or β, which is probably due to the higher Zn content in this phase comparatively to α or β phases as confirmed by SEM-EDS microanalysis for binary alloys.

Another condition used for brass phase identification was phase corrosion sensitivity behaviour (preferential etching or preferential long term corrosion), according to the following sequence of reactivity: α < β < γ, for the richer the binary brass is in Zn, the higher is its reactivity due to this element low reduction potential ($E^o_{(Zn)}$= -0.76 V) comparatively to the main alloy element Cu, ($E^o_{(Cu)}$= 0.34 V).

Calculations were performed in order to better define the X-ray diffraction angles of α and β phases according to their Zn content. The low intensity of specific peaks from the β phase in the analysed coin diffractograms do not allow the differentiation between an ordered or disordered β phase but, according to Gialanella *et al.* [1997], even after a faster solidification – likely when casting coins – the β phase at room temperature should be the ordered one (β').

For binary Cu-Zn alloys in as-cast conditions, up to ~32.5 wt.% Zn in the alloy, there is formation of a monophasic α phase dendritic structure, usually cored. This is visible in micrographs after etching (Fig. 2.11, #2763).

Zinc contents in the narrow range from 32.5 to 37 wt% give rise to a biphasic structure resulting from a peritectic reaction to form β phase in an α phase matrix. When the Zn content rises above ~37 wt.%, there is an α phase precipitation, forming a Widmanstätten type structure (e.g. Fig. 2.11, #2786), in a primary β phase matrix.

When the Zn contents range between ~45 and ~49 wt.%, a monophasic β structure (Fig. 2.11, coin X) is formed. Above ~49 wt.% Zn in the alloy, there is an interdendritic γ phase precipitation in the β phase matrix (Fig. 2.11, #2723).

2.3. Bronzes

2.3.1. Southern Song dynasty coins (1174 – 1265 AD)

The Southern Song were established south of Shanghai and assumed a resistance position against an opposing regime in the North (*Jin*). After a period of calm, when the culture continued to expand, they were overthrown by the Mongols, which founded the Yuan dynasty in 1280 AD.

Although coin minting was a priority during this period, the shortage of copper as well as iron, lead and tin, caused frequent production interruptions. After 1162, the "*official copper content of the coins was reduced to 54% (in practice no more than 40% Cu, 5% tin and the balance lead).*", according to Hartill [2005]. The shortage of money increased the use of paper money, used in China since the Tang dynasty, which further aggravated the economic situation. From 1180 AD onwards, a character was added to the coin reverse to identify the year of coinage and hence discourage counterfeiting.

All the studied coins from this dynasty are of unattributed production mint.

2.3.1.1. Chun Xi Yuan Bao coins (1174 – 1189 AD)

Three coins (ref.: #2416; #2419; #2421) are 1-cash size while two others are 2-cash (ref.: #2427; #2433) were analysed: see coins in Fig. 2.12. Besides the EDXRF analysis performed on all coins (see Table 2.1), #2416, #2421 and #2427 were observed under SEM-EDS for phase and inclusion characterization.

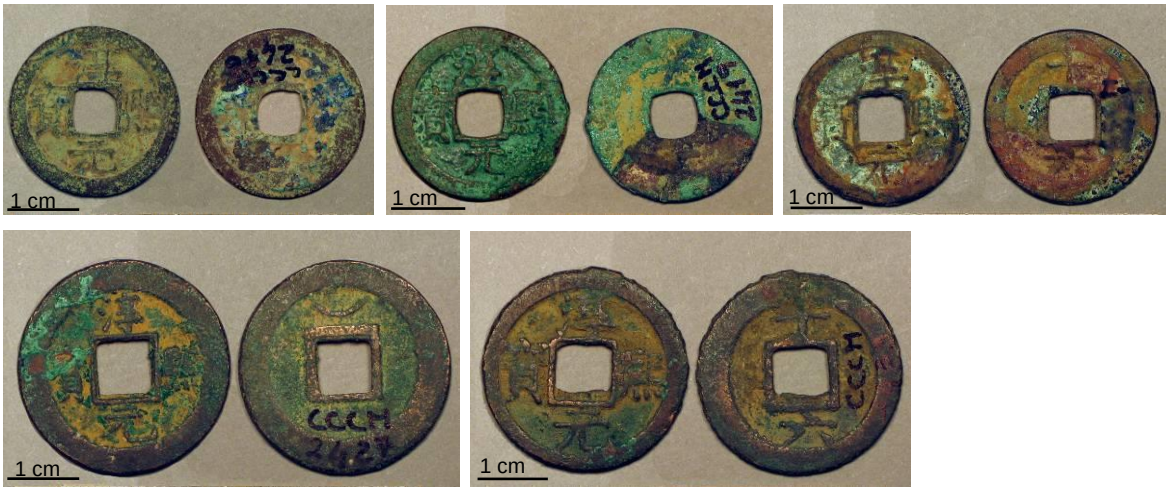

Fig. 2.12 Obverse and reverse of Chun Xi Yuan Bao coins (from left to right and top to bottom, ref.: #2416; #2419; #2421; #2427; #2433)

The Sn contents vary between 2.0 and 5.1 wt.%. The 1-cash coins seem to be slightly richer in Pb. Iron is always above 1.0 wt.%. Arsenic seems to be an impurity in the alloys, being almost always below 0.5 wt%. Comparing the micro-EDXRF results with the macro-EDXRF, from the surface, there seems to be a superficial enrichment in Cu (#2419, #2421) or in Pb (#2416, #2433), probably due to the corrosion layer composition on the surface (see Appendix VII, Table VII.3).

Table 2.1 EDXRF results and microstructural observation of the Chun Xi coins. The values in italic are from macro-EDXRF from the surface, while the remaining are from micro-EDXRF from the cleaned metal edge.

Reference	Composition (wt.%) Cu	Sn	Pb	Fe	As	Observed Phases	Inclusions
2416	*44.9*	*6.2*	*46.8*	*1.8*	*n.d.*	α; (Pb); F_1	C_1 or B_1
	60.5	3.7	34.6	1.2	n.d.		
2419	*66.0*	*2.5*	*29.7*	*1.3*	*n.d.*	α; (Pb); F_1	C_1 or B_1
	59.2	2.8	35.4	2.2	0.67		
2421	*62.4*	*3.3*	*30.7*	*3.2*	*n.d.*	α; (Pb); F_1	C_1
	57.9	2.0	38.7	1.0	0.12		
2427	*60.3*	*4.8*	*33.0*	*1.7*	*n.d.*	α; (Pb); F_1	C_1 or B_1
	63.3	5.1	29.0	1.9	0.42		
2433	*56.1*	*2.6*	*38.6*	*2.5*	*n.d.*	α; (Pb); F_1	C_1 or B_1
	61.6	2.4	33.6	1.8	0.33		

The coins have similar microstructures (see Fig. 2.13). Contrary to common copper-based alloys, solidification seems to have started with the formation of a primary grey phase, instead of the extensive beige α phase matrix. SEM-EDS analysis (coins #2416; #2421; #2427) showed that this phase is Fe-rich. This grey phase will be referred to as F_1 because it is probably a ferrite phase (α-Fe) that results from the transformation of austenite phase (γ-Fe) at low temperatures, as will be further explained in Chapter 3.

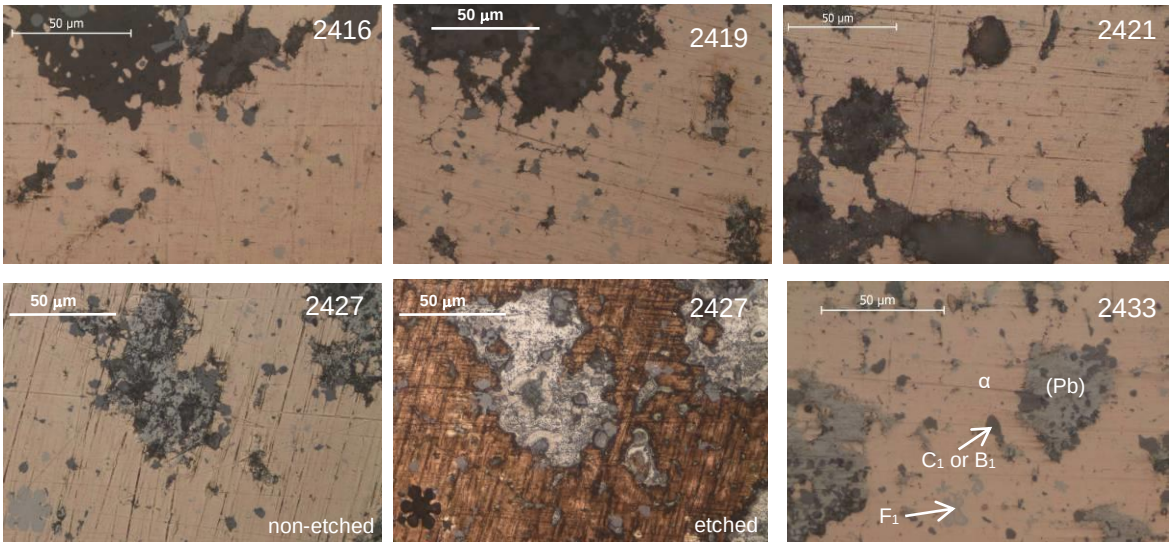

Fig. 2.13 Details of microstructures in the Chun Xi coins

In Fig. 2.13, the microstructures present "dirty" grey (coins #2427 and #2433) or almost black (#2416, #2419 and #2421) globular formations in OM (white in BSE-SEM), which were found to Pb-rich or Pb,O-rich by SEM-EDS analysis, respectively. Grey Pb globules seem to be well preserved, while the black ones seem to be oxidized. As Pb is in high amounts in these coins (see Table 2.1), these Pb-rich globules are sometimes quite large.

Considering the coins metallic matrix, Sn seems to be in solid solution: coring is evident in SEM-EDS analysis (Fig. 2.14 (b),(c),(d): spots #1 and #2).

Dark grey inclusions are Cu,S-rich or Cu,Fe,S-rich. These phases will be referred to as C_1 and B_1, because they are probably chalcocite (Cu_2S) and bornite[14] (Cu_5FeS_4) respectively. Their presence will be further explained in Chapter 3.

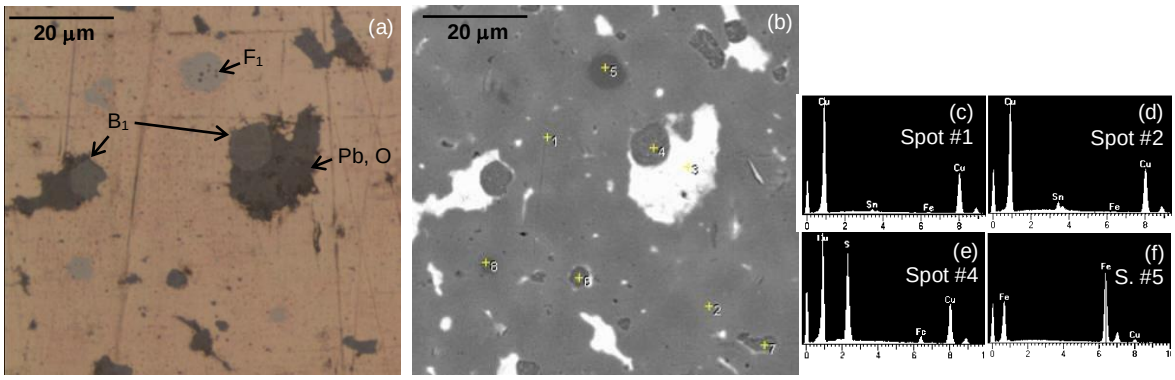

Fig. 2.14 Coin #2416: detail of polished microstructure in (a) BF-OM; (b) BSE-SEM. EDS spectra of (c) spot #1 (lower Sn content); (d) spot #2 (higher Sn content); e) spot #4 (Cu-Fe-S inclusion); f) spot #5 (Fe-rich phase).

2.3.1.2. Qing Yuan Tong Bao coins (1195 – 1200 AD)

Although this period lasted only 6 years, coins continued being produced the following year (1201 AD) for lack of new orders (Hartill, 2005). Coins #2471 and #2479 are 2-cash coins, while the remaining studied coins from this period are 1-cash coins (see Fig. 2.15).

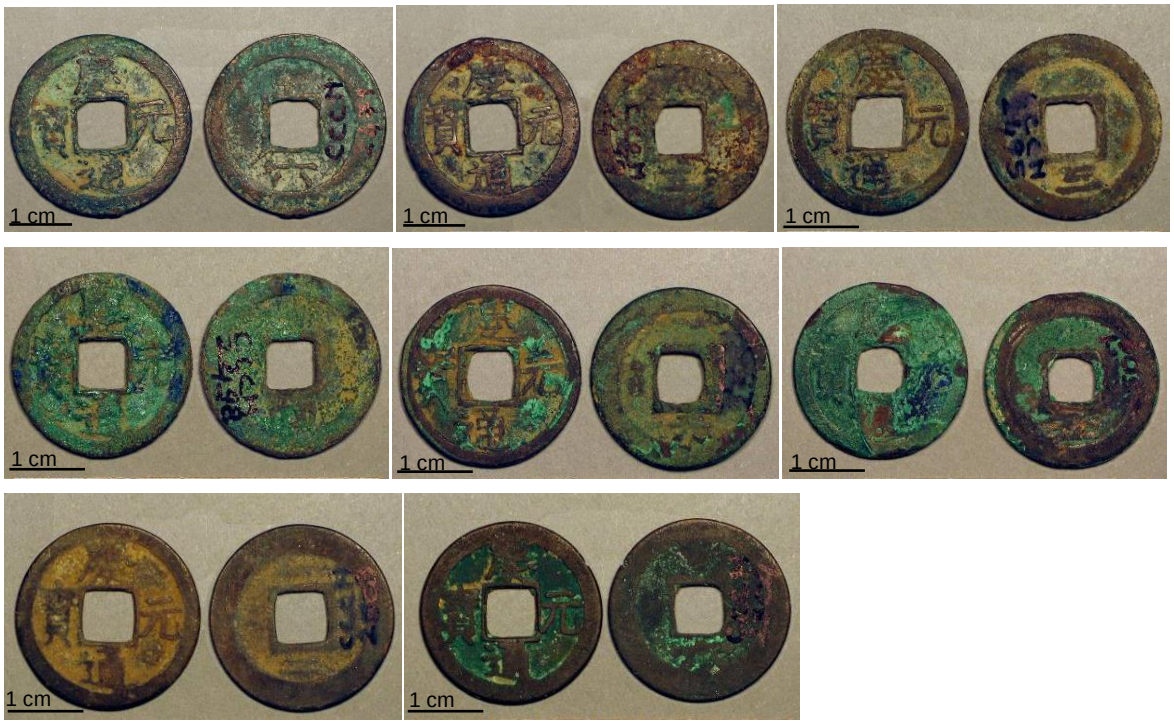

Fig. 2.15 Obverse and reverse of the Qing Yuan reign coins (from left to right and top to bottom, ref.:#2471; #2479; #2495; #2498; #2500; #2501; #2503; #2504)

[14] According to P. Golas [1999], this is one of the common ores extracted in China to obtain copper.

Compositional values are similar among them; however #2503 and #2504 seem to be Cu-richer and Pb-poorer. This may be due to changes in composition in the various casting years, or compositional disparities between different minting provinces. Iron content continues to range the ~1-2 wt.% as in the previous reign, while As can also still be considered an alloy impurity.

Table 2.2 EDXRF results and microstructural observation of the Qing Yuan coins. The values in italic are macro-EDXRF from the surface, while the remaining are micro-EDXRF from the cleaned metal edge.

Reference	Composition (wt.%) Cu	Sn	Pb	Fe	As	Observed Phases	Inclusions
2471	*50.4* 62.6	*2.4* 2.4	*45.1* 32.6	*1.8* 1.4	*n.d.* 0.76	α; (Pb); F_1	C_1 or B_1
2479	*42.5* 60.5	*4.0* 2.9	*46.9* 34.4	*6.3* 1.9	*n.d.* 0.36	α; (Pb); F_1	C_1 or B_1
2495	*62.1* 61.0	*2.9* 1.8	*32.5* 35.8	*2.3* 1.3	*n.d.* 0.30	α; (Pb); F_1	C_1 or B_1
2498	*64.6* 61.3	*3.7* 2.7	*29.5* 34.6	*1.9* 1.4	*n.d.* n.d.	α; (Pb); F_1	C_1 or B_1
2500	*62.2* 64.6	*4.4* 3.6	*30.8* 31.0	*2.3* 0.8	*n.d.* n.d.	α; (Pb)	C_1
2501	*72.2* 59.8	*3.2* 2.8	*22.2* 35.2	*1.2* 1.4	*n.d.* 0.81	α; (Pb); F_1	C_1 or B_1
2503	*43.1* 69.6	*5.6* 3.6	*48.1* 24.6	*2.5* 1.3	*n.d.* 0.92	α; (Pb); F_1	C_1 or B_1
2504	*70.4* 72.8	*2.9* 2.6	*25.6* 22.0	*0.85* 1.6	*n.d.* 0.51	α; (Pb); F_1	C_1 or B_1

Regarding the microstructures (see Fig. 2.16), taking into account the determined compositions, the phases encountered are very similar to the Chun Xi coins: alpha Cu matrix, with primary Fe-rich phase (F_1) and dark grey Cu-S inclusions (C_1) in the interdendritic regions. Pb-rich globules (Pb) were found in their metallic form or sometimes partially or totally corroded.

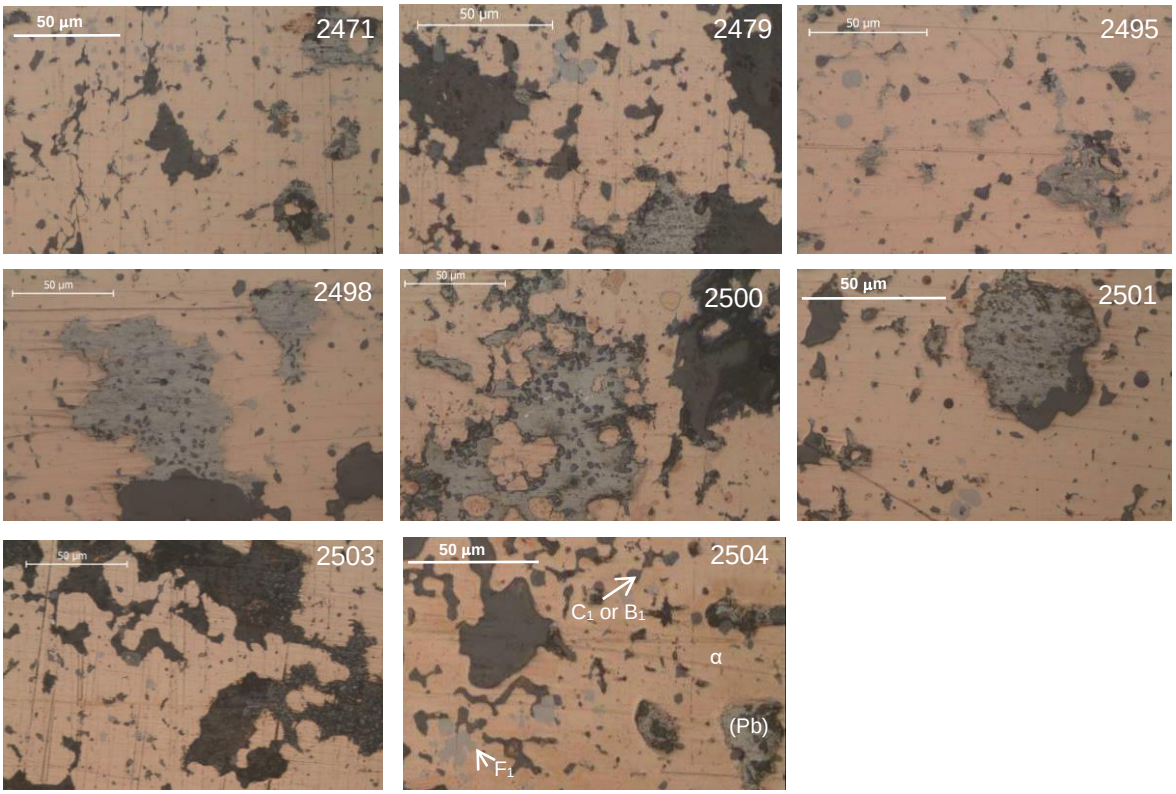

Fig. 2.16 Details of microstructures in the Qing Yuan coins (all in BF-OM, non-etched)

2.3.1.3. Jia Ding Tong Bao coins (1208 – 1224 AD)

The characters on the reverse correspond to the numeral year of reign in which the coin was cast [Hartill, 2005]. All the coins are 1-cash size, except for #2534 and #2544 that are 2-cash size (see Fig. 2.17).

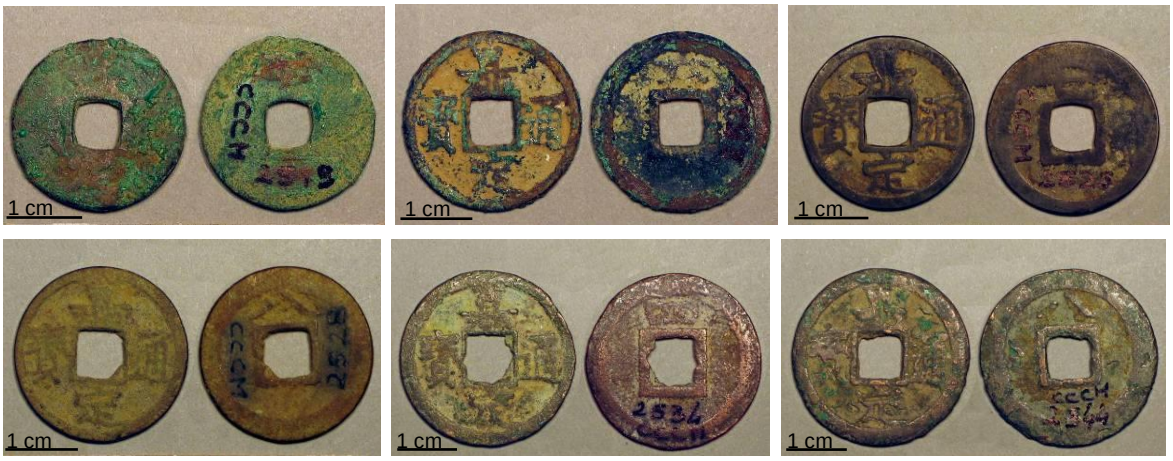

Fig. 2.17 Obverse and reverse of the Jia Ding reign coins (from left to right and top to bottom, ref.: #2519; #2522; #2525; #2528; #2534; #2544)

All the coins seem to have similar elemental contents for Cu and Pb, except for #2519 and #2544. This last one seems to have had an over-estimation of the Pb content due to the micro-EDFRX spots coinciding with large Pb-rich globules that are present in the cleaned area (see Fig. 2.18(c)). When assessing data obtained by SEM-EDS, from a region without large globules (Fig. 2.18(b)), the Pb content drops to less than half the value of the obtained by micro-EDXRF (~55 wt.% to ~20 wt.%) (see Table 2.3), which when considered alone, can also lead to a Pb content underestimation. The first coin, #2519, has an unexpected high As content and a low Pb content. It may have been produced in a province or time of copper abundance. Coin #2534 has no Sn but a small amount of Sb, which was probably non-intentional.

Table 2.3 EDXRF results and microstructural observation of the Jia Ding coins. The values in italic are macro-EDXRF from the surface, while the remaining are micro-EDXRF from the cleaned metal edge. Grey-highlight corresponds to a SEM-EDS analysis of region in Fig. 2.18 (b).

Reference	Composition (wt.%) Cu	Sn	Pb	Fe	As	Observed Phases	Inclusions
2519	*84.9*	*1.1*	*11.7*	*1.0*	*0.77*	α; (Pb); D_1	C_1
	90.0	1.0	2.3	0.6	6.0		
2522	*77.0*	*0.5*	*20.1*	*2.1*	*n.d.*	α; (Pb); F_1	C_1 or B_1
	63.1	3.7	32.2	1.0	0.30		
2525	*49.6*	*5.0*	*42.3*	*2.3*	*n.d.*	α; (Pb); F_1	C_1 or B_1
	60.1	2.0	35.3	2.1	0.40		
2528	*72.2*	*4.1*	*21.1*	*2.4*	*n.d.*	α; (Pb); F_1	C_1 or B_1
	67.1	3.0	28.4	0.9	0.43		
2534	*32.5*	*0.2*	*65.7*	*1.3*	*n.d.*	α; (Pb); F_1	C_1 or B_1
	64.9	0.2*	31.6	1.7	1.6		
2544	*26.1*	*0.8*	*70.4*	*2.6*	*n.d.*		
	41.1	1.9	54.8	2.0	0.67	α; (Pb); F_1	C_1 or B_1
	75.2	3.2	18.2	1.9	1.50		

* Sb, not Sn.

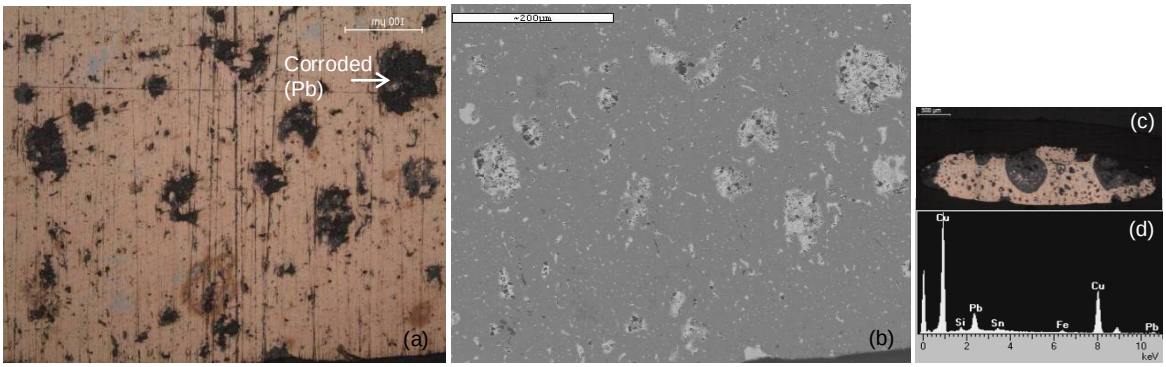

Fig. 2.18 Detail of coin #2544 in: (a) BF-OM and (b) BSE-SEM. (c) clean edge area where the micro-analyses were performed. (d) SEM-EDS spectra collected from the scanned region (b).

Microstructurally, with exception of coin #2519, all coins have an α matrix in which Pb-rich globules (grey, metallic or dark, corroded) exist, as well as a dendritic lighter grey Fe-rich phase, F_1 (see Fig. 2.19). Dark grey Cu-S (C_1) or Cu-S-Fe (B_1) inclusions are sometimes observed. Concerning the As-rich coin, #2519, a dark grey Cu,As-rich phase exists in the interdendritic regions of the α matrix. It will be refered to as D_1 (it was later identified as domeykite, a copper arsenide, Cu_3As), which will be explained in Chapter 3.

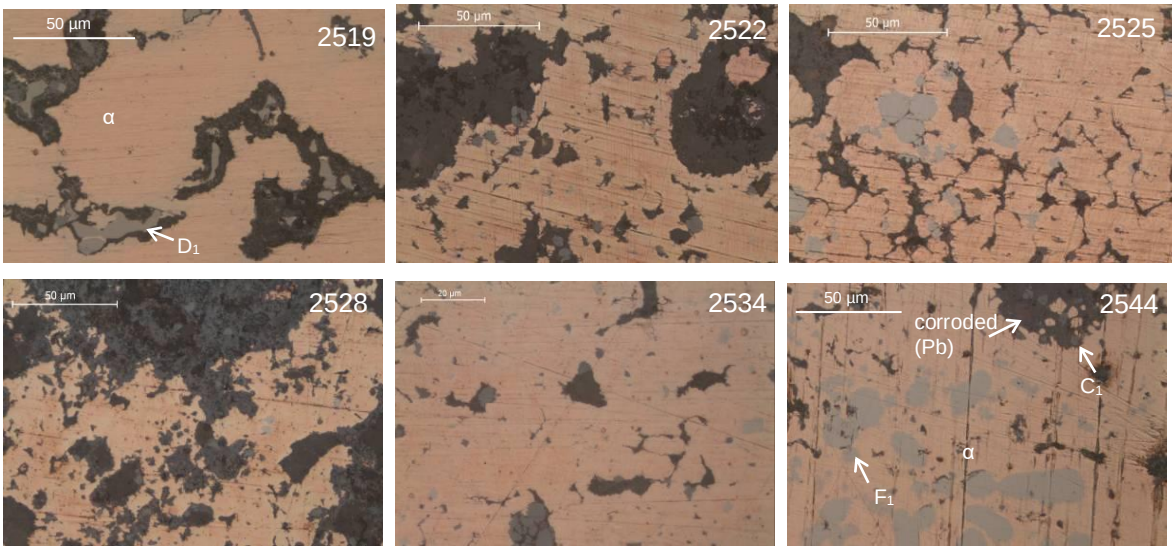

Fig. 2.19 Details of microstructures in the Jia Ding coins (all in BF-OM, non-etched).

2.3.1.4. Shao Ding Tong Bao coins (1228 – 1233 AD)

The characters on the reverse correspond to the numeral year of reign in which the coin was cast [Hartill, 2005].

All coins are 1-cash size except for #2568 and #2571 that are 2-cash size (see Fig. 2.20).

The elemental contents are presented in Table 2.4. The main element contents range from ~60 to ~70 wt.% Cu and ~20 to ~40 wt.% Pb. Tin contents are similar: ~2 to ~3 wt.% except for #2564, with ~5 wt.% Sn. Iron is present in all coins and goes from 1 to 5 wt.%. As is always below 0.5 wt.%.

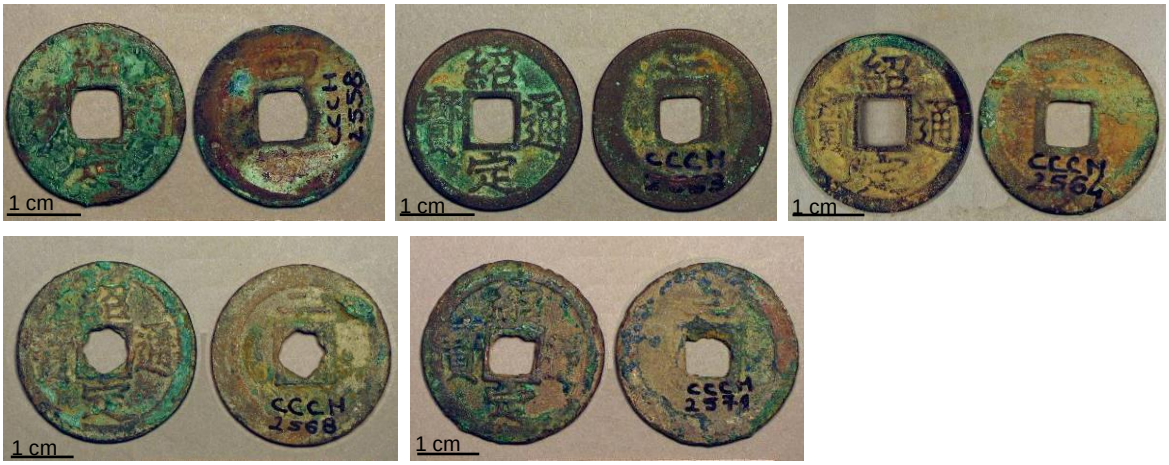

Fig. 2.20 Obverse and reverse of the Shao Ding reign coins (from left to right and top to bottom, ref.: #2558; #2563; #2564; #2568; #2571)

Table 2.4 EDXRF results and microstructural observation of the Shao Ding coins. The values in italic are macro-EDXRF from the surface, while the remaining are micro-EDXRF from the cleaned metal edge.

Reference	Composition (wt.%) Cu	Sn	Pb	Fe	As	Observed Phases	Inclusions
2558	*64.3*	*3.4*	*30.3*	*1.6*	*n.d.*	α; (Pb); F_1	C_1 or B_1
	61.7	2.7	30.2	5.0	0.2		
2563	*61.3*	*3.5*	*33.7*	*1.3*	*n.d.*	α; (Pb); F_1	C_1 or B_1
	69.8	3.2	24.0	2.4	0.37		
2564	*39.2*	*8.0*	*49.6*	*2.8*	*n.d.*	α; (Pb); F_1	C_1 or B_1
	72.4	5.1	21.2	1.1	0.36		
2568	*46.6*	*2.1*	*49.6*	*1.4*	*n.d.*	α; (Pb); F_1	C_1 or B_1
	56.7	1.8	39.0	2.3	0.25		
2571	*34.1*	*1.1*	*62.8*	*1.9*	*n.d.*	α; (Pb); F_1	C_1 or B_1
	65.6	1.8	30.0	2.4	0.39		

Regarding the microstructures, taking into account the determined compositions, the phases encountered are very similar to the previous coins: α matrix, with primary Fe-rich phase (F_1) and Pb globules (Pb) and Cu-S inclusions (C_1 or B_1) in the interdendritic regions. Lead-rich globules are in their metallic form or sometimes partially or totally corroded, presenting a dark colour in BF-OM.

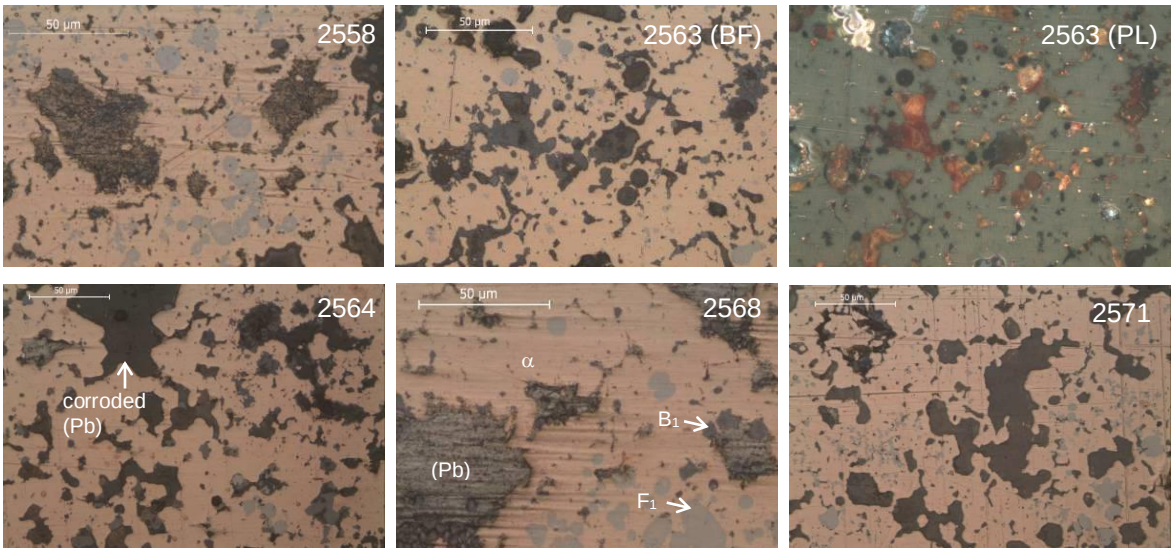

Fig. 2.21 Details of microstructures in the Shao Ding coins (all non-etched, in BF-OM except for #2563, in PL)

2.3.1.5. Chun You Yuan Bao coins (1241 – 1252 AD)

The characters on the reverse correspond to the numeral year of reign in which the coin was cast [Hartill, 2005]. All coins are 1-cash size.

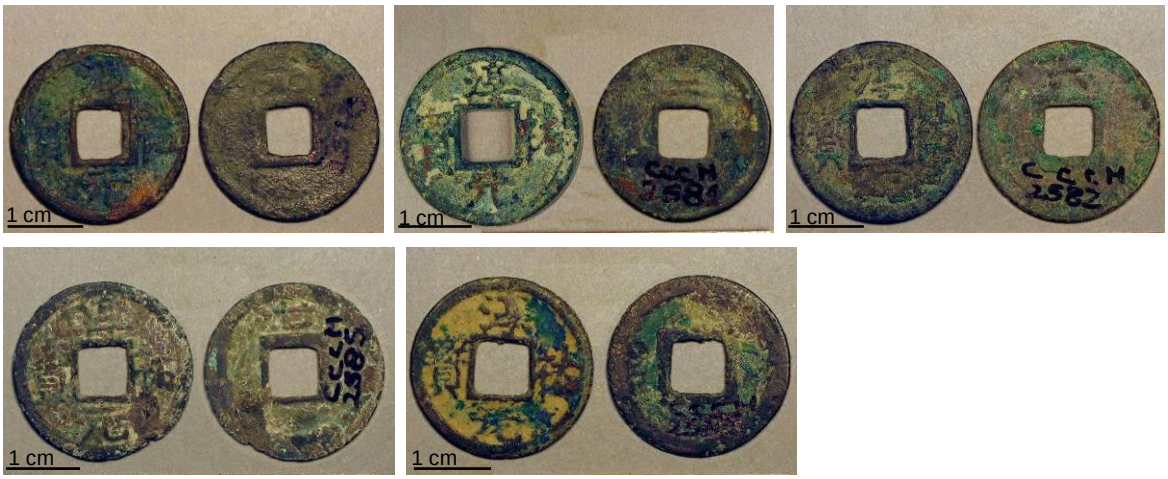

Fig. 2.22 Obverse and reverse of the Chun You reign coins (from left to right and top to bottom, ref.: #2578; #2581; #2582; #2585; #2588)

Copper has a content variation range between ~50 and ~70 wt.% and Pb between 24 and 44 wt.%. Tin contents range between ~2 to ~3 wt.%, and Fe between 1 and ~3 wt.%. Arsenic contents reaches ~0.5 wt.%.

Table 2.5 EDXRF results and microstructural observation of the Chun You coins. The values in italic are macro-EDXRF from the surface, while the remaining are micro-EDXRF from the cleaned metal edge.

Reference	Composition (wt.%) Cu	Sn	Pb	Fe	As	Observed Phases	Inclusions
2578	*45.7*	*3.9*	*48.0*	*2.2*	*n.d.*	α; (Pb); F_1	C_1 or B_1
	59.4	2.8	34.2	3.2	0.38		
2581	*64.9*	*1.9*	*31.7*	*1.3*	*n.d.*	α; (Pb); F_1	C_1 or B_1
	61.4	1.9	34.3	2.5	0.26		
2582	*48.3*	*1.8*	*47.3*	*2.8*	*n.d.*	α; (Pb); F_1	C_1 or B_1
	62.2	2.4	34.0	1.0	0.44		
2585	*35.7*	*2.0*	*60.8*	*1.2*	*n.d.*	α; (Pb); F_1	C_1 or B_1
	51.1	2.2	44.0	2.1	0.48		
2588	*48.2*	*2.2*	*47.3*	*2.2*	*n.d.*	α; (Pb); F_1	C_1 or B_1
	69.7	3.1	24.0	2.3	0.55		

Microstructurally they are similar to the previous coins: α matrix, with primary Fe-rich phase (F_1) and Pb globules (Pb) and Cu,S inclusions (C_1 or B_1) in the interdendritic regions. Lead globules are in a metallic form or sometimes partially or totally corroded.

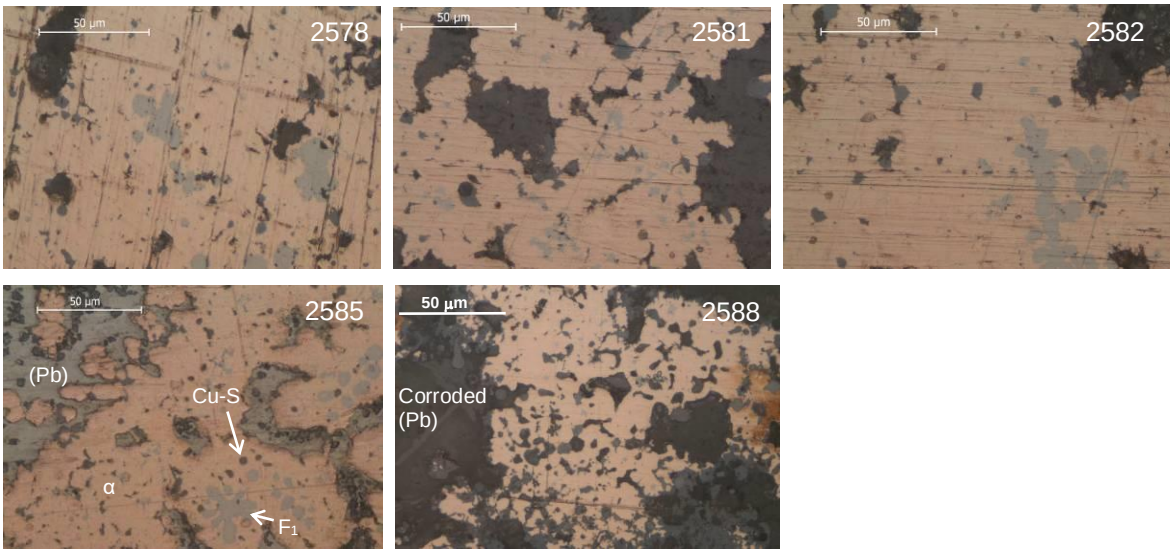

Fig. 2.23 Details of microstructures in the Chun You coins (all in BF-OM, non-etched).

2.3.1.6. Jing Ding Yuan Bao coin (1260 – 1264AD)

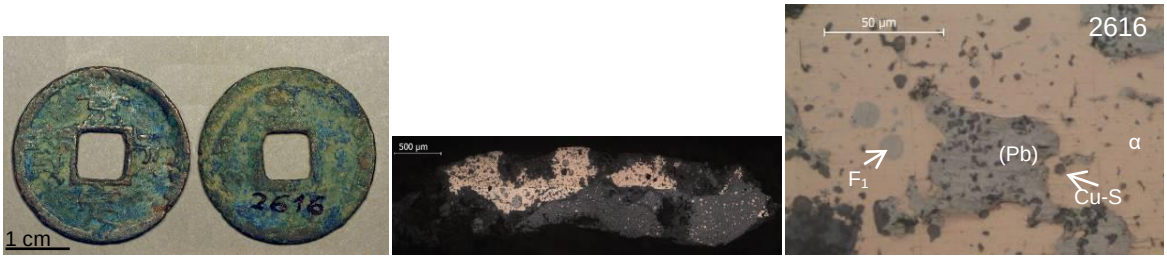

Fig. 2.24 Coin from the Jing Ding reign (ref.: #2616): obverse and reverse; clean area and detail (BF-OM, non-etched).

This is 2-cash size coin. Compositionally (Table 2.6) and microstructurally (Fig. 2.24) it is similar to the coins from the previous reign.

Table 2.6 EDXRF results and microstructural observation of the Jing Ding coin. The values in italic are macro-EDXRF from the surface, while the remaining are micro-EDXRF from the cleaned metal edge.

Reference	Composition (wt.%) Cu	Sn	Pb	Fe	As	Observed Phases	Inclusions
2616	*49.1*	*3.3*	*45.7*	*1.7*	*n.d.*	α; (Pb); F_1	C_1 or B_1
	59.9	3.1	34.2	1.9	0.36		

2.3.1.7. Xian Chun Yuan Bao coins (1265 – 1274 AD)

During the last years of the Southern Song dynasty (1275-1279 AD), no coins were produced due to the turbulence caused by the Mongols persecution [Hartill, 2005].

All the coins are 1-cash size except for #2621, #2624, #2625, #2626 and #2631, that are 2-cash (see Fig. 2.25).

Copper content ranges between ~52 to ~73 wt.% and Pb between 20 and 45 wt%. Tin ranges from 1.4 to 5.0 wt.%. Iron, with exception to coin #2621, with more than 7.0 wt.%, ranges from 1.0 to ~3 wt.%; and As, is as in previous analysed coins, up to 0.5 wt.% (see Table 2.7).

Fig. 2.25 Coins from the Xian Chun reign (from left to right and top to bottom, ref.: #2614; #2615; #2617; #2619; #2621; #2623; #2624; #2625; #2626; #2631)

Table 2.7 EDXRF results and microstructural observation of the Xian Chun coins. The values in italic are macro-EDXRF from the surface, while the remaining are micro-EDXRF from the cleaned metal edge.

Reference	Composition (wt.%) Cu	Sn	Pb	Fe	As	Observed Phases	Inclusions
2614	*51.2* 61.8	*6.2* 5.0	*40.6* 31.0	*1.9* 2.0	*n.d.* 0.29	α; (Pb); F_1	C_1 or B_1
2615	*62.7* 60.8	*2.6* 2.5	*30.2* 33.0	*3.5* 2.5	*n.d.* 0.55	α; (Pb); F_1	C_1 or B_1
2617	*44.1* 58.4	*4.0* 3.2	*48.2* 34.9	*3.5* 2.7	*n.d.* 0.35	α; (Pb); F_1	C_1 or B_1
2619	*63.7* 73.2	*5.1* 4.1	*29.4* 20.0	*1.5* 1.8	*n.d.* 0.45	α; (Pb); F_1	C_1 or B_1
2621	*35.9* 55.9	*1.6* 1.6	*60.2* 35.0	*2.1* 7.2	*n.d.* 0.34	α; (Pb); F_1	C_1 or B_1
2623	*38.0* 55.3	*5.6* 3.5	*53.9* 38.2	*2.2* 2.4	*n.d.* 0.39	α; (Pb); F_1	C_1 or B_1
2624	*47.1* 53.8	*5.3* 4,2	*44.7* 39.2	*2.4* 2.6	*n.d.* 0.36	α; (Pb); F_1	C_1 or B_1
2625	*59.9* 52.3	*1.0* 1.4	*37.9* 45.0	*1.0* 1.0	*n.d.* 0.31	α; (Pb); F_1	C_1 or B_1
2626	*20.4* 62.7	*0.5* 3.6	*78.4* 30.4	*0.7* 2.6	*n.d.* 0.50	α; (Pb); F_1	C_1 or B_1
2631	*42.1* 63.7	*3.6* 4.5	*52.5* 30.2	*1.6* 1.3	*n.d.* 0.44	α; (Pb); F_1	C_1 or B_1

Microstructurally, these coins are similar to the previous observed coins: primary Fe-rich phase (F_1) in α matrix, occasionally presenting large Pb-rich globules (Pb) and some Cu-S inclusions (C_1 or

B_1). Sometimes, inside the larger Pb-rich globules, α phase segregations are observable, in a quasi-globular or dendritic formations (see Fig. 2.26, coin #2624).

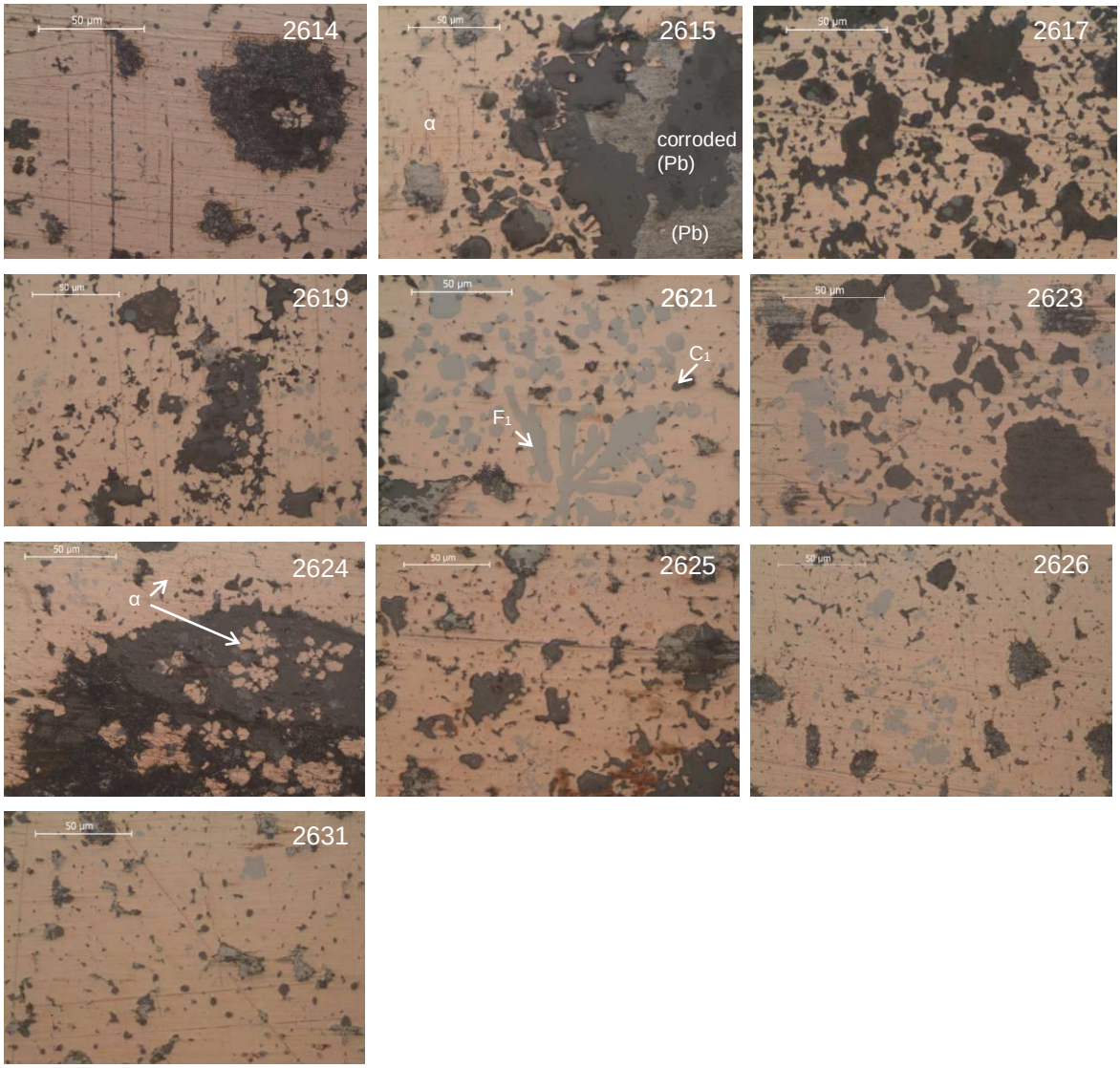

Fig. 2.26 Details of microstructures in the Xian Chun coins in BF-OM (all in BF-OM, non-etched).

2.3.2 Other dynasties bronze coins

2.3.2.1. Eastern Han dynasty (25-220 AD)

Coin #2209 is a Xiao Wu Zhu (little Wu Zhu) from the Eastern Han Dynasty, attributed to 40 AD. It seems a rather detailed and perfect item, and seems to have some kind of superficial lustrous protective film (see Fig. 2.27). Hartill [2005] refers that Wu Zhu coins bearing a raised rim in the inner hole are a special edition with very high standards.

In Table 2.8 are the elemental results obtained from this coin: nominal compositions of Xiao Wu Zhu coins are considered of high quality [Hartill, 2005], having a high Cu content and significant few minor elements. A peculiar characteristic is the amount of S present in the grey globules (~29 wt.%, by SEM-EDS), not seen in any other coin in this collection as in this one.

Table 2.8 EDXRF results and microstructural observation of the Xiao Wu Zhu coin. The values in italic are macro-EDXRF from the surface, while the remaining are micro-EDXRF from the cleaned metal edge.

Reference	Composition (wt.%) Cu	Sn	Pb	Zn	Fe	As	Observed Phases	Inclusions
2209	*82.5*	*5.7*	*6.0*	*n.d.*	*5.5*	*n.d.*	α; F_1; (Pb)	B_1
	89.0	4.2	2.0	n.d.	3.9	0.3		

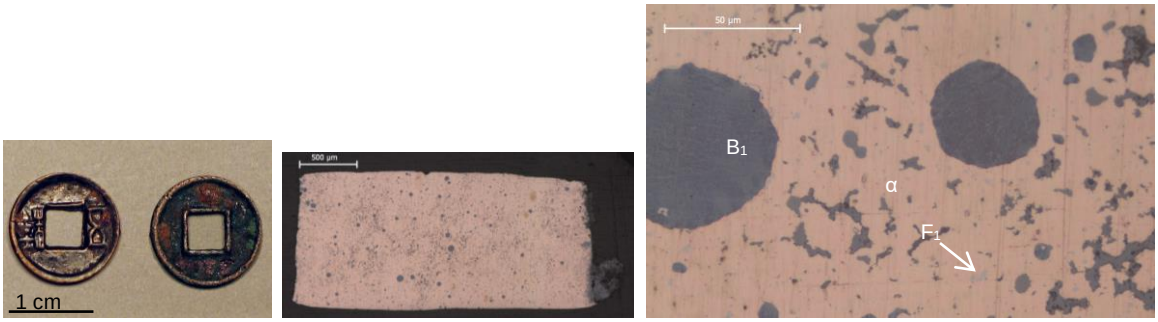

Fig. 2.27 Obverse and reverse images of coin #2209, its BF-OM cleaned edge area and a detail (non-etched).

Its microstructure presents an α matrix with round, large, dark grey Cu,Fe,S-rich globules (B_1) in BF-OM. The interdendritic regions are also filled with this phase. A few primary Fe-rich phase grains (F_1), in light grey, are also observed.

2.3.2.2. Tang dynasty (618-906 AD)

Coin #2242 is a Kai Yuan Tong Bao attributed to 621 AD. It was chosen because, unlike the other Kai Yuans in the collection, it had almost no patina and its rims and characters were very detailed and defined (see Fig. 2.28).

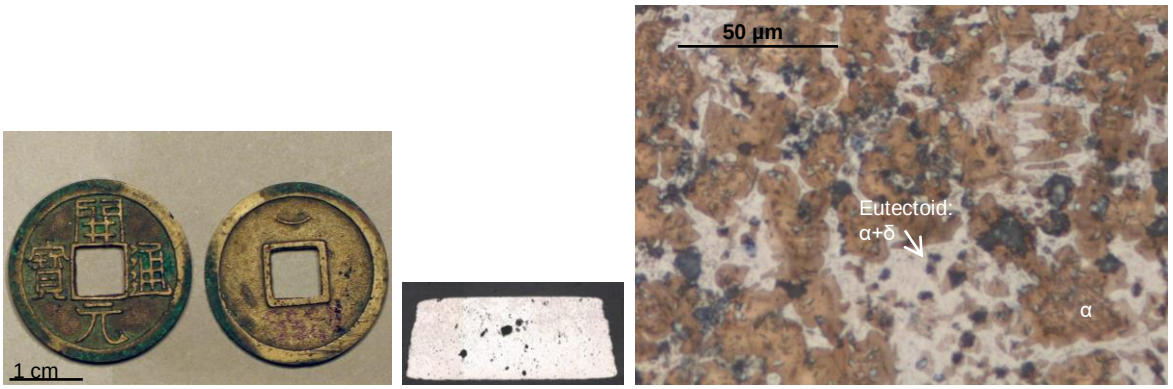

Fig. 2.28 Obverse and reverse image of coin #2242, its BF-OM cleaned edge area (non-etched) and a detail micrography (etched).

This coin also has very good quality, similar to coins of the same period in the BM collection [Wang, 2005]. Regarding its composition (see Table 2.9): a high Cu content and a very high - the highest in the collection - Sn content (15.2 wt%), causes the formation of an α+δ eutectoid constituent (delta phase is light grey in BF-OM, in Fig. 2.28). Minor phases include Fe-rich, F_1, and Pb-rich globules.

Table 2.9 EDXRF results and microstructural observation of the Kai Yuan Tong Bao coin. The values in italic are macro-EDXRF from the surface, while the remaining are micro-EDXRF from the cleaned metal edge.

Reference	Composition (wt.%) Cu	Sn	Pb	Fe	As	Observed Phases	Inclusions
2242	*71.8*	*16.6*	*9.1*	*0.53*	*0.19*	α; δ; F_1; (Pb)	C_1
	70.4	15.2	9.9	3.1	0.69		

2.3.2.3. Qing dynasty (1644-1912 AD)

Coins #2704 and #2977 belong to the *Shun Zhi Tong Bao* (1644-1661 AD) and the *Tong Zhi Tong Bao* (1862-1874 AD) reigns respectively (see Fig. 2.29). Coin #2704 is of unknown cash size, and coin #2977 is a 10-cash.

Micro-EDXRF results show both coins have higher Sn contents when compared with identical exemplars from the same reigns (see Table 2.10).

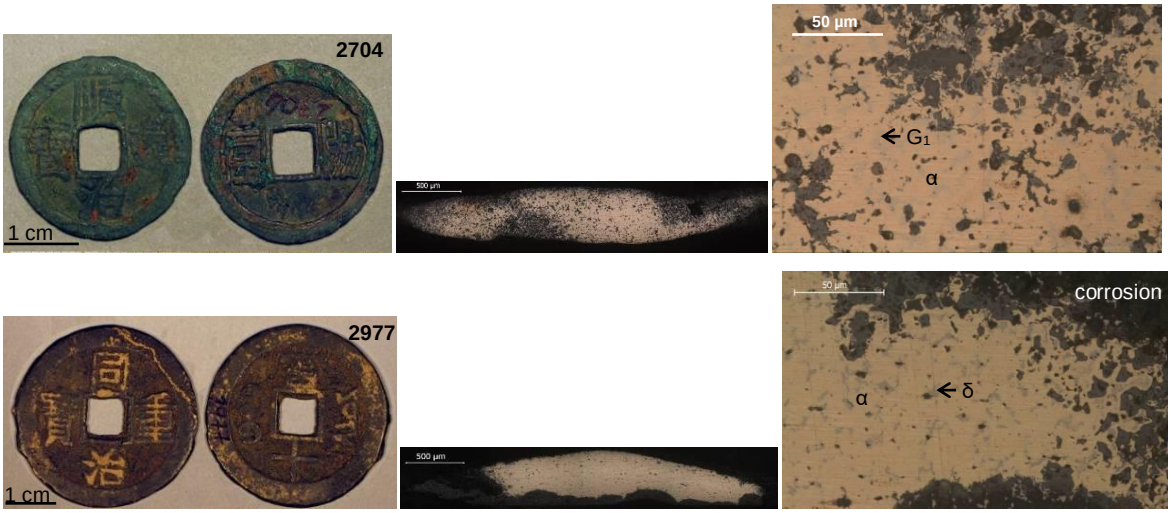

Fig. 2.29 Obverse and reverse images of coins #2704 and #2977 and their BF-OM cleaned edge areas and details (non-etched).

Table 2.10 EDXRF results and microstructural observation of the Jing Ding coin. The values in italic are macro-EDXRF from the surface, while the remaining are micro-EDXRF from the cleaned metal edge.

Reference	Composition (wt.%) Cu	Sn	Pb	Zn	Fe	As	Observed Phases	Inclusions
2704	*53.7*	*12.8*	*27.0*	*3.6*	*2.0*	*n.d.*	α+G_1; (Pb)	C_1
	68.3	5.0	15.3	10.3	0.3	0.34		
2977	*64.4*	*18.6*	*11.1*	*0.7*	*3.2*	*1.67*	α+δ; (Pb)	-
	73.3	10.1	13.3	0.27	0.7	1.90		

Microstructurally, both coins present an apparently similar as-cast structure with a light grey interdendritic eutectoid or eutectic product in a beige Cu-based matrix, and a dispersion of Pb-rich small globules. But while #2977 has an α+δ eutectoid, micro-analysis by SEM-EDS showed that the light grey phase of the eutectoid in coin #2704 was much richer in Zn, besides a small amount of Sn. So, this phase will be referred to as G_1 because it is probably the γ-brass phase. This α+G_1 structure of coin #2704 cannot be explained using the Cu-Sn or the Cu-Zn binary phase diagrams alone (see Fig. 2.10 and 2.11). Considering the Cu-Zn system, possible phase combinations include α, α+β, β, β+γ, γ, γ+(Zn) and (Zn). This α+G_1 phase combination, almost proof of the

complex microstructures that these coins can possess, was observed not only in this particular coin but in several other brass coins from the Ming and Qing dynasties in the studied collection. This special phase constitution points to certain combinations of three elements, Cu, Zn and Sn, to promote its formation. These results will be further discussed in Chapter 3.

In Fig. 2.30 are plotted the elemental contents obtained from the surface of these coins (macro and micro-EDXRF) and from a cleaned edge (micro-EDXRF). Micro and macro-EDXRF were performed on the surface of both coins and the results were very similar, except when considering the Cu and Pb contents in coin #2704, which can be accountable to Pb corrosion products concentration at the analysed micro-EDXRF spot. Both coins present analogous Pb contents; in coin #2704 the corrosion layer seems to be enriched in this element. Both coins have similar corrosion thicknesses (~50 to ~100 micron); so probably, according to the corrosion environment, Pb was differently leached out in each coin.
Both micro and macro-EDXRF showed a notorious superficial enrichment in Sn (see Table 2.10), and a consequent decrease in Cu. Iron is enriched at the coins surface, probably as a consequence of a burial environment. In coin #2704, Zn seems to have been intentionally added to the alloy, contrary to coin #2977, where the contents found point towards an impurity. Comparing micro-EDXRF from the clean edge and macro-EDXRF from the surface, values in this coin suggest that Zn corrosion products have been leached from the surface.

As for their abnormal contents in Sn (when comparing these coins with others of the same period belonging to this collection and also to the British Museum collection, whose data were accessed in [Wang, 2005]), the production of coin #2704 can be traced, by the reverse characters that indicate the production mint, to a garrison: *Yanghe*, in the Shanxi province [Hartill, 2005]. While many factors may be responsible for this Sn content, the reuse of metal for coin casting, especially alloys used in weaponry (with a higher Sn content) can be a plausible hypothesis. As for coin #2977, Hartill [2005] reports this specific coin title (*Tong Zhi Zhong Bao*, dated 1862 AD) as a commemorative edition, which justifies the noble mother-cash composition (Sn richer). However, its appearance is puzzling (the calligraphy details should be finer) which also allows the hypothesis of it having been minted in the Yunnan province as a regular issue (this province was known for its copper-rich mines and coins).

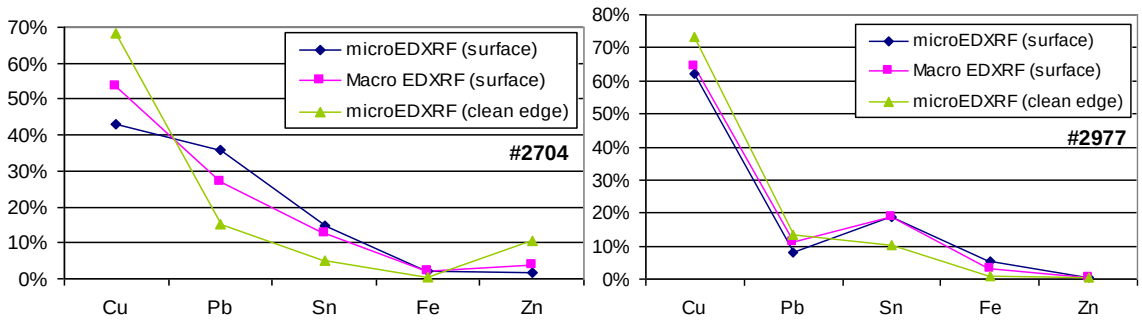

Fig. 2.30 Elemental contents of coins #2704 and #2977, from the surface and from a cleaned edge area.

2.4. Brasses

Compositionally and microstructurally, the brass studied coins are much more complex than the bronze cash. Lead and Sn are usually still present in the alloy but in a less important content while Zn emerges as the second or sometimes first larger element in the alloy. Other than Sn and Pb, some other minor elements present are often Fe, As and Sb, increasing the complexity and diversity of possible alloys and microstructures.

2.4.1. Ming dynasty coins (1368-1644 AD)

After rebellion overthrew the Mongol rule, the Ming dynasty arose, in 1368. The calm period that followed allowed the growth of science and arts. Portuguese made contact with the Chinese Empire for trading and religious purposes. Coins and notes circulated freely, including money from other countries, such as Spain. Although the capital moved from Nanking to Beijing in 1421, both cities had a Board of Revenue and a Board of Works, and minting was done officially by many government departments throughout the empire as well as by many corrupt mint officers. The production reached 250,000 strings of coins per year in 1503 and 500,000 strings in 1630. Four coin categories circulated after 1620, being the last two predominant: the *yang qian* coins (fine quality and full weight); the *feng qian* coins (second quality, for salaries and emoluments); an intermediate quality coin (circulation money among the people); and *shang qian* coins (small and thin, fragile issues, similar to private minting coins, to pay government employees) [Hartill, 2005].

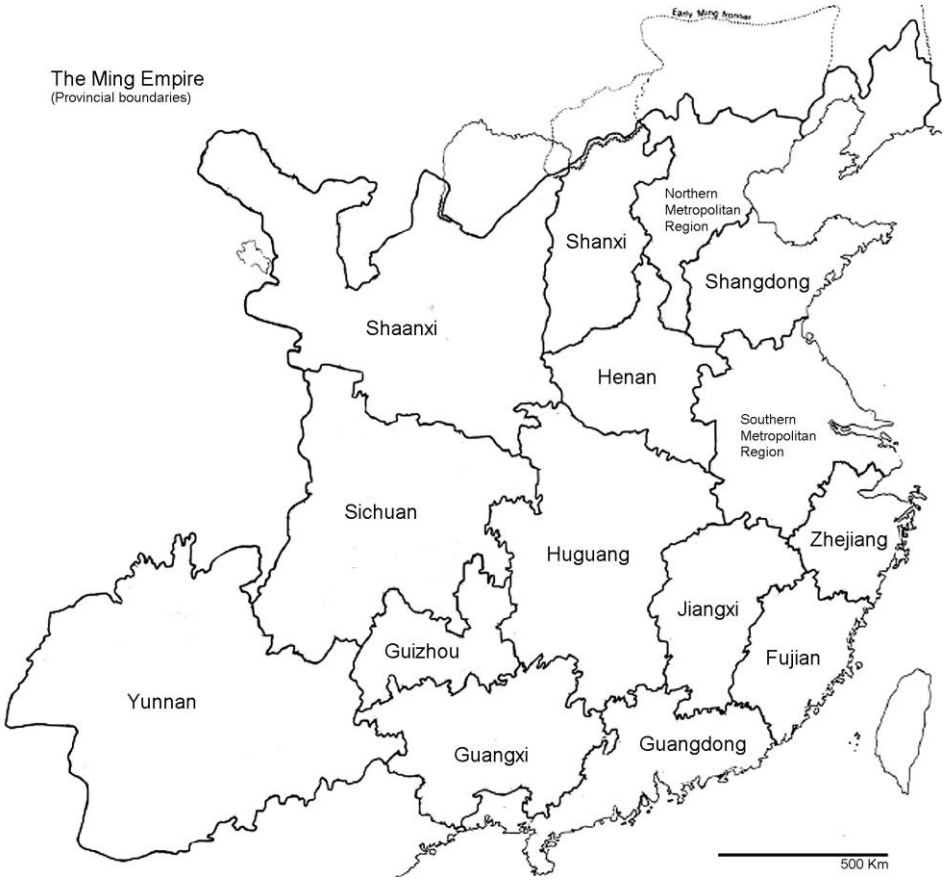

Fig. 2.31 Administrative regions of the Ming Empire (adapted from [Twitchett and Mote, 2008])

There were different finishing stages of production originating three types of coins: *xuanbian*, with smooth and even rims; *jinbei*, the "gold reverse" coins made of a finer Cu alloy, smelted four times instead of the regular two; and the "baked lacquer" coins, *huoqi*, in which the field was covered in dark lacquer for corrosion protection purposes [Kumanotani *et al.*, 1979, Cowell *et al.*, 2005a; Song, 1637]. Therefore, in spite of their specific designation, each issue could have different elemental compositions, weight and finishing aspect.

Since the Ming dynasty, cash coins were minted with only one title per reign, i.e., during the period of a reign, there was only one designation for all the coins issued, e.g., in the Wan Li reign, only Wan Li Tong Bao coins were issued (even if earlier coins circulated).

Given that the origin provinces and mints were not supplied with the studied coins, the investigation of the coins reverse allowed obtaining some information on the coins, especially after the Chong Zhen period, when Ming coins started to have the mint characters on the reverse.

2.4.1.1. Wan Li Tong Bao (1573 – 1620 AD)

After many periods of mintage suspension, in 1576 casting was resumed at Beijing and Nanking, and other provinces followed soon after. Wan Li coins were cast in the "gold reverse" and "baked lacquer" types, and the alloy was characterized by Hartill [2005] as "93.8% brass and 6.2% tin". Minting continued until 1579, when the rising price of copper and the lack of skilled men and distribution from the mints caused production to cease.

Coin #2650 is a 1-cash size and #2653 is a 2-cash size (see Fig. 2.32), both of them attributed to the year 1576 AD. Coin #2653 seems to have traces of a compact paste in the character crevices which may be related to the documented habit of lacquering the coins fields.

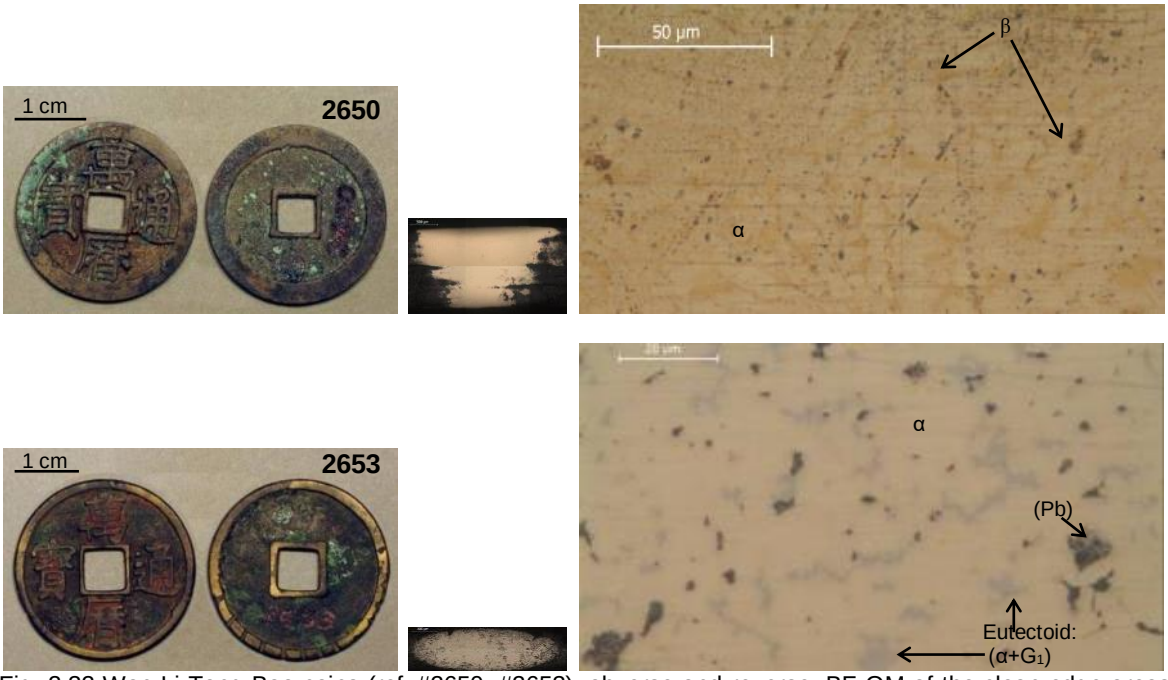

Fig. 2.32 Wan Li Tong Bao coins (ref.:#2650; #2653): obverse and reverse; BF-OM of the clean edge areas and detail.

The straight angles and symmetry of coin #2650 indicate it must have been a mother-cash or a special edition of this coin.

Table 2.11 EDXRF results and microstructural observation of the Wan Li coins. The values in italic are macro-EDXRF from the surface, while the remaining are micro-EDXRF from the cleaned metal edge.

Reference	Composition (wt.%) Cu	Zn	Pb	Fe	As	Sn	Sb	Observed Phases
2650	*60.9*	*37.5*	*1.0*	*0.1*	*n.d.*	*0.40*	*n.d.*	α; β
	61.9	37.0	0.8	0.1	n.d.	n.d.	n.d.	
2653	*63.1*	*10.9*	*17.9*	*1.2*	*n.d.*	*6.68*	*n.d.*	α+G_1; (Pb)
	70.1	11.0	13.7	0.4	n.d.	4.90	n.d.	

Their microstructure is highly dependent on the Zn content: while #2650 presents an α+β Widdmanstätten type structure (with 37 wt.% Zn); #2653 presents an α matrix and a two-phase mixture, α+G_1, as well as Pb-rich globules in the interdendritic regions. The identification of the light grey color phase G_1 and this particular eutectoid formation – impossible in the Cu-Zn binary system – will be discussed in the next chapter.

2.4.1.2. Tai Chang Tong Bao (1620 AD)

Emperor Guang Zong issued these coins during his one-month reign, but his successor, Xi Zong, continued their coinage during the first year of his reign.

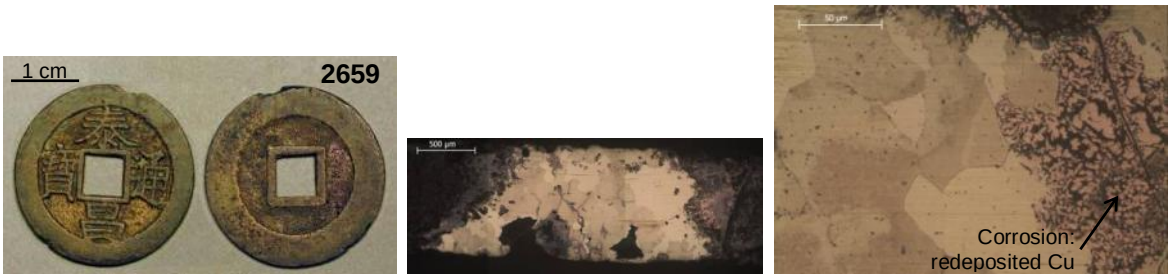

Fig. 2.33 Tai Chang Tong Bao coins (ref.:#2659): obverse and reverse; BF-OM (non-etched) of the clean edge area and detail.

This is a 1-cash coin. Its composition is similar to a coin from the same reign analysed by Dai and Zhou [1992]: 63%Cu; 2.6%Pb; 0.2%Sn; 32%Zn; 0.2%Fe (in wt.%).

Table 2.12 EDXRF results and microstructural observation of the Tai Chang coin. The values in italic are macro-EDXRF from the surface, while the remaining are micro-EDXRF from the cleaned metal edge.

Reference	Composition (wt.%)* Cu	Zn	Pb	Fe	As	Sn	Sb	Observed Phases
2659	*66.5*	*31.2*	*1.2*	*0.7*	*0.16*	*n.d.*	*0.22*	α; (Pb)
	72.7	24.7	1.3	0.5	0.50	n.d.	n.d.	

* (0.38 wt.% Bi by micro-EDXRF)

This coin has a puzzling structural feature (Fig. 2.33, BF-OM): although its composition places it in the α dominium in the Cu-Zn diagram, it shows (in both polished areas assessed) very distinct grain limits and different grain colorations in spite of not having been etched. This coloration is visible immediately after polishing and persists inaltered. No other coin presents this feature; so a hypothesis is that the coin may have suffered annealing and the α grains may have quite different orientations hence presenting different tones. Another possible explanation is that the edge had

suffered tensions that caused it to crack and the solution retained in these fissures is making the grains around it oxidise rapidly after polishing.

2.4.1.3. Tian Qi Tong Bao (1621 – 1627 AD)

Tian Qi coins started to be produced in 10-cash value, but were soon debased. In 1623 the reported elemental contents were *"only 20 or 30 percent* [copper]*, and their lead or slag content 70 or 80 percent. They were so brittle and thin that if thrown on the floor they could break (...). The officials were not strict enough (...)"* in Hartill [2005]. This author comments that the *"melting down of copper artefacts of great historical and religious significance from the government store-houses for coinage upset conservative officials and added to the bad reputation of Tianqi coins"*.

Previously, in 1358 AD, in the Hubei province, the Yuan Rebels had minted *Tian Qi Tong Bao* coins with identical inscriptions. These coins were later also used during the Ming dynasty. Six of the studied coins with the characters *Tian Qi Tong Bao* were attributed to the Yuan Dynasty (14th century AD) according to the information on their card containers. However, after the preliminary macro-EDXRF analysis, it was found these coins were made of a brass alloy, which is incongruent with the zinc-less alloy used to produce coins during the Yuan dynasty [Bowman *et al.*, 2005; Dai and Zhou, 1992]. As such, coin experts Helen Wang (British Museum) and Zhou Weirong (China Numismatic Museum) were contacted and confirmed the coins in fact belong to the Ming dynasty reign that has the same designation (*Tian Qi*, 1621-27 AD), where brass alloys were already well-established.

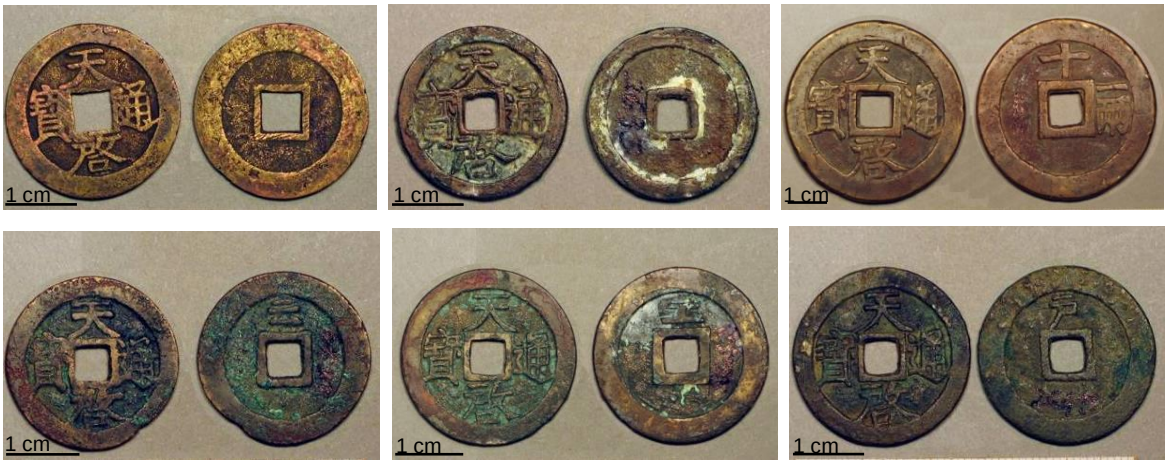

Fig. 2.34 Tian Qi Tong Bao coins (from left to right and top to bottom, ref.: #2632; #2635; #2636; #2639; #2642; #2645)

With exception from #2636, a 10-cash size, the remaining five coins are 1-cash coins.

The composition seems to be very similar inspite of the diffent cash-sizes. Coin #2639 seems to have somewhat more copper than the rest of the coins and also a higher content in As (almost 1 wt.%). The other coins have between ~54 and ~66 wt.%Cu and ~25 and ~40 wt.%Zn. Lead goes

up to 10 wt.% and Fe and As are usually under 0.5 wt.%. Only one coin presents a Sn content above 1 wt.% (#2642).

The microstructures encountered vary from monophasic α to biphasic α+β and α+γ. Lead is present in small to larger interdendritic globules.

Table 2.13 EDXRF results and microstructural observation of the Tian Qi coins. The values in italic are macro-EDXRF from the surface, while the remaining are micro-EDXRF from the cleaned metal edge.

	Composition (wt.%)							
Reference	Cu	Zn	Pb	Fe	As	Sn	Sb	Observed Phases
2632	*64.8*	*30.5*	*2.5*	*0.8*	*0.18*	*1.0*	*0.12*	α; β; (Pb)
	54.3	41.4	2.4	0.7	n.d.	1.3	n.d.	
2635	*50.8*	*46.5*	*1.6*	*0.5*	*n.d.*	*0.4*	*0.14*	α; β
	60.2	37.4	1.0	0.3	0.32	0.5	n.d.	
2636	*64.5*	*33.6*	*1.4*	*0.4*	*n.d.*	*n.d.*	*n.d.*	α
	65.9	32.3	1.3	0.3	n.d.	n.d.	n.d.	
2639	*84.9*	*8.7*	*4.5*	*0.6*	*0.37*	*n.d.*	*0.67*	α; (Pb); G_1?
	80.4	12.5	5.0	0.4	0.95	0.2	0.39	
2642	*56.6*	*29.8*	*9.2*	*0.7*	*n.d.*	*3.6*	*n.d.*	α; G_1; (Pb)
	61.9	24.6	9.7	0.4	n.d.	3.5	n.d.	
2645*	*55.6*	*26.5*	*14.5*	*0.9*	*n.d.*	*2.4*	*n.d.*	α; G_1; (Pb)
	63.9	28.2	6.0	0.3	0.17	1.2	n.d.	

* 0.42 wt.% Bi, by micro-EDXRF

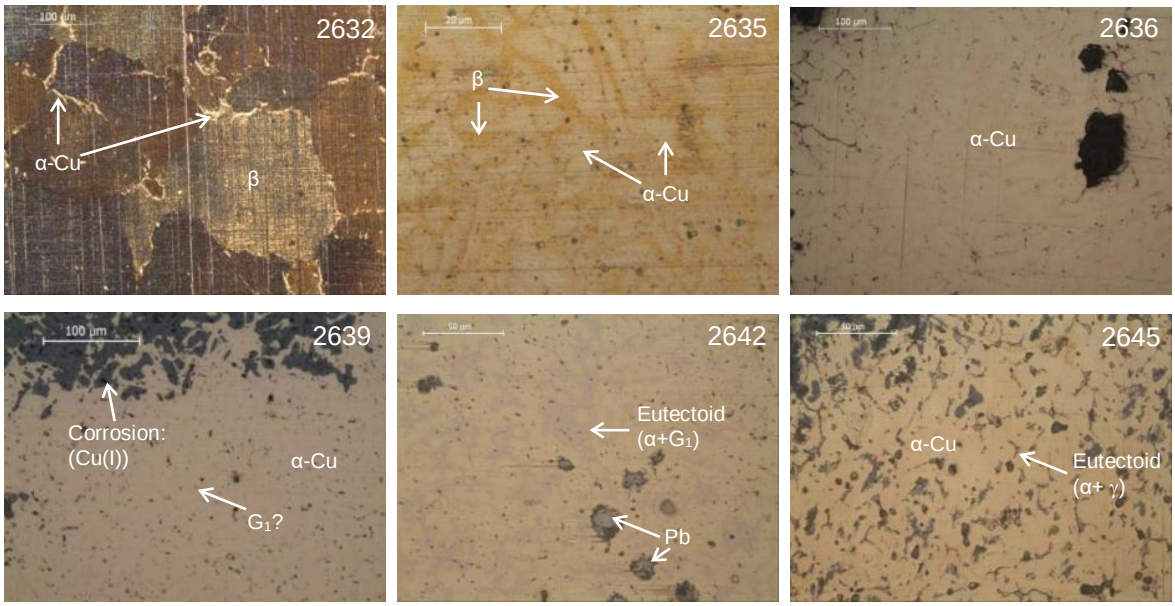

Fig. 2.35 Details of microstructures in the Tian Qi coins (all in BF-OM, #2632 & #2635 etched)

2.4.1.4. Chong Zhen Tong Bao (1628 – 1644 AD)

Hartill refers to the mark system these coins present (on the reverse) as "not fully understood": the characters *Zhen* and *Tong* (inscribed on the obverse) suffered variations, and the reverse had several characters that may be related with the minting year or provenance. Later on, this influenced the system adopted by the Southern Ming and Qing dynasties.

Coin #2667 is a 5-cash size, #2670 is a 2-cash size, but the rest are 1-cash size.

The coins main element is Cu, ranging from ~50 to ~71 wt.%. Zinc is the second larger element ranging from ~25 to ~46 wt.%. Lead varies between ~1 and ~14 wt.%. Iron is present in almost every coin but rarely above 1 wt.% while As, Sn and Sb are sometimes not present at all. These coins show a distinct presence of Sb from the coins already shown: some coins have Sb instead of Sn in the similar amounts expected for this element.

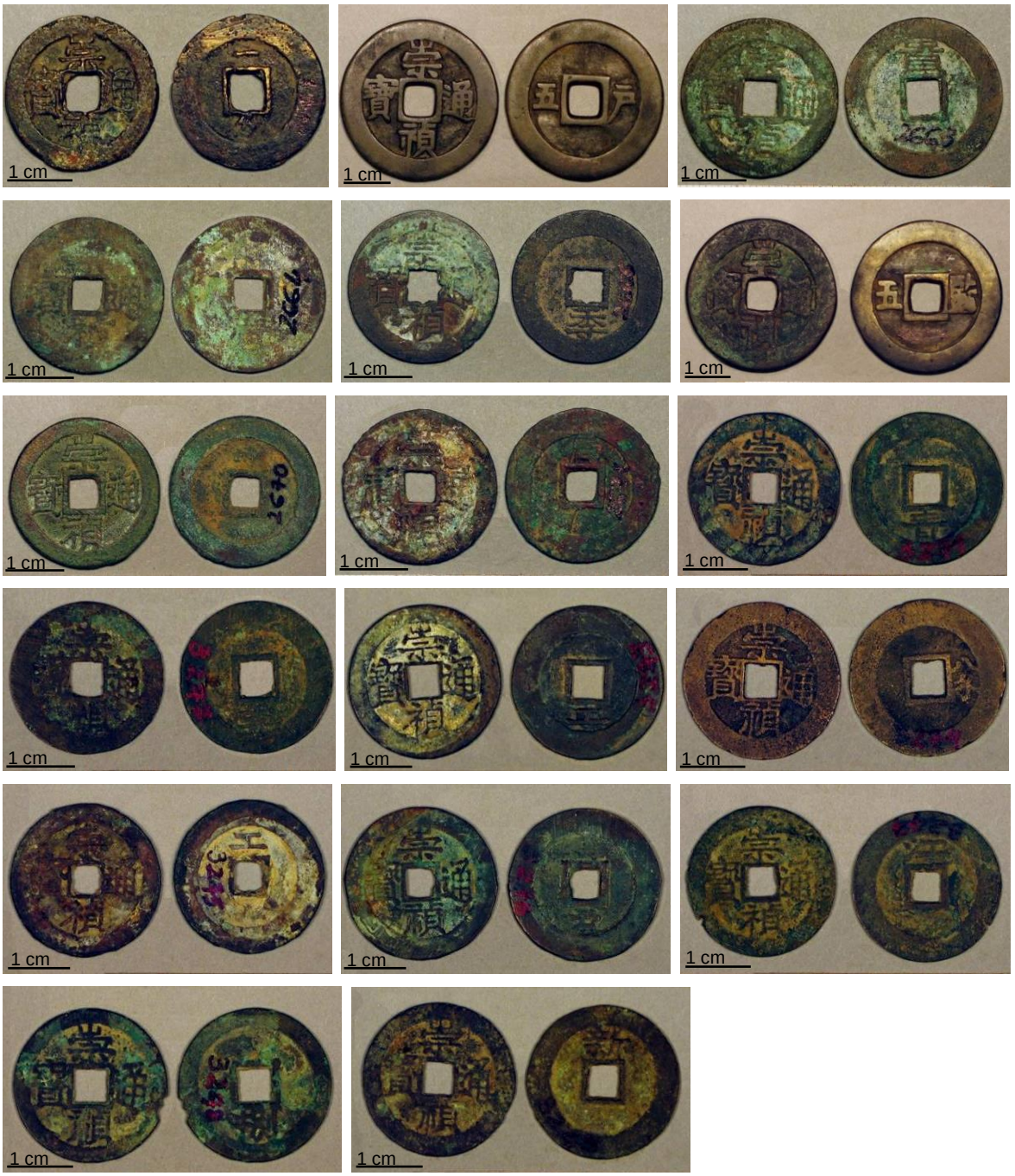

Fig. 2.36 Chong Zhen Tong Bao coins (from left to right and top to bottom, ref.: #2661; #2662; #2663; #2664; #2666; #2667; #2670; #2671; #3271; #3272; #3273; #3274; #3275; #3276; #3277; #3278; X)

Microstructurally, the multitude of elements and different content ranges cause the formation of multiphase microstructures: α, α+β, α+γ, α+β+γ, β+γ. The main and most common phase is α but

there are also 2 coins with high enough Zn contents to create β matrixes. The minor phase (Pb) is also present in many coins in the interdendritic regions. A two-phase mixture composed of α and a grey phase was observed. As mentioned before (in section 2.3.2)., when tin is present in sufficient amounts it seem to promote the G_1 phase for lower Zn contents. The presence of antimony seems to work in a similar way, promoting a phase that will be referred to as G_2, although they can actually be the same phase (this effect will be discussed in the next chapter).

Table 2.14 EDXRF results and microstructural observation of the Chong Zhen coins. The values in italic are macro-EDXRF from the surface, while the remaining are micro-EDXRF from the cleaned metal edge.

	Composition (wt.%)							Observed
Reference	Cu	Zn	Pb	Fe	As	Sn	Sb	Phases
2661	*67.8*	*29.1*	*1.0*	*1.8*	*n.d.*	*n.d.*	*n.d.*	α; F_1
	71.5	25.6	1.0	1.7	n.d.	n.d.	n.d.	
2662	*63.3*	*31.6*	*2.6*	*0.6*	*0.32*	*0.9*	*0.56*	α
	63.5	32.2	2.1	0.4	0.40	0.7	0.44	
2663*	*58.8*	*38.9*	*1.6*	*0.3*	*0.22*	*n.d.*	*n.d.*	α; β
	62.1	36.0	1.0	0.1	0.43	n.d.	n.d.	
2664	*30.7*	*60.5*	*5.8*	*1.0*	*n.d.*	*1.1*	*0.94*	α; β
	53.3	38.2	6.7	0.6	n.d.	0.8	0.38	
2666	*47.5*	*42.9*	*4.4*	*0.9*	*n.d.*	*0.5*	*3.78*	β; G_2
	52.3	38.0	5.3	0.5	0.45	n.d.	3.13	
2667	*64.5*	*28.2*	*3.7*	*1.9*	*n.d.*	*1.2*	*0.34*	α; G_1
	67.6	26.0	4.2	0.5	0.41	1.0	n.d.	
2670+	*63.8*	*20.3*	*11.7*	*1.8*	*n.d.*	*2.2*	*0.15*	α; G_1; (Pb);
	57.3	25.8	14.3	0.4	0.30	1.7	n.d.	
2671	*35.9*	*40.7*	*17.0*	*1.9*	*n.d.*	*3.4*	*1.00*	α; G_1 and/or G_2; (Pb);
	57.1	26.7	9.7	0.6	0.43	3.8	1.57	
3271	*52.3*	*34.5*	*6.9*	*1.4*	*n.d.*	*0.3*	*4.65*	α; G_2; (Pb);
	56.0	29.9	8.0	1.1	0.98	n.d.	3.67	
3272	*54.2*	*35.4*	*6.4*	*1.3*	*n.d.*	*0.1*	*2.52*	α; G_2; (Pb);
	54.7	33.5	8.7	0.9	n.d.	n.d.	2.30	
3273	*41.6*	*47.7*	*7.3*	*1.1*	*n.d.*	*0.1*	*2.14*	α; β; G_2; (Pb);
	52.2	34.6	10.0	0.8	0.32	n.d.	1.93	
3274	*53.0*	*37.5*	*3.1*	*1.6*	*0.36*	*0.7*	*3.67*	β; G_2
	50.3	39.5	6.0	0.9	0.49	n.d.	2.73	
3275	*41.0*	*52.6*	*4.9*	*1.1*	*n.d.*	*n.d.*	*0.39*	α; β
	54.7	40.3	4.2	0.7	n.d.	n.d.	n.d.	
3276	*47.2*	*46.0*	*5.4*	*0.6*	*n.d.*	*n.d.*	*0.65*	α; β
	54.3	38.8	5.7	0.3	0.26	n.d.	0.56	
3277	*51.7*	*39.2*	*5.7*	*1.1*	*n.d.*	*n.d.*	*2.15*	α; β
	56.2	37.1	4.7	0.4	n.d.	n.d.	1.60	
3278	*52.9*	*38.4*	*5.7*	*1.0*	*n.d.*	*0.4*	*1.50*	α; β; G_2
	54.3	39.1	4.1	0.6	0.74	n.d.	1.10	
X	*58.7*	*35.9*	*3.4*	*1.4*	*n.d.*	*n.d.*	*0.48*	β
	51.3	46.1	1.6	0.5	0.10	n.d.	0.20	

*0.97 wt.% Bi; +0.3 wt.% Bi;

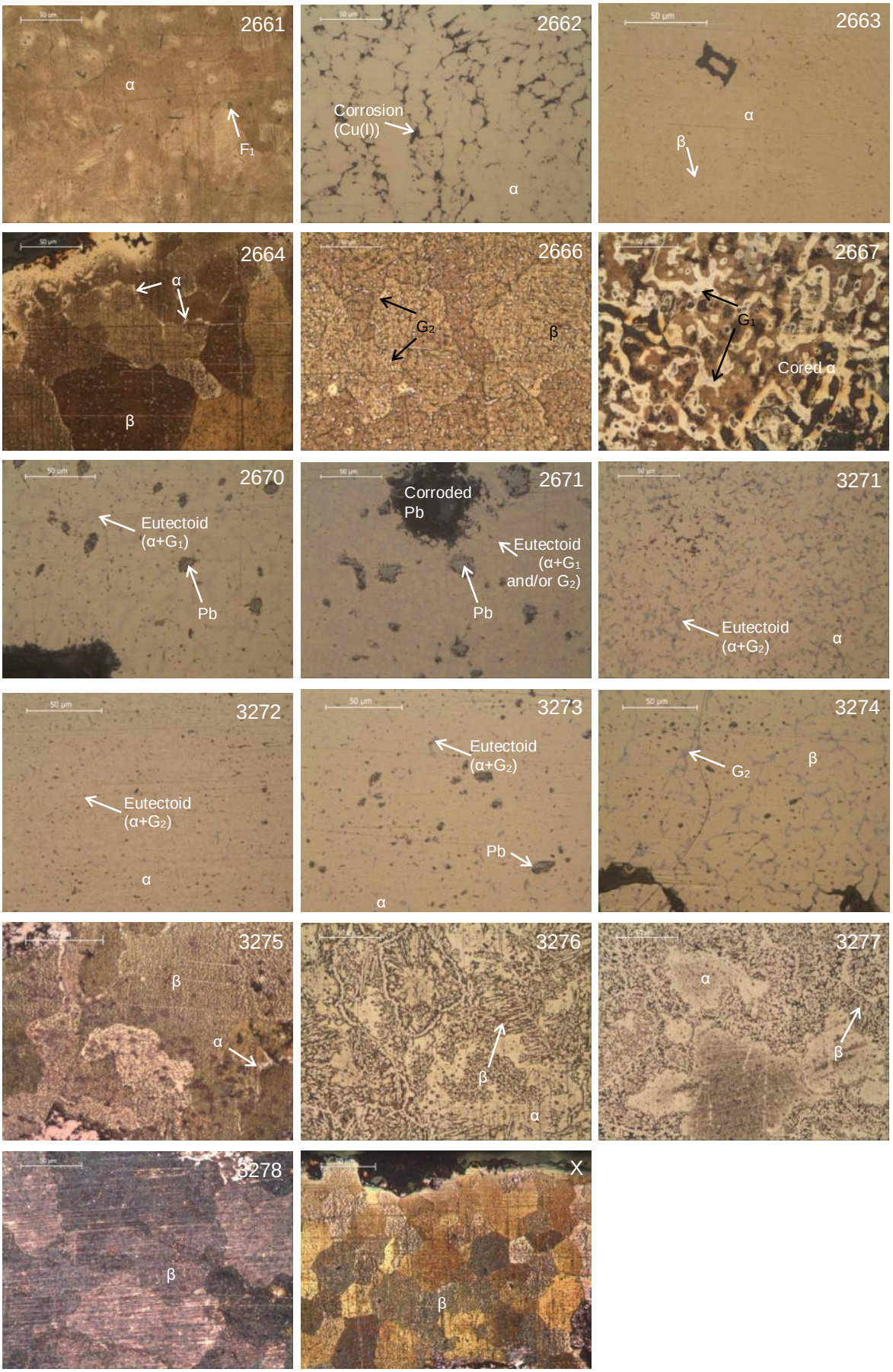

Fig. 2.37 Details of microstructures in the Chong Zhen coins (BF-OM, all etched except for #2662, #2663, #2670, #2671, #3271, #3272, #3273, #3274)

2.4.2. Qing dynasty coins (1644 – 1912 AD)

The Ming dynasty was overthrown in 1644 by Manchu rebels. Stability facilitated the cultural growth at least during some of the earlier reigns. During this dynasty, following the Ming dynasty practice, mint names appear in the reverse of the coins, in Chinese characters, Manchu or both, which makes possible provenance determination. The production method had a significant alteration as master cash (high quality positive moulds of cash coins) were introduced to perform the imprints, reducing the amount of unintentional variations in coin morphology [Burguer, 1976; Hartill, 2005].

As there was a copper shortage up until the 18th century, this metal was imported from Japan. After the 19th century, the Yunnan copper mines were fully exploited and cash coin production increased considerably. After that, copper shortage continued, creating an "intermittent and of poor quality" casting [Hartill, 2005]. As such, these shortages caused metal recycling to be frequently performed during this dynasty. Economic decline eventually settles due to the use of old money, the increasing counterfeiting of new money and the corruption of high-rank officials that lead to a spiralling deflation. Alloy composition was increasingly debased while maintaining face value, which made salaries and commodities inflate [von Glahn, 1996]: while in 1644, the official copper content was ~70%, in 1852 it had decreased to 54%.

Fig. 2.38 Map of China's Provinces during the Qing dynasty (adapted from Wikipedia)

2.4.2.1. Kang Xi Tong Bao (1662-1722 AD)

During this reign, the rule was finally secure and stability as well as economic growth occurred. Rebellions were appeased and Taiwan was finally conquered. Copper shortage made several mints close and re-open, but also caused a reduction in the official coin weight and in the copper content.

All six coins are 1-cash size.

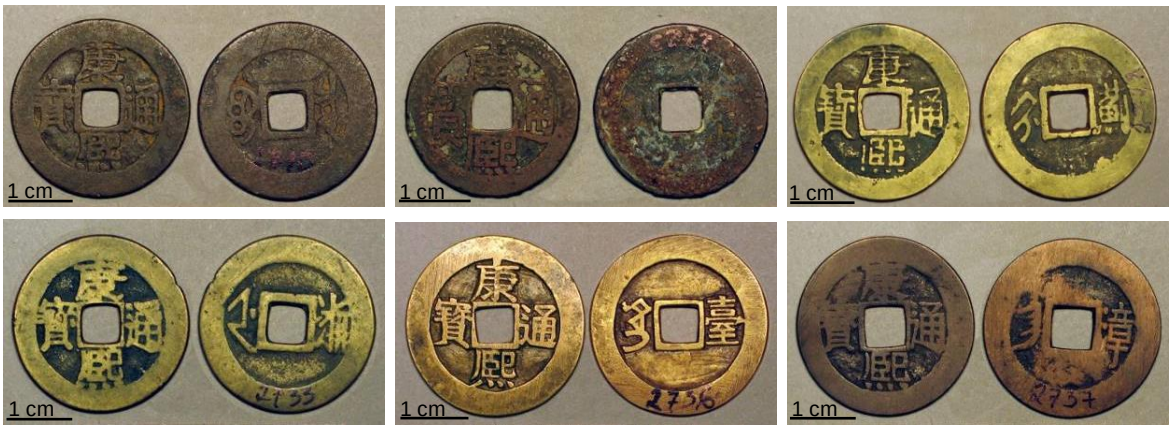

Fig. 2.39 Kang Xi Tong Bao coins (from left to right and top to bottom, ref.: #2710; #2723; #2728; #2733; #2736; #2737)

Other than coins #2723 and #2737, the Zn content ranges between ~24 and ~33 wt.%. The major element is still copper and minor elements are Fe and As, up to ~1 wt.% and Sn or Sb, up to ~2.5 wt.% and ~1.4 wt.% respectively. Pb can go up to ~14 wt.%.

Table 2.15 EDXRF results and microstructural observation of the Kang Xi coins. The values in italic are macro-EDXRF from the surface, while the remaining are micro-EDXRF from the cleaned metal edge.

Reference	Province (Mint)	Composition (wt.%) Cu	Zn	Pb	Fe	As	Sn	Sb	Observed Phases
2710	Beijing	*65.7*	*15.6*	*13.2*	*1.2*	*n.d.*	*3.4*	*0.89*	α; G_1; (Pb)
	(B. Revenue)	56.6	29.2	10.2	0.6	0.16	2.5	0.78	
2723	Hunan(?)	*54.0*	*43.0*	*1.5*	*1.3*	*n.d.*	*n.d.*	*n.d.*	β; γ
	(?)	46.9	51.6	0.4	1.0	n.d.	n.d.	n.d.	
2728	Zhili	*67.2*	*23.0*	*6.0*	*0.8*	*n.d.*	*2.0*	*1.00*	α; G_1; (Pb)
	(Jizhou)	65.1	24.0	7.2	0.6	0.24	1.8	0.93	
2733	Zhejiang	*64.6*	*24.0*	*6.4*	*0.8*	*n.d.*	*2.2*	*1.95*	α; G_1 and/or G_2; (Pb)
	(Hangzhou)	65.3	23.4	7.0	0.6	0.21	1.7	1.36	
2736	Taiwan	*63.2*	*32.4*	*2.3*	*0.8*	*n.d.*	*0.7*	*2.32*	α; G_1; F_1; (Pb)
	(?)	61.5	32.7	3.3	0.8	0.6	0.7	0.30	
2737	Fujian	*79.2*	*4.3*	*14.0*	*0.6*	*n.d.*	*1.8*	*n.d.*	α; G_1; (Pb)
	(Zhangzhou)	78.6	3.5	14.3	0.4	1.03	2.1	n.d.	

The microstructures are highly influenced by the minor elements present. Coin #2723 has Cu, Zn and a small Fe content, and is a common binary and biphasic β+γ structure. However, the remaining coins present secondary phases (light grey colour) probably related to the Sn and/or Sb contents. Pb is distributed along the interdentritic regions.

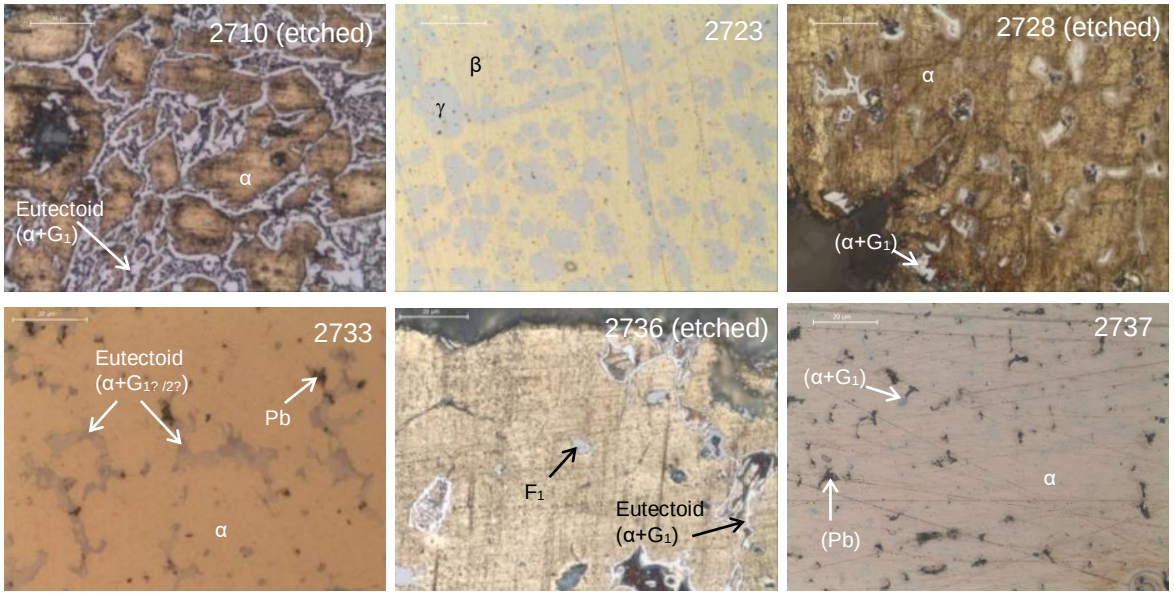

Fig. 2.40 Details of microstructures in the Kang Xi coins (in BF-OM, etched coins are signalled).

.

2.4.2.2. Qian Long Tong Bao (1736 – 1795 AD)

This was also a prosperous period for the arts and literature as well as for military purposes: Hartill considers it to be “the highest point of the dynasty”. During this 60-year reign, the mintage decrease due to Cu shortage except during the years the Yunnan mines were explored, reaching a peak of 3.7 million strings per year.

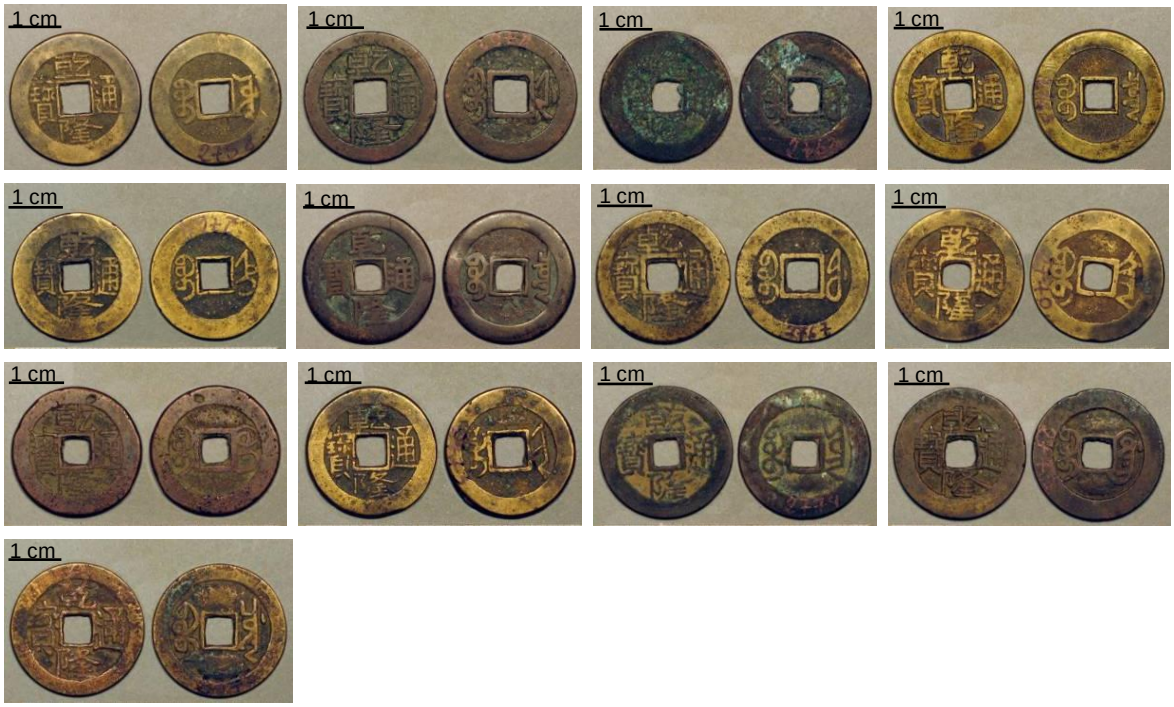

Fig. 2.41 Qian Long Tong Bao coins (from left to right and top to bottom, ref.: #2758; #2761; #2762; #2763; #2764; #2766; #2767; #2770; #2772; #2773; #2774; #2775; #2776)

All coins are 1-cash size.

Coin #2766 is larger and fits the characteristics of a Palace coin: “a larger coin”: Ø of ~27 mm, weighing 5-7 g; “their alloy a high quality brass composed of 60% Cu and 40% Zn”. These coins were introduced in 1752 for use in the Imperial Palace by the guards and eunuchs.

The Cu content has a variation range of ~20 wt.% (~47 to ~68 wt.%). Compositions seem to be independent of the original production mint: coins #2758, #2763 and #2766 have different elemental contents albeit being from the same region and probably the same mint. Furthermore, they are even from the empire’s capital, where content control was supposedly higher.

Table 2.16 EDXRF results and microstructural observation of the Qian Long coins. The values in italic are macro-EDXRF from the surface, while the remaining are micro-EDXRF from the cleaned metal edge.

Coin ref.	Province (Mint)	Composition (wt.%) Cu	Zn	Pb	Fe	As	Sn	Sb	Observed Phases
2758	Beijing	*53.8* 53.1	*34.3* 35.0	*8.0* 8.3	*0.9* 0.3	*n.d.* n.d.	*2.8* 2.9	*0.14* 0.30	α; β; G_1; (Pb)
2761	Zhejiang (Hangzhou)	*50.7* 49.8	*36.1* 36.8	*10.9* 12.0	*0.9* 0.6	*n.d.* n.d.	*1.3* 1.0	*n.d.* 0.15	α; β; (Pb)
2762	Hubei (Wuchang)	*42.8* 54.6	*45.6* 39.1	*10.5* 5.5	*0.9* 0.6	*n.d.* n.d.	*0.2* 0.2	*0.13* 0.14	α; β; (Pb)
2763	Beijing	*68.7* 68.2	*28.6* 30.0	*1.3* 0.8	*1.0* 0.5	*n.d.* 0.48	*n.d.* n.d.	*0.32* n.d.	α
2764	Zhili (Baoding)	*51.6* 53.9	*39.7* 38.3	*6.2* 6.1	*0.8* 0.3	*n.d.* n.d.	*1.6* 1.3	*0.10* 0.14	α; β; (Pb)
2766	Beijing	*66.2* 65.5	*31.4* 32.6	*1.0* 0.7	*0.4* 0.4	*0.4* 0.4	*n.d.* n.d.	*0.47* 0.34	α
2767	Fujian (Fuzhou)	*45.9* 46.9	*42.5* 41.3	*7.3* 6.6	*1.7* 1.8	*n.d.* 1.20	*2.5* 2.1	*n.d.* 0.19	β; G_1; F_2; (Pb)
2770	Shaanxi	*56.0* 55.3	*33.2* 35.0	*7.8* 7.0	*0.5* 0.3	*n.d.* n.d.	*2.4* 2.1	*n.d.* 0.15	α; β; G_1; (Pb)
2772	Guangxi (Guilin)	*53.9* 46.7	*39.2* 47.9	*5.2* 4.2	*1.6* 1.3	*n.d.* n.d.	*n.d.* n.d.	*n.d.* n.d.	β; γ; (Pb)
2773	Shanxi (Taiyuan)	*49.8* 53.7	*37.5* 38.1	*10.8* 6.6	*0.8* 0.3	*n.d.* n.d.	*1.1* 0.9	*n.d.* 0.14	α; β; (Pb)
2774	Yunnan (Yunnan-fu)	*45.9* 48.1	*47.6* 46.7	*4.5* 4.1	*1.5* 0.9	*n.d.* n.d.	*0.4* 0.4	*n.d.* n.d.	β; G_1; F_1; (Pb)
2775	Guangdong (Guangzhou)	*53.4* 49.6	*41.6* 45.0	*3.9* 4.7	*0.9* 0.5	*n.d.* 0.17	*n.d.* n.d.	*0.11* n.d.	β; (Pb)
2776	Sichuan (Chengdu)	*60.1* 58.8	*31.4* 32.5	*7.4* 8.0	*0.8* 0.2	*n.d.* n.d.	*n.d.* 0.2	*0.26* 0.23	α; β; (Pb)

Microstructurally, although α is still the predominantly main phase, the number of coins with α+β structures or main β phase is increasing comparatively to the previous reign, undoubtfully due to the higher Zn content in these coins, perhaps due to the previously mentioned Cu scarceness. The presence of the γ phase can be associated to the small Sn or Sb contributions to these alloys, as previously mentioned (section 2.3.2).

Also in this group of coins, more specifically in coin #2767, an unexpected dark-grey phase appears, next to the light-grey gamma phase, G_1. Elemental analysis (SEM-EDS) of this phase revealed it to be Fe,As-rich. This phase will be referred to as F_2 because it should be the iron arsenide (Fe_2As), found in this and other coins from subsequent reigns. This will be further explained in Chapter 3.

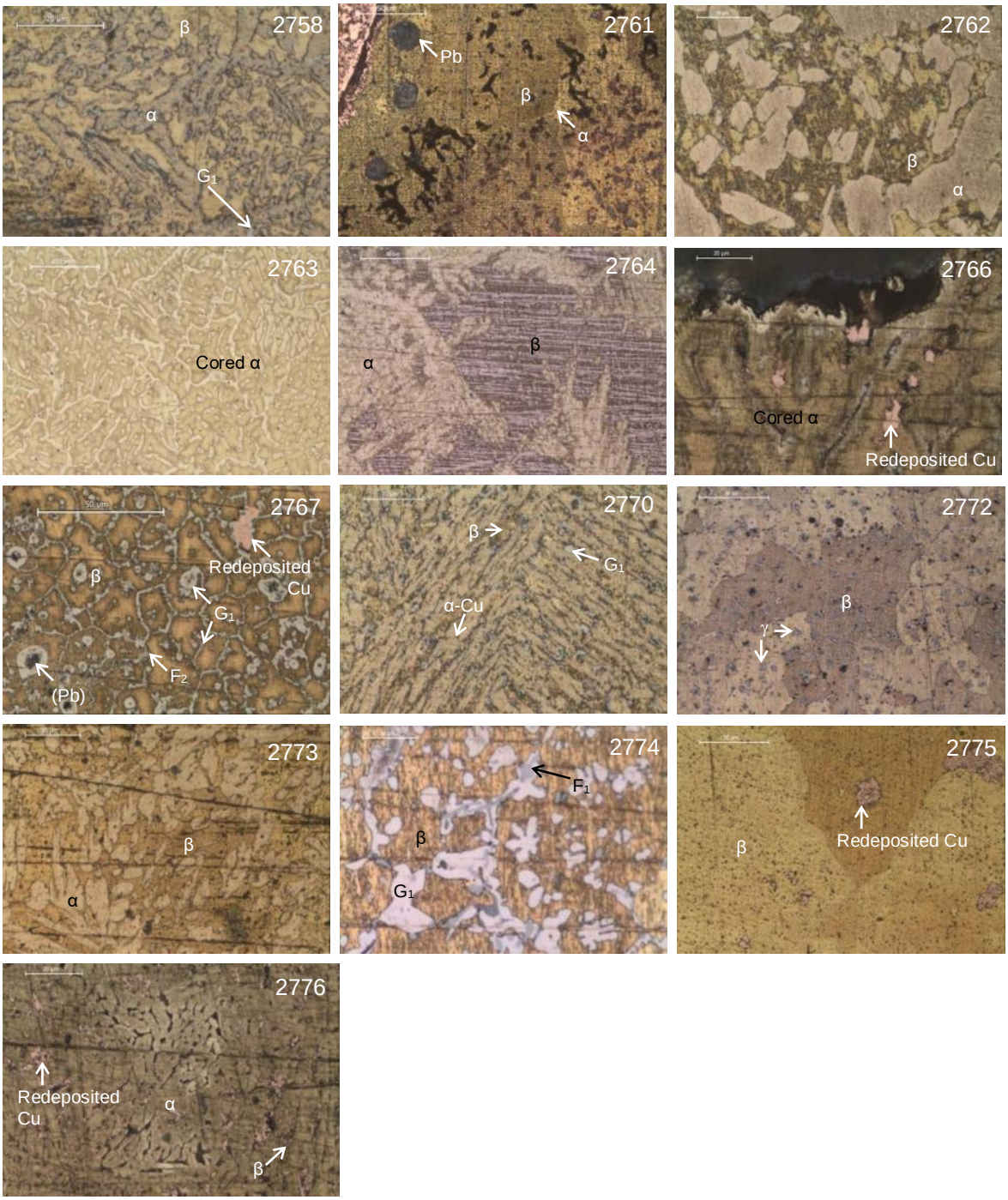

Fig. 2.42 Details of microstructures of the Qian Long coins (in BF-OM, etched)

2.4.2.3. Jia Qing Tong Bao (1796 – 1820AD)

After several years of food shortage, the high-numbered population and the internal conflicts had weakened the empire. The coin debasement had made it urgent to reform the coinage and in 1796 both Peking and the provincial mints issued good quality brass coins with 60-40% Cu-Zn. Over time, the alloy changed to 54% Cu, 43% Zn and 3% Pb [Hartill, 2005].

Very few coins of this group respect the 60-40 Cu-Zn established composition, they are however closer to the 54-43-3 Cu-Zn-Pb composition, although with higher Pb content (up to 10 wt.%) and

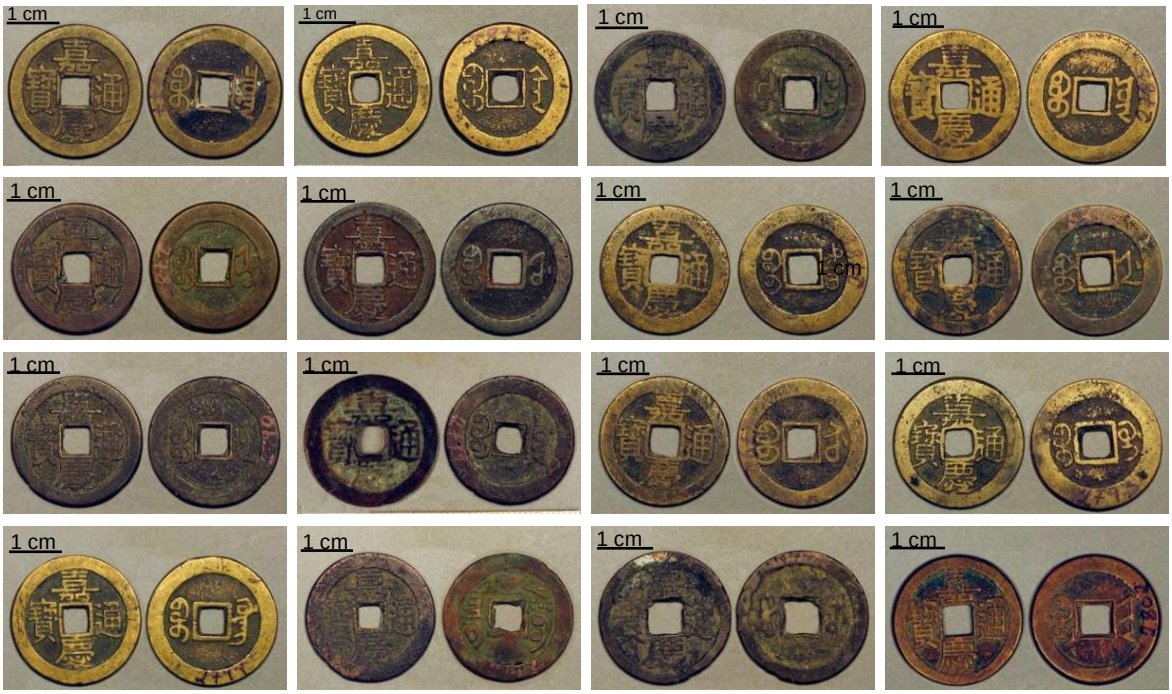

Fig. 2.43 Jia Qing Tong Bao coins (from left to right and top to bottom, ref.: #2777; #2782; #2783; #2785; #2786; #2787; #2788; #2789; #2790; #2791; #2792; #2793; #2794; #2796; #2799; #2802)

Table 2.17 EDXRF results and microstructural observation of the Jia Qing coins. The values in italic are macro-EDXRF from the surface, while the remaining are micro-EDXRF from the cleaned metal edge.

Reference	Province (Mint)	Composition (wt.%) Cu	Zn	Pb	Fe	As	Sn	Sb	Observed Phases
2777	Beijing	*59.3* 64.4	*33.7* 30.1	*2.7* 2.4	*1.6* 1.0	*0.39* 0.65	*n.d.* n.d.	*2.19* 1.26	α; G_2; (Pb)
2782	Shaanxi	*49.3* 52.9	*34.2* 37.4	*11.6* 6.6	*2.6* 1.5	*0.87* 2.7	*0.3* n.d.	*1.14* 1.06	α; β; G_2; (Pb); F_1 and/or F_2
2783	Jiangxi	*46.8* 46.8	*43.9* 42.9	*6.8* 7.0	*1.9* 1.8	*n.d.* 1.56	*0.3* n.d.	*n.d.* n.d.	β; (Pb); F_2
2785	Yunnan (Yunnan-fu)	*54.0* 52.3	*31.8* 30.8	*7.6* 9.7	*2.1* 2.3	*0.55* 1.57	*n.d.* n.d.	*3.64* 3.30	α; G_2; (Pb); F_1; F_2
2786	Zhili (Baoding)	*54.0* 59.0	*42.8* 39.1	*1.7* 1.4	*1.3* 0.5	*n.d.* n.d.	*n.d.* n.d.	*n.d.* n.d.	α; β
2787	Fujian (Fuzhou)	*67.1* 55.2	*17.0* 34.4	*11.6* 7.1	*3.3* 1.6	*0.3* 1.01	*0.5* 0.5	*0.20* n.d.	α; β; (Pb); F_1; F_2
2788	Yunnan (Dong Chuan)	*54.5* 55.1	*34.9* 35.8	*8.8* 7.6	*1.6* 1.4	*n.d.* 0.20	*n.d.* n.d.	*n.d.* n.d.	α; β; (Pb)
2789	Zhejiang (Hangzhou)	*49.6* 51.3	*39.0* 36.9	*8.6* 8.8	*1.9* 1.7	*n.d.* 0.55	*0.8* 0.8	*n.d.* n.d.	α; β; (Pb); F_1
2790	Henan (Kaifeng)	*52.4* 53.8	*37.3* 38.0	*8.6* 6.8	*0.8* 0.1	*n.d.* 0.59	*n.d.* n.d.	*0.76* 0.55	α; β; G_2; (Pb)
2791	Sichuan (Chengdu)	*44.0* 43.7	*49.7* 50.8	*4.7* 4.4	*1.6* 1.2	*n.d.* n.d.	*n.d.* n.d.	*n.d.* n.d.	β; γ; (Pb)
2792	Jiangsu (Suzhou)	*51.2* 53.6	*36.9* 34.1	*8.5* 6.6	*1.5* 0.8	*1.30* 4.05	*n.d.* n.d.	*0.46* 0.42	α; β; G_2; (Pb); F_2; D_1
2793	Guangxi (Guilin)	*49.9* 53.2	*30.3* 31.4	*14.9* 10.0	*0.7* 0.3	*n.d.* 1.70	*n.d.* n.d.	*4.07* 3.37	α; G_2; (Pb); D_1?
2794	Guangdong (Guangzhou)	*59.5* 56.1	*33.6* 34.7	*4.9* 7.0	*1.0* 0.8	*0.47* 1.14	*0.2* n.d.	*0.15* n.d.	α; β; (Pb); F_2
2796	Guizhou (Guiyang)	*47.8* 45.6	*48.4* 52.0	*1.9* 0.7	*1.9* 1.5	*n.d.* 0.13	*n.d.* n.d.	*n.d.* 0.13	β; γ
2799	Hubei (Wuchang)	*30.0* 43.2	*62.9* 49.5	*5.2* 5.3	*1.6* 1.4	*n.d.* 0.18	*n.d.* n.d.	*0.21* 0.27	β; γ; (Pb)
2802	Shanxi (Taiyuan)	*62.5* 61.8	*33.2* 32.7	*3.4* 4.8	*0.7* 0.4	*n.d.* n.d.	*n.d.* 0.3	*n.d.* n.d.	α; β; (Pb)

lower copper content. These coins seem to have no Sn, which seems to have been substituted by Sb, when present. Three coins also present an As content above 1 wt.%, and Fe contents also usually above this value.

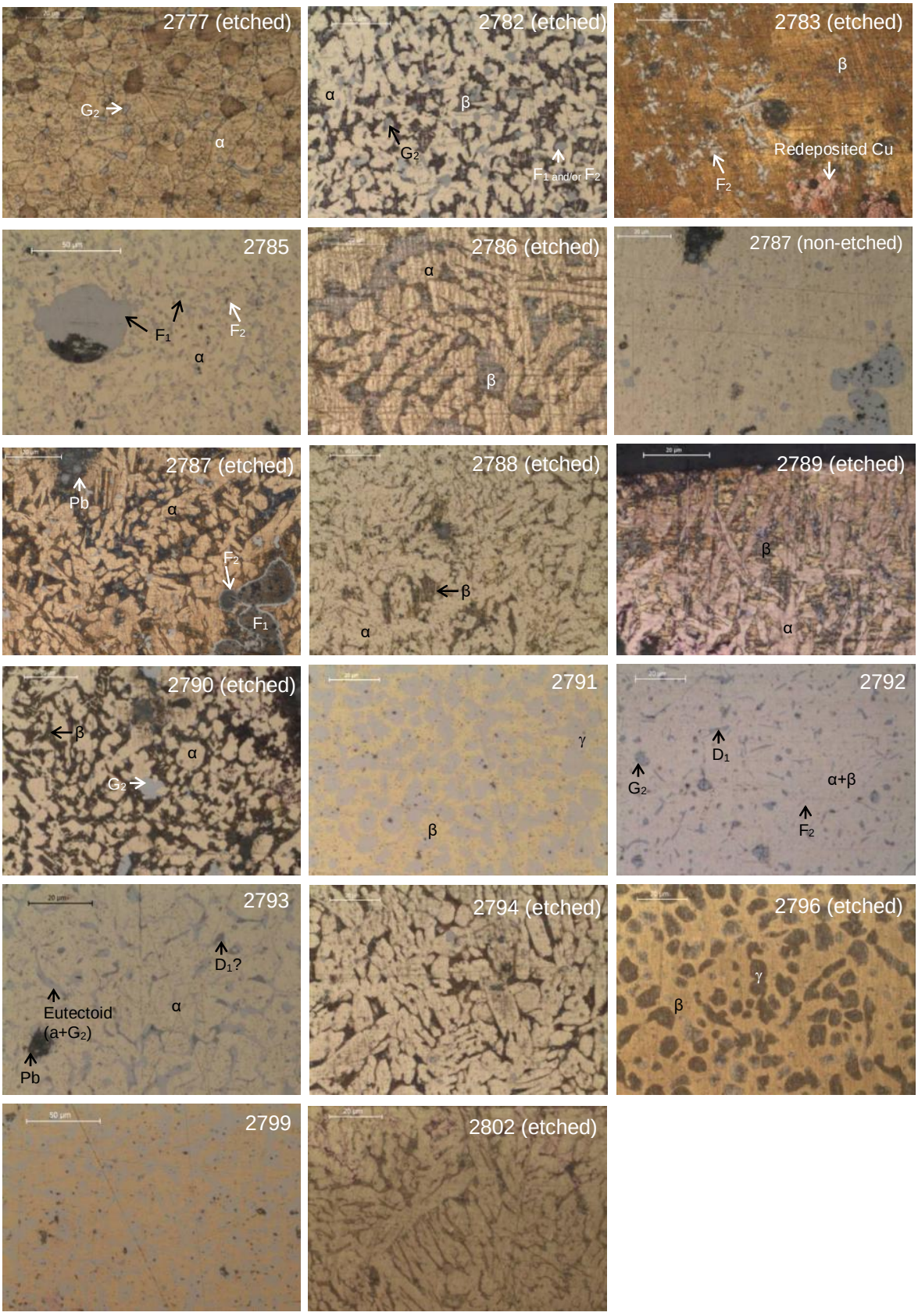

Fig.2.44 Details of microstructures of the Jia Qing coins (in BF-OM, etched coins are signalled)

Due to higher Zn contents in these coins, β, γ and/or G_2 phases are present in all structures. The G_2 phase seems to be associated with the presence of Sb in the alloy, as well as with the higher Zn contents in these coins. This reign group also presents Fe and As rich phases, in grey colour, detected by SEM-EDS. The iron-rich phase (F_1) seems to have been primarily formed, due to its dendritic shape (see Fig. 2.44, coin #2783), while the Fe,As-rich phase (F_2) seems to be mainly of interdendritic formation (see Fig. 2.44, coin #2782) or a solid state precipitation around the F_1 phase (see Fig. 2.44, coin #2787), with ~1 μm thickness.

2.5. Copper coins

Several coins of the Qing dynasty were found to be of almost pure Cu (see Table 2.18). This phenomena occurs especially after the beginning of the exploration of the copper mines in Yunnan [Tsu-yu, 1991; Golas, 1999], as Hartill states in his "*Cast Chinese Coins*" [2005] about the Qianlong reign: "*At the beginning of the reign there was a shortage of cash, but as more and more copper became available from the Yunnan mines, casting rapidly increased, both in Beijing and in the provinces.*"

All the ~99 wt.% Cu coins found in this collection are from the Xinjiang region (Northwest China), conquered in 1759. Minting began shortly after, acquiring the established regional habit of using pure Cu (as in native *pul* coins). These coins were called *hong qian* (red cash), due to their reddish color from the high Cu-content. This difference in composition occurred due to the difficulty of obtaining Zn in this province. Two of the coins (#2771 and #2779) are attributed to 1736, but they are probably posthumous issues of the Qian Long coins, ordered by the successor of Emperor Qianlong, Jiaqing [Hartill, 2005].

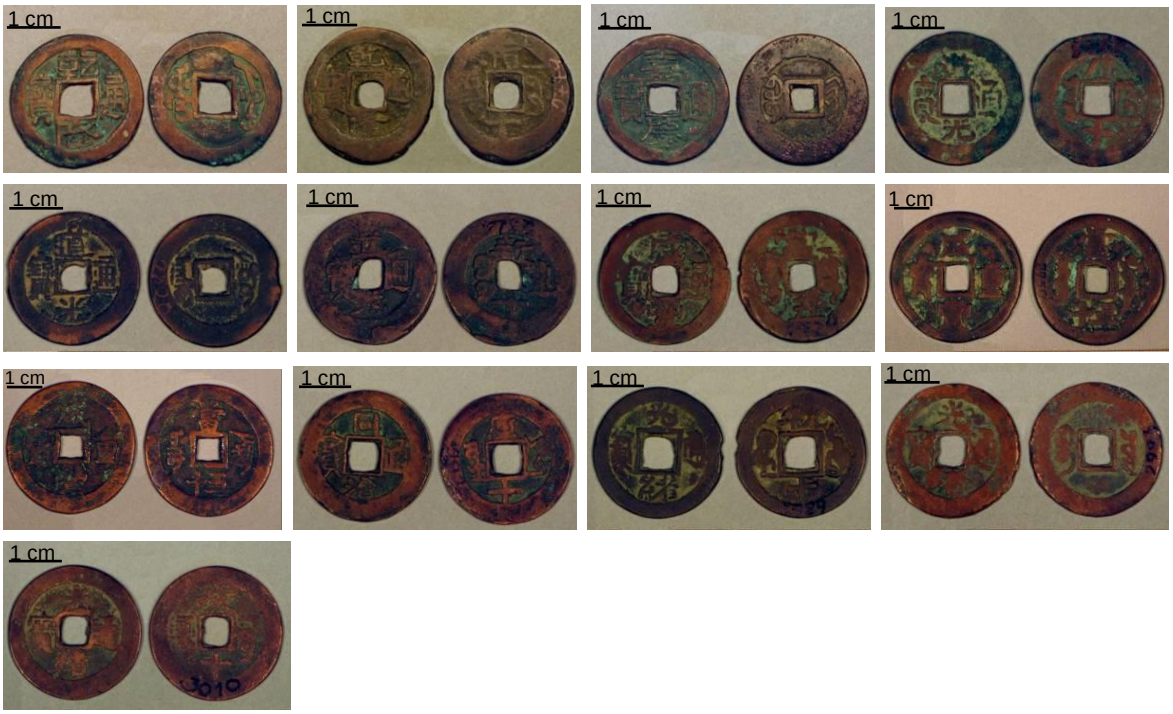

Fig. 2.45 Copper-rich coins from the Qing Dynasty (from left to right and top to bottom, ref.: #2771; #2779; #2797; #2818; #2820; #2826; #2924; #2950; #Y; #2970; #2989; #2993; #3010)

Coin #2924 is a 5-cash size. Coins #2779, #2818, #2826, #2970 and #3010 are 10-cash size. Coins #2950 and Y are 50-cash size, and the remaining coins are 1-cash size.

Composition is nearly 100% Cu, sometimes with trace amounts of Zn, Pb or Fe. Only three coins (#2771; #2779 and #2797) were chosen to perform edge polishing. They all show similar elemental composition and a dendritic α structure with gray inclusions at the interdendritic regions. SEM-EDS analysis determined these inclusions to be Cu,S-rich (C_1 phase). The remaining coins also present similar compositions, except for #2826, that shows a Fe superficial enrichment on the surface (this could be attributed to soil contaminations during burial).

Table 2.18 EDXRF results and microstructural observation of the copper coins. The values in italic are macro-EDXRF from the surface, while the remaining are micro-EDXRF from the cleaned metal edge.

Ref.	Name	Date	Province (Mint)	Composition (wt.%) Cu	Zn	Pb	Fe
2771	Qian Long Tong Bao	1736?	Xinjiang (Ushi)	*99.3*	*0.2*	*n.d.*	*0.3*
				99.5	n.d.	0.2	0.1
2779	Qian Long Tong Bao	1736?	Xinjiang (Aksu)	*99.4*	*0.2*	*n.d.*	*0.3*
				99.5	n.d.	n.d.	0.1
2797	Jia Qing Tong Bao	1796	Xinjiang (Aksu)	*99.4*	*0.2*	*n.d.*	*0.3*
				99.6	n.d.	n.d.	n.d.
2818	Dao Guang Tong Bao	1821	Xinjiang (Kucha)	*99.0*	*0.2*	*n.d.*	*0.6*
2820	Dao Guang Tong Bao	1821	Xinjiang (Aksu)	*99.3*	*<q.l.*	*n.d.*	*0.4*
2826	Dao Guang Tong Bao	1821	Xinjiang (?)	*96.2*	*0.22*	*0.28*	*3.1*
2924	Xian Feng Tong Bao	1854	Xinjiang (Aksu)	*99.2*	*n.d.*	*0.23*	*0.3*
2950	Xian Feng Zhong Bao	1854	Xinjiang (Yarkand)	*98.4*	*0.41*	*0.76*	*0.3*
Y	Xian Feng Zhong Bao	1854	Xinjiang (Aksu)	*99.1*	*<q.l.*	*0.22*	*0.4*
2970	Tong Zhi Tong Bao	1862	Xinjiang (Kucha)	*99.3*	*0.2*	*n.d.*	*0.4*
2989	Guang Xu Tong Bao	1875	Xinjiang (Kucha)	*98.4*	*<q.l.*	*0.49*	*0.7*
2993	Guang Xu Tong Bao	1875	Yunnan (Yunnan-fu)	*99.1*	*0.20*	*n.d.*	*0.5*
3010	Guang Xu Tong Bao	1875	Xinjiang (Kashgar)	*99.3*	*0.20*	*n.d.*	*0.4*

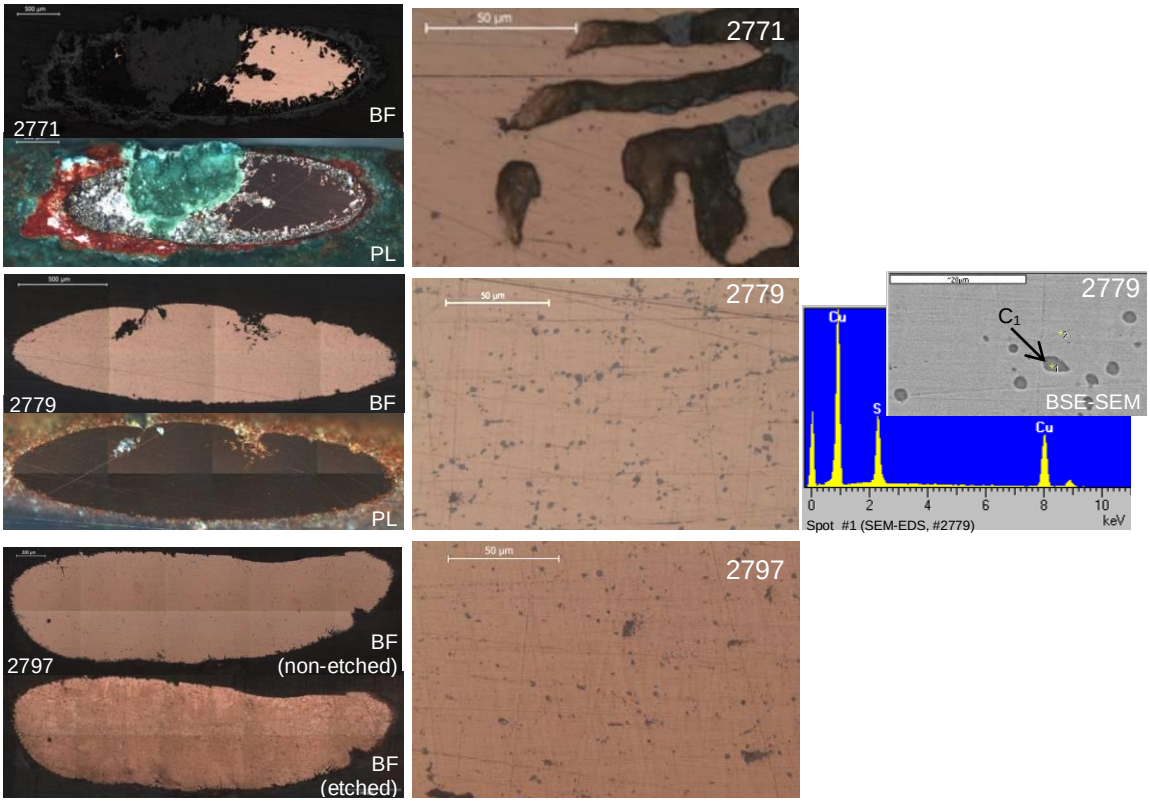

Fig. 2.46 OM images of the cleaned sections and details of the copper-rich coins #2771, #2779 and #2797. Detail of coin #2779 in SEM-BSE: inclusions consist of Cu and S (spectra of spot #1).

Corrosion seems to develop intergranularly and in coin #2771 it is visible the red cuprite layer next to the metal and then a green carbonate outside layer. The central area is also attacked and micro-XRD found chloride corrosion compounds as atacamite, nantokite and paratacamite: this topic will be discussed in Chap. 4.

2.6. General Remarks

The results permitted to group the analysed coins in 3 categories according to their main elements: bronzes, brasses and coppers. Up until the 16th century, most coins were cast in high-leaded bronze, and after that, almost always in brass alloy or pure copper (the later, a regionalism in *Xinjiang* province during the late Qing dynasty). The other main elements found were tin, lead or zinc. Tin and/or antimony were also found as minor elements in brass coins after the 16th century; and Pb reached its peak use during the 12th and 13th century.

Macro-EDXRF analysis shows a superficial enrichment in Pb and Sn in bronze coins, and a superficial enrichment in Zn in brass coins with lower Sn values. Pb is the only element that shows a large variation within the obverse and reverse of the same coins, which can be related to its globular distribution.

Micro-EDXRF of several cleaned areas allowed verification of the representativeness of the clean edge areas, from where OM observations were also obtained. Minor elements found were Fe, Ni, Zn (in bronzes), Sn and Sb (in brasses), As and Bi. Iron and niquel are present in almost every coin and Fe reaches a higher content in bronze coins. Optical microscope observations corroborated the production process of sand casting and showed the fine structures with grain size ranging from 5 to 100 micron, and also evidence of little to no post-production work. Elemental composition and microstructure varies within the same reign, dynasty and province, showing a range of contents that diverge from the officially established alloys.

Bronze coin microstructures are tipically α or α+δ eutectoid, with other phases like (Pb); F_1 (ferrite?); C_1 (chalcocite?); B_1 (bornite?); or D_1 (domeykite?). Brass coins microstructures can present α, α+β, β, β+γ and α+G_n (Sn and or Sb-rich) main phase combinations. The hypothesis of a γ-brass phase formation due to Sn or Sb additions will be analysed in the next chapter. Brass coins also exhibit other phases as (Pb); D_1 (domeykite?); F_1 (ferrite?) and F_2 (iron arsenide?). Almost pure copper coins usually present an α structure and copper sulphide inclusions, C_1 (chalcocite?).

3.1. Effects of the presence of other elements in copper alloys

The other main elements in most of the studied copper based coins are Sn, Zn and Pb. So, for bronze coins the main alloying elements are Cu, Sn and Pb; and for brasses, Cu, Zn and sometimes Pb. As Pb is almost immiscible in copper phases, including in bronze and brass phases, the interpretation of its microstructural effects will be considered separately. Considering bronze coins, minor/trace elements are Fe, Ni, Zn, As and sometimes Sb or Bi, mostly derived from ore impurities or metal recycling.

When considering brasses, the minor elements are also Fe, Ni, As as well as Sn and Sb. Alloy compositions are very variable even within the same reign period (as the SD values in Fig. 3.1 indicate). In addition to a complex composition, the fine and uncommon phase constitution makes it much more difficult to interpret the microstructures. Elemental association between Sn-Sb and Fe-As are present in brass coins, and each pair exhibits similar microstructural effects. This elemental association leads to an important simplification in microstructural interpretations.

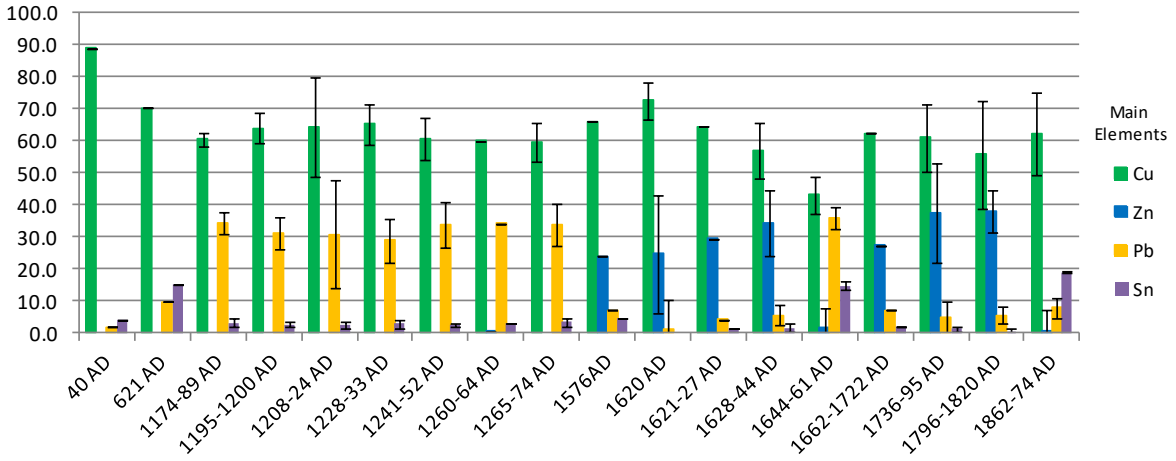

Fig. 3.1 Micro-EDXRF average results and SD error bars for the main elements (for 108 from the 109 analised coins: the 109th is an archaeological find of unknown date).

Elemental composition agrees with the analysis performed on other Chinese cash coins collections [Sano and Tominaga, 1982; Notsu and Mabuchi, 1979; Cowell *et al.*, 2005a; Misner and Benvenuto, 2007; Lei *et al.*, 2003]: until the 16th century, the main alloy was bronze and after that brass became the mostly used alloy although there are sporadic bronze issues (see 1644-61 AD and 1862-74 AD in Fig. 3.1). Out of the 109 bulk analysed coins, Table 3.1 synthesizes the types of alloy present (iron, nickel and lead were ignored because they exist in every coin). While the As content may have been unintentional (derivative of copper ore smelting) rarely surpassing 1 wt% until the end of the 18th century, after that it seems to have been more common, reaching up to 4 wt%. Looking at Table 3.1, it is noticeable that compositions of both bronze and brass alloys used for minting cash coins can vary substantially and only rarely are binary alloys. In the studied coins,

at least 6 different alloys were found for bronzes and 8 for brasses: even within each type, compositions are not constant. There can be up to 5 and 6 alloying elements (and this is disregarding Fe and Ni, always present in higher or lower values in these coins) simultaneously, which can render the microstructure quite difficult to interpret.

Table 3.1. Elements present in the 109 cleaned and analysed coins (3 of them are pure coppers and were not accounted for; elements between brackets are present in small amounts, <1 wt.%)

Bronzes	*Nº of coins*
Cu+Sn	3
Cu+Sn+(As)	34
Cu+Sn+(Sb+As)	2
Cu+Sn+(Zn+As)	3
Cu+As+(Sb)	1
Cu+Sn+As	1

Brasses	*Nº of coins*
Cu+Zn	8
Cu+Zn+(Sn)	5
Cu+Zn+(Sb)	2
Cu+Zn+As	7
Cu+Zn+Sn+(As)	6
Cu+Zn+Sb+(As)	16
Cu+Zn+(Sn+Sb)	8
Cu+Zn+(As+Sn+Sb)	10

Iron, nickel and lead were present in all the coins. Iron and lead will be discussed during this chapter due to the effects they promote in the microstructures. Nickel is totally soluble in Cu, with no visible effects in the microstructures, as displayed by the Cu-Ni equilibrium phase diagram (see Appendix IV, Fig. IV.1) and is a minor element reaching up to 0.36 wt.% in the alloy. Therefore it will not be further discussed.

3.1.1. Microstructural influence of Pb[15]

Lead seems to have a preponderant place in Chinese coinage, especially before the transition from bronzes to brasses [Bowman *et al.*, 2005]. Misner and Benvenuto [2007] found that there is certainly more lead present in these coins than the amounts actually required to achieve lower working temperatures for molten alloys.

This element is almost immiscible in copper, as shown by the Cu-Pb equilibrium phase diagram (see Fig.3.1) and also with other metals, such as Fe, As, Sn or Sb; therefore, during cooling, Pb is segregated into a Pb-rich liquid (L_2):

- For hypomonotectic alloys (Pb < 36 wt.%), due to primary α-Cu solidification and the monotectic decomposition ($L_1 \rightarrow$α-Cu+L_2), L_2 should be segregated into the interdendritic regions forming Pb-rich globules;
- In hypermonotectic alloys (36 wt.% < Pb < 87 wt.%), before solidification begins, two immiscible liquids (L_1+L_2) are formed. While this larger fraction of Pb-rich liquid, L_2, should give rise to the formation of larger Pb globules, the L_1 will form the previously described hypomonotectic structure.

[15] Part of the results presented in this section was presented as an oral communication: M.J.Furtado, M.F.Araújo, R.J.C.Silva - *Pb in Ancient Chinese Cu-based Coins: a multi-analytical survey*. EXRS 2010, Figueira da Foz (Portugal), June 2010.

For both types of alloys, at lower temperature (328 ºC), L_2 solidifies in 99.9 % Pb eutectic [Cao and Wei, 2002].

Chase [1994] writes: "*Lead does not really affect the solidification structures; since it does not go into solution in copper, it remains in globules, which can be small and well distributed in low-lead bronzes or large and irregular in highly leaded bronzes. Some of the Chinese bronzes contain more than 50% lead. These have usually been solidified rapidly; the highly leaded alloys were used for casting objects such as coins, which could be cast thin (for rapid solidification) and which did not require good physical properties (…).*"

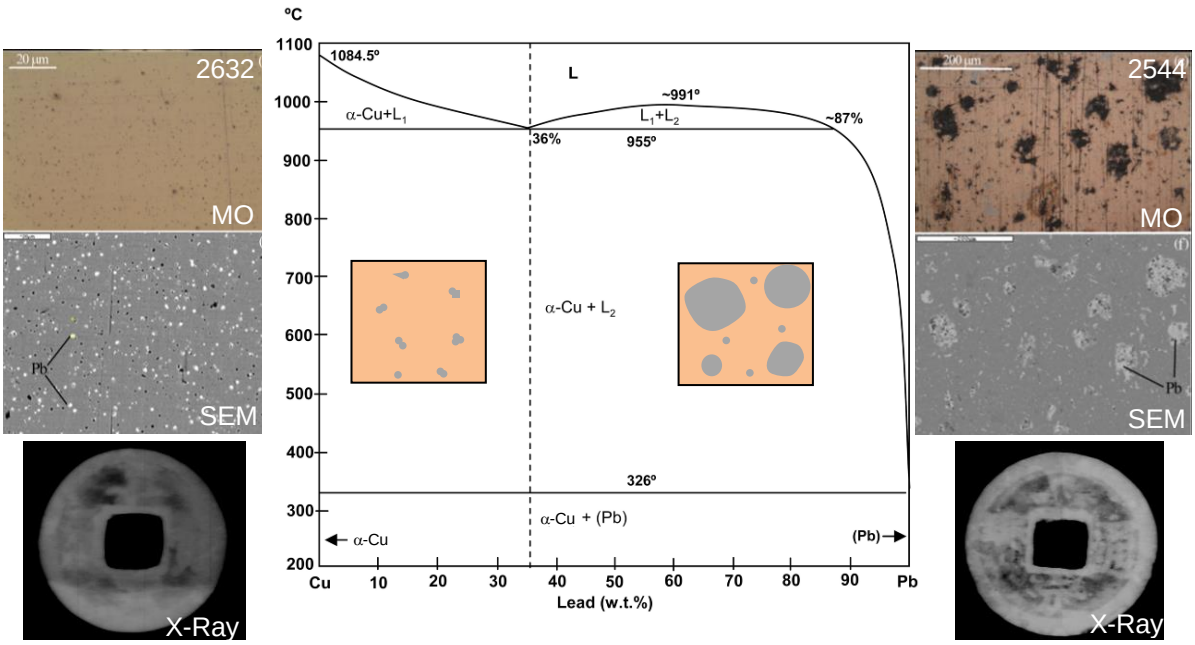

Fig. 3.1 Cu-Pb equilibrium phase diagram (adapted from Metals Handbook 3: Alloy Phase Diagrams, ASM, 1980) and examples of a hypo and a hypermonotectic alloy (coins #2632 and #2544, with 2 and 55 wt.% Pb respectively).

Those general descriptions are in agreement with our microstructural observations:

- For lower Pb hypomonotectic alloys, the Pb-rich phase in the coins is disperse throughout the α-Cu matrix in small interdendritic globular forms. In the case of higher Pb contents, ~14 wt.% up to ~30 wt.% Pb, larger irregular globules are also observed (these globular morphologies were also experimented by Wang and Ottaway [2004] and reported by Lei *et al.* [2003]), some of them revealing an interdentritic morphology (according to Martyushev [2010], "as Pb crystallizes last, the Pb-rich phase takes the form of the surrounding copper dendrites").
- For hypermonotectic alloys, very large round-like globules (up to 500 µm in diameter) are observed, as seen in Fig. 3.2 (a). Those larger globules often show important fractions of dendrites or globular α-Cu phase and Cu-S inclusions inside them, as Fig. 3.3 exemplifies (SEM-EDS spots #3 & #1, respectively).

These are a consequence of L_1 fractions being “trapped” in the Pb-rich liquid (L_2), resulting in a “globule-inside-globule” type structure (as stated by Cao and Wei [2002], the α-Cu that segregates from L_2 is often located around the inner edge of the Pb-rich globule). Meanwhile, L_1 fractions decompose into a monotectic α-Cu+L_2, which contribute to a higher level of chemical heterogeneity in the coins.

Digital X-ray radiography was performed on 20 Southern Song bronze coins (micro-EDXRF results show an average Pb content of ~33 wt%) and on 14 Ming and Qing brass issues (average Pb content of ~6 wt.%). The radiographic images show that the Pb-rich phase is consistently distributed throughout the coin: the large globules are clearly visible (white spots), while small globule sizes (not very distinguishable by this technique) seem to give an homogeneously blur image, especially in low-leaded coins (see Appendix VIII). They are, however, even if not clearly noticeable by OM, discernible by SEM observations (see images of coin #2632 in Fig.3.1). This

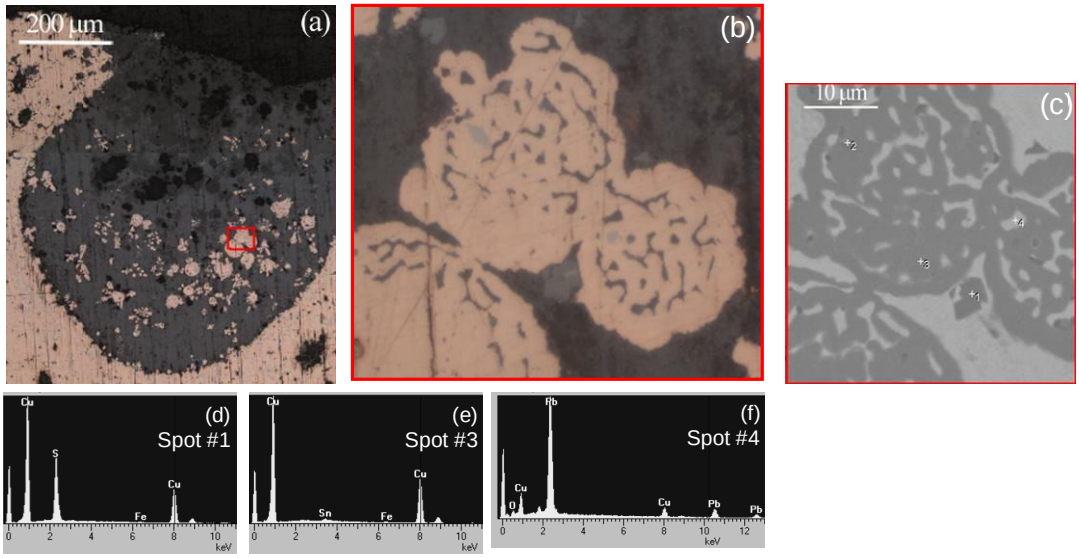

Fig. 3.2 Coin #2544 (55 wt.% Pb): (a) detail of a Pb globule (BF-OM); (b) detail of (a) (BF-OM); (c) BSE-SEM of (b); (d), (e), (f): EDS spots in (c).

homogeneous distribution of the Pb-rich phase is explained by Campbell [2003]: although Pb has a higher density than the other alloying elements, its distribution is free from gravitational influence due to the convection movements during solidification. As Pb has a lower melting point than Cu, it remains liquid while Cu phases are already solid. This annuls the effect of its density in its distribution. The absence of Pb gravitational segregation may also be caused by fast solidification due to the coins thin thickness.

The existence of significant deep transglobular corrosion in large globules (see EDS spot #4 in Fig. 3.2(c): Pb & O) makes the current Pb content assessment below the original value in some of the lead rich coins. This underestimation explains why some coins, that exhibit a typical hypermonotectic structure, have an average Pb content <36 wt.% by micro-EDXRF. A morphological assessment was performed on a set of 20 Pb-rich coins using an image analysis software, Image J (version 1.43u [Rasband, 2011]). This software allowed the determination of the fraction areas originally occupied by Pb-rich globules (including corroded regions inside each

globular form, Fig. 3.2). Using those fraction areas and taking into account the phase densities of α-Cu and (Pb), a higher average Pb content was confirmed (~50 wt.%), comparatively to the average value (~33 wt.%) obtained by micro-EDXRF performed on the same areas, as shown in Fig. 3.3. In the same figure it is also clear that the Pb contents obtained by EDXRF of the coins surface are usually above the values obtained from the micro-EDXRF from the cleaned section. Therefore, when dealing with coins with such high Pb contents, the elemental analysis but also the microstructural observation of these analysed areas are important in achieving an accurate interpretation.

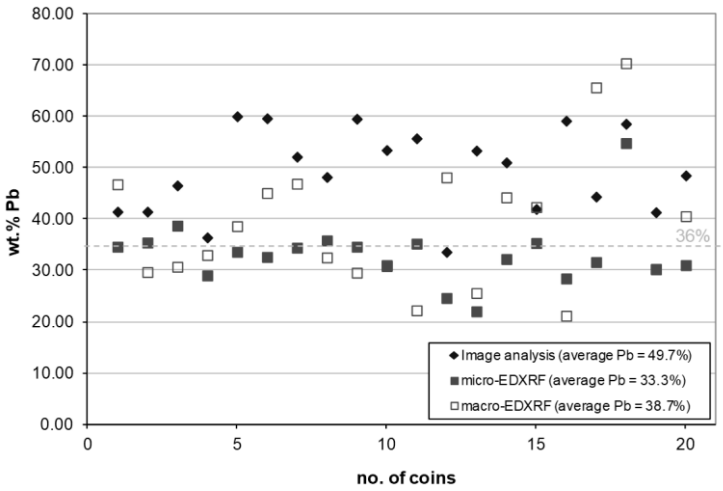

Fig. 3.3 Pb average content of 20 high-leaded coins obtained through image processing and micro-EDXRF of the observed cross-sections and macro-EDXRF from the coins surfaces.

3.1.2. Microstructural influence of Sn[16]

Tin is present in the studied collection, especially in coins earlier to the 16th century, in values ranging between 1.4 - 5.1 wt% (exception made for coins #2242 with ~15 wt.% and #2977 with 10 wt.%, the only ones presenting eutectoid, α-Cu + δ-Cu_4Sn). In brass coins from the 16th to 18th century, tin values ranged between 0 - 3.5 wt.%, with two exceptions: #2653 and #2704, ~5 wt.% Sn. Concerning brass coins, as shown in Chapter 2 (see Fig. 2.11), looking at the Cu-Zn phase diagram for contents above ~49wt.% Zn there is formation of a γ phase, (Cu_5Zn_8) [Predel, 1994b] (see Fig. 3.4, coin #2723).

Observing the zinc content of two brass coins, #2763 and #2710 (Fig. 3.4), one would expect to obtain the same phase constitution. However, the presence of Sn in the later coin seems to promote the formation of a light grey G_1 phase that precipitates at grain boundaries of the previous solid phases. SEM-EDS of α-Cu and G_1 phase in coin #2710 showed their Zn content was almost the same (~29 wt.%) but the G_1 phase was 4 times richer in Sn than α-Cu phase (from 1.7 to 7.6

[16] Part of the results presented in this section were published as: M.J.Furtado, R.J.C.Silva, M.F.Araújo, F.M.Braz Fernandes *Composition and microstructure of imperial brass Chinese coins*. Materials Science Forum, Vols. 636-637 (2010) pp.531-537.

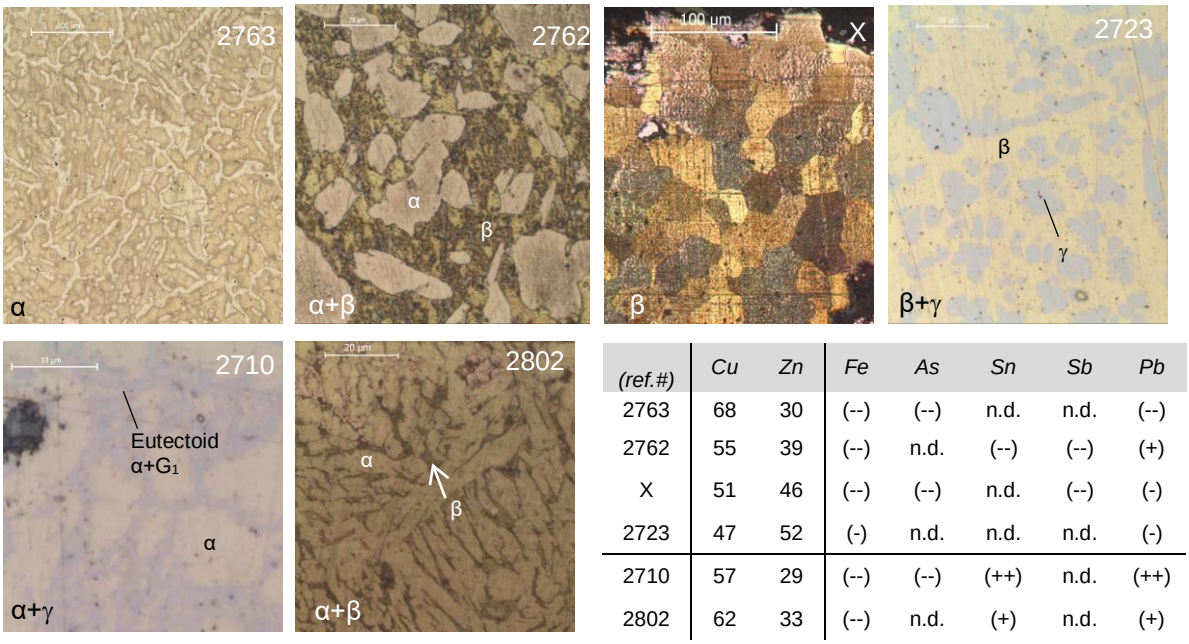

(ref.#)	Cu	Zn	Fe	As	Sn	Sb	Pb
2763	68	30	(--)	(--)	n.d.	n.d.	(--)
2762	55	39	(--)	n.d.	(--)	(--)	(+)
X	51	46	(--)	(--)	n.d.	(--)	(-)
2723	47	52	(-)	n.d.	n.d.	n.d.	(-)
2710	57	29	(--)	(--)	(++)	n.d.	(++)
2802	62	33	(--)	n.d.	(+)	n.d.	(+)

Fig. 3.4 OM microstructures of brass coins (BF, etched except for 2723 and 2710, non-etched) and their elemental compositions.

wt% Sn). The same occurs for coins #2762 and #2802 (Fig. 3.4): although both present α+β structures, the Zn content of #2802 would be, according to Cu-Zn equilibrium diagram, insufficient to promote the formation of beta phase, which should occur due to the presence of a small amount of Sn in this phase, confirmed by SEM-EDS. When dealing with coins presenting a β+γ or β+G_1 structures (e.g., coin #2767, Fig. 3.5), SEM-EDS analysis shows that both phases have similar Zn contents (~45 wt%) but G_1 phase is about 4.5 times Sn-richer than beta phase (1.5 to 6.8 wt.% Sn).

According to Smith and Levine [1973] and Bochvar *et al.* [2007], tin additions in Cu-Zn alloys are responsible for the formation of an eutectoid structure, α+γ, resulting from a high temperature (~520ºC) decomposition of brass β phase. Chou and Chen [2006] confirms, as all the authors above, that there are no new ternary compounds in the Cu-Sn-Zn system and that molten Sn has tie-lines with all the binary Cu-Zn compounds at 250 and 230 ºC. Jantzen and Spencer [2008] add that "*a ternary excess term for the β phase was used to describe the experimental solubility between the Cu-Zn and Cu-Sn binary systems.*"

The use of an isothermal section of the ternary phase diagram for Cu-Sn-Zn system at 450 ºC[17] (see Fig. 3.5) seems to explain these less common phase constitutions observed in tin brasses. Accessing this ternary isothermal section, one can see that small additions of tin promote the formation of β or γ phases in the Cu-Zn system for lower Zn contents than the dictated by the binary system Cu-Zn, as supported by Jantzen and Spencer [2008]: "*The activity of Zn increases with small additions of tin, (...).*"

[17] The use of an isothermal section of the ternary diagram Cu-Sn-Zn at 450ºC is due to the fact that a section at a lower temperature was not found in the literature, and considering the rapid cooling of these coins in production the variation in the diagram at a lower temperature is minimal.

For example, an α+γ structure is impossible to occur in binary brasses but can be explained in the presence of small amounts of Sn. This is also true for the occurrence of triphasic systems, α+β+γ (as in coin #2770, in Fig. 3.5, where γ consists of a fine light grey precipitate scattered at grain boundaries. So, the observed G_1 phase could be interpreted as the γ-brass phase (from now on the G_1 phase will be assumed as γ).

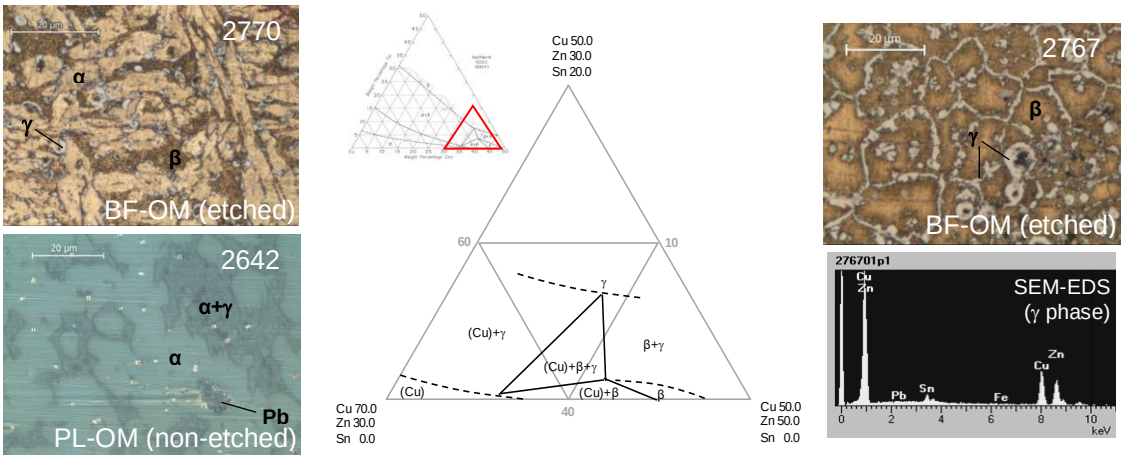

Fig. 3.5 Partial isothermal section (450 ºC) of the Cu-Sn-Zn phase diagram, adapted from [Vilarinho *et al.*, 2004; Smith and Levine, 1973], and microstructural examples of selected coins: #2642, α+γ; #2770, α+β+γ; and #2767, β+γ. An EDS spectrum of γ phase in coin 2767 shows the presence of Sn in this phase.

This light grey coloured γ-brass phase is considered structurally equivalent to δ-bronze phase according to the ternary diagram Cu-Sn-Zn [Smith and Levine, 1973], although Bochvar *et al.* [2007] and Vilarinho *et al.* [2004] indicate they are not the same phase (see Table 3.2). Moreover Lee *et al.* [2007] claims that Cu_3Sn (ε phase in the Cu-Sn system) corresponds to the γ-brass phase.

Table 3.2 Crystallographic data of gamma and delta phases Cu-Zn and Cu-Sn systems

Phase (diagram)	*Chemical formula*	*Space Group (Pearson Symbol)*	*References*
γ (Cu-Zn)	Cu_5Zn_8	I-43m (cI52)	[Bochvar *et al.*, 2007]
δ (Cu-Sn)	$Cu_{41}Sn_{11}$ ~ Cu_4Sn	F-43m (cF416)	[Ghosh, 2007]
ε (Cu-Sn)	Cu_3Sn	Cmcm (oC80)	[Saunders and Miodownik, 1994]

Micro-XRD of the γ-brass phase on the Cu-Zn diffusion couple produced in laboratory showed identical peaks to the micro-XRD on γ-tin brass phase of selected coins (for example, #2710 or #2767), in spite no Sn is present in the diffusion couple (see Fig. 3.6). Also, when comparing the XRD patterns of Cu_5Zn_8 (γ-brass) and Cu_4Sn (δ-bronze), there seem to be only small shifts on the 2-theta axis of the main peaks of the considered phases (see Fig. IV.2, in Appendix IV). So, these phases seem to be very similar crystallographically. Although still controversial, the δ-bronze and γ-brass phases will be assumed as one in the present thesis for the Cu-Sn-Zn alloys.

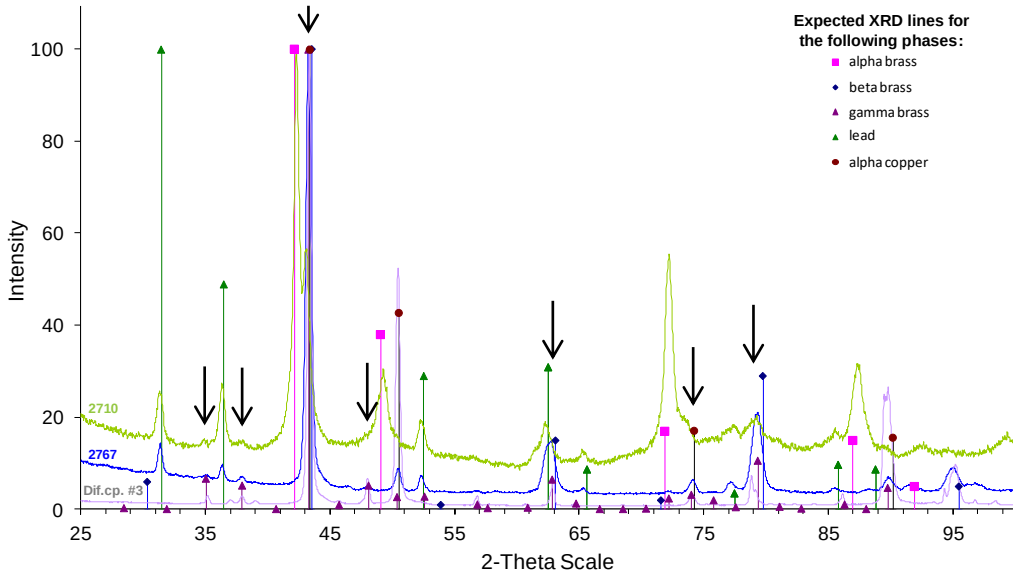

Fig. 3.6 Micro-XRD diffractograms (relative intensities versus two-theta angles for Cu(Kα) radiation) obtained for the diffusion couple Cu-Zn (grey line); coin # 2767 (blue line) and coin #2710 (green line). The black arrows indicate the most significant detected peaks in gamma brass phase.

The γ phase identification by XRD is difficult because the most intense peak (2θ at 43.2º) is usually overlapped with other major peaks of more abundant phases: β-brass or α-Cu (including from redeposited Cu), see Fig. 3.6. Also, some of the medium intensity peaks are overlapped with peaks from α-Pb or Fe_2As phases. However, taking into account the overall set of peak positions and their relative intensities, the presence of this phase seems certain (see Fig. 3.6).

3.1.2.1. Microstructural influence of Sb

Antimony and tin have adjacent atomic numbers; furthermore, microstructural observations seem to confer to Sb in Cu-rich alloys a similar microstructural effect (see Appendix IV for physical properties of each element). Concerning the studied brass coins there are four occurring cases: 1) no Sn or Sb; 2) small amounts of Sn; 3) small amounts of Sb; and 4) small amounts of Sn and Sb. Like Sn, when Sb content is sufficient, there is formation of a phase at grain boundaries, rich in Sb (SEM-EDS analysis in Fig. 3.7), that displays in OM a very similar grey colour to the Sn-rich γ phase.

SEM-EDS analysis showed that in Cu-Zn-Sn-Sb alloys, the grey phase is simultaneously rich in Sn and Sb (see coin #2733, Fig.3.7). This is in agreement with the ternary diagram Cu-Sb-Sn [Lee *et al.*, 2007]. According to the isothermal section at 400 ºC for the Cu-Sb-Sn system [Lee *et al.*, 2007], Sb could completely replace Sn in the δ-bronze phase – see Fig. 3.8(a). Our microstructural observations seem to confirm this behaviour. This Sb distribution was also observed in a study of ancient Chinese bronze coins [He *et al.*, 2011]. Observing the Cu-rich corner of the Cu-Sn-Sb ternary section, it is visible that up to 18 at.% Sb and 24 at.%Sn, an α+δ biphasic region exists,

where the δ phase should represent the common δ phase of the Cu-Sn and Cu-Sb binary systems, as seen in Figs. 3.8(b) and 3.8(c), [Blalock *et al.*, 1973].

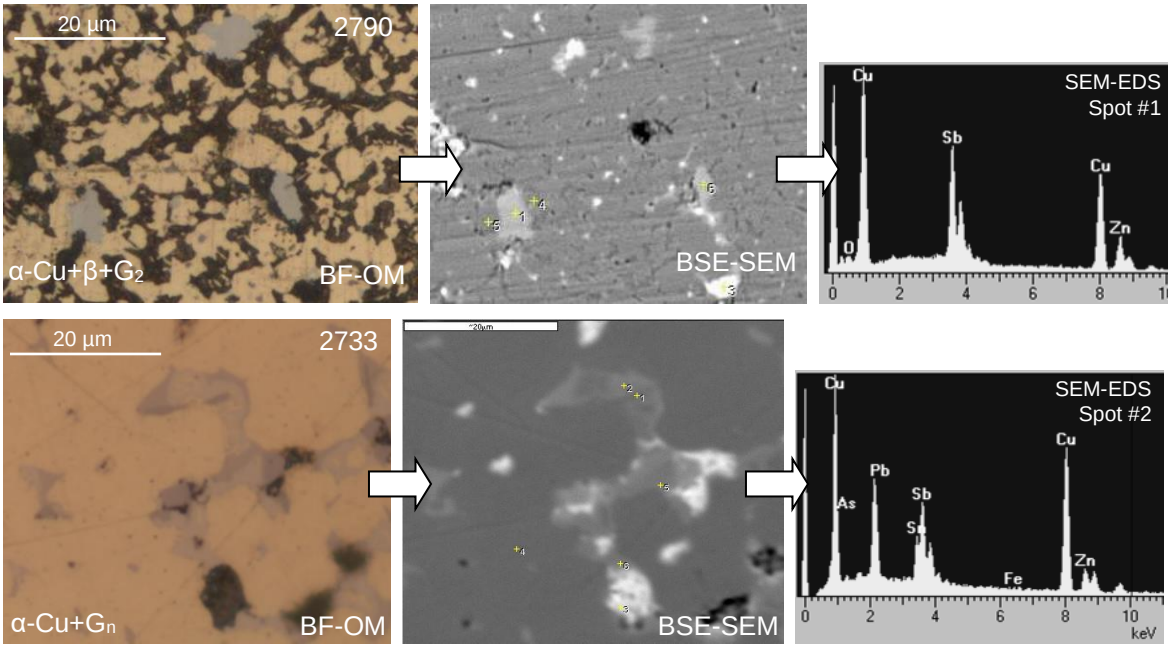

Fig. 3.7 Microstructural observation of coins #2790 (etched) and #2733 (non-etched) in OM-BF and in BSE-SEM. Spectra of spot #1 and spot #2 in SEM-EDS shows grey phases (BF-OM) in both coins are Sb and Sn,Sb-rich, respectively.

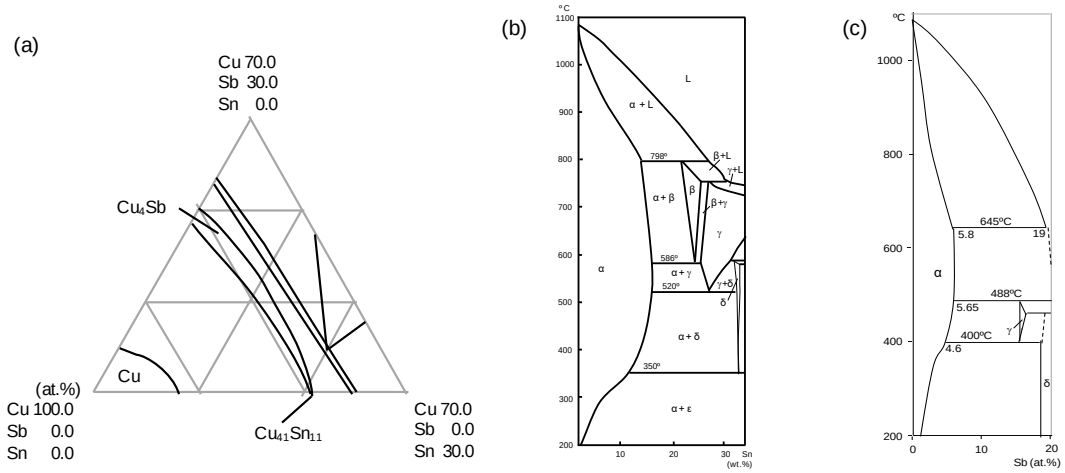

Fig. 3.8 (a) Isothermal section of the ternary diagram Cu-Sn-Sb at 400 ºC, adapted from [Lin *et al.*, 2007]; (b) partial binary Cu-Sn diagram, adapted from [CTIF, 1967]; (c) partial binary Cu-Sb diagram, adapted from [Subramanian and Laughlin, 1994; Fürtauer, 2010].

Lin *et al.* [2007] compares the ε phase, Cu_3Sn – from the binary system Cu-Sn – to Cu_3Sb (from the binary system Cu-Sb); it also compares δ phase, $Cu_{41}Sn_{11}$, to Cu_4Sb not only as having the same homogeneous content range structure but also very similar lattice parameters in both cases. Lee *et al.* [2007], in a follow-up review of this, alters the parallelism to Cu_3Sn (ε phase) and Cu_4Sb, whose patterns are very much coincident (see Fig. IV.3, in Appendix IV). The article proposes a continuous solid solution between Cu_3Sn and Cu_4Sb at 260ºC in the ternary Cu-Sb-Sn due to the isomorphism of the cited phases from the Cu-Sn and Cu-Sb systems. According to Fürtauer [2010], δ-Cu,Sn has a cubic lattice and δ-Cu,Sb has an hexagonal symmetry, due to the more covalent

character of the Cu-Sb bindings: the author finds face centered cubic and hexagonal close packed structure can convert into one another (see Table 3.3). This could explain why both phases have similar properties and generally appear to be associated.

Table 3.3. Crystallographic data of delta phase in Cu-Sb and Cu-Sn systems

Phase (diagram)	Chemical formula	Space Group / Geometry (Pearson Symbol)	References
δ (Cu-Sb)	$Cu_{78}Sb_{20}$ ~ Cu_4Sb	$P6_3/mmc$ / hexagonal (hP2)	[Fürtauer, 2010; Motai *et al.*, 1993; Lebrun *et al.*, 2007]
δ (Cu-Sn)	$Cu_{41}Sn_{11}$ ~ Cu_4Sn	F-43m / cubic (cF416)	[Fürtauer,2010; Ghosh, 2007]

Two coins containing Sb but no Sn (#3271 and #2666) were analysed by micro-XRD to try to identify the light grey phase observed in OM. Although some major peaks are coincident with other compounds, and minor peaks are very small, the XRD difractograms do not exclude the possibility of a Cu_4Sb phase in both coins (see Fig. 3.9).

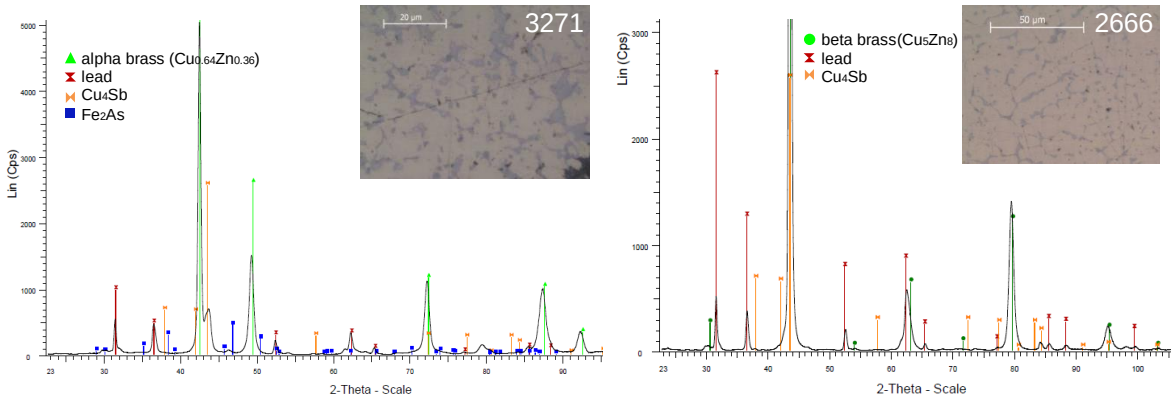

Fig. 3.9 Micro XRD diffractograms of coins #3271 and #2666: antimony rich phase in orange colour.

So, like Sn, Sb seems to promote the appearance of rich-Zn phases (beta and gamma). In the light of these findings, for the purpose of positioning the coins in an isothermal section of the ternary Cu-Sn-Zn diagram, a Sn equivalent content given by Sn+Sb was used to represent the coins compositions in the ternary system (see Fig. 3.10). Lead, iron and arsenic were ignored as they do not seem to significantly influence brass phases constitution [Furtado *et al.*, 2010c].

The major brass phases identification obtained by microscope observations (MO and SEM) were also confronted in this isothermal section (only three coins were not represented because they fall on the far left of the represented section: Ming dynasty coins #2639 and #2653, α+γ; and also Qing dynasty coin #2737, α+γ). Taking into account the compositional complexity and the non-equilibrium conditions (as-cast structures) of the analysed brass coins, the isothermal section of the ternary Cu-Sn-Zn diagram seems to explain relatively well the Sn and Sb microstructural effects. This also means that the G_2 phase observed in the Sb-brass coins could also be attributed as γ-brass phase.

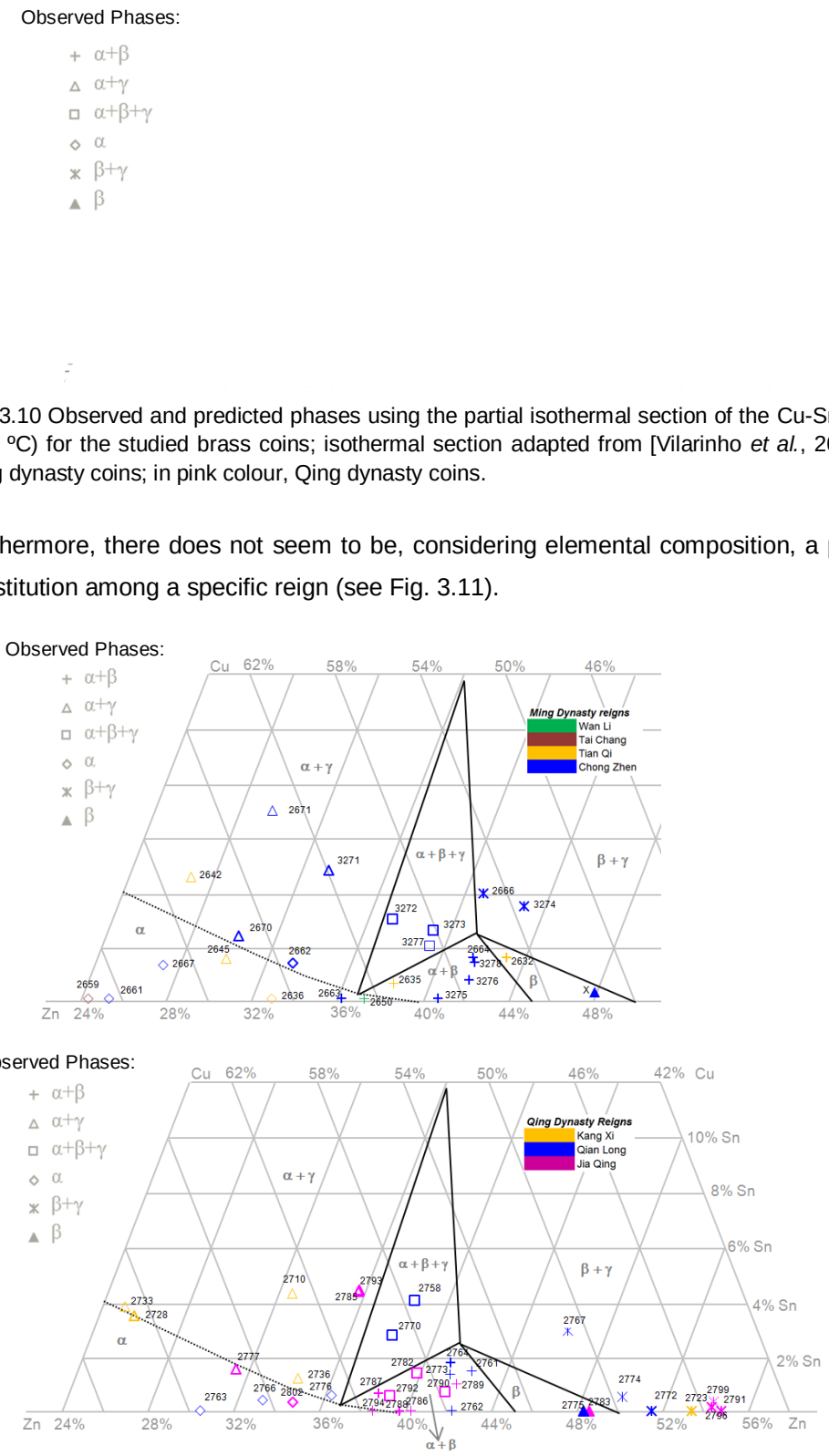

Fig. 3.10 Observed and predicted phases using the partial isothermal section of the Cu-Sn-Zn phase diagram (450 ºC) for the studied brass coins; isothermal section adapted from [Vilarinho *et al.*, 2004]. In blue colour, Ming dynasty coins; in pink colour, Qing dynasty coins.

Furthermore, there does not seem to be, considering elemental composition, a preferential phase constitution among a specific reign (see Fig. 3.11).

Fig. 3.11 Representation by reigns of the studied brass coins on the partial isothermal section of the Cu-Sn-Zn phase diagram (450 ºC); isothermal section adapted from [Vilarinho *et al.*, 2004]. The various studied periods are in different colours: (a) Ming dynasty coins; (b) Qing dynasty coins.

3.1.4. Microstructural influence of Fe[18]

Concerning the minor element Fe, it is present in almost all the studied coins. It was seen in the previous chapter that Fe contents are higher in bronze issues and lower in the first brass issues, with a erratic rise over time, but generally its content is very heterogeneous which can signify Fe was an impurity in the alloy (from raw material, metal recycling or contaminations).

Most of the coins with higher Fe contents present a primary dark grey Fe-rich phase defined as F_1. SEM-EDS analysis of this phase confirmed high Fe content and some Cu (coins #2416, #2421, #2427). According to the Cu-Fe phase diagram, the formation of a primary Fe-rich phase, γ-Fe (austenite), is expected for Fe contents above 2.8 wt.% (see Fig. 3.12). During cooling, austenite subsequently suffers an allotropic transformation to α-Fe (ferrite). X-ray diffractometry of coin #2785 (see Fig.3.15) evidences the strongest α-Fe peak, Miller Indices (110). So the F_1 phase should be α-Fe (ferrite).

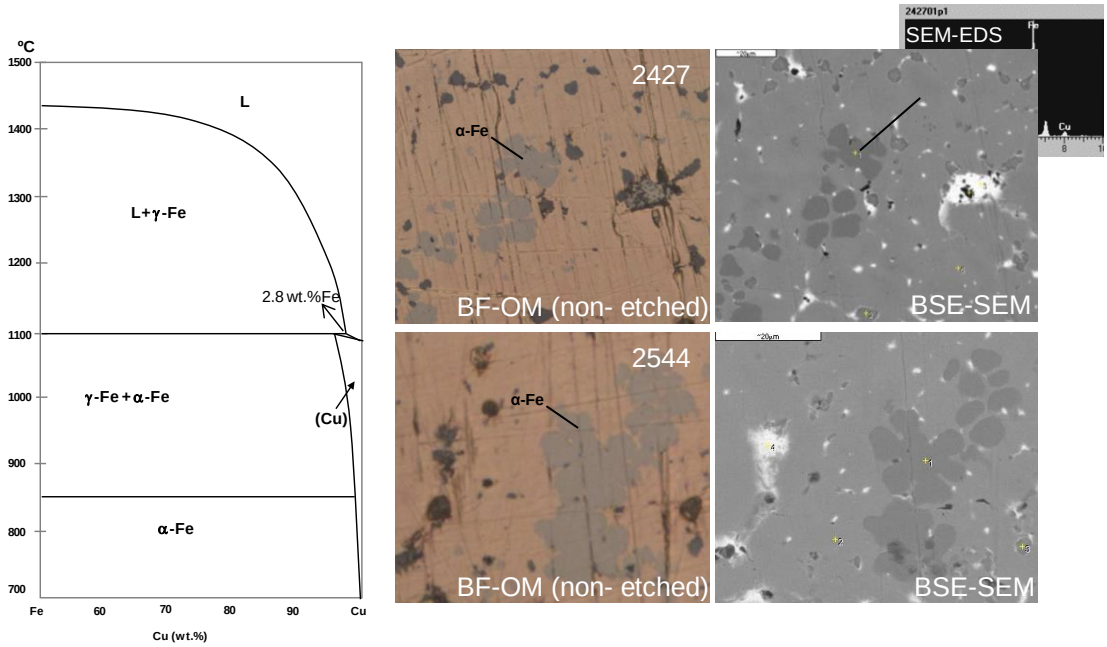

Fig. 3.12 Partial Cu-Fe phase diagram (adapted from [Hansen and Anderko, 1958]). Ferrite (α-Fe) in coin #2427 and #2544 (SEM-EDS of point #1 in both BSE-SEM images: ~93 at.% Fe; ~7at.% Cu)

Coin observations show that the Fe-rich primary phase appears even for lower Fe contents (~2 wt.%) than the minimum content dictated by the Cu-Fe phase diagram (~2.8 wt.% Fe). This can be related to non-homogeneous production conditions or due to the thermodynamic influence of other elements in the system. Ferrite promotes ferromagnetic properties in cash coins (e.g., #2209, #2242, #2785), easily detected with a magnet (they are immediately attracted to it), which could be a quick and inexpensive method of assessing the Fe phase in coins [Saitou *et al.*, 1998; Tanner *et al.*, 1979].

The Fe-richer bronze coins were represented in the Cu rich corner of the isothermal section at 900 ºC of the Cu-Fe-Sn phase diagram (see Fig. 3.13). This ternary isothermal section seems to

[18] Part of the results presented in this section were published as: M.J.Furtado, R.J.C.Silva, M.F.Araújo, F.M.Braz Fernandes *Influence of minor elements in ancient Chinese brass coins microstructures*. TOFA Conference Proceedings, Porto, 2010.

explain relatively well the main effect of Fe in promoting an Fe-rich primary phase in the coins. According to our microstructural observations, all bronze coins that fall into the monophasic α-Cu region, with the exception of coin #2528, do not display the α-Fe phase. The presence of some intergranular ferrite in coin #2528 could also be explained by the binary Cu-Fe phase diagram as a solid-state precipitation at lower temperatures.

On the other hand, all Fe-richer brass coins exhibited the α-Fe and clearly fall in the α-Cu+(γ-Fe) region at 900 ºC (for the sake of simplicity, those are not represented in the isothermal section of Fig. 3.13).

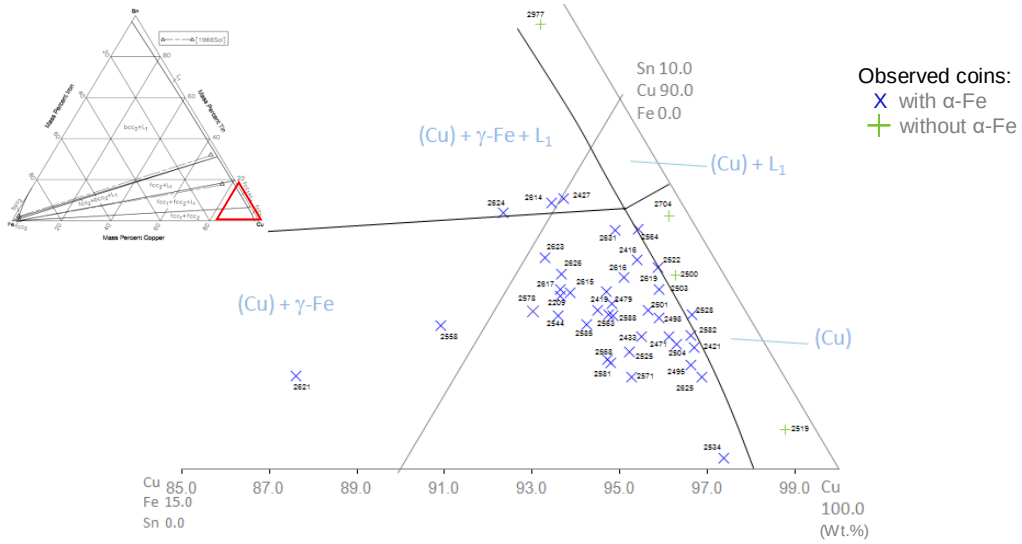

Fig. 3.13 Bronze coins Fe phase constitution on a partial Cu-Fe-Sn ternary diagram (isothermal section at 900ºC). Adapted from [Raghavan, 2009; Miettinen, 2008]. Coins #2242 and #2977 are not represented but fall in the α-Cu+(γ-Fe)+L_1 and α-Cu+L_1 regions, respectively.

3.1.4.1. Microstructural influence of Fe and As

In the studied coins, the presence of As is mainly associated with Fe – as observed by SEM-EDS mapping (see Fig. 3.14, coin #2782) – in a dark grey coloured phase (see Fig. 3.18, BF-OM detail) that usually precipitates or is segregated around Fe-rich grains. A semi-quantification analysis attempt of this phase by SEM-EDS gave 77.7 at.% Fe and 22.3 at.% As (ratio of 3.5:1), which inspite of this proportion could be Fe_2As, taking into account that this phase coexists next to α-Fe

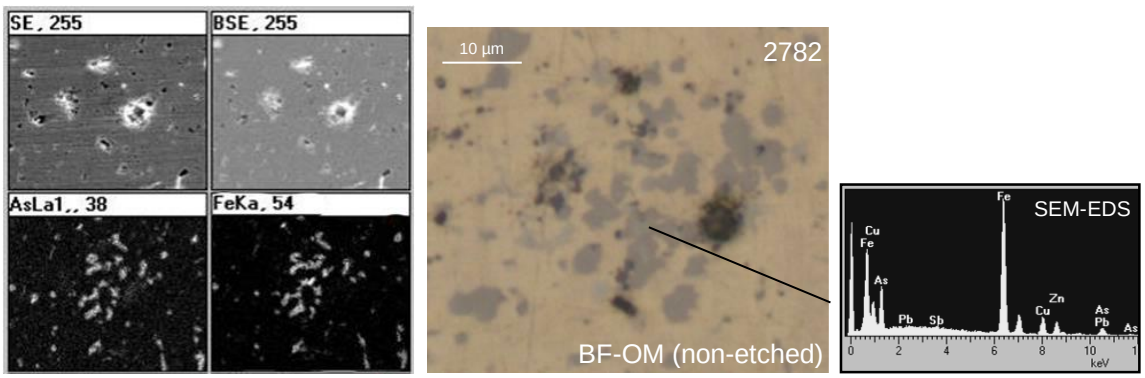

Fig. 3.14 Coin #2782 (~1.5Fe wt.%; ~2.7As wt.%): SEM mapping of a region with grey coloured phase (in BF-OM), Fe- and As-rich according to SEM-EDS analysis.

phase grains. So, the F_2 phase observed in the coins is most likely the Fe_2As.

This was later confirmed by micro-XRD analysis (see Fig.3.15), and is in agreement with the As-Cu-Fe phase diagram. According to the As-Fe system [Okamoto, 1991], Fe_2As could be formed by an eutectic reaction (L→α-Fe+Fe_2As), resulting in a triphasic alloy of α-Cu+α-Fe+Fe_2As [Raghavan, 1992]. Most of the coins possessing Fe and As are situated within this domain (see Fig. 3.16).

In coin #2785 (Fig. 3.15), a peculiar morphology was observed: the ferrite grains were encapsulated by a thin iron arsenide layer, as if this phase precipitated on the ferrite grain boundaries.

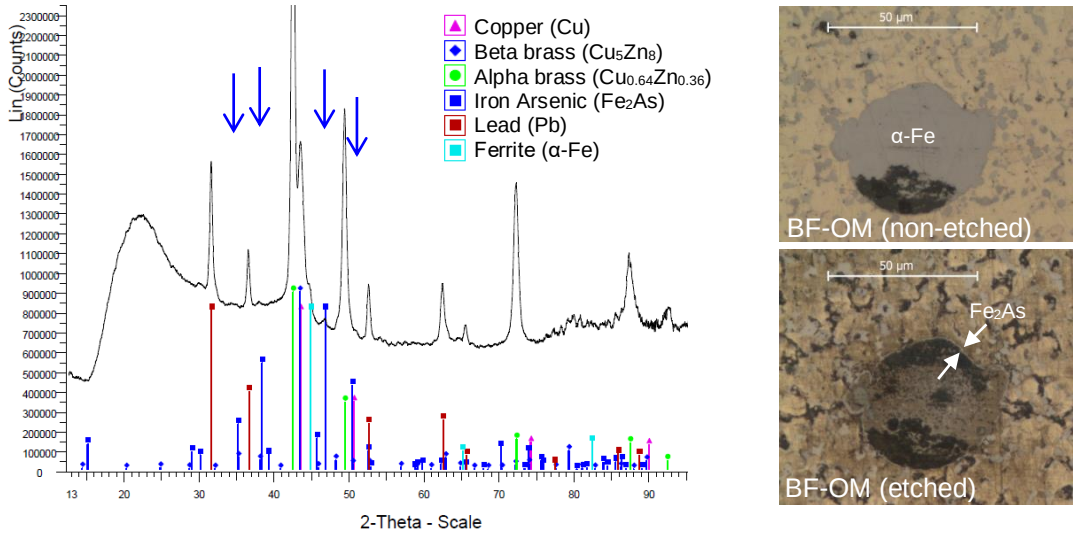

Fig. 3.15 On the left: micro-XRD diffractogram of coin #2785 (the blue arrows show the prominent Fe_2As peaks). On the right, OM images of coin #2785, detailing the Fe and As rich phases.

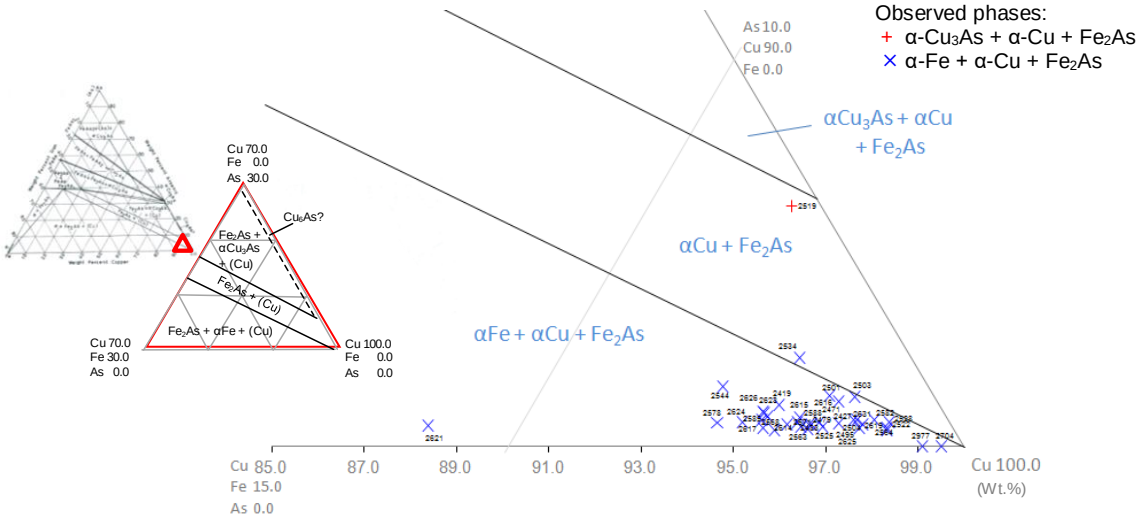

Fig. 3.16 Bronze coin (with As>0 wt.%) distribution according to Cu, Fe and As contents, in a partial isothermal section of Cu-Fe-As phase diagram at 25 ºC [Raghavan, 1992]. The red cross marks coin #2519, that presented an As-rich phase, possibly $αCu_3As$.

3.1.5. Microstructural influence of As

Arsenic is present in some coins, in variable amounts (up to ~6.0 wt.%). According to the As-Cu equilibrium phase diagram (in Fig. 3.17), this element exists in an α-Cu solid solution up to ~6.5 wt.%. Higher contents cause the formation of a copper arsenide, Cu_3As (domeykite) [Raghavan, 2009]. As clearly observed in coin #2519 (with 5.97 wt.% As), the D_1 phase is likely to be the Cu_3As intermetallic, inspite its composition falls below that limit in the Cu-As diagram. The presence of Cu_3As could be due to non-equilibrium solidification, resulting in a higher As segregation. Micro-XRD performed on coin #2519 does not allow a clear identification of the As-containing phases (Fig. 3.17).

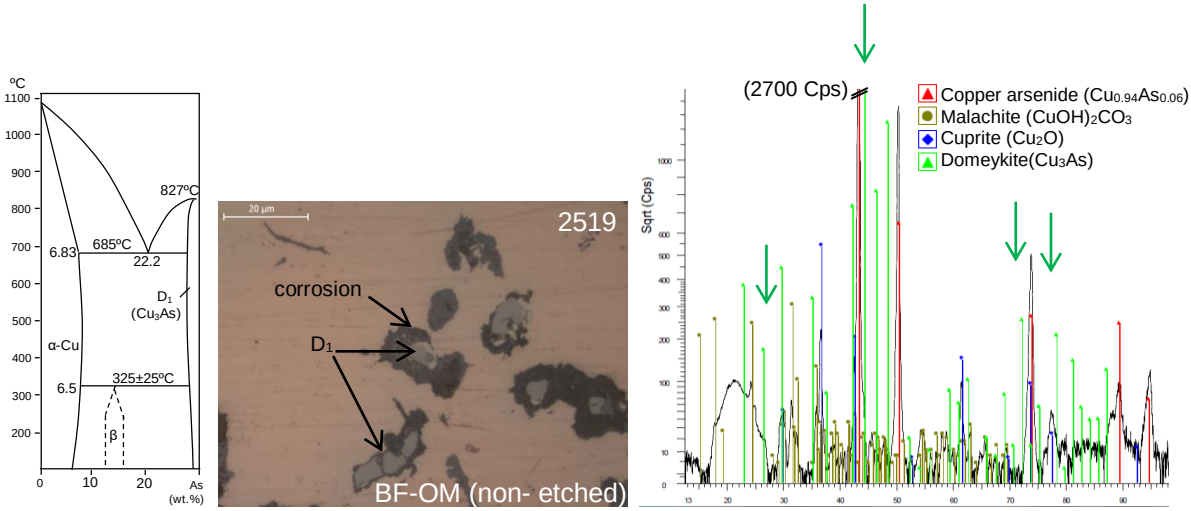

Fig. 3.17 Partial Cu-As phase diagram (adapted from Junk [2003]). OM of coin #2519 showing a grey As-rich phase. Micro-XRD diffractogram of same coin with the most intense peaks of copper arsenide (Cu_3As) signaled in green.

3.1.6. Microstructural influence of S

The presence of S compounds in these coins points towards a Cu un-refinement, as Cu-S compounds are often associated with other Cu minerals in hydrothermal veins. Sulphur may derive from processing of the raw material employed to obtain the metal (namely sulphidic ores as chalcopyrite, covellite or bornite), or from impurities present in oxidized copper ores. Although it is not a metal and does not form metallic phases, sulphur is present in most of the bronze and copper coins that were studied, resulting in non-metallic inclusions of a dark-grey colour in BF-OM.

Copper sulphides were identified by SEM-EDS analysis of coin #2779, an almost pure copper coin. SEM-EDS results of the round grey inclusions (up to 3µm Ø) showed a stoichiometry of ~2:1 (Cu:S) (Fig. 3.18), which, taking into account the Cu-S equilibrium diagram [Chakrabarti and Laughlin, 1983] point towards chalcocite (Cu_2S), a grey phase formed at low temperatures [Predel, 1994a]. So, the observed phase assigned as C_1 should be chalcocite. These inclusions seem to have been formed by sulphur segregation during solidification towards interdendritic regions due to the low S miscibility in α-Cu. Large globular formations (see Fig. 3.19a) can be attributed to a two-liquid immiscibility in the higher S content section of the Cu-S system.

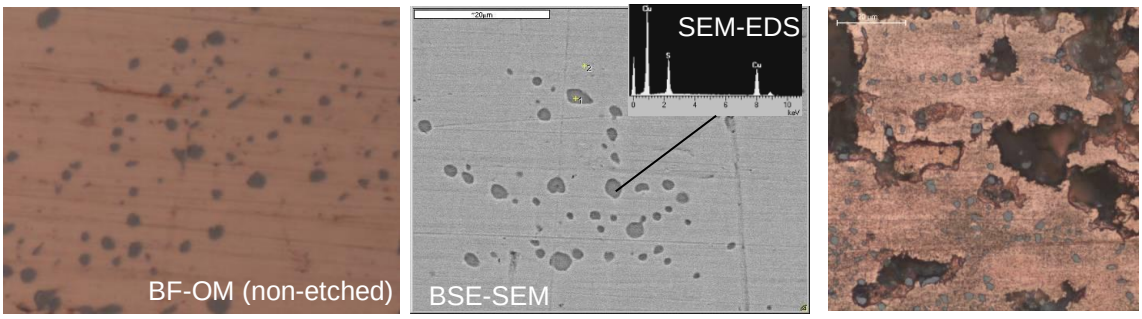

Fig.3.18 – Coin #2779 (99.5%Cu, 0.1%Fe, 0.3%Ni, by μEDXRF): (a) Detail of polished microstructure in OM-BF (non-etched); (b) SEM image of a different area (BSE); (c) detail of corroded area, in OM-BF (etched).

Copper sulphide inclusions are chemically stable in archaeological context, remaining in the corroded regions after the α phase has been leached [Valério *et al.*, 2010b], as can be seen in Fig. 3.18(c).

A more complex case emerges when Fe is present, promoting the formation of a ternary phase with copper, iron and sulphur (B_1 phase in Chapter 2). The occurrence of S and Fe rich inclusions in the microstructure seems to contribute to increase alloy hardness [Chernyck *et al.*, 1998] although this may not have been the actual purpose in cash coins.

The most evident example is coin #2209 (Fig. 3.19), presenting large round grey globules. Micro-analysis by SEM-EDS showed these grey inclusions are rich in Cu, S and Fe (~45 at.%Cu, ~44 at.%S and ~11 at.%Fe), and inside them there is α-Pb precipitation (Fig. 3.19). Consulting the Cu-Fe-S ternary diagram [Yund and Kullerud, 1966] and by micro-XRD, the B_1 phase is identified as bornite, Cu_5FeS_4, a phase sometimes present in bronze objects [Walker, 1980].
Phase equilibrium experiments in the system Cu-Fe-S have shown immiscibility in Fe-poor, Cu-rich compositions [Brenan and Haider, 2008]. This miscibility gap could explain the globular formation of bornite. Isothermal section of the Cu-Fe-S phase diagram at 700 ºC exhibits a triphasic region constituted by α-Cu, α-Fe and B_1, which is in agreement with the microstructure presented in Fig. 3.19.

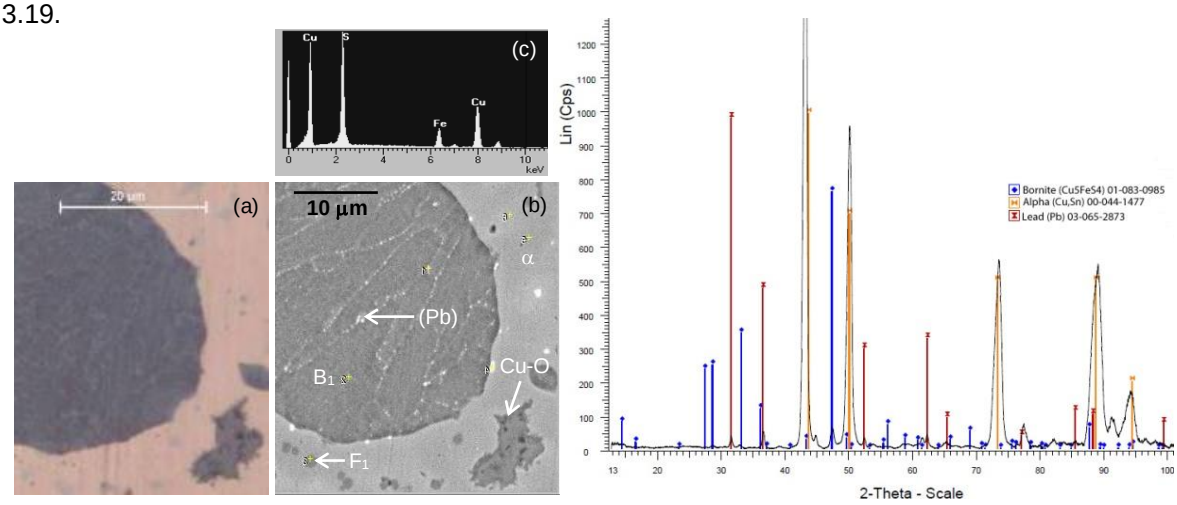

Fig. 3.19 - Coin # 2209 (3.6%Fe, 82%Cu; 4.5%Sn, 2%Pb, by μEDXRF): (a) detail of polished microstructure in OM-BF; (b) SEM image in BSE mode; (c) EDS spectra of the large grey globule; (d) micro-XRD diffractogram of the area.

3.2. General Remarks

Elemental analysis and microstructural observation show that brass coins are more complex than bronze coins due to the presence of more minor elements and the formation of minor phases.

Some of the minor phases in the studied coins, sometimes difficult to distinguish in the microstructures due to their reduced size and distribution, were initially of dubious identification. Combining the various available methods as EDXRF, SEM-EDS, OM, XRD and digital X-radiography and resorting to binary and ternary phase diagrams, allowed most of the times a clear identification of the coins phase constituition.

Microstructural observation correlated to the compositional analysis reveals Pb has a bimodal distribution according to a lower or higher content in the alloy. When its content is low (falling on the hypomonotectic range of the Cu-Pb system), it is interdendritically homogeneously distributed throughout the coin. When close or above the hipermonotectic content range, Pb is distributed throughout the coin in irregular globular size, which may interfere with finer microanalysis – especially when corrosion is present – due to beam size and reduced area of analysis: that is why OM observation may help to interpret the original content based on its distribution.

The presence of tin in small contents (5>Sn(wt.%)>1) in brasses promotes the formation of beta and gamma (also referred to G_1 in the previous chapter) phases for lower Zn contents than expected in the Cu-Zn system. Also, Sn-rich γ brass phase (G_1) was considered structurally equivalent to the bronze δ phase. Antimony seems to have a similar microstructural behaviour to Sn in brasses and appears associated with Sn in the microstructural phases. The Sb-rich γ phase (also referred to as G_2 in the previous chapter) was found to be compatible and convertible with the Sn-rich γ phase (G_1); so a (Sn+Sb) content was taken into account for microstructural purposes.

Ferrite (α-Fe, also referred to as F_1 in the previous chapter) dendrites are common in coins with iron contents above 2 wt.%, with the particularity of rendering the coin magnetic (which was verified in several coins). Arsenic seems to be present in some coins: in higher contents, it can form domeykite (Cu_3As, also referred to as D_1), but usually it is present in low contents and remains in solid solution with copper or iron. It is associated with Fe or around Fe-rich phases to form an iron arsenide (Fe_2As, also referred to as F_2).

Sulfur inclusions are also frequent in most bronze coins or, in late 19th century pure copper issues, attesting to the use of unrefined copper. Most common inclusions are chalcocite (Cu_2S, also referred to as C_1) and bornite (Cu_5FeS_4, also referred to as B_1), and both seem to be corrosion resistant.

Chapter 4 - Considerations on corrosion

Having had access to the metal-corrosion interface in view of the general objectives of this work, some remarks on phase corrosion susceptibility regarding the influence of secondary alloy elements were thought to be a valuable addition to the present thesis. Even in small amounts, these elements can form uncommon metallic phases in bronzes and brasses that can contribute to variable corrosion resistance. Although environmental conditions are very important to the corrosion processes, phase constitution is essential to understand degradation mechanisms. These artifacts are, first of all, cultural heritage and previsions on the long term corrosion behaviours of their alloys can be relevant to their preservation.

It is known now that small additions of other metals to copper-based alloys can influence their corrosion behaviours [Davies, 1993]. It is doubtful, however, to think that in 16^{th}-18^{th} century China this was already developed, especially attending to the object in question (common coins) and the fact that both metals that promoted or prevented dezincification in brasses were added to the melt (Fe and Sn, respectively). It is interesting to observe the influence such a small amount of a certain element has on the microstructure, protecting it from corrosion or potentiating it. Davies [1993] says:

> *"(…) the literature is very clear about complex alloys; it is difficult to establish the effect of individual elements on general corrosion and dezincification rates for there may be synergistic effects for certain combinations of elements".*

In ancient copper-based alloys, the main corrosion products, developed in a non-marine environment and in the absence of chloride salts, are typically Cu oxides and Cu carbonates [Scott, 2002]. After minting, copper initially forms cuprous oxides like cuprite (Cu_2O), in the inner layers, and tenorite (CuO) – see equations (4.1) and (4.2) – that can be converted into a stabler copper basic carbonates due to rising enthalpies – see equations (4.3) and (4.4).

$4Cu + O_2 \leftrightarrows 2Cu_2O$ [cuprite] (4.1)

$2Cu + O_2 \leftrightarrows 2CuO$ [tenorite] (4.2)

$Cu_2O + H_2O + CO_2 + {}^1/_2O_2 \leftrightarrows Cu_2(OH)_2CO_3$ [malachite] (4.3)

$3Cu_2O + 2H_2O + 4CO_2 + {}^3/_2O_2 \leftrightarrows 2Cu_3(CO_3)_2(OH)_2$ [azurite] (4.4)

The transformation rate depends on kinetic factors as the environment composition and the nature and solubility of the corrosion products [Walker, 1980]. Hence, the corrosion phenomena is dependent on both extrinsic as intrinsic factors as the nature of the surface film and the chemical reactions happening in that film [Davies, 1993].

4.1. Coppers

In one of the 13 studied copper coins, the polished area presented thick corrosion layers of oxides, carbonates and chlorides. It is noticeable that corrosion advances inwards through the α-Cu

dendrite interfaces, forming Cu[I] products, as cuprous ions are partially leached to the outer surface and oxidised, precipitating as Cu[II] products, as carbonates (Fig. 4.1).

Prolongued contact with chlorides (e.g., in burial conditions), can lead to the formation of atacamite [$CuCl_2.3Cu(OH)_2$], a dark green product – see equation (4.6). Nantokite, CuCl, a pale green and waxy compound – see equation (4.5) – can also occur in the inner layer (see Fig. 4.1). Nantokite is unstable in aerated conditions and can cause the "bronze disease", an autocatalytic corrosion that can ultimately lead to artifact destruction [Walker, 1980].

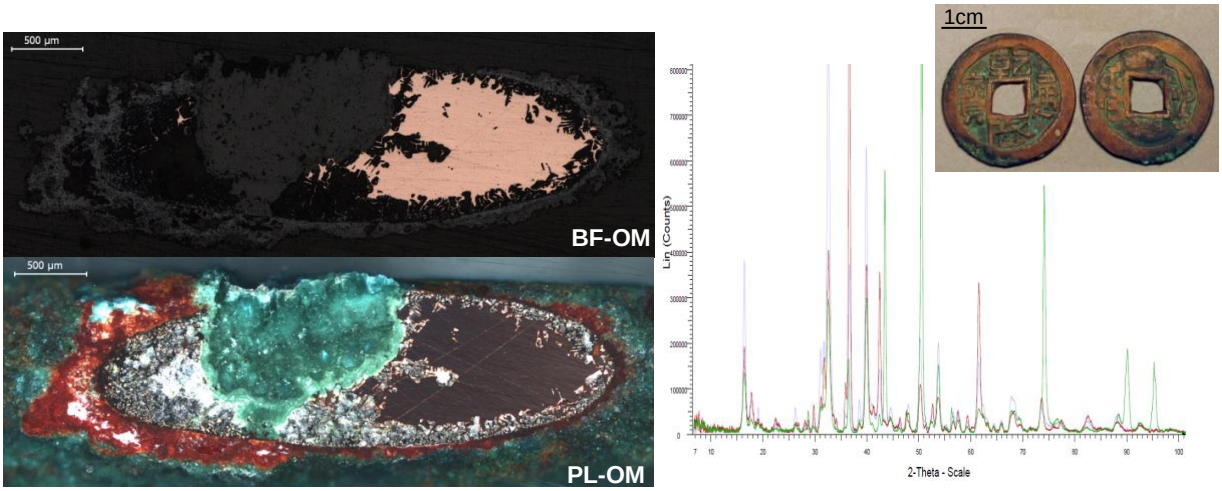

Fig. 4.1 On the left, OM images of the polished rim in coin #2771. On the right, micro-XRD diffractogram of 3 areas: red line - red layer (cuprite), green central area and blue line - white central area (copper chlorides).

$Cu_2O + 2Cl^- + 2H^+ \leftrightarrows H_2O + 2CuCl$ [nantokite] (4.5)

$2CuCl + 3H_2O \leftrightarrows 3H^+ + Cl^- + 2e^- + Cu_2Cl(OH)_3$ [atacamite] (4.6)

4.2. Bronzes

As the bronze coins are older, they usually present thicker corrosion layers and/or deep intergranular or transglobular corrosion, consisting of oxides, carbonates and sulphides of the major elements in the alloy: Cu, Sn or Pb.

4.2.1. Sn effect

As the tin content in the studied coins is generally below 6 wt.%, the ratio of Sn corrosion products is quite small. There is, however, a perceptible Sn superficial enrichment in the inner corrosion layer (immediately under the original surface) that denotes the low solubility of tin corrosion products, SnO_2. Figure 4.2 shows the elemental distribution in a small area of two bronze coins. The superficial region (the outer corrosion layer should be partially missing) is richer in O and Sn. Similar results were obtained by Ling *et al.* [2007] when observing Chinese bronze vases, where he identified tin oxide SnO_2 (cassiterite). For biphasic bronzes (α+δ), in aerated mediums, the α-Cu is preferentially corroded towards the interior (low oxygen potential), the δ phase could be the only corroded phase [Silva, 2008]; however this was not observed in the selected bronze coins that presented delta phase (#2242, #2704 and #2977).

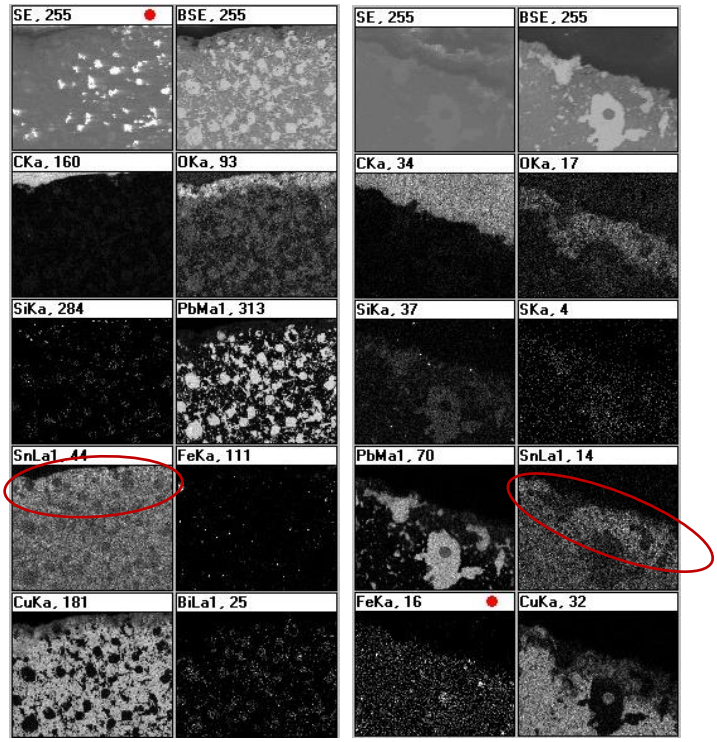

Fig. 4.2 SEM-BSE elemental mapping of clean areas in coins (a) 2421 and (b) 2427: notice the Sn and O accumulation across the surface area (and Cu depletion).

4.2.2. Pb effect

The most common corrosion issue in these coins is the transglobular corrosion of Pb-rich phase (see Fig. 4.3, coin #2544). Pb is leached towards the surface and the globules are filled with Pb or Cu corrosion products, as also observed by Mccann [1999] in ancient bronze money-trees.

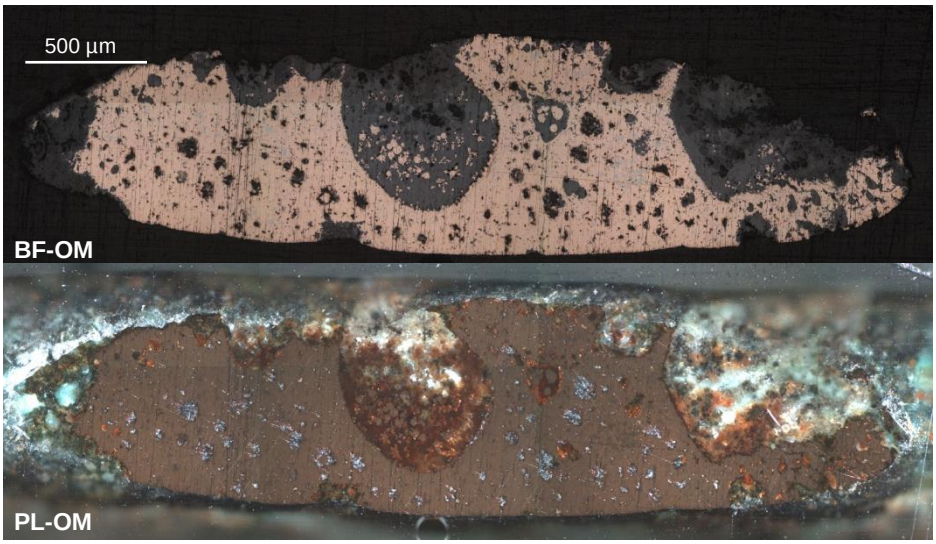

Fig. 4.3 Polished rim area of coin #2544: the Pb-rich phase is corroded.

Sub-superficial corroded Pb globules present a black color in BF-OM and a translucent to milky-gray colored crystals in PL-OM (see Fig. 4.4): SEM-EDS analysis showed these Pb globules were oxidized, presenting Pb, O and C. Inside the globular space it is also visible, in polarized lighting,

the presence of cuprite, Cu_2O (red colour). Also in older Pb-richer coins, elemental X-ray maps showed a superficial Pb enrichment in the corroded layers, as seen in Fig. 4.5(a). This indicates that part of the Pb tends to be leached towards the surface where it precipitates as outer corrosion products and part stays as corrosion in the initial globules. This is reported by Trentelman *et al.* [1999], in the study of Han dynasty money-trees. She suggests the probable sequence of corrosion: oxidation of metallic Pb and migration out of the bronze alloy with subsequent migration of Cu[I] ions into the regions formerly occupied by the Pb globules to form cuprite, which can later further oxidize in other Cu(II) products.

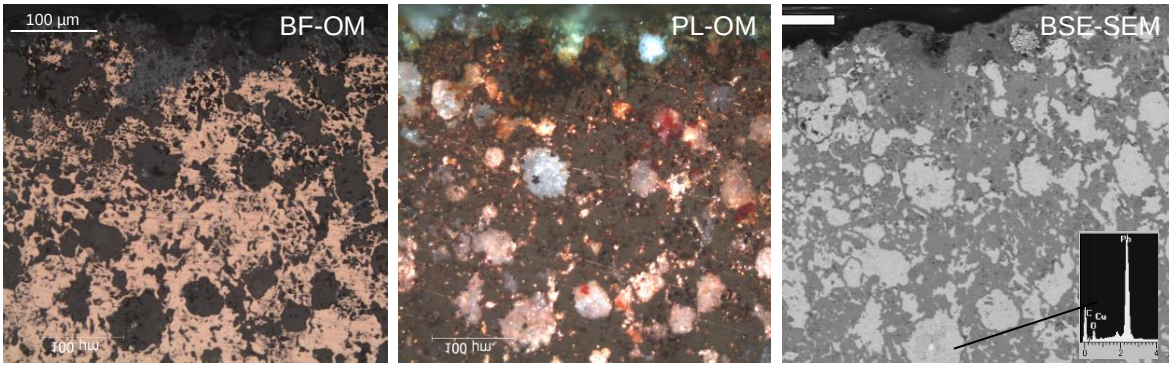

Fig. 4.4 Coin #2421 (~40 wt.% Pb): presents transglobular corrosion. Lead-rich phase was replaced by Pb corrosion products.

Trentelman *et al.* [1999] also refers to a superficial alteration of the sectioned metallic surface, where Pb protruded out of the surface after a few weeks in a worm-like manner. A similar phenomenon was observed in one studied coin but in acicular form (like the one referred by [Fang *et al.*, 2003]), and according to Trentelman, confirms the theory that Pb migration towards the surface is also driven by pressure exerted due to volume expansion when Pb oxidates, noting that this happens in a much faster rate than for Sn or Cu.

A curious case was found in brass coin M117, see Fig. 4.5(b), an archaeological find from the ruins of St. Paul in Macau, where Pb concentrates in an intermediate corrosion layer of ~5µm thick, probably due to two distinct environmental corrosion conditions over time.

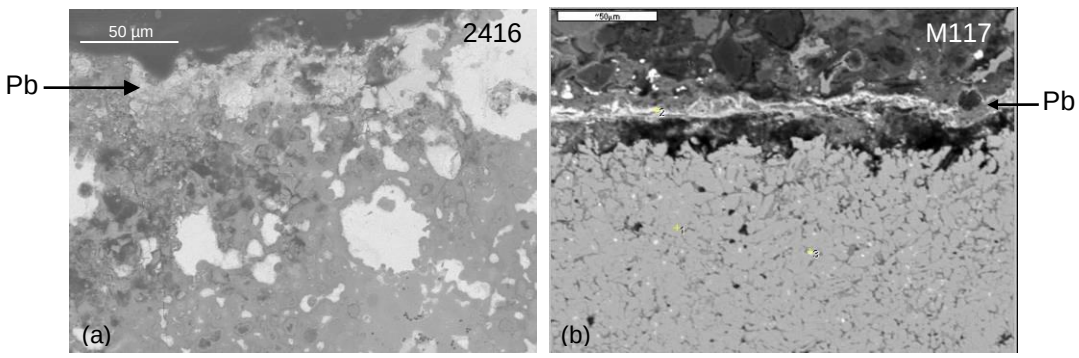

Fig. 4.5 BSE-SEM images of coins a) #2416 and b) #M117 (superficial areas) where there is a noticeable Pb deposition on the surface.

In coin #2522, micro-XRD was performed on the corroded globules and several Pb corrosion products were identified (see Fig. 4.7): lead carbonates (cerussite [$PbCO_3$] and hydrocerussite [$Pb_3(CO_3)_2(OH)_2$]) [Schotte and Adriaens, 2006], as well as lead chloride hydroxide, laurionite [PbCl(OH)], common in Pb containing alloys [Junior *et al.*, 2007; Graedel, 1994; Selwyn, 2005; Walker, 1980].

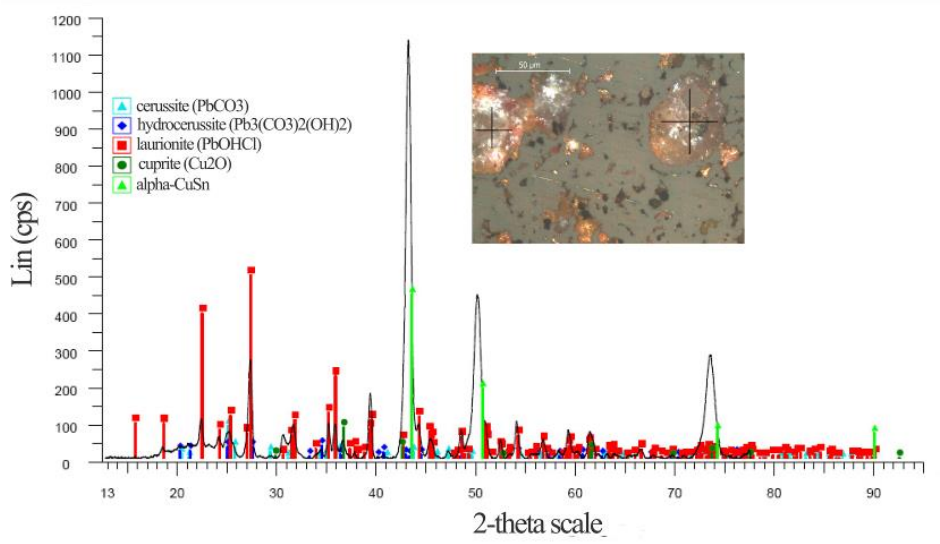

Fig. 4.7 micro-XRD diffractogram of a corroded Pb-rich globule in coin #2522

Fang *et al.* [2003] writes that in coins possessing a layer of cerussite, Pb contents in the bulk are lower than expected based on a superficial analysis due to Pb being leached out to the corrosion layers. The same conclusion was reached by Figueiredo *et al.* [2007b] concerning bronze artefacts. Ling *et al.* [2007] found in ancient Chinese bronze vases several lead compounds, such as PbO, $PbCO_3$, Pb_3O_4 and PbCl(OH) by XRD analysis; and also refers to a higher outer layer lead content "probably because of the deposition of lead oxide and lead carbonate corrosion products". He *et al.* [2011] also reports the presence of Pb_3O_4 in ancient Chinese bronze coins.

The Pb assessment in these coins showed a Pb dispersion variability that is strongly dependent on Pb the content. While micro-EDXRF gave an approximate Pb content, OM and SEM observations permitted to confirm the Pb-rich globular distribution but also a Pb content estimation based on the image analysis from the cleaned edges (see section 3.1.1). Also, the investigation on the leaching and corrosion products formed allowed stating Pb vulnerability to corrosion, which can mean a significant volume loss in high-leaded coins, or increased fracture risk: the high Pb content in some bronze coins may be related to a higher fracture rate. As shown in Fig. 4.8 (coin #2582), SEM images show the fracture site and EDS determined the presence of lead and oxygen in the area, as demonstrated by Campbell [2003].

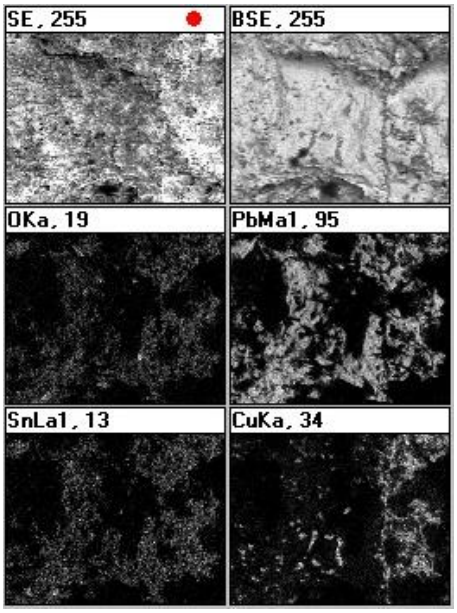

Fig. 4.8 Fracture area of coin #2582 (SEM-EDS). Notice how the majority of the area is rich in Pb and O.

4.3.2. Fe effect

In leaded bronze coins, α-Fe (ferrite) is generally not affected by corrosion (see Fig. 4.9). Instead, Pb (an electrochemically less active element, when passivated) is preferentially corroded, which can be due to specific burial conditions.

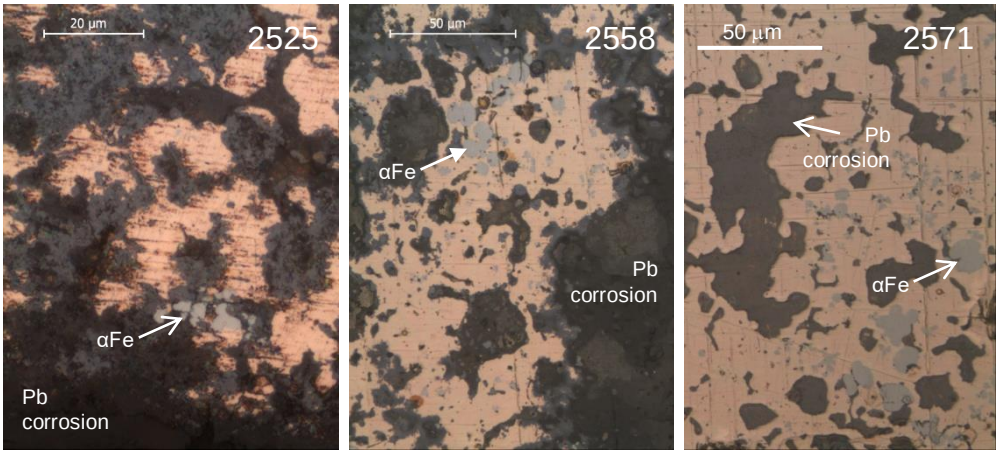

Fig. 4.9 Corroded regions in bronze coins (BF-OM): ferrite (grey phase) seems to be unaltered.

4.3. Brasses

The overall corrosion mechanism observed in the studied brass coins is dezincification, mostly of the plug-type [Furtado *et al.*, 2010b; Davies, 1993]. When dealing with brasses, since Zn has a lower standard reduction potential than Cu, it is preferentially corroded. While Zn is leached out of the alloy, Cu ions undergo a cathodic redeposition on the corroded regions in a permeable and porous manner [Fontana, 1987]. The Cu redeposition provides the continuous dissolution of more Zn in the alloy in a process known as dezincification that is consistent with a preferential Zn loss (see Fig. 4.10, coin #2761). This selective Zn depletion, very common in brasses, is more expressive in microstructures with more than one brass phase [Jones, 1996], where higher Zn

content phases, in general, are preferentially corroded. As the corrosion progresses, the redeposited Cu is also oxidized and gradually leached. When extensive, this process can contribute to elemental differences observed in EDXRF results from the surface and bulk metal: a copper enrichment is sometimes observed at the surface due to Zn depletion.

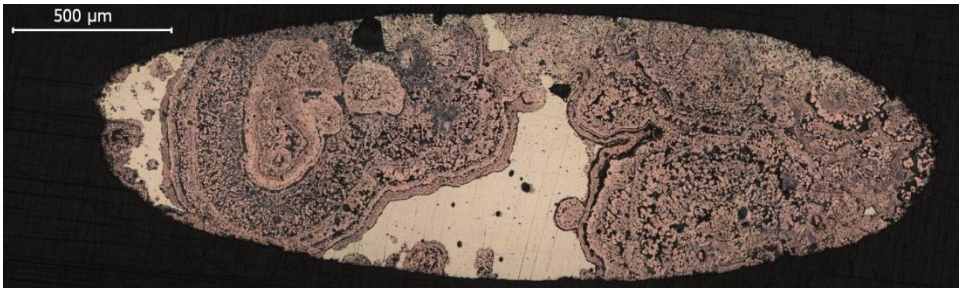

Fig. 4.10 Polished rim area of coin #2761 (37 wt.%; α+β) presenting important Cu redeposition due to a dezincification process.

The expected sequence of corrosion resistance for brass phases is α>β>γ, i.e., it decreases with the increase of Zn content in the phase [Davies, 1993]. However, this relation is not linear, depending on the phase constitution: Davies reports the following sequence of corrosion resistance: α>α+β>β, adding that alloys under 15 wt% Zn rarely dezincify. Figure 4.11(a) illustrates an α+β structure where there is an evident preferential corrosion susceptibility of β phase, Zn richer than α phase. The corrosion pattern shows that beta phase is primarily corroded. In Figure 4.11(b), for a β+γ structure, the γ phase, Zn richer, is preferentially corroded: notice the blue-pinkish colour of the gamma dendrites that indicates the phase has already lost Zn (the uncorroded colour for this phase is light-grey). Eventually, the beta phase is also corroded: the voids left by the Zn depletion in both phases are partially filled with porous redeposited Cu that eventually oxidizes.

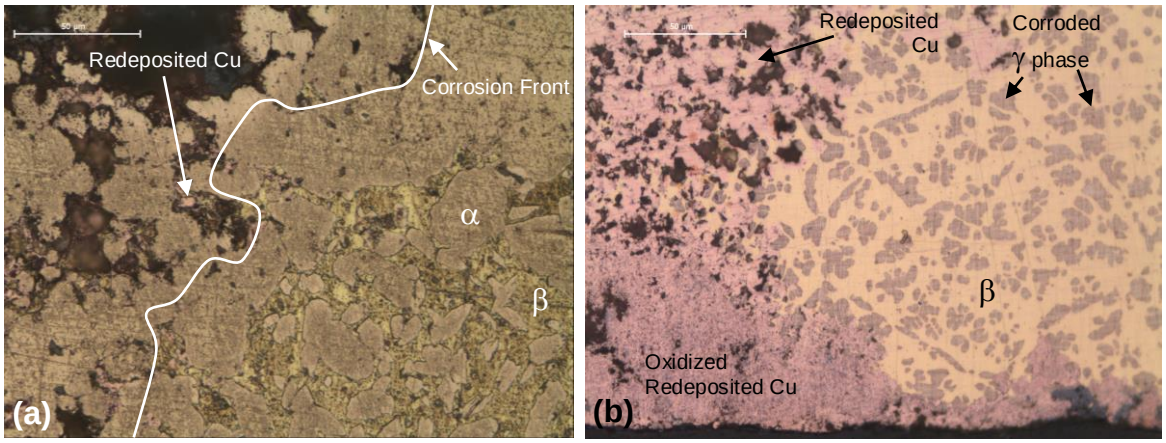

Fig. 4.11 Etched microstructures (OM-BF) of leaded brass coins (a) 2762 (39.1wt.% Zn), an α+β structure, where secondary α grains (yellow) precipitate in a β matrix (brighter yellow), that is being replaced by redeposited Cu (pink) due to a dezincification process; and (b) 2723 (51.6 wt.% Zn), a β+γ structure showing preferential corrosion of the γ phase.

4.3.1. Sn or Sb effect

When dealing with tin brasses (assuming Sn+Sb contents as previously explained), for α+β structures the corrosion sequence corresponds to the previously described. However, this

behaviour seems to be altered when looking at β+γ structures, where the β phase is preferentially corroded instead of the γ phase - Fig. 4.12(a) -, even though in the analysed coins both phases have similar Zn contents. It seems that the higher are the Sn and/or Sb contents of this γ phase, albeit small, they may confer it some form of protection, also reported by Davies [1993]. When observing coins with the α+γ phase constitution, most coins show a clear preferential γ corrosion - Fig. 4.12(b). In these coins the (Sn+Sb) content is higher in the gamma phase (which should be protective of this phase); however, they present high Zn/(Sn+Sb) ratios.

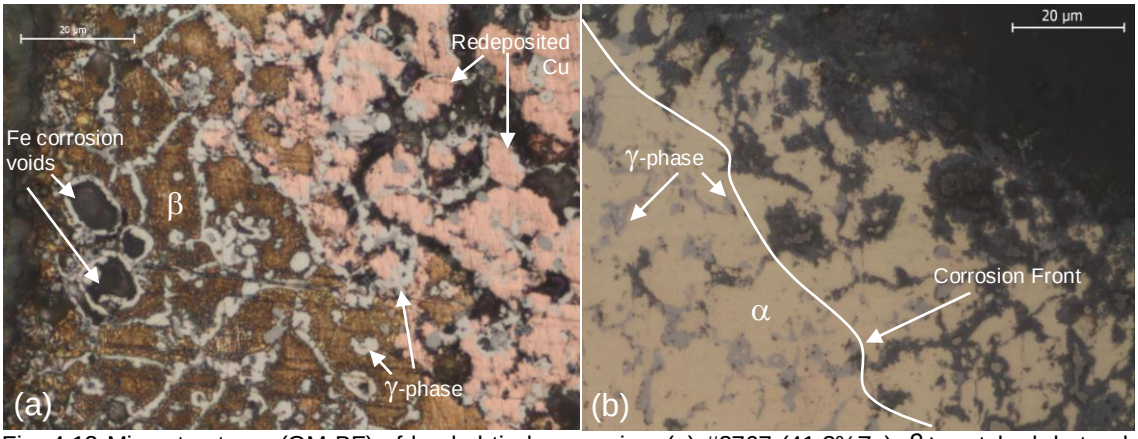

Fig. 4.12 Microstructures (OM-BF) of leaded tin brass coins: (a) #2767 (41.3%Zn), β+γ, etched, beta phase (brown colour) is being preferentially corroded. Fe-rich phase is also preferentially corroded and leached out of the alloy; (b) #3271 (29.9%Zn), α+γ, non-etched, eutectoid γ phase (light grey colour) is being preferentially corroded.

An exception occurs in two coins that have in common a relatively low Zn/(Sn+Sb) ratio (displayed within the dotted region in the phase diagram of Fig. 4.13) [Furtado *et al.*, 2010b]. In these coins, there was preferential corrosion of the α phase. Davies [1993] suggests this happens in view of the high tin + low copper levels in the gamma phase relatively to the extra low tin + high copper levels in the alpha phase.

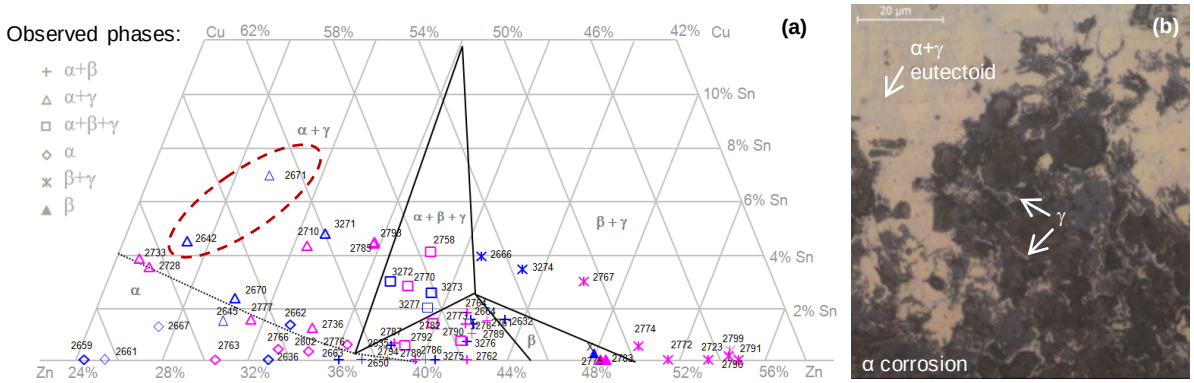

Fig. 4.13 (a) Phase constitution of most of the brass coins superimposed to a partial isothermal section of the Cu-Zn-Sn phase diagram (450ºC), adapted from [Vilarinho *et al.*, 2004]. In blue colour: Ming Dynasty coins; in pink colour: Qing Dynasty coins. (b) Microstructure of coin #2671, showing γ phase resistance to corrosion.

Also, according to Smith and Levine [1973], the γ brass phase is considered structurally equivalent to δ bronze phase (as previously mentioned in Chapter 3). So, for brasses with low zinc contents a

corrosion behaviour similar to bronze alloys should be expected, as observed in coins #2671 and #2642, where the δ phase exhibits higher corrosion resistance.

In tryphasic structures α+β+γ (Fig. 4.14 coin #2770), beta phase seems to corrode preferentially to the other two phases with dezincification and consequent copper redeposition.

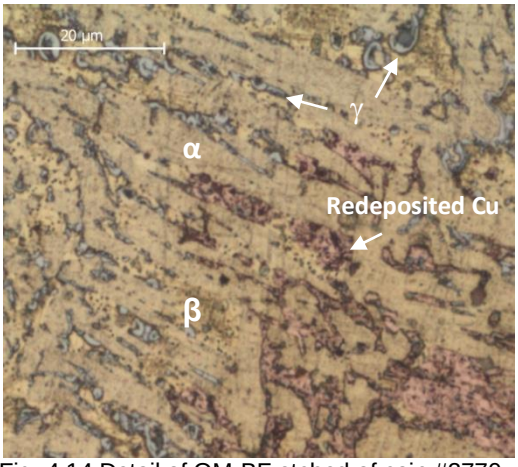

Fig. 4.14 Detail of OM-BF etched of coin #2770.

So, these results point to a general additional corrosion protection in Sn and Sb richer phases.
The corrosion resistance for tin brasses can be sorted as α>γ(high Zn/(Sn+Sb) ratio)>β or γ(low Zn/(Sn+Sb) ratio)>α>β.

4.3.2. Fe-As effect

For brass coins, ferrite seems to be preferentially corroded (see Fig. 4.12(a)). Davies [1993] demonstrates that the additions of Fe to all-alpha (70Cu-30Zn), alpha+beta (60-40) and all-beta brasses accelerate the dezincification process in brasses. It was also verified that when present, As is in association with Fe, promotes the formation of an iron arsenide (see Chapter 3). A micro-XRD analysis of coin #2785 identified α-Fe and Fe_2As phases. While α-Fe is preferentially corroded instead of the brass phases (Fig. 4.15, OM-BF-etched), the iron arsenide seems to have an improved corrosion resistance, remaining unaffected in the structure after the ferrite had corroded (see Fig. 4.15, SEM-EDS mapping). Although Davies [1993] cites several authors on As being unable to stop dezincification in brasses in most cases, in the studied coins it seems to confer this Fe,As-rich phase some protection.

4.3.3. Pb effect on corrosion

Conversely to the observed bronzes [Furtado *et al.*, submitted], concerning leaded brasses, it was observed that Pb globules are relatively stable, probably due to its higher standard reduction potential than Zn. Davies [1993] suggested that small amounts of Pb accelerated dezincification; however this was not evident in the studied coins.

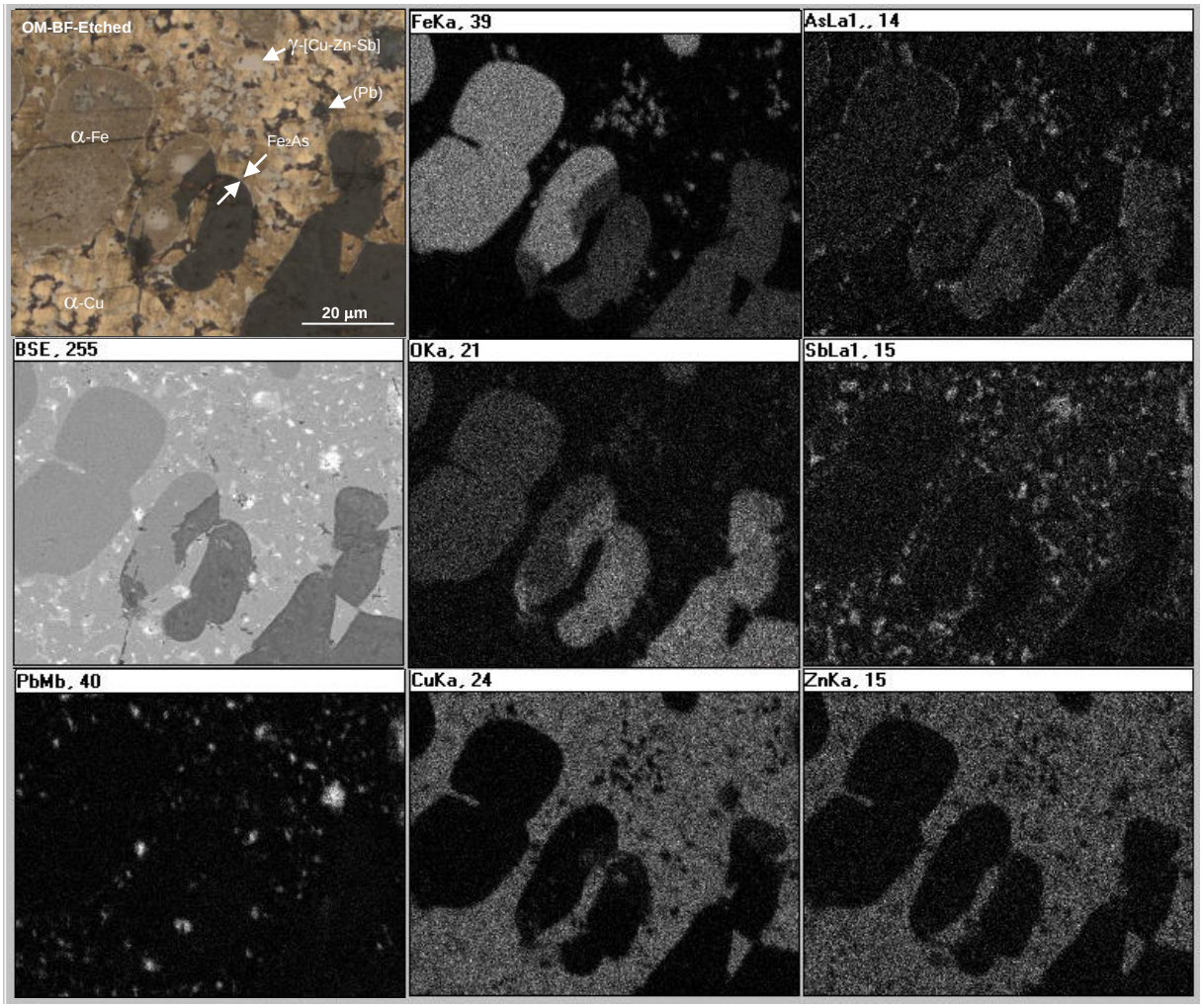

Fig. 4.15 Microstructure of coin #2785 (OM-BF-etched & SEM-BSE-non etched) and SEM-EDS X-ray mapping. Primary Fe-rich dendrites are contained in an α+γ matrix. The Fe_2As phase surrounds the α-Fe dendrites. Pb globules are finely scattered across the matrix.

4.4. General Remarks

Besides the common copper corrosion products, like cuprite (Cu_2O), malachite ($Cu_2(OH)_2CO_3$) or azurite ($Cu_3(CO_3)_2(OH)_2$), chloride corrosion products were detected in copper and bronze coins (nantokite, atacamite or laurionite). Tin tends to be leached from the alloy and remain at the surface in the form of oxide (cassiterite, SnO_2). Lead-rich globules in high leaded coins suffer from transglobular corrosion: Pb is leached towards the surface (remaining or eventually being leached) and its initial globular form is filled with Cu oxide (cuprite, Cu_2O) and/or Pb carbonate (cerussite, $PbCO_3$; hydrocerussite, $Pb_3(CO_3)_2(OH)_2$). The later products seem to render the coins brittle. Image analysis of the cleaned areas helped to assess the original Pb content in the clean sections.

While Pb transglobular corrosion is prominent in bronze coins, dezincification is the main corrosion issue in brass coins. Zinc is leached out of the alloy and copper is redeposited in its place. This is a cyclical process that renders the structure porous, permeable and usually, Cu-rich. Corrosion resistance in higher Zn content phases was observed in the presence of Sn and/or Sb. It was observed in α+γ structures that preferential corrosion also depended of the elemental ratio between

Zn and the protective elements (Sn or Sb). For higher Sn+Sb and lower Zn contents, the brass alloys seem to have a similar corrosion behaviour to bronze alloys, where α phase is less corrosion resistant than δ phase. This is in agreement with the fact that δ bronze and γ brass with high Sn+Sb contents and low Zn contents may in fact be equivalent phases. Consequently, for tin brasses, a sequence of corrosion susceptibility of the phases was established as: α > γ(high Zn/(Sn+Sb) ratio) > β or γ(low Zn/(Sn+Sb) ratio) > α > β.

The iron-rich phase in brass coins seems to be preferentially corroded except when associated with As, for iron arsenide appears to be more corrosion resistant.

General Conclusions

The present work focused on the study of cash coins, a type of coin commonly used in daily transactions for over 2000 years (up to the 20th century AD), not only in China but in several surrounding regions as well. Although widespread in space and time, and with a well established production process, the study and divulgation of Chinese coins research in western languages is uncommon. From a human sciences approach, it has usually concerned research of historical sources and observation of its stylistic work; and from the material or exact sciences approach, it usually regards elemental composition or superficial corrosion products. Microstructural studies of copper-based cash coins are rare, so this work has contributed to a simultaneous first-time glance into three aspects that are often disconnected: history, elemental composition and microstructural constitution. The fact that these alloys are made of several elements other than copper, tin or zinc creates a microstructural variability that had not been studied to date.

Regarding the methodology, a minimum invasive approach was designed in order to safeguard the coins value and aesthetics, but permitting the gathering of relevant data from both the surface and small cleaned metallic regions, manually and mechanically polished to obtain a fresh and levelled surface. The semi-quantitative EDXRF analysis of the surface proved important for various reasons: 1) to determine the alloying elements and distinguish between bronzes, brasses and almost pure copper in a non-invasive expedite manner; 2) although the corrosion layers are usually very thin, in cases where the corrosion products were thicker, it allowed perception of which elements are present in higher contents on the surface; and 3) realize the difference in the Pb distribution from the obverse-reverse contents. The micro-EDXRF analysis of cleaned areas in selected coins permitted to determine the alloys average elemental contents in an also non-invasive and rapid way, as well as to obtain the elemental composition on specific corrosion spots on the coins surface. The metallographic preparation and OM observation of these coins corroborated the process involved in their production – sand casting – and showed 1) the presence of small to large quantities of other phases other than the commonly expected ones in copper, brasses and bronzes; as well as 2) the corrosion features heterogeneity and porosity. The SEM observation and SEM-EDS analysis bonded much of the obtained information on microstructural observations and alloy elemental contents, as it allowed 1) to see S, Sn, Sb, Fe, As and Pb dispersion on the metallic matrix and hence characterize the elements of most metallic phases; 2) in spite of the low contrast between elements (Sn and Sb, or Cu and Zn) due to the proximity of atomic number between these two pairs of elements, it was possible e.g. to distinguish between alpha and beta brass phases and determine their relative compositions; 3) to detect the lighter elements: C and O, and hence characterize the elemental composition of the corrosion products and their distribution in the corrosion layer. Micro-XRD was performed on a few coins, in order to identify or to confirm some of the present metallic phases or corrosion products, when OM observation or SEM-EDS elemental analysis alone or combined were not enough. Since the available area for analysis was approximately 1mm^2, a collimator of 1mm^2 was used to obtain a

good counts-background ratio. Most of the detected compound peaks were partially overlapped because the incident beam always comprised a region with several phases; so the identification was performed through analysing the minor peaks and taking into account the elemental composition and the microstructural observation. Digital radiography performed was successfully used to verify lead distribution within the coin area, but it also served to observe casting defects and corrosion hidden decoration.

Due to the specificity of the analysed objects and the necessity to reduce invasive procedures, many technical adaptations were performed depending on the used instrumentation, which can be of importance when dealing with the analysis of similar objects. Mostly, this work showed that optimal results can be reached through the cleaning of a small area only, which is of extreme importance when dealing with cultural artefacts.

Regarding the elemental characterization, this study permitted the 380 coins that integrated the collection to be divided into 3 main groups: bronzes, brasses and a few almost pure coppers. This was straight forward important because initially the whole collection had been classified as "bronzes". The results show that, until the 16th century (before the Ming dynasty), the most common alloys in cash coin casting were leaded tin bronzes. Thereafter, inspite bronze coins were sporadically cast, brass was the chosen alloy for these cash coins, which is in agreement with most of the coins attributed dates and reigns and also with the previously published works by other authors in the study of similar coin collections, and in written sources of the time. Although composition was officially established by the central government, elemental contents evidence that there was a great discrepance between compositions within the same reign and provinces, which is explained by the inherently fiduciary character of Chinese coinage. The raw material availability in the various provinces where minting took place is probably the most important factor in the elemental content differences within the same reign. Also, disregarding counterfeiting, private minting was encouraged in periods of coin shortage as a way to regulate the economy, although both operations (illicit and private minting) favour elemental composition dispersion due to the lack of regulation enforcement. Plotting compositions and phases of brass coins showed there is no preferential phase constitution among a specific reign/dynasty, which is supported by this historical data.

The copper content decreased over time, undoubtedly due to the constant debasement in alloy composition derived from economical reasons. Tin or zinc are the secondary alloying elements, although tin is in much lesser contents than zinc (Sn<15%; Zn up to 63%). The lead content is very erratic, and its ranges can vary from 5 to 60% within the same time period, reaching its peak content during the 12th and 13th century. Other minor elements such as Fe, Ni, As, Sn and Sb (the first two almost always present and the last two, as minor elements in brasses) are also present in significant and variable amounts, probably due to ore contamination or metal recycling, a very common activity in cash coin production.

The elemental characterization allowed the correction of the previous dating attribution to 6 brass coins (*Tian Qi* Ming dynasty brass coins) from the 16th century that have the same designation as bronze ones issued during the 14th century, during the Yuan rebels period. The use of almost pure copper in Qing dynasty coins was found to be related to a regional issue (Xinjiang province) but can also occur due to the proximity copper-mining sites (like Yunnan).

On the subject of microstructural interpretation, all the observed coins evidence having been mould cast and have not undergone any intentional thermo-mechanical processes. Brass microstructures were considered more complex because of the phase constitution variability but also because of the minor phases that arise from the presence of minor elements in the alloy. Almost pure copper coins are the simplest ones with only sulphur inclusions amongst the Cu matrix.

Pb tends to segregate in small to large Pb-rich globules evenly distributed throughout the coin, according to its content in the alloy. Large globules were found to limit microanalysis results, although OM observation and image assessment may be complementary techniques for a better interpretation. Tin and Sb seem to be associated in promoting Zn-rich phases in brass alloys. Similarly, Fe and As seem to associate in a corrosion resistant iron arsenide. All these usually very finely grained phases, as well as Cu-S inclusions, possess a grey-like coloration which renders its identification rather complex. Ferrite and domeykite, Fe-rich and an As-rich phase respectively, are also grey; so elemental analysis (both by microEDXRF and SEM-EDS) was very important in "decifring" the phase constitution of brass coins.

Although minor elements are considered impurities of the main alloy, and could cause difficulties during the melting and casting of the alloy, the very fine structure of the coins must have overriden this problem. This characteristic is also important in corrosion issues, for finer grain size improves boundary corrosion resistance [Campbell, 2003]. This is probably the reason that even in multiphase alloys, with one or more susceptible phases, corrosion isn't very problematic, as the coins seem to apparently be in a fair conservation condition. The sometimes dramatic differences in corrosion behaviours of objects with similar alloy compositions can be due to the exposure to different environments [Trentelman *et al.*, 1999].

Although corrosion products are strongly dependant on extrinsic factors (like environment), it was found that intrinsic factors as small changes in composition also have great relevance in protecting or potentiating corrosion. The main results obtained by EDXRF from the surface showed, especially in coins with thicker corrosion layers, a superficial enrichment in Pb and Sn, in bronze coins. Pb transglobular corrosion seems to render high-leaded bronze coins brittle and prone to fracture upon impact, which can be relevant information when dealing with these coins. Dezincification occurs very frequently in brass coins, but the presence of Sn and/or Sb seems to reduce the susceptibility of the Zn-rich phases and, as such, may delay the progression of the

corrosion process. In tin brasses a sequence of corrosion susceptibility of the phases was established as: α>γ(high Zn/(Sn+Sb) ratio)>β or γ(low Zn/(Sn+Sb) ratio)>α>β.
Chloride corrosion products were detected in copper and bronze coins, reinforcing the necessity for a dechlorination procedure or tight storage conditions.

Future work in this field may include a systematic review in English (or other alphabetical languages) of the most relevant work published in the Far-East regarding cash coins to favour knowledge transmission on this subject since there is already some work done on the subject. In the same way, experimental archaeometallurgy in order to try to replicate the microstructures in Chinese coins by testing different casting conditions and alloy compositions, similarly to other studies performed on other object typologies [Wang and Ottaway, 2004], would be motivating work. Another area worth exploring would be corrosion studies, for example to characterize the corrosion products using other instrumental methods like Raman or FTIR spectroscopy for compound identification. Also worthy of investigation would be to see which phases are more corrosion susceptible according to different environmental setups, by replicating these complex alloys and testing them for corrosion. It has been noticed that, in spite of the low Fe content in some brass coins, the electrochemistry between these elements in certain conditions potentiates cyclical processes which can destroy the artefact [Xia *et al.*, 2010]. Taking into account the results, tests on the inhibitors commercially available could be performed to help decide accordingly which would bring the most benefits to a specific alloy. It would also be interesting to try to determine the lead provenance by studying their Pb isotopes, seen that most of them are quite rich in this element. Although there seems to be no record of a database with the Pb isotopes distribution in the Chinese territory, several studies have been performed on this subject with good results [Tian *et al.*, 2010; Peng *et al.*,1991; Saitou *et al.*, 1998; Golas, 1999]. The use of a LA-ICP-MS [Günther and Hattendorf, 2005] could also be a worthy technique to explore as it has been tested on coins [Talib *et al.*, 2003; Sarah *et al.*, 2007], reducing even more the abrasion area required for analysis.

In the overall, this work revealed the complex copper-based alloys microstructures of Chinese Cu-cash coins and related them with their elemental composition. This was highly favoured by working in a blossoming Portuguese Archaeometallurgical research group that continuously develops interesting projects in this area. This group is composed of conservation scientists, archaeologists, analytical chemists and metallurgists, maximizing the data extraction and analysis of the studied materials. As a conservation scientist, it was very important to have developed methods that minimized damage and maximized results, for this information can be used in future similar studies.

References

Araújo, M.F.; Alves, L.C.; Cabral, J.M.P. 1993. Comparison of EDXRF and PIXE in the analysis of ancient gold coins. *Nuclear Instruments and Methods in Physics Research B: Beam Interactions with Materials and Atoms* 75 (1), 450-453.

Araújo, M. F., Conceição, A., Barbosa, T., Lopes, M. T., Humanes, M. (2003). Elemental composition of marine sponges from the Berlengas natural park, western Portuguese coast. *X-Ray Spectrometry*, 32(6), 428-433. doi:10.1002/xrs.660

ASM International. 1992. Alloy Phase Diagrams*, ASM Handbook,* Vol. III, Metals Park, USA.

Barbieri-Low, A. 2007. *Artisans in Early Imperial China*. University of Washington, Washington.

Bavarian, B. 2005. *Unearthing Technology's Influence on the Ancient Chinese Dynasties through Metallurgical Investigations*. California State University Northridge, California.

Bayley, J. 1998. *The production of Brass in Antiquity with particular reference to Roman Britain*. In 2000 Years of Zinc and Brass, P.Craddock (Ed). British Museum, London. ISBN: 0861591240

Blalock, J.M.; Harding, J.V.; Pell-Walpole, W.T. 1973. Cu-Sb-Sn (Copper-Antimony-Tin). *Metals Handbook. Metallography, Structural Phase Diagrams* 8, 428-430. American Society for Metals, Metals Park, OH.

Bochvar, N.; Lysova, E.; Rokhlin, L.; Ivanchenko, V. 2007. Copper-Tin-Zinc. In *Landolt-Börnstein*, IV, 11C3, 422-435. Springer, Berlin.

Bosi, C.; Garagnani, G.L.; Imbeni, V.; Martini, C.; Mazzeo, R.; Poli, G. 2002. Unalloyed copper inclusions in ancient bronze artefacts. Journal of Materials Science, 37(20), 4285-4298.

Bowman, S.; Cowell, M.; Cribb, J. 2005. Two thousand years of coinage in China: an analytical survey. In *Metallurgical Analysis of Chinese Coins at the British Museum*, Wang, H., Cowell, M., Cribb, J., Bowman, S. (Eds.). British Museum, London.

Brenan, J. M., Haider, N. 2008. Experimental Evaluation of Liquid Immiscibility in a Portion of the System Fe-Ni-Cu-S Using High Gravitational Acceleration. *Economic Geology*, 103, 1563-1570.

Bronk, H.; Röhrs, S.; Bjeoumikhov, A.; Langhoff, N.; Schmalz, J.; Wedell, R.; Gorny, H.-E.; Herold, A.; Waldschläger, U. 2001. ArtTAX - a new mobile spectrometer for energy-dispersive micro X-ray fluorescence spectrometry on art and archaeological objects. *Fresenius Journal of Analytical Chemistry*, 307-316. doi: 10.1007/s002160100989

Burger, W. 1976. *Ch'ing Cash until 1735.* Mey Ya Publications, Taipei.

Burstein, G.T.; Liu, C.; Souto, R.M.; Vines, S.P. 2004. Origins of pitting corrosion. *Corrosion Engineering, Science And Technology*, 39(1), 25-30. doi:10.1179/147842204225016859

Cabral, J.M.P.; Possolo, A.; Marques, M.G. 1979. Non-destructive analysis of reais and fortes of Dom Fernando of Portugal by X-ray Spectrometry. *Archaeometry*, 21(2), 219-231.

Cabral, J.M.P.; Marques, M.G.; Araújo, M.F.; Marinho, J.R. 1998. Application of XRF Spectrometry to the Study of Visigothic Coinage. In *Metallurgy in Numismatics* vol.4, Oddy, A. & Cowell, M. (Eds), 472-482. Royal Numismatic Society, London.

Cabral, J.M.P. 1995. *Métodos Físicos e Químicos de Análise no Estudo da Composição das Ligas de que são feitas as moedas*. In ANEJOS AespA, Mª P. García-Bellido, R.M. Sobral (Eds), XIV, 15-24. CSIC, Madrid.

Caestecker, J.C. 2011. *Chinese Metallic Money and Cash.* Museum of the National Bank of Belgium, Brussels.

Caley, E. R. 1945. Methods of Distinguishing Cast from Struck Coins. *Numismatic Review*, 21-24.

Calliari, I.; Magrini, M.; Zambon, A.; Guerriero, P.; Martini, R. 1999. Microstructural and Compositional Characterization of Roman Coins. *X-ray Spectrometry*, 28, 86-90.

Campbell, J. 2003. *Castings*. 2nd ed., Butterworth-Heinemann, Oxford.

Canberra. 2003. *WinAxil Operational Guide*. Canberra Eurisys Benelux N.V., Canberra.

Cao, C.; Wei, B. 2002. Microstructure Evolution of Cu-Pb Monotectic Alloys Processed in Drop Tube. *J. Mater. Sci. Technol.*, 18(1), 73-76.

Casaletto, M.P.; Caruso, F.; Ingo, G.M.; Caro, T.; Riccucci, C. 2008. Recovering Bronze Metallurgy from Archaeological Artefacts for the Production of Reference Materials. *Archaeometallurgy in Europe*, Vol. 39, Aquileia, Italy.

CDA, 1992. Equilibrium Diagrams: Selected copper alloy diagrams illustrating the major types of phase transformation. *Copper Development Association*, 94.

Chakrabarti, D.J.; Laughlin, D.E. 1983. The Cu-S (copper-sulfur) system. *Bulletin of Alloy Phase Diagrams*, 4(3), 254-271.

Chase, W.T. 1994. *Chinese Bronzes, Casting, Finishing, Patination and Corrosion*. Ancient and Historic Metals - Conservation and Scientific Research, Getty Conservation Institute, USA. ISBN: 0892362316

Chen, T. 1991. *China's Copper Production in Yunnan Province (1700-1800).* In Money, Coins and Commerce: Essays in the monetary history of Asia and Europe (from Antiquity to Modern Times). E. Von Cauwenberghe (Ed). Leuven University Press, Belgium. ISBN: 9061864852

Cheng, C.F.; Schwitter, C.M. 1957. Nickel in Ancient Bronzes. American Journal of Archaeology, 61, 351-365.

Chernykh, E.N.; Prusakov, B.A.; Katkova, L.V. 1998. A Study of Ancient Copper. *Metal Science and Heat Treatment*, 40(9-10), 368-373.

Chou, C.; Chen, S. 2006. Phase equilibria of the Sn–Zn–Cu ternary system. *Acta Materialia*, 54(9), 2393-2400. doi:10.1016/j.actamat.2006.01.014

Ciliberto, E.; Spoto, G. (Eds.) 2000. *Modern Analytical Methods in Art and Archaeology*. John Wiley & Sons, USA. ISBN 0-471-29361-X

Combarieu, R.; Dauchot, G.; Delamare, F. 1998. *Étude de l'adsorption du benzotriazole sur le fer, le cuivre et le laiton alpha par Tof-SIMS et XPS*. In Metals 98 (Proceedings of the International Conference on Metals Conservation), 223-228. W. Mourey & L. Robbiola (Eds). James & James, London.

Coole, A.; Kozono, H.; Bowker, H. 1967. *A bibliography on Far Eastern Numismatology and a coin index*. In Encyclopedia of Chinese Coins. Vol.I, Inter-collegiate Press, USA.

Coole, A. 1981. *Earliest round coins of China.* In Encyclopedia of Chinese Coins, Vol. VII, Quarterman Publications, USA.

Cowell, M.; Cribb, J.; Bowman, S.; Shashoua, Y. 2005a. *The Chinese Cash: composition and production.* In Metallurgical Analysis of Chinese Coins at the British Museum. Helen Wang; Michael Cowell, Joe Cribb; Sheridan Bowman (Eds). British Museum, London.

Cowell, M.; Wang, H. 2005b. *Metal supply for the metropolitan coinage of the Kangxi period (1662-1721)*. In Metallurgical Analysis of Chinese Coins at the British Museum. Helen Wang; Michael Cowell, Joe Cribb; Sheridan Bowman (Eds). British Museum, London.

Craddock, P.T. 1995. *Early mining and metal production*. Edinburgh University Press, Edinburgh.

Craddock, P. 1998. *2000 years of zinc and brass*. British Museum, London. ISBN: 0861590503

Craddock, P. 2008. An Early Zinc-smelting Retort from China. In *Historical Metallurgy Society*, 69, 3-4.

Craddock, P.T. 2009. *Metals II: Metalwork and coins*. In "Scientific investigation of copies, fakes and forgeries", Elsevier / Butterworth-Heinemann, Oxford, 157-185.

Cresswell, O.D. 1979. *Chinese cash.* Sanford J. Durst Numismatic Publications, New York. ISBN: 0900696346

Cribb, J. 1996a. *Chinese coin finds from South India and Sri Lanka*. Maheshwari, K.K., Rath, B. (eds), In Numismatic Panorama, Essays in Memory of late Shri S.M. Shukla. New Delhi, 253-69.

Cribb, J.; Potts, D. 1996b. Chinese coin finds from Arabia and the Arabian Gulf. *Arabian Archaeology and Epigraphy*, 7, 108-18.

CTIF (Centre Technique des Industries de la Fonderie) 1967. Atlas métallographique des alliages cuivreux. Éditions Techniques des Industries de la Fonderie, Paris.

Dai, Zhiqiang. 1985. Bei Song tongqian jinshu chengfen chutan. *Zhongguo Qianbi*, 3, 7-16.

Dai, Zhiqiang; Zhou, Weirong. 1992. Studies of the alloy composition of more than two thousand years of Chinese coins (5th century BC – 20th century AD). *Journal of the Historical Metallurgy Society*, 26, 45-55.

Dalgado, S. R. 1982 (1st edition 1921). Glossário Luso-Asiático, II. Helmut Buske, Hamburg.

Davies, D.D. 1993. *A note on the dezincification of brass and the inhibiting effect of elemental additions.* Copper Development Association, New York.

Davis, J.R. 2001. *Copper and Copper Alloys.* ASM International Handbook Committee, ASM International. ISBN 0871707268

Denker, A.; Bohne, W.; Opitz-Coutureau, J.; Rauschenberg, J.; Rohrich, J.; Strub, E. 2005. Influence of corrosion layers on quantitative analysis. *Nuclear Instruments & Methods in Physics Research Section B-Beam Interactions with Materials and Atoms*, 239(1-2), 65-70.

Deshpande, V. 1996. A note on ancient zinc-Smelting in India and China. *Indian Journal of History and Science*, 31(3), 275-279.

Eagleton, C.; Williams, J. 2007. *Money - A History*. The British Museum Press, London. ISBN: 978-0-7141-1814-7.

Earl, B.; Adriaens, A. 2000. Initial experiments on arsenical bronze production. *Journal of the Minerals Metals & Materials Society (JOM)*, 52(3), 14-16.

Faltermeier, R.B. 1998. A corrosion inhibitor test for copper-based artifacts. In *Studies in Conservation* (43) 121-128.

Fang, J.N.; Tan, L.P. ; Huang, E. 2003. Modes and textures of secondary minerals on Chinese coins of different ages. *Mineralogical Magazine*, 67(1), 23-29. doi:10.1180/0026461036710081

Fell, V. 1995. *X-radiography and archaeometallurgy.* Datasheet no.14, Historical Metallurgy Society.

Figueiredo, E.; Valério, P.; Araújo, M.; Senna-Martinez, J.C. 2007a. Micro-EDXRF surface analyses of a bronze spear head: Lead content in metal and corrosion layers. Nuclear Instruments and Methods in Physics Research Section A, 580(1), 725-727. doi:10.1016/j.nima.2007.05.135

Figueiredo, E.; Araújo, M.F.; Silva, R.J.C.; Senna-Martinez, J.C. 2007b. Corrosion of bronze alloy with some lead content: implications in the archaeometallurgical study of Late Bronze Age metal artefacts from "Fraga dos Corvos" (North Portugal). *Metal 07*(1), 61-66.

Figueiredo, E.; Silva, R.J.C.; Araújo, M.F.; Senna-Martinez, J.C. 2010. Identification of ancient gilding technology and Late Bronze Age metallurgy by EDXRF, Micro-EDXRF, SEM-EDS and metallographic techniques. *Microchimica Acta*, 168, 283-291. doi: 10.1007/s00604-009-0284-6

Fontana, M.G. 1987. *Corrosion Engineering*. McGraw-Hill, USA.

Furtado, M.J. 2004. *Conservação de Objectos Orientais do Acervo do Museu do Centro Científico e Cultural de Macau*. Thesis presented on the final year of the Degree in Conservation and Restoration by FCT-UNL. (non-published)

Furtado, M.J.; Silva, R.J.C.; Araújo, M.F.; Braz Fernandes, F.M. 2010a. Composition and Microstructures of Imperial Brass Chinese Coins. *Materials Science Forum,* 636-637, 531-537. doi:10.4028/www.scientific.net/MSF.636-637.531

Furtado, M.J.; Silva, R.J.C.; Araújo, M.F.; Braz Fernandes, F.M. 2010b. *Some corrosion issues in ancient Chinese brass coins - Influence of minor elements in the corrosion susceptibility*. Eurocorr 2010 (CD Proceedings), 1-8.

Furtado, M.J.; Silva, R.J.C.; Araújo, M.F.; Braz Fernandes, F.M. 2010c. Influence of minor elements in ancient chinese brass coins microstructures. TOFA 2010 (Proceedings). ISBN: 978-972-752-126-5.

Furtado, M.J. 2008. *Moedas Kangxi.* In Tomás Pereira - Um Jesuíta na China de Kangxi. Museu do Centro Científico e Cultural de Macau, Lisboa.

Furtado, M.J. 2011. Moedas Imperiais Chinesas da colecção do Museu do Centro Científico e Cultural de Macau. *Numismática*, 114, (38/4).

Fürtauer, S. 2010. *Investigation of relevant phase diagrams for high temperature solder materials: The binary systems Cu-Sn and Cu-Sb.* MSc Thesis. Universität Wien (University of Vienna).

Gaines, T.; McGrath, E.; Iduma, V.; Kuzava, R.; Frederick, S.; Benvenuto, M. 2002. Chemical compositions of Chinese coins of emperor Ch'ien Lung (Qian Long) and Annamese coins of emperor Thanh Thai via energy-dispersive X-ray fluorescence. *Archaeological Chemistry: Materials, Methods, and Meaning*, American Chemical Society Sympos., 831, 231-244. doi:10.1021/bk-2002-0831.ch015

Ghosh, G. 2007. Cu-Sb-Sn (copper-antimony-tin). In Landolt-Börnstein, IV/2, 11C2. Springer, Berlin.

Gialanella, S.; Baró, M.D.; Amils, X.; Suriñach, S.; Yavari, A.R. 1997. Rapid Solidification and Mechanical Grinding of Cu-Zn alloys. *Materials Science Forum*, 235-238, 571-76. doi:10.4028/www.scientific.net/MSF.235-238.571

Giumlia-Mair, A. 2005. On surface analysis and archaeometallurgy. *Nuclear Instruments and Methods in Physics Research*, B, 239, 35-43.

Glamann, K. 1953. The Dutch East India Company's trade in Japanese copper, 1645-1736. *Scandinavian Economic History Review*, I, 40-80.

Golas, P.J. 1999. Chemistry and Chemical Technology, part XIII: Mining. In *Science and Civilization in China,* vol. 5. Cambridge University Press, Cambridge.

Gorny, N. F. 2003. Northern Song Dynasty Cash Variety Guide, Volume 2. *Kosen Daizen (Song Yuan to Jing You, A. D. 968 – 1034)*. Published by the author, Oregon.

Gosen, M. 1963. Annan senpu (Vietnamise Coins Catalogue), 3 Vols. Tokyo.

Graedel, T.E. 1994. Chemical Mechanisms for the Atmospheric Corrosion of Lead. *Journal of The Electrochemical Society*, 141(4), 922-927. doi:10.1149/1.2054858

Gu, Z. 1954. *Tu shi yu ji yao (1667).* Needham, J. Ed. In Science and Civilization in China, V:2, p.231. University Press, Cambridge.

Guerra, M. F. (2008). An overview on the ancient goldsmith's skill and the circulation of gold in the past: the role of x-ray based techniques. *X-Ray Spectrometry*, 37, 317-327. doi:10.1002/xrs

Günther, D.; Hattendorf, B. 2005. Solid sample analysis using laser ablation inductively coupled plasma mass spectrometry. *Trends in Analytical Chemistry*, 24(3), 255-265. doi:10.1016/j.trac.2004.11.017

Hansen, M.; Anderko, K. 1958. *Constitution of Binary Alloys.* 2nd ed., McGraw-Hill, New York, 581.

Hartill, D. 2003. *Qing Cash.* Royal Numismatic Society Special Publication, 37. London.

Hartill, D. 2005. *Cast Chinese Coins - A historical catalogue.* Trafford Publishing, Canada.

He, L.; Liang, J.; Zhao, X.; Jiang, B. 2011. Corrosion behavior and morphological features of archeological bronze coins from ancient China. *Microchemical Journal*, 99(2), 203-212. doi:10.1016/j.microc.2011.05.009

Heidemann, S. 2004. Collections of Oriental Coins in Germany. *Oriental Numismatic Society Newsletter*, 179, 5-9.

Huang, R. 1974. *Taxation and Governmental Finance in Sixteenth Century Ming China*. Cambridge University Press, Cambridge. ISBN: 05212202833

Ingo, G.M.; Manfredi, L.I.; Bultrini, G.; LoPiccolo, E. 1997. Quantitative analysis of copper-tin bronzes by means of glow discharge optical emission spectrometry. *Archaeometry*, 39, 59-70.

Ingo, G.M.; Angelini; E., Bultrini, G.; Caro, T.D.; Pandolfi, L.; Mezzi, A. 2002. Contribution of surface analytical techniques for the microchemical study of archaeological artefacts. *Surface and Interface Analysis*, 34, 328-336. doi:10.1002/sia.1311

Ingo, G.M.; Balbi, S.; De Caro, T.; Fragala, I.; Angelini, E.; Bultrini, G. 2006. Combined use of SEM-EDS, OM and XRD for the characterization of corrosion products grown on silver roman coins. *Applied Physics a-Materials Science & Processing*, 83(4), 493-497.

IUPAC, 1978. Nomenclature, symbols, units and their usage in spectrochemical analysis II. Data interpretation. *Spectrochimica Acta B,* 33, p.242-245.

Jantzen, T.; Spencer, P.J. 1998. Thermodynamic assessments of the Cu-Pb-Zn and Cu-Sn-Zn systems. *Calphad*, 22(3), 417-434.

Jenkins, R.; Gould, R.W.; Gedcke, D. 1995. Quantitative X-Ray Spectrometry. 2nd Ed., Marcel Dekker, New York. ISBN 0-8247-9554-7.

Jones, D.A. 1996. Principles and Prevention of Corrosion. Prentice-Hall, USA.

Junior, J. de Figueiredo; Lins, V. de Freitas Cunha; de Bellis, V. 2007. Surface characterization of a corroded bronze-leaded alloy in a salt spray cabinet. *Applied Surface Science*, 253(17), 7104-7107. doi:10.1016/j.apsusc.2007.02.053

Junk, M. 2003. *Material properties of copper alloys containing arsenic, antimony, and bismuth. The material of Early Bronze Age ingot torques* (PhD Dissertation). Freiberg University of Technology, Freiberg.

Kulkarni, A.D. 1973. *Cu-Ni diagram.* Lyman, T., Hawkins, D., Hultgren, R. (Eds.), In Constitution of binary alloys, Metals Handbook, Vol. 8, American Society for Metals, 294.

Kumanotani, J.; Achiwa, A.; Oshuna, R.; Adachi, K. 1979. Attempts to understand Japanese lacquer as a superdurable material. *Cultural Property and Analytical Chemistry,* 51-62.

Lebrun, N.; Bätzner, C.; Ferro, R.; Rokhlin, L.; Tedenac, J.-Claude 2007. *Cu-Sb-Zn (Copper – Antimony – Zinc)*. Landolt-Bornstein IV/5. Materials Science International Team MSIT. doi:10.1007/978-3-540-47000-7_38

Lee, C.; Lin, C.; Yen, Y. 2007. The 260°C phase equilibria of the Sn–Sb–Cu ternary system and interfacial reactions at the Sn–Sb/Cu joints. *Intermetallics*, 15 (8), 1027-1037. doi:10.1016/j.intermet.2006.12.002

Lei, J.; Zeng, L.; Tong, H.; Yu, X.; Liu, J.; Hu, J. 2003. Characterization of Kangxi Coins of Tsing Empire by SEM-EDS. *Microchimica Acta*, 142(1-2), 123-127. doi:10.1007/s00604-003-0016-2

Lei, J.-Feng; Zhu, Z.-Hong; Zeng, L.-Bo; Tong, H.; Hu, J.-Ming. 2004. Fast Dating of Yongzheng Copper Coins in Tsing Empire by SEM-EDS. *Wuhan University Journal of Natural Sciences*, 9(1), 89-92.

Li, X. J.; Martinón-Torres, M.; Meeks, N.D.; Xia, Y.; Zhao, K. 2011. Inscriptions, filing, grinding and polishing marks on the bronze weapons from the Qin Terracotta Army in China. *Journal of Archaeological Science*, 38(3), 492-501. Elsevier Ltd. doi:10.1016/j.jas.2010.09.012

Li, X., Han, R. 1992. A study of the metallic artifacts unearthed from the Tubo Tombs, Dulan County, Qinghai Province. In *Studies in the History of Natural Sciences*, 11(3), 278-288. [in mandarin]

Lin, C.-Y.; Lee, C.; Yen, Y.; Ting, C. 2007. The 400°C phase equilibria of the Sn–Sb–Cu ternary system and interfacial reactions at the Sn–Sb/Cu joints.

Lin, E.K.; Shen, C.T.; Yu, Y.C.; Wang, C.W.; Hsieh, C.H.; Wu, S.C. 1994. External-beam PIXE analysis of ancient chinese coins. *Nuclear Instruments and Methods in Physics Research*, B, 85(1-4), 869-873.

Ling, H.; Qingrong, Z.; Min, G. 2007. Characterization of corroded bronze Ding from the Yin Ruins of China. *Corrosion Science*, 49(6), 2534-2546. doi:10.1016/j.corsci.2006.11.005

Lockhart, James (Sir). 1975. *The Stewart Lockhart collection of Chinese copper coins, by Sir James H. Stewart Lockhart.* 2nd Ed.: Lawrence, Mass., Quarterman Publications. ISBN: 0880000562

Loeper-Attia, M.-A.; Robbiola, L. 1998. Étude de la déchloruration de dépôts de CuCl formés sur du cuivreen absenceet en presence de benzotriazole (BTA). In *Metals 98* (Proceedings of the International Conference on Metals Conservation), 215-222. W. Mourey & L. Robbiola (Eds). James & James, London.

Lutz, J.; Pernicka, E. 1996. Energy dispersive X-ray fluorescence analysis of ancient copper alloys: empirical values for precision and accuracy. *Archeometry*, 38(2), 313-323.

Mabuchi, H.; Notsu, K.; Nishimatsu, S.; Fuwa, W.; Iyam, H.; Tominaga, T. 1979. Kodai kahei kagaku soshiki [Chemical compositions of ancient coins]. *Nippon Kagaku kaishi*, 5, 586-90. [in Japanese]

Mabuchi, H.; Yamaguchi, S.; Kanno, H.; Nakai, T. 1978. Chemical analysis of ancient oriental coins by atomic absorption spectrometry. *Scientific Papers on Japanese Antiques and Art Crafts*, 22, 20-23.

Mandel, E.J. 1972. *Cast coinage of Korea*. Racine (Wis.), Western Pub. Co.

Martyushev, N. 2010. Parameters of the dendritic structure of copper alloys. *Chem. Met. Alloys* 3, 197-200.

Mccann, L. I.; Trentelman, K.; Possley, T.; & Golding, B. 1999. Corrosion of Ancient Chinese Bronze Money Trees Studied by Raman Microscopy. *Journal of Raman Spectroscopy*, 30, 121-132.

Mei, Jianjun; Rehren, Thilo (eds). 2009. *Metallurgy and Civilisation: Eurasia and Beyond*. London, Archetype.

Miettinen, J. 2008. Thermodynamic description of the Cu–Fe–Sn system at the Cu–Fe side. *Calphad*, 32(3), 500-505. doi:10.1016/j.calphad.2008.06.003

Misner, J.; Boats, J.; Benvenuto, M. 2007. Chemical Compositions of Song Dynasty, Chinese, Copper-Based Coins via Energy Dispersive X-Ray Fluorescence. In: M. D. Glascock, R. J. Speakman, & R. S. Popelka-Filcoff (Eds.), *Archaeological Chemistry: Analytical Techniques and Archaeological Interpretation*. Washington D.C., American Chemical Society.

Motai, K.; Watanabe, Y.; Hashimoto, S. 1993. Laticce Modulation of the epsilon phase in a Cu-Sb alloy. *Acta Crystallographica* B49, 655-661.

Notsu, K.; Mabuchi, H. 1979. Simultaneous multi-elementar analysis of coins by inductively coupled plasma emission spectrometry. In: *Proceedings 2nd International Symposium on Conservation and Restoration of Cultural Property*, 111-24.

Okamoto, H. 1991. The As-Fe (arsenic-iron) system. *Journal of Phase Equilibria* 12(4), 457-461. doi:10.1007/BF02645968

Ouyang, Zhongshi; Wang, Youfen. 2008. Chinese Calligraphy. *Yale University Press*, Yale. ISBN: 9780300121070.

Pan, C.; Liao, L.; Hu, Y. 2007. Functions and Morphology of Metal Lead Addition to Ancient Chinese Bronzes. *Advanced Materials and Processing* 26-28, 523-526.

Peng, Xinwei. 1965. *Zhongguo Huobi Shi*. Shangai. (A monetary history of China). Translated from mandarin by Edward H. Kaplan (1994). 2vols. Bellingham WA, Western Washington University. ISBN: 091458481]

Peng, Z.; Li, X.; Zhang, B.; Li, Z.; Li, K.; Wan, F. 1991. Lead isotope studies of metal sources for the earliest bronze drums in Yunnan Province, China. *Chinese Journal of Geochemistry* 10 (4), 357-362. DOI: 10.1007/BF02841096

Petersen, J.O. 1990. Traditional zinc smelting in the Guima district of Hezhang County. In: *2000 Years of Zinc and Brass,* British Museum Occasional Paper 50, 103-22.

Petrie, A.E.H. 1964. *An illustrated guide to Chinese cash pieces of the Manchu mints, A.D. 1662-1796*. Otava, Collectors Research.

Pollard, A.M.; Batt, C.M.; Stern, B.; Young, S.M.M. 2007. *Analytical Chemistry in Archaeology*. Cambridge, Cambridge University Press. ISBN: 13978-0-521-65209-4

Predel, B. 1994a. Cu-S (Copper-Sulfur). Madelung, O. (Ed.). Landolt-Börnstein Database. SpringerMaterials. doi: 10.1007/10086090_1113

Predel, B. 1994b. Cu-Zn (Copper-Zinc). Madelung, O. (Ed.). Landolt-Börnstein Database. SpringerMaterials. doi: 10.1007/10086090_1134

Raghavan, V. 1992. The As-Cu-Fe (arsenic-copper-iron) system. *Phase Diagrams of Ternary Iron Alloys*, part 6, 244-249. Calcutta: Indian Institute of Metals.

Raghavan, V. 2004. As-Cu-Fe-S (Arsenic-Copper-Iron-Sulfur). *Journal of Phase Equilibria & Diffusion* 25(5), 455-457. doi:10.1361/15477030420854

Raghavan, V. 2009. Cu-Fe-Sn (Copper-Iron-Tin). *Journal of Phase Equilibria and Diffusion* 30(4), 384-385. doi:10.1007/s11669-009-9548-4

Rasband, W.S. 1997-2011. *Image J*, U. S. National Institutes of Health, Bethesda, Maryland, USA, http://imagej.nih.gov/ij/.

Robbiola, L.; Portier, R. 2006. A global approach to the authentication of ancient bronzes based on the characterization of the alloy–patina–environment system. *Journal of Cultural Heritage* 7, 1-12.

Rovira Llorens, S.; Gómez Ramos, P. 2003. Las primeras etapas metalúrgicas en la Península Ibérica. *III. Estudios Metalográficos*. Madrid, Fundación José Ortega y Gasset. ISNB: 849-225629-X

Saitou, T.; Takahashi, T.; Nishikawa, Y. 1998. Chemical Study of the Medieval Japanese Mochu-sen (Bronze Coins). *IMES Discussion Paper Series* 98-E-13. Tokyo, Bank of Japan. http://www.imes.boj.or.jp/research/papers/english/98-E-13.pdf

Sano, Y.; Tominaga, T. 1982. Segregation of elements in ancient Chinese coinage. In: *Scientific Papers on Japanese Antiques and Art Crafts* 27, 12-17.

Sano, Y.; Notsu, K.; Tominaga, T. 1983. Studies on chemical composition of ancient coins by multivariate analysis. In: *Scientific Papers on Japanese Antiquities and Art Crafts* 28, 44-58.

Sarah, G.; Gratuze, B.; Bompaire, M.; Barrandon, J.-n. 2007. A new approach for the investigation of ancient silver coins: depth profile analysis by laser ablation inductively coupled plasma mass spectrometry (LA-ICP-MS). In Proceedings of the *2nd International Conference Archaeometallurgy in Europe* (Aquileia).

Saunders, N.; Miodownik, A.P. 1990. The Cu-Sn (Copper-Tin) System. In *Bulletin Of Alloy Phase Diagrams* 11, 278-287.

Saunders, N.; Miodownik, A.P. 1994. Cu-Sn (Copper-Tin). In: Subramanian, P.R., Chakrabarti, D.J., Laughlin, D.E. (Eds.), *Phase Diagram of Binary Copper Alloys*. Materials Park (OH), ASM International, 412-418.

Schjöth, F. 1965. *Chinese Currency (Currency of the Far East), a comprehensive text: Zhou Dynasty (1122 BC-225 BC) through Qing Dynasty (1644 AD-1911 AD)*. Virgil Hancock (Ed.). Iola (WI), Krause Publ.

Schotte, B.; Adriaens, A. 2006. Treatments of Corroded Lead Artefacts. *Studies in Conservation* 51, 1-8.

Schweizer, F. 1972. Analysis of ancient coins using a point source linear X-ray spectrometer. A critical review. In Royal Numismatic Society Special Publication (8), 153-169. London.

Scott, D.A. 1991. *Metallography and Microstructure of Ancient and Historic Metals*. Los Angeles, Archetype Books. ISBN: 0-89236-195-6

Scott, D.A. 2002. *Copper and Bronze in Art – Corrosion, colorants, conservation*. Getty Publications, USA.

Scott, D. 2010. *Ancient Metals: microstructures and metallurgy* (vol.1). Los Angeles, Conservation Science Press. ISBN: 978-0-9829338-0-0

Scott-Dodd, A. 1939. *Counterfeit coins. Meeting of the Scottish Section* 64, 861-866. doi:10.1039/an9396400861

Selwyn, L. 2005. Health and Safety Concerns Relating to Lead and Lead Compounds in Conservation Health and Safety. *Journal of the Canadian Association for Conservation* 30.

Serra, I. S. 2005. Estudio preliminar de la colección de moneda china y japonesa del Museo Arqueológico Nacional de Madrid. In: C. Alfaro, C. Marcos, & P. Otero (Eds.). *XIII Congresso Internacional de Numismática* Actas II, 9-11. Madrid: Secretaría General Técnica. Retrieved from http://en.calameo.com/read/0000753359af1d450140e

Serra, I. S. 2006. Monedas Chinas En El Museo Cerralbo - Chinese Coins From The Cerralbo Museum (Madrid , Spain). *Documenta & Instrumenta* 4, 151-167.

Shen, Xiongqing. 1929. Zhongquo zhiqian zhi dingliang fenxi. In: *Huaxue Gongye* vol.5(1),117-18.

Shigeshi, K. 1959. Zhongguo Jinji Shi Kaozheng. Translated by Wu Jie. Beijing: Shangwu yin shuguan, juan I, 147-55.

Silva, R.J.C.; Figueiredo, E.; Araújo, M.F.; Pereira, F.; Braz Fernandes, F.M. 2008. Microstructure Interpretation of Copper and Bronze Archaeological Artefacts from Portugal. Mat. Sci. Forum, 587-588, 365-369.

Smith, C. S.; Levine, E. D. 1973. Cu-Sn-Zn (copper-tin-zinc). *Metals Handbook. Metallography, Structure. Phase Diagrams*. 8, 431. Metals Park, OH: ASM International.

Song, Yingxing. 1637. *Tian gong kai wu: Chinese Technology in the Seventeenth Century*. Translated from mandarin with preface by E-Tu Zen Sun and Shiou-Chuan Sun (1966). University Park, Pennsylvania State University Press.

Steinhoff, D.; Bandhari, V.B. 2007. Design of Machine Elements. Tata McGraw-Hill, New Delhi.

Subramanian, P.R.; Laughlin, D.E. 1994. Cu-Sb (Copper-Antimony). In : *Phase Diagram of Binary Coppers*. ASM, Materials Park, OH, 372-383.

Talib, D.; Ma, R.; Mcleod, C. W.; Green, D. 2003. Multielement Analysis of Modern and Ancient Coins using Diamond Lapping Film and Laser Ablation ICP Mass Spectrometry. *Canadian Journal Of Analytical Sciences And Spectroscopy* 3.

Tanner, B.K.; Macdowall, D.W.; Maccormack, I.B.; Smith, R.L. 1979. Ferromagnetism In Ancient Copper-Based Coinage. *Nature* 280, 46-48.

Teng, S. 2000. The Original Significance of Bi Disks: Insights Based on Liangzhu Jade Bi with Incised Symbolic Motifs. *Journal of East Asian Archaeology*. 2, 1/2, 165-194.

Thierry, F. 1987. *Catalogue des monnaies Vietnamiennes.* Paris, Bibliothèque Nationale de France.

Thierry, F. 1992. *Monnaies de Chine (vol. I).* Paris, Bibliothèque Nationale de France.

Thierry, F. 2003. *Monnaies de Chine - Des Qin aux Cinq Dynasties (vol. II).* Paris, Bibliothèque Nationale de France.

Thierry, F. 2001. La Fiduciarité Idéale À L'épreuve Des Coûts De Production: Quelques Éléments Sur La Contradiction Fondamentale De La Monnaie En Chine. *Revue Numismatique*, 6 (157), 131-152. DOI:10.3406/NUMI.2001.2323

Tian, J. H.; Jin, Z. Y.; Li, R. L.; Yan, L. F. ; Cui, J. Y. 2010. An Elemental And Lead-Isotopic Study On Bronze Helmets From Royal Tomb No. 1004 In Yin Ruins. *Archaeometry* 52, 1002–1014. doi: 10.1111/j.1475-4754.2010.00519.

Trentelman, K.; Stodulski, L.; Lints, R.; & Kim, C. 1999. A Comparative Study Of The Composition And Corrosion Of Branches From Eastern Han Dynasty Money Trees. *Studies In Conservation* 44(3), 170-183.

Tsu-yu, Chen. 1991. China's Copper Production in Yunnan Province. 1700-1800. In: Cauwenberghe, Eddy Van. (Ed.) *Money, Coins, and Commerce: Essays in the Monetary History of Asia and Europe* 95-117. Leuven, Leuven University Press. ISBN: 9061864852´

Twitchett, D.; Mote, F.W. (Eds.) 2008. The Ming Dynasty, 1368-1644 (part 2). In *The Cambridge History of China* (vol.8). Cambridge University Press, Cambridge.

Tylecote, R.F. 1979. The effect of soil conditions on the long-term corrosion of the buried tin-bronzes and copper. *Jour. Archaeological Science* 6, 345-347.

U.S. Congress. 1901. Congressional Edition, vol. 4303. Washington D.C., USGPO.

Valério, P.; Silva, R.J.C.; Araújo, M.F.; Soares, A.M.M.; Braz Fernandes, F.M.. 2010a. Microstructural Signatures of Bronze Archaeological Artifacts from the Southwestern Iberian Peninsula. *Mat. Sci. Forum* 636-637, 597-604. doi: 10.4028/www.scientific.net/MSF.636-637.597

Valério, P.; Silva, R.J.C.; Soares, A.M.M.; Araújo, M.F.; Braz Fernandes, F.M.; Silva, A.C.; Berrocal-Rangel, L. 2010b. Technological continuity in Early Iron Age bronze metallurgy at the South-Western Iberian Peninsula – a sight from Castro dos Ratinhos. *J. Archaeological Science*, 37, 1811-1919. doi:10.1016/j.jas.2010.01.038

Vilarinho, C.; Soares, D.; & Castro, F. 2004. Contribution to the knowledge of the Cu-Sn-Zn system for compositions close to brass alloys. *Journal of Alloys and Compounds* 379(1-2), 161-165. doi:10.1016/j.jallcom.2004.02.020

Vogel, H. U. 1987. Chinese Central Monetary Policy, 1644-1800. In: *Late Imperial China*, vol.8, 2, 1-52.

Von Glahn, R. 1996. *Fountain of Fortune: Money and monetary policy in China, 1000-1700*. University of California Press, Berkeley (California). ISBN: 0-520-20408-5.

Voort, G. F. V. 2004. Color Metallography. In: A. International (Ed.). *Metallography and Microstructures*, vol. 9, 493-512. doi:10.1361/asmhba0003752

Voort, G. F. 1984. *Metallography - Principles and Practice*. USA: McGraw-Hill.

Wagel, S. 1915. *Chinese Currency and Banking*. Shanghai, North-China Daily News & Herald.

Walker, R. 1980. Corrosion and preservation of bronze artifacts. *Journal of Chemical Education* 4, 277-280. Madison.

Wang, C.Y. 1919. *Antimony*. 2nd Ed. London, Charles Griffin & Company, Ltd.

Wang, J. *et al*. 1995. *Zhongguo Gudai Jinshu Huaxue ji Jin Danshu. Shanghai: Zhongguo kexue tushu yiqi gongsi*, 21-28.

Wang, Q.; Ottaway, B. 2004. *Casting Experiments and Microstructure of Archaeologically Relevant Bronzes* (BAR International Series 1331). Oxford, Archaeopress. ISBN: 1841716766.

Wang, H.; Cowell, M.; Cribb, J.; Bowman, S. (Eds.). 2005. *Metallurgical Analysis of Chinese Coins at the British Museum* (British Museum Press, London.

Wayman, M. 2000. Archaeometallurgical contributions to a better understanding of the past. *Materials Characterization* 45, 259-267, 2000. doi: 10.1016/S1044-5803(00)00108-X

Wayman, M.L.; Wang, H. 2003. Cast Iron Coins of Song Dynasty China: a Metallurgical Study. In: *Historical Metallurgy* 37 (1) 6-24. (and also in: Wang, H., Cowell, M., Cribb, J., Bowman, S. (Eds.). 2005. *Metallurgical Analysis of Chinese Coins at the British Museum*. London, British Museum).

Wu, Chengluo. 1929. Zhongquo gu qian fenxi jieguo. *Huaxue Gongye* vol.4, 2, 127-28.

Xia, D.-qing; Qin, Y.; Mao, Z.-wei; Jin, P.-jun; Dong, Y.-wei. 2010. Corrosion Products and Its Mechanism Analysis on Several Brass Coins Excavated from Ezhou of Hubei Province. *Corrosion Science and Protection Technology (Guang Pu Xue Yu Guang Pu Fen Xi)* 22(3), 234-237.

Xian Wen Wu Bao Hu Xiu Fu Zhong Xin (Xian Heritage Conservation Repair Centre). 2004. *Mint coins Official Site of Han Zhong***.** Science Press. ISBN: 7030136225

Yang, Lien-Sheng. 1952. *Money and Credit in China (A short story)*. Cambridge, Harvard University Press.

Yoshimasa, Koga. 1911. *Suiyo Kaishi*, vol. I, no.8. Nippon Kyoto Teikoku Daigaku (Tokyo Imperial University), Japan. [in Japanese]

Yund, R. A.; Kullerud, G. 1966. Thermal Stability of Assemblages in the Cu-Fe-S System. *Journal of Petrology* 7(3), 454-488.

Zhao, K.; Wang, W.; Hua, J.; Zhang, H. 1986. An analysis of the Chemical composition of Northern Song brass coins and a preliminary investigation of coins with an addition of tin. *Zi Ran Ke Xue Shi Yan Jiu [Studies in the History of Natural Sciences]* 5, 3, 229-46. [in Mandarin Chinese]

Zhou, W; Fan, X. 1993. A study on the development of brass for coinage in China. In: *Bulletin of the Metals Museum*, vol. 20, II, 35-45. Sendai, Japan.

Zhou, W. 2004. Zhongguo gudai qianbi hejin chengfen yanjiu (Chinese coins: alloy composition and metallurgical research). *Beijing: Zhonghua shuju*. ISBN: 7-101-04089-6/H.195

Zhou, W. 2007. The origin and invention of zinc-smelting technology in China. In: Susan La Niece; Duncan Hook & Paul Craddock (Eds.) *Metals and Mines – Studies in archaeometallurgy*. London, Archetype Publications. ISBN: 978-1-904982-19-7

APPENDIX

APPENDIX I – Glossary

Acicular – That possesses a needle-like form.

Alloy – A material mixture of two or more elements: it can be formed from a mixture of two of more metals e.g. copper and tin to form bronze, or by a mixture of a metallic and non-metallic element e.g. iron and carbon to form steel, or cast iron.

Alpha Brass – Low zinc brass. An alloy of copper and zinc with no more than 38% zinc so that the beta phase is not formed. In antiquity, the cementation process for the manufacture of brass meant that only up to 28% zinc might be absorbed in the copper when the zinc ore was reduced in situ. Most ancient brasses do not contain over 28% zinc.

Alpha-Beta Brass – A brass with sufficient zinc present to allow the development of the beta phase. The equilibrium range of the alpha-beta composition varies with temperature, being 33.5 to 36.8% at the solidus temperature, and 35 to 46.6 % at room temperature.

Alpha-delta eutectoid (in bronze) – A hard constituent normally present in the structure of cast bronze containing more than about 6% tin (delta phase intermetallic composition).

Annealing – Process of heating a material (metal or glass) above its recrystallization temperature, maintaining it for a certain period of time and cooling it at a specific rate. It is used in metallurgy to homogenize the alloy and reduce internal stresses, especially when the aim is to further mechanically work the alloy, altering the microstructural or chemical structure of the metal to the advantage of the metal-worker.

Archaeometallurgy – The application of the materials science to archaeological studies. In particular the study of the processing of metals from ore to final artefact, the trade and use of the artefact and the processes involved its deposition and subsequent corrosion.

As-cast structure – The metallurgical structure (distribution of phases and grain structure) formed during the solidification of the metal after casting. Such structures are often composed of heavily cored dendrites. The grain sizes and shape vary with distance from the mould surface. The chemical composition may also vary as a result of elemental segregation during freezing; as a result a gravity segregation, inverse segregation and heavily cored structures can be produced.

Board of Revenue - Was in charge of taxation, and of the state monopolies over items like salt and tea. The department was charged with revenue collection and the financial management of the government. The Board of Revenue mint [*bao quan*] was used for the Provincial Coinage Service established in each province in 1368, superseding the previous Jiangxi Coinage Service [*huo quan ju*]. It was responsible for the production of coins in accordance with the orders of the central government following designs issued by the Board of Works. From 1380, this entity was also responsible for the production and circulation of paper money.

Board of Works - Handled all governmental building projects, including palaces, temples and the repairs of waterways and flood canals. It was also in charge of minting coinage: it had a mint [*Bao*

Yuan]. From 1421 to the end of the Ming there was another Bao Yuan at Nanking. After 1625, the Board of Revenue became the chief agency for coinage matters.

Beta brass – The beta phase of the copper-zinc equilibrium phase diagram is an intermetallic phase and is much harder that alpha but will only withstand a small amount of mechanical deformation at room temperature. However at 470°C the ordered beta prime phase changes to the disordered beta phase which is easier to work, and by 800°C the beta phase is easier to work than the alpha.

Bronze – An alloy of copper and tin. Usually with up to 14% Sn, but many examples of ancient alloys are known with higher tin contents. 14% Sn is the limit of solid solution of tin in well annealed alpha-bronzes. Leaded bronze contains a significant quantity of lead that has been added deliberately. Many early copper alloys contain some lead due to impurities in the constituent metals (under 1 wt.%). The addition of up to about 2% Pb can improve the castability of the metal, but in some cases far greater quantities were added for other reasons. However, when present in large amounts it weakens the metal as it will tend to segregate into weak lead-rich inclusions

Cash coin – Round Chinese coin with a concentric round or square hole.

Cementation – The alloying process for obtaining brass where zinc ore (zinc sulphides – spharelite - or zinc carbonates - calamine) was directly mixed with copper instead of the Zn metal. Although efficient, this made it very difficult to control the amount of zinc in the alloy and impossible to obtain brasses containing more than c. 33% Zn. Brass obtained in this process also contains undesirable impurities derived from the ore, particularly lead and iron.

Coring – The micro-segregation of an alloy on successive freezing to the solid. This means there is a change in composition from the dendrite centre to its periphery: as result of solute rejection during solidification, concentrating in outer layers of the dendrite branches. It is most evident after etching or in SEM observation, appearing as onion-like layers around a central core. It is especially common in ancient cast bronzes, or accentuated in alloys with a wide separation between liquidus and solidus curves.

Crucible – A container for melting metal normally made from a refractory clay, often graphitized. Now there is wide range of ceramic materials and surface protective washes to choose from.

Dendrite – An arborescent crystalline growth (i.e., with a fern-like conformation) formed during solidification of most pure metals and alloys.

Etchant – in this work, it refers to an acid solution used to alter the natural colour of microstructural features, in order to make them discernible from each other, especially when they have the same colour and optical methods are insufficient to compare them.

Equilibrium phase diagram – A diagram in two or more dimensions giving a plot of the phases present at a given temperature and composition. Two dimensional phase diagrams plot the composition of two elements (horizontal) against temperature (vertical); when three or more elemental are involved it becomes more complex to illustrate the phase diagram. What is usually displayed is a triangular plot of composition, with the temperature of phase boundaries marked, or with the solidus or liquidus surfaces plotted as contour maps. It describes the situation at

equilibrium, but it may be necessary to consider non-equilibrium conditions, especially in ancient and historical alloys.

Etching – A process in which corrosive solutions are used to selectively remove or stain selected microstructural components from a polished metal surface so that the microstructure can be seen using a reflected light (metallurgical) microscope. There are many hundred different etch solutions, each one will reveal one or more specific micro-structural components.

Eutectic – (1) An isothermal transformation in which a liquid transforms into two separate solid phases. This sort of transformation can only occur at a set composition and temperature. This will be the lowest melting point for any composition composed of those phases where the liquidus and solidus temperatures are the same. (2) An alloy having the eutectic composition. (3) A microstructure consistent with having solidified from a melt of eutectic or near eutectic composition. At moderate cooling rates the simultaneous growth of two phases results in morphologies with fine regular dispersions of one phase in the other.

Eutectoid – The solid state transformation equivalent of a eutectic, in which one solid phase transforms into two other different phases.

Face value – Value of a coin, attributed by the minting authority. While the face value usually refers to the true value (as with circulation coins) it can sometimes be largely symbolic or determined by the issuing authorities.

Fiduciary system – System that attributes a value to an object, not based on its intrinsic value, but on the trust of the users in the entity that emits it.

Flux – Material used to improve the melt fluidity and prevent metal oxidation and even promote its reduction by lowering the melting point.

Hanyu Pinyin – Common romanization of the Mandarin phonetics.

Liquidus Temperature – The boundary on a phase diagram that shows the temperature at which solidification begins upon cooling from the melt.

Loess – A geologic term attributed to silt deposits (sediment with particles under 80 microns in diameter) very common in central China, that have been laid down by wind action.

Monotectic – Alloy in which at a certain temperature and content a liquid turns into 2 imiscible liquids.

Mint – a place where coins were produced under government authority. The name also refers to the mint offices and location.

Phase – a material that has uniform physical properties and a homogeneous chemical composition that constitutes state of matter of a thermodynamic system.

Plug-type dezincification – Localized dezincification process penetrates deeply into the object within surrounding surfaces mostly unaffected by corrosion.

Segregation – When there is no longer a uniform distribution of the chemical elements in the alloy. All castings segregate to some extent due to solute partition between solid and liquid phases during solidification.

Smelting – The metallurgical process by which a metal is extracted from its ore. It uses heat and a chemical reducing agent – usually charcoal – to change the oxidation state of the metal ore.

Solidus temperature – The theoretical line or plane corresponding to the last liquid melt to solidify in a cast object and consequently, the metallic core of the object.

Speltering – Process in which brass is obtained mixing copper and metallic zinc together. There is record of metallic zinc production as early as the 1st millenium AD in India and in the first half of 17th century in China.

Sprue system – channels carved on the mould, designed to pour the melt into it. They connect the positive mould parts between one another.

Striking (manual or machine) – Method that consists in striking with a single heavy blow a negative carved/cut die of hard material placed on a blank disk of a softer material. The metal of the blank is therefore compressed into the indentations of the die. This process causes characteristic stress features in the microstructure, like internal defects and superficial cracks.

Tinning – Process of submerging an object in molten tin or washing it with molten tin.

White Spirit - a common organic solvent derived from petroleum.

Widmanstätten structure – A structure formed by the solid state decomposition of one phase into one or more phases, with the new phase developing along specific crystallographic planes of the original phase. In brasses, when the alpha grains that precipitate in a beta matrix grow according to a geometrical pattern on the crystallographic orientations of the beta lattice.

Zinc flaring – Occurs in alloys with over 20 wt.% zinc and consists on raising the melt temperature to permit greater zinc vapour formation. Although this process causes Zn loss, the high pressure Zn vapour purges gases as hydrogen from the melt, preventing its entry and reducing its diffusion in the melt.

Appendix II – Chinese Chronology

Table II.1. Main Chinese Dynasties (adapted from J. Needham's Science and Civilization in China, Cambridge University Press, 1954-2004)*

Dynasty		**Dates**
Xia Kingdom (legendary)		c. 2000 to c. 1520 BC
Shang (or Yin)		c.1520 to c. 1030 BC
Zhou	Western Zhou	c.1030 to 722 BC
	Eastern Zhou	722 to 480 BC
	Warring States	480 to 221 BC
Qin		221 to 207
Han	Western Han	202 BC to 9 AD
	Wang Mang period	9 to 23 AD
	Eastern Han	25 to 220 AD
Sui		581 to 618 AD
Tang		618 to 906 AD
Wu Tai (5 dynasty period)		907 to 960 AD
Song	Northern Song	960 to 1226 AD
	Southern Song	1227 to 1279 AD
Yuan (Mongol)		1260 to 1368 AD
Ming		1368 to 1644 AD
Qing (Manchu)		1644 to 1911 AD
Republic		1912 to 1948 AD
People's Republic		1949 AD to present day

* In the period of 220 to 581 AD there are simultaneous conflicting powers across the country. It was a time of great disunity in China.

Table II.2. Chronological table of the reigns present in the studied coins

Dynasty	**Era Names (reigns)**	**Date**	**Name of coin**
Eastern Han	-	40 AD	Xiao Wu Zhu
Tang	Wude	618-626 AD	Kai Yuan Tong Bao
Southern Song	Chun Xi	1174-1189 AD	Chun Xi Yuan Bao
	Qing Yuan	1195-1200 AD	Qing Yuan Tong Bao
	Jia Ding	1208-1224 AD	Jia Ding Tong Bao
	Shao Ding	1228-1233 AD	Shao Ding Tong Bao
	Chun You	1241-1252 AD	Chun You Yuan Bao
	Jing Ding	1260-1264 AD	Jing Ding Yuan Bao
	Xian Chun	1265-1274 AD	Xian Chun Yuan Bao
Ming	Wan Li	1572-1620 AD	Wan Li Tong Bao
	Tai Chang	1620 AD	Tai Chang Tong Bao
	Tian Qi	1620-1627 AD	Tian Qi Tong Bao
	Chong Zhen	1627-1644 AD	Chong Zhen Tong Bao
Qing	Shun Zhi	1644-1661 AD	Shun Zhi Tong Bao
	Kang Xi	1662-1722 AD	Kang Xi Tong Bao
	Qian Long	1736-1795 AD	Qian Long Tong Bao
	Jia Qing	1796-1820 AD	Jia Qing Tong Bao
	Dao Guang	1821-1850 AD	Dao Guang Tong Bao
	Xian Feng	1850-1862 AD	Xian Feng Tong Bao Xian Feng Zhong Bao
	Tong Zhi	1862-1874 AD	Tong Zhi Tong Bao
	Guang Xu	1875-1908 AD	Guang Xu Tong Bao

Appendix III – Polishing and clean area representativeness

III.1 Clean area representativeness

Theoretical calculations were performed to see how far the abraded edge areas were reaching into the metallic core (see Fig. III.1.1).

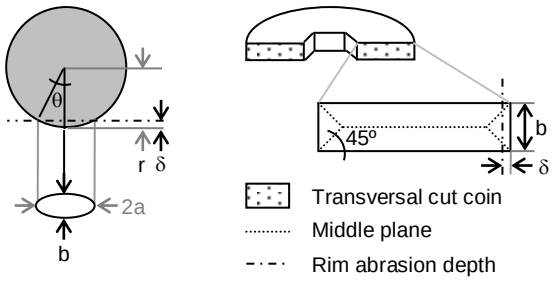

Coin averages:
a= 2 mm (2a=4 mm)
b = 1 mm
r = 12.5 mm

Removed thickness:
sen θ = a / r <=> sen θ = 0.16 <=> θ = 9.25º
cos θ = (r-δ) / r <=> δ = r – r x cos θ <=>
<=> δ = 12.5-12.5 x cos (9.25º) <=>
<=> δ = 0.163mm = 163 μm

Middle plane depth (s): b/2 = 500 μm

Ratio: (s-δ)/s = (500-163)/500 **~ 2/3 from the middle plane**

Fig. III.1.1 Schematics used to explain the calculations of the analysed depth in polishing

These calculations show that in spite of the small abrasion depth achieved (~2/3 to the middle plane of thickness of the coin), the region is representative of the metallic core of the coin, as demonstrated by Schweizer [1972], that is, far enough from the superficial area (with purer phases) and also from the middle area (last to solidify and thus more segregated).

However, the representativeness of these areas was tested by comparing the results obtained by OM observation and micro-EDXRF analysis on the cleaned edge of several coins with: 1) a second cleaned edge area (coin #2792), to account for the reproducibility of the edge results; 2) from the radial cut of an already broken coin (coin #M117), to account for the edge representativeness regarding the metallic core; 3) from a rim abrasion on the reverse of the coins, made for micro-DRX analysis (coins #2666 and #3271), to assess a clean area on the side of the coins.

In the first case, the results show that both abraded areas of the edge of coin #2792 are very similar, both in microstructure (Fig. III.1.2., Edge1 and Edge2) and elemental composition (see Table III.1.1.).

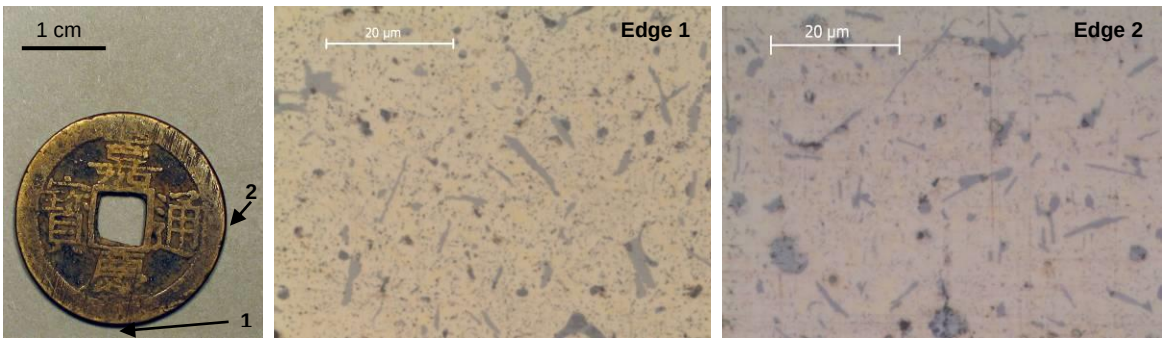

Fig. III.1.2 OM observation of two distinct abraded areas from the edge of coin #2792.

Table III.1.1 Micro-EDXRF analysis of 2 distinct cleaned areas of the edge of coin #2792

2792 (μ-EDXRF)	Fe wt.%	Cu wt.%	Zn wt.%	As wt.%	Sb wt.%	Pb wt.%
Edge 1	0.8	53.6 ± 0.9	34.1 ± 0.7	4.1	0.4	6.7
Edge 2	0.7	53.3 ± 1.1	33.7 ± 0.6	4.1	0.5	8.0

In the second case, both the cleaned edge and radial cut were observed and analysed and their results were also very similar (Fig. III.1.3 and Table III.1.2).

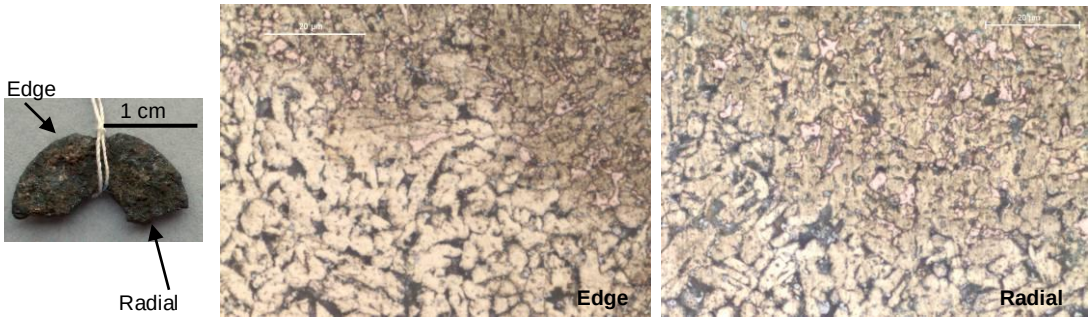

Fig. III.1.3 Coin #M177: the presented half was polished and observed: edge and radial cut microstructures (OM-BF, Etched).

Table III.1.2 Micro-EDXRF analysis of cleaned areas of the edge and radius of coin #M117

M117 (μ-EDXRF)	Fe wt.%	Cu wt.%	Zn wt.%	As wt.%	Sn wt.%	Sb wt.%	Pb wt.%
Edge	1.0	60.7 ± 1.6	29.7 ± 1.5	0.7	1.3	0.5	6.7
Radial	0.9	61.7 ± 0.5	26.7 ± 0.3	1.3	2.0	0.6	7.0

In the third case, as in the previous two, both the OM observation as micro-EDXRF results show a congruent similarity between two different abraded areas - reverse and edge - (see Fig. III.1.4 and Table III.1.3) that assures the edge sampling representativeness.

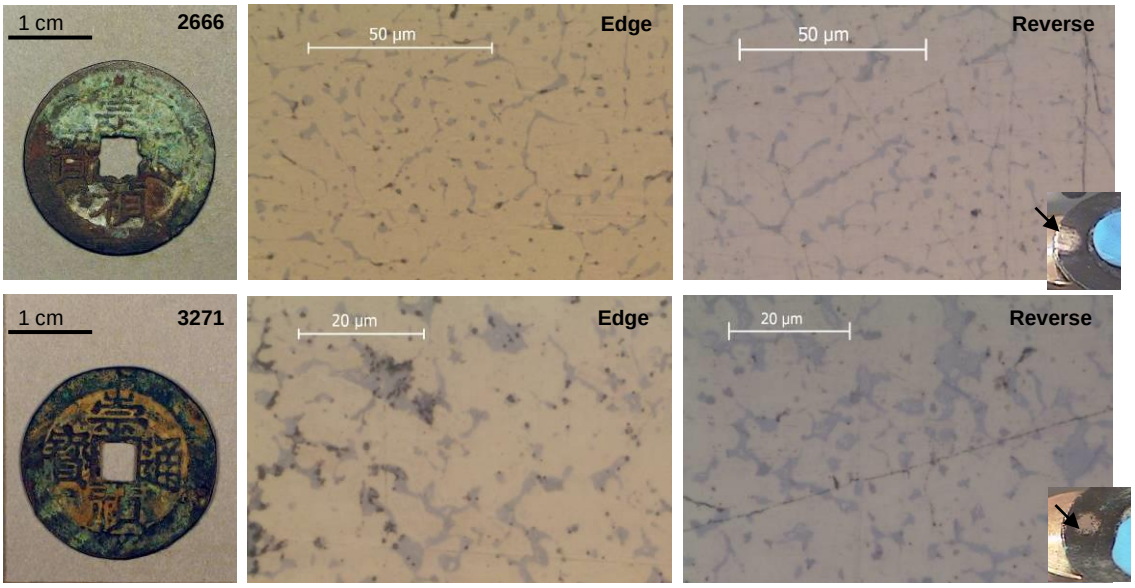

Fig. III.1.4 Coins #2666 and #3271. The edge MO images were acquired from a clean area on the south edge of each coin. The reverse MO images were acquired from a clean area on the reverse rim of each coin.

Table III.1.3 Micro-EDXRF analysis of cleaned areas of the edge and reverse rim of coins 2666 and 3271

μ-EDXRF	Fe wt.%	Cu wt.%	Zn wt.%	As wt.%	Sb wt.%	Pb wt.%
2666 – edge	0.5	52.3 ± 0.2	38.0 ± 0.1	0.5	3.1	5.3
2666 - reverse	0.5	52.0 ± 0.0	37.7 ± 0.6	0.5	3.4	6.0
3271 - edge	1.1	56.0 ± 0.2	29.9 ± 0.1	1.0	3.7	8.0
3271 - reverse	1.0	57.0 ± 0.0	29.3 ± 0.6	1.3	4.1	7.3

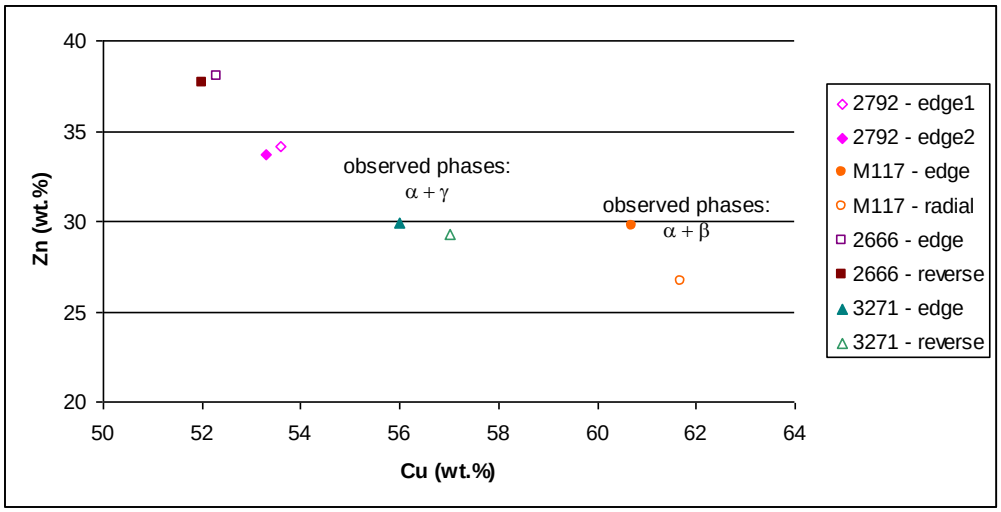

Fig. III.1.5 Micro-EDXRF results of the two main elements of 4 coins in 2 distinct cleaned areas.

The results show (see Fig. III.1.5) all the cleaned areas (edge abrasion, radial cut and reverse abrasion) present similar results both for the major elements as for the minor ones, therefore showing the chosen area (edge) is in fact representative of the composition of the entire coin.

III.2 Coin sample holder

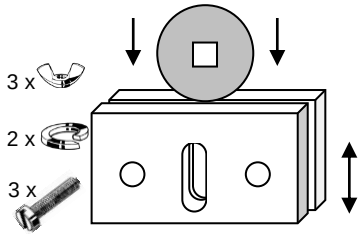

A folded film of latex – made from hand gloves – was placed between the walls of the holder and the coin to absorb chock and prevent scratches.
A helical spring lock washer was placed in each of the lateral holes, between the walls of the holder, to prevent excessive pressure on the coin.
The central hole allows the middle screw to move up and down in order to place the edge of the coin on the face of the sample holder.
The interior edge of the coins was protected from being scratched by covering the screws thread with a Teflon tape (plumbers tape).

Fig. III.2.1 Schematics of the sample holder developed

Appendix IV – Elements and compounds chemical and physical properties

Antimony (symbol: Sb) - Element with atomic number 51, atomic weight 121.75, mp 630 ºC, specific gravity 6.62. It's a lustrous metal with a bluish silvery-white appearance. The metal does not tarnish readily on exposure to air and can be used as a decorative coating. Antimony is found in some copper alloys of antiquity in particular in combination with arsenic. Copper alloys with antimony contents of ~3% show clear hardening.

Arsenic (symbol: As) – Element with atomic number 33, atomic weight 74.9214, specific gravity (grey form) 5.73. The usual variety is grey arsenic which sublimates at 610ºC. Arsenic is a steel-grey colour with a metallic lustre and was the first alloying element of importance. Arsenic contents usually vary from ~1 to 8%.

Copper (symbol: Cu) – An element with atomic number 29, atomic weight 63.54, mp 1083 ºC, specific gravity 8.96. Pure copper is reddish in colour and malleable and ductile. It occurs in native copper in dendritic masses and has been known and used since the later part of the Neolithic period.

Iron (symbol Fe) – Element with atomic number 26, atomic weight 55.85, mp 1538ºC, specific gravity ~7. Pure iron is silver coloured, but very rare to occur in nature. On the other hand, iron ores are the 4th most common mineral on earth. If usually occurs as impurities in copper ores.

Lead (symbol: Pb) – Element with atomic number 82, atomic weight 207.19, mp 327.4°C, specific gravity 11.35. Pure lead recrystallizes at room temperature when deformed. Lead was commonly extracted from galena, lead sulphide, and was often a by-product of the extraction of silver from galena, since many of these lead ores are argentiferous. Lead is a useful addition to bronzes and brasses, especially for making castings. The relative abundance of its various isotopes may give an indication as to the source of the metal.

Nickel (symbol: Ni) – An element with atomic number 28, atomic weight 58.71, melting point 1453ºC, specific gravity 8.9, and a whitish colour.

Tin (symbol: Sn) – Element with atomic number 50, symbol Sn, atomic weight 118.71, mp 231.8 ºC, specific gravity (grey) 5.75, (white) 7.31. A soft white lustrous metal obtained mainly from the mineral cassiterite, SnO_2, but stannite (Cu_2SnFeS_4) occasionally occurs in ore grade concentrations. Tin is not affected on exposure to air at ordinary temperatures.

Zinc – Element of atomic number 30, symbol Zn, atomic weight 65.37, mp 419.58ºC, specific gravity 7.13. Zinc ores were used for making brass by cementation long before the metal was used in its pure form. The limit of zinc that can enter into solid solution in copper by this process is 28%. The Romans made extensive use of brass and, in India, zinc was being made by distillation in retorts during the 13th century A.D. The metal was not known in Europe until rediscovered in 1746. Zinc is a bluish-white, lustrous metal, brittle at ordinary temperatures but malleable at 100-150ºC.

Table IV.1 Chemical and physical characteristics of the alloying elements

Element	Element Group/ Period	Atomic Number	Molar Mass ($g.mol^{-1}$)	Electron Configuration	Atomic Radius (pm)	Electronegativity (Pauling's Method)
Fe	8 / 4	26	55.85	[Ar] $4s^2\,3d^6$	126	1.83
Ni	10 / 4	28	58.69	[Ar] $4s^2\,3d^8$	124	1.91
Cu	11 / 4	29	63.55	[Ar] $4s^1\,3d^{10}$	128	1.90
Zn	12 / 4	30	65.38	[Ar] $4s^2\,3d^{10}$	134	1.65
As	15 / 4	33	74.92	[Ar] $4s^2\,3d^{10}\,4p^3$	119	2.18
Sn	14 / 5	50	118.71	[Kr] $5s^2\,4d^{10}\,5p^2$	140	1.96
Sb	15 / 5	51	121.75	[Kr] $5s^2\,4d^{10}\,5p^3$	141	2.05
Pb	14 / 6	82	207.20	[Xe] $6s^2\,4f^{14}\,5d^{10}\,6p^2$	175	2.33

[from **Chang, R. 1994.** *Chemistry* (5th ed). McGraw-Hill. ISBN: 0-07-011003-4 and **Cotton, F.A.; Wilkinson, G.; Gaus, P.L. 1995.** *Basic Inorganic Chemistry* (3rd ed). John Wiley & Sons. ISBN: 0-471-50532-3]

Table IV.2 Optical observation of metallic phases and inclusions in copper-based alloys

Alloy	**Designation**	**Colour (BF-OM)**	
		Non-etched	**Etched ($FeCl_3$)**
Cu-Sn or Cu-Sb	α phase (Cu++)	Pink to bright yellow	darker yellow
	δ phase (Sn++)	Light grey	Light grey
Cu-Zn	α phase (Cu++)	Pink to bright yellow	Darker yellow
	β phase (Zn++)	Darker yellow	Dark yellow to brown
	γ phase (Zn+++)	Light grey	Light grey
Either of the above	α-Fe	Dark grey	Brownish to black
	Iron Arsenide (Fe_2As)	Dark grey	Dark grey
	α-Pb	Grey (glitters in PL)	Grey
	Cu^0	Pink	Pink
Inclusions	Cu-S	Dark grey	Blue
	Cu_2O	Grey (red in DF&PL)	Red

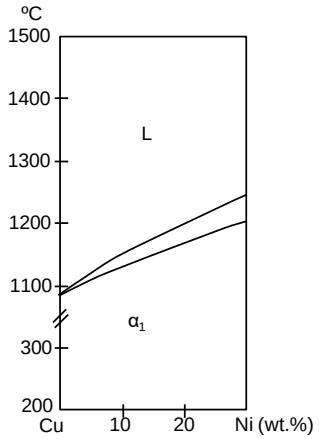

Fig. IV.1 Cu-Ni equilibrium diagram (adapted from [AMS, 1992])

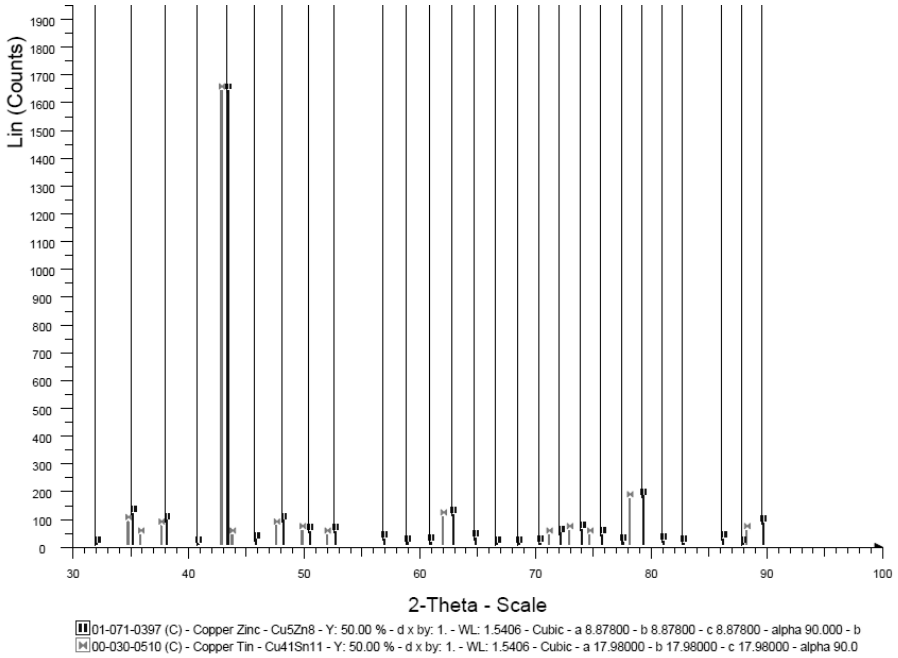

Fig. IV.2 X-ray diffractograms for brass gamma phase (Cu_5Zn_8) and bronze delta phase ($Cu_{41}Sn_{11}$) [Bruker Database 2008]

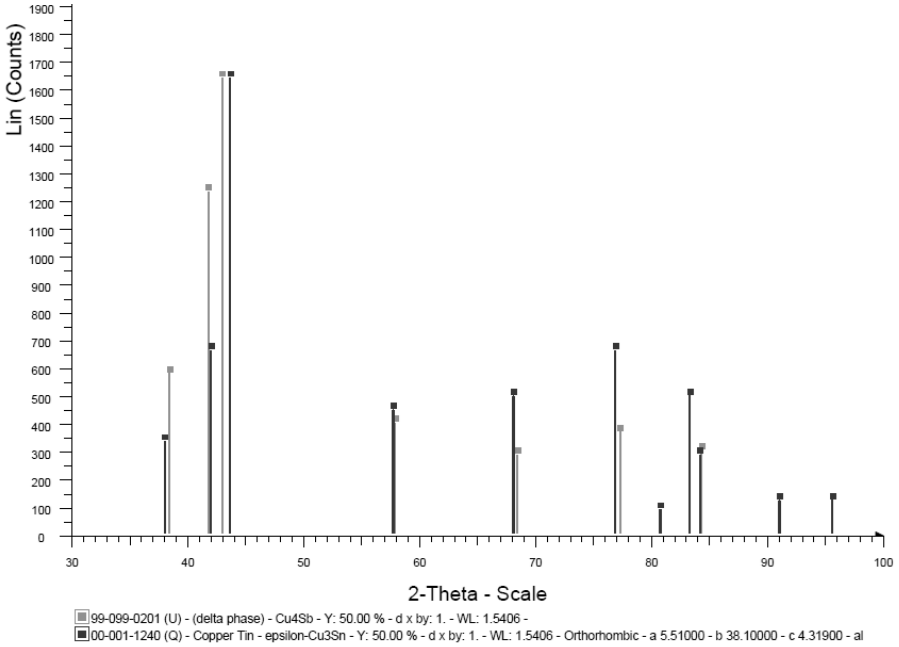

Fig. IV.3 X-ray diffractograms for bronze epsilon phase (Cu_3Sn) and Cu-Sb delta phase (Cu_4Sb) [Bruker Database 2008]

Appendix V - Cu-Zn Diffusion Couple

A 99.99 wt.% Cu tube with ~15 mm in diameter was cut to a length of 6 cm and pressed to acquire an elliptical section. In the interior, ~10 g of 99.99 wt.% Zn pellets were placed and both ends of the Cu tube were arc-welded shut. This concoction was taken to an electrin oven at 500 ºC for ~10h. After cooling, the tube was cut to show a set of 4 distinct phases by OM. EDS microanalysis of the different phases is stated in Table V.1.

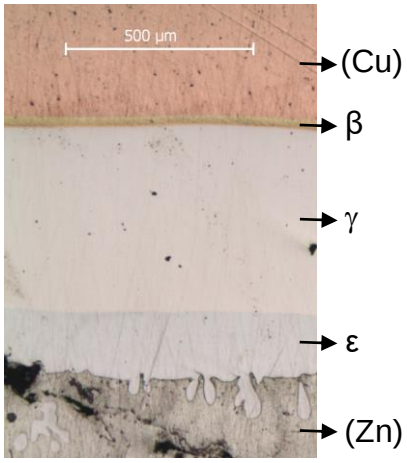

Fig. V.1 Cross-section of the Cu-Zn diffusion couple in O.M.

Table V.1 SEM-EDS of diffusion couple Cu-Zn

Phase	α	β	γ	ε	(Zn)
Zn (wt.%)	~0	48.9	66.0	86.4	98.3

Note: remaining, Cu content.

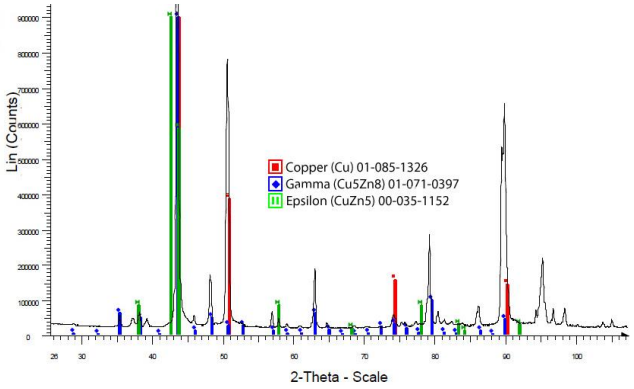

Micro-diffraction of this sample permitted to identify the 3 main phases: α phase, γ phase (Cu_5Zn_8) and ε phase ($CuZn_5$), as the micro-XRD performed on the gamma phase (see Fig. V.2) exemplifies.

Fig. V.2 Micro-XRD diffractogram of a spot of the Cu-Zn diffusion couple

Appendix VI - Comparing macro-EDXRF and micro-EDXRF

In order to see if the values obtained by macro-EDXRF and micro-EDXRF can be compared, some micro-EDXRF analysis were performed on the surface of about 15 selected coins. The results are very similar to the ones obtained by macro-EDXRF, for the major elements (Fig. VI.1). Some discrepancies are visible in the Cu contents: the coins below the tendency line have a higher micro-EDXRF Cu content, probably due to the spots having been acquired in relatively clean areas (see Fig. VI.2, coin 2782), while the macro-EDXRF was performed on the whole area and has a contribution of corrosion of the coin field, which accumulates corrosion products that are not worn out with coin handling. The coins above the tendency line show a distinct corrosion patina, and a lower Cu content in micro-EDXRF than in macro-EDXRF, probably due to the influence other elements present in the patina and the fact that macro-EDXRF has a higher penetration rate and can better overcome the patina influence, reaching the metallic bulk.

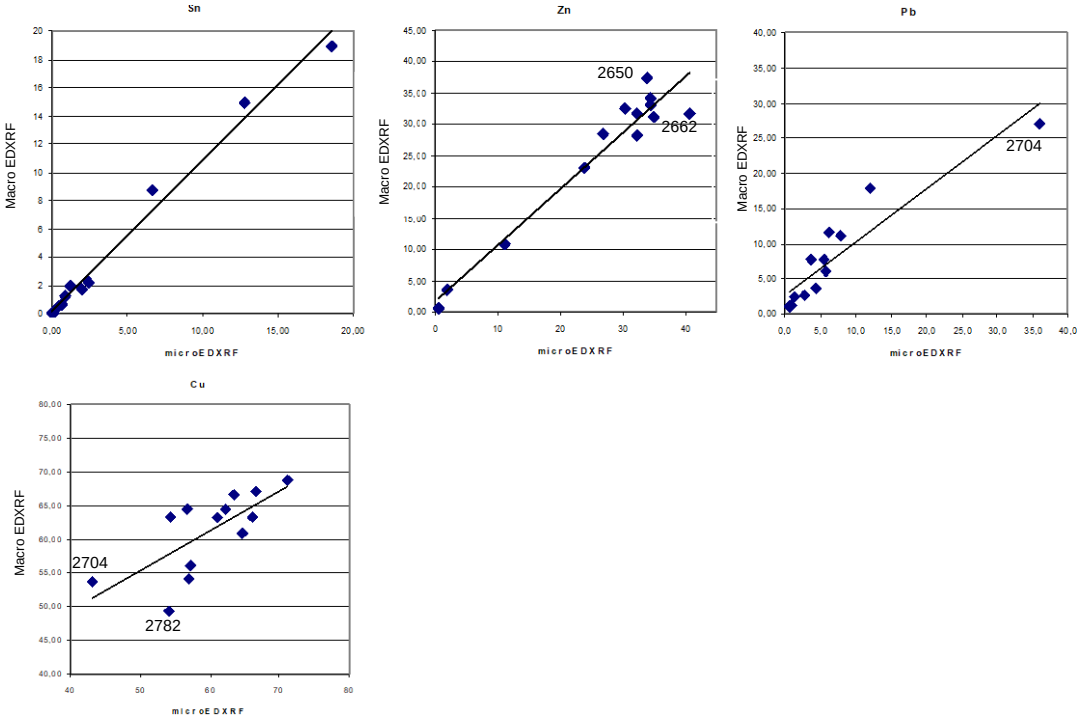

Fig. VI.1 EDXRF vs micro-EDXRF results (wt.%) obtained from the surface of 14 selected coins.

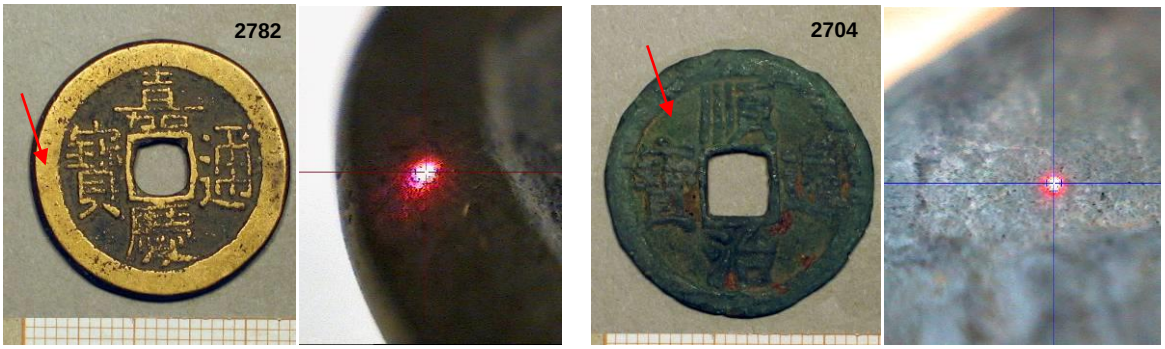

Fig. VI.2 Coins #2782 and #2704 (obverses). EDXRF analysis area corresponds to the whole obverse/reverse areas; the red arrow indicates the areas where micro-EDXRF was performed.

Appendix VII – Coin data: information and analysis

Table VII.1 Coin attributed data, physical measurements and EDXRF

Ref.	Name	Cash #	Dynasty	Minting start-end date	Mint name, province	Ø (mm)	Maximum Thickness (mm)	weight (g)	Macro-EDXRF averages [obverse & reverse] (wt%)							
									Cu ave.	Sn ave.	Zn ave.	Pb ave.	Fe ave.	Ni ave.	As ave.	Sb ave.
2133	Xiao Ban Liang (B)	*unk.*	Western Han	206 BC	*unknown*	16	1.5	1	70.8	12.5	<q.l.	16.1	0.26	0.16	-	0.11
2137	Xiao Ban Liang	*unk.*	Western Han	206 BC	*unknown*	14	1	0.5	54.0	3.58	<q.l.	41.7	0.39	0.15	-	0.12
2152	Wu Zhu	*unk.*	Western Han	115 BC : 8 AD	*unknown*	26	2.5	4	34.0	2.87	<q.l.	55.5	5.36	<q.l.	-	2.06
2155	Wu Zhu	*unk.*	Western Han	115 BC : 8 AD	*unknown*	25.5	1.75	5	86.8	3.30	<q.l.	7.7	0.66	0.13	-	1.26
2158	Wu Zhu	*unk.*	Western Han	115 BC : 8 AD	*unknown*	25.5	1	3	92.3	3.50	<q.l.	2.2	1.16	0.12	0.46	<q.l.
2165	Wu Zhu	*unk.*	Western Han	73 BC	*unknown*	25	1.5	4	71.9	3.06	<q.l.	18.4	1.30	0.18	-	4.98
2167	Wu Zhu	*unk.*	Western Han	73 BC	*unknown*	25	1.5	4	41.9	6.53	0.25	39.7	1.37	0.10	-	10.21
2169	Da Quan Wu Shi	*unk.*	Western Han	7 AD	*unknown*	25.5	2	3	85.7	6.39	<q.l.	5.8	1.30	0.12	-	0.52
2172	Da Quan Wu Shi	*unk.*	Western Han	7 AD	*unknown*	24.5	1.5	3	75.3	3.12	<q.l.	20.2	0.72	0.17	-	0.28
2175	Da Quan Wu Shi	*unk.*	Western Han	7 AD	*unknown*	26.5	2	5	73.6	3.79	<q.l.	18.6	3.28	0.15	-	0.37
2181	Bu Quan	*unk.*	Xin	14 AD	*unknown*	26	1.5	4	86.7	4.57	<q.l.	7.7	0.27	0.20	-	0.50
2186	Huo Quan	*unk.*	Xin	14 AD	*unknown*	22.5	2	4	68.1	3.96	<q.l.	26.6	0.62	0.14	-	0.42
2199	Huo Quan (cake coin)	*unk.*	Xin	14 AD	*unknown*	27	4.2	10.6	78.0	6.42	<q.l.	13.5	1.30	0.14	-	0.54
2200	Huo Quan	*unk.*	Xin	14 AD	*unknown*	20.5	1.2	3	78.4	9.08	0.21	9.8	1.69	0.17	-	0.63
2202	Huo Quan	*unk.*	Xin	14 AD	*unknown*	21	1.3	2	80.7	5.01	0.22	11.0	2.43	0.12	-	0.52
2209	Xiao Wu Zhu	*unk.*	Eastern Han	40 AD	*unknown*	12.5	1	1	82.5	5.70	0.19	6.0	5.46	0.10	-	<q.l.
3270	Wu Jin	*unk.*	unkown	190-960 AD	*unknown*	21.8	1.4	2	66.8	17.41	<q.l.	14.0	1.29	0.17	-	0.29
2242	Kai Yuan Tong Bao	*unk.*	Tang	621 AD	*unknown*	25	1.5	4	71.8	16.58	<q.l.	9.1	1.75	0.53	0.19	<q.l.
2246	Kai Yuan Tong Bao	*unk.*	Tang	621 AD	*unknown*	23	1.5	4	54.0	0.19	<q.l.	40.2	2.75	0.21	1.82	0.81
2250	Kai Yuan Tong Bao	*unk.*	Tang	621 AD	*unknown*	22	1	2	60.7	15.45	0.20	22.3	1.10	0.21	-	0.04
3269	Kai Yuan Tong Bao	*unk.*	Tang	621 AD	*unknown*	23.9	1.8	5	64.1	0.12	<q.l.	32.7	0.73	0.27	1.07	1.02
2256	Qian Yuan Zhong Bao	*unk.*	Tang	759 AD	*unknown*	24.5	1.2	4	68.3	7.88	<q.l.	15.1	8.39	0.10	-	<q.l.
2259	Qian Yuan Zhong Bao	*unk.*	Tang	759 AD	*unknown*	26	1.2	5	60.0	17.71	0.24	19.9	1.58	0.14	-	0.36
2258	"Hui Chang" Kai Yuan TB	*unk.*	Tang	845 AD	*unknown*	23	1.5	4	69.4	15.19	<q.l.	13.9	1.07	0.17	-	0.11
2274	"Hui Chang" Kai Yuan TB	*unk.*	Tang	845 AD	*unknown*	22	1.2	4	54.5	12.38	<q.l.	28.2	3.10	0.12	1.27	0.30
3265	"Hui Chang" Kai Yuan TB	*unk.*	Tang	845 AD	*unknown*	24.1	1.3	4	69.2	13.61	<q.l.	15.8	0.43	0.15	0.26	0.42
3266	"Hui Chang" Kai Yuan TB	*unk.*	Tang	845 AD	*unknown*	23.7	1.3	3	70.9	12.02	<q.l.	15.5	0.46	0.18	0.49	0.36
3268	"Hui Chang" Kai Yuan TB	*unk.*	Tang	845 AD	*unknown*	24	1.6	4	70.2	14.17	0.19	14.6	0.55	0.19	-	0.14
2298	Song Yuan Tong Bao	*unk.*	Northern Song	960 AD	*unknown*	23.5	1	3	58.0	1.03	<q.l.	38.1	2.10	<q.l.	0.48	<q.l.
2322	Zhi He Tong Bao	*unk.*	Northern Song	1054 AD	*unknown*	24	0.75	3	49.2	9.78	<q.l.	39.5	1.24	<q.l.	-	<q.l.
2348	Yuan You Tong Bao	*unk.*	Northern Song	1086-93 AD	*unknown*	24.5	1	4	44.0	13.10	0.37	40.0	2.44	<q.l.	-	<q.l.
2408	Qian Dao Yuan Bao	2	SouthernSong	1165 AD	*unknown*	28	1.1	7	46.3	3.74	<q.l.	47.1	2.74	0.11	-	<q.l.
2416	Chun Xi Yuan Bao	*unk.*	SouthernSong	1174 AD	*unknown*	23.5	1.2	3	44.9	6.17	<q.l.	46.8	1.84	0.10	-	0.10
2419	Chun Xi Yuan Bao	*unk.*	SouthernSong	1174 AD	*unknown*	23.5	1.2	3	66.0	2.54	0.30	29.7	1.32	0.14	-	<q.l.
2421	Chun Xi Yuan Bao	*unk.*	SouthernSong	1174 AD	*unknown*	24	1.1	3	62.4	3.34	<q.l.	30.7	3.23	0.10	-	0.13
2427	Chun Xi Yuan Bao	2	SouthernSong	1174 AD	*unknown*	29.5	1.8	9	60.3	4.75	<q.l.	33.0	1.72	0.11	-	<q.l.
2433	Chun Xi Yuan Bao	2	SouthernSong	1174 AD	*unknown*	29	1.5	7	56.1	2.56	<q.l.	38.6	2.53	0.11	-	<q.l.
2447	Shao Xi Yuan Bao	*unk.*	SouthernSong	1190 AD	*unknown*	23	1	3	52.8	3.68	<q.l.	39.2	3.61	0.12	-	0.48
2458	Shao Xi Yuan Bao	*unk.*	SouthernSong	1190 AD	*unknown*	29	1.5	7	57.0	2.81	<q.l.	38.1	1.81	0.10	-	<q.l.
2461	Shao Xi Yuan Bao	2	SouthernSong	1190 AD	*unknown*	28.5	1.3	7	45.0	2.14	0.17	51.1	1.42	0.10	-	<q.l.
2463	Shao Xi Yuan Bao	2	SouthernSong	1190 AD	*unknown*	30	1.5	7	53.0	3.35	<q.l.	40.7	2.79	<q.l.	-	<q.l.
2471	Qing Yuan Tong Bao	2	SouthernSong	1195 AD	*unknown*	29.5	1.1	5	50.3	2.35	<q.l.	45.1	1.81	<q.l.	-	0.26
2479	Qing Yuan Tong Bao	2	SouthernSong	1195 AD	*unknown*	29	1.5	5	42.5	4.04	<q.l.	46.9	6.29	<q.l.	-	0.13
2495	Qing Yuan Tong Bao	*unk.*	SouthernSong	1195 AD	*unknown*	24	0.95	3	62.1	2.89	<q.l.	32.5	2.26	0.10	-	0.13
2498	Qing Yuan Tong Bao	*unk.*	SouthernSong	1195 AD	*unknown*	24.5	1.1	3	64.6	3.68	<q.l.	29.5	1.86	0.13	-	<q.l.
2500	Qing Yuan Tong Bao	*unk.*	SouthernSong	1195 AD	*unknown*	23.5	1.1	3	62.2	4.41	<q.l.	30.8	2.34	<q.l.	-	<q.l.
2501	Qing Yuan Tong Bao	*unk.*	SouthernSong	1195 AD	*unknown*	23.5	0.95	4	72.2	3.17	1.04	22.2	1.19	0.12	-	<q.l.
2503	Qing Yuan Tong Bao	*unk.*	SouthernSong	1195 AD	*unknown*	24	0.9	3	43.1	5.59	<q.l.	48.1	2.51	<q.l.	-	0.42
2504	Qing Yuan Tong Bao	*unk.*	SouthernSong	1195 AD	*unknown*	24	0.9	4	70.4	2.91	<q.l.	25.6	0.85	0.13	-	0.10
3255	Xian Yuan Tong Bao	5	SouthernSong	1195 AD	*unknown*	33.3	2.2	10	66.2	11.1	<q.l.	21.6	0.74	<q.l.	-	0.13
2505	Jia Tai Tong Bao	*unk.*	SouthernSong	1201 AD	*unknown*	24	0.9	2	35.6	3.47	<q.l.	57.5	3.20	<q.l.	-	0.13
2515	Jia Tai Tong Bao	2	SouthernSong	1201 AD	*unknown*	29	0.95	5	39.7	2.11	<q.l.	55.8	2.24	<q.l.	-	0.12
2510	Kai Xi Tong Bao	*unk.*	SouthernSong	1205 AD	*unknown*	24	1	3	72.6	1.25	<q.l.	25.0	0.88	0.12	-	<q.l.
2513	Kai Xi Tong Bao	*unk.*	SouthernSong	1205 AD	*unknown*	24	0.9	3	60.0	2.97	<q.l.	35.6	1.11	0.11	-	<q.l.
2516	Kai Xi Tong Bao	*unk.*	SouthernSong	1205 AD	*unknown*	24.5	0.95	4	39.6	3.49	0.56	51.8	4.42	<q.l.	-	<q.l.
2520	Kai Xi Tong Bao	2	SouthernSong	1205 AD	*unknown*	30	1.4	6	60.5	1.30	<q.l.	36.7	1.37	<q.l.	-	<q.l.
2519	Jia Ding Tong Bao	*unk.*	SouthernSong	1208-24 AD	*unknown*	23.5	2	4	84.9	1.10	0.28	11.7	1.02	0.16	0.77	<q.l.
2521	Jia Ding Tong Bao	*unk.*	SouthernSong	1208-24 AD	*unknown*	25	1	3	77.0	0.46	<q.l.	20.1	2.07	0.10	-	0.15
2522	Jia Ding Tong Bao	*unk.*	SouthernSong	1208-24 AD	*unknown*	24.5	1.2	4	46.2	4.65	<q.l.	44.2	4.71	0.11	-	<q.l.
2525	Jia Ding Tong Bao	*unk.*	SouthernSong	1208-24 AD	*unknown*	24	1	4	49.6	5.03	0.51	42.3	2.34	0.18	-	<q.l.
2527	Jia Ding Tong Bao	*unk.*	SouthernSong	1208-24 AD	*unknown*	24.5	1	4	51.8	0.26	<q.l.	45.7	1.58	<q.l.	-	0.49
2528	Jia Ding Tong Bao	*unk.*	SouthernSong	1208-24 AD	*unknown*	24.5	1	4	72.2	4.07	<q.l.	21.1	2.35	0.10	-	<q.l.
2531	Jia Ding Tong Bao	2	SouthernSong	1208-24 AD	*unknown*	29.5	1.5	7	58.0	0.33	<q.l.	39.2	1.72	0.14	-	0.48
2533	Jia Ding Tong Bao	*unk.*	SouthernSong	1208-24 AD	*unknown*	24	1	3	61.2	3.80	0.22	32.8	1.82	0.10	-	<q.l.
2534	Jia Ding Tong Bao	2	SouthernSong	1208-24 AD	*unknown*	29.5	0.9	6	32.5	0.15	<q.l.	65.7	1.32	<q.l.	-	0.15
2535	Jia Ding Tong Bao	*unk.*	SouthernSong	1208-24 AD	*unknown*	24	0.95	3	54.5	5.78	<q.l.	37.7	1.61	0.14	-	<q.l.
2537	Jia Ding Tong Bao	2	SouthernSong	1208-24 AD	*unknown*	29	1.1	7	62.4	0.38	<q.l.	35.3	1.24	0.13	-	0.40
2540	Jia Ding Tong Bao	2	SouthernSong	1208-24 AD	*unknown*	29.5	2	7	55.9	0.54	<q.l.	40.3	2.25	<q.l.	-	0.82
2542	Jia Ding Tong Bao	2	SouthernSong	1208-24 AD	*unknown*	30	1.1	7	63.5	5.00	<q.l.	30.2	1.06	0.10	-	<q.l.
2544	Jia Ding Tong Bao	2	SouthernSong	1208-24 AD	*unknown*	30	1.1	6	26.1	0.75	<q.l.	70.4	2.61	<q.l.	-	<q.l.
2545	Jia Ding Tong Bao	2	SouthernSong	1208-24 AD	*unknown*	29	1.1	7	49.5	2.73	<q.l.	45.7	1.83	0.11	-	<q.l.
2547	Jia Ding Tong Bao	2	SouthernSong	1208-24 AD	*unknown*	29.5	1.1	6	49.4	0.93	<q.l.	47.5	1.86	0.11	-	0.14
2548	Jia Ding Tong Bao	2	SouthernSong	1208-24 AD	*unknown*	29	1.1	6	43.3	2.61	<q.l.	52.1	1.83	<q.l.	-	<q.l.
2553	Da Song Yuan Bao	*unk.*	SouthernSong	1225 AD	*unknown*	24	1	2	53.8	3.99	<q.l.	40.2	1.70	0.12	-	<q.l.
2554	Da Song Yuan Bao	2	SouthernSong	1225 AD	*unknown*	28.5	1.2	5	42.9	3.60	0.25	51.0	2.06	0.11	-	<q.l.
2559	Da Song Yuan Bao	*unk.*	SouthernSong	1225 AD	*unknown*	24	0.95	2	54.8	5.16	<q.l.	36.6	2.96	0.12	-	0.12
2555	Shao Ding Tong Bao	*unk.*	SouthernSong	1228-33 AD	*unknown*	23.75	0.95	3	64.6	2.73	<q.l.	30.1	2.32	<q.l.	-	<q.l.

Cu | bronze | brass | unk. - unknown | <q.l. - below quantification limit

Table VII.1 Coin attributed data, physical measurements and EDXRF (continued)

Ref.	Name	Cash #	Dynasty	Minting start-end date	Mint name, province	Ø (mm)	Maximum Thickness (mm)	weight (g)	Macro-EDXRF averages [obverse & reverse] (wt%) Cu ave.	Sn ave.	Zn ave.	Pb ave.	Fe ave.	Ni ave.	As ave.	Sb ave.
2558	Shao Ding Tong Bao	*unk.*	SouthernSong	1228-33 AD	*unknown*	24	1.2	3	64.3	3.39	0.35	30.3	1.60	0.11	-	<q.l.
2560	Shao Ding Tong Bao	*unk.*	SouthernSong	1228-33 AD	*unknown*	23.5	1.1	3	43.5	3.52	<q.l.	51.1	1.64	0.12	-	<q.l.
2563	Shao Ding Tong Bao	*unk.*	SouthernSong	1228-33 AD	*unknown*	24	0.9	4	61.3	3.49	<q.l.	33.7	1.27	0.11	-	<q.l.
2564	Shao Ding Tong Bao	*unk.*	SouthernSong	1228-33 AD	*unknown*	24	1.1	3	39.2	8.00	0.19	49.6	2.82	<q.l.	-	<q.l.
2565	Shao Ding Tong Bao	2	SouthernSong	1228-33 AD	*unknown*	29.5	1.5	6	44.6	4.89	<q.l.	48.3	1.94	<q.l.	-	<q.l.
2568	Shao Ding Tong Bao	2	SouthernSong	1228-33 AD	*unknown*	29.2	1.1	7	46.6	2.11	<q.l.	49.6	1.43	<q.l.	-	<q.l.
2571	Shao Ding Tong Bao	2	SouthernSong	1228-33 AD	*unknown*	29.5	1.5	6	34.1	1.10	<q.l.	62.8	1.85	<q.l.	-	<q.l.
2566	Duan Ping Tong Bao	5	SouthernSong	1234 AD	*unknown*	34.5	2.1	12	63.7	6.44	<q.l.	27.5	2.12	0.10	-	0.10
2574	Duan Ping Yuan Bao	*unk.*	SouthernSong	1234 AD	*unknown*	23.5	1.1	3	58.9	1.62	<q.l.	36.7	2.54	<q.l.	-	0.13
2567	Jia Xi Tong Bao	*unk.*	SouthernSong	1237 AD	*unknown*	24.5	0.95	3	47.9	2.86	0.19	47.4	1.53	0.13	-	0.09
2572	Jia Xi Tong Bao	*unk.*	SouthernSong	1237 AD	*unknown*	23.5	0.95	3	46.1	3.35	<q.l.	48.1	2.08	0.12	-	0.11
2575	Jia Xi Tong Bao	*unk.*	SouthernSong	1237 AD	*unknown*	24.9	1.2	4	38.6	1.51	<q.l.	58.2	1.31	<q.l.	-	<q.l.
2576	Jia Xi Tong Bao	2	SouthernSong	1237 AD	*unknown*	28.5	1.2	7	64.8	3.85	0.22	29.4	1.65	0.11	-	<q.l.
2577	Jia Xi Tong Bao	2	SouthernSong	1237 AD	*unknown*	29	1.5	8	62.8	2.89	0.23	32.1	1.74	0.16	-	<q.l.
2580	Jia Xi Tong Bao	2	SouthernSong	1237 AD	*unknown*	28.5	1	5	39.9	1.96	<q.l.	56.1	1.70	<q.l.	-	0.11
2583	Jia Xi Tong Bao	2	SouthernSong	1237 AD	*unknown*	29.5	1	5	41.5	1.79	<q.l.	55.0	1.39	<q.l.	-	0.11
2586	Jia Xi Zhong Bao	5	SouthernSong	1237 AD	*unknown*	36.5	3.5	17	62.6	5.07	<q.l.	30.6	1.32	0.10	-	0.15
2578	Chun You Yuan Bao	*unk.*	SouthernSong	1241-52 AD	*unknown*	24	1.4	3	45.7	3.91	<q.l.	48.0	2.17	<q.l.	-	0.16
2579	Chun You Yuan Bao	*unk.*	SouthernSong	1241-52 AD	*unknown*	23.7	0.7	2	44.7	6.17	<q.l.	45.6	3.16	0.12	-	0.15
2581	Chun You Yuan Bao	*unk.*	SouthernSong	1241-52 AD	*unknown*	24.1	0.8	3	64.9	1.88	<q.l.	31.7	1.27	0.11	-	<q.l.
2582	Chun You Yuan Bao	*unk.*	SouthernSong	1241-52 AD	*unknown*	24	0.95	3	48.2	1.82	<q.l.	47.3	2.41	<q.l.	-	<q.l.
2585	Chun You Yuan Bao	*unk.*	SouthernSong	1241-52 AD	*unknown*	24	0.9	3	35.7	2.02	<q.l.	60.8	1.21	<q.l.	-	<q.l.
2588	Chun You Yuan Bao	*unk.*	SouthernSong	1241-52 AD	*unknown*	23.5	0.7	3	48.2	2.16	<q.l.	47.3	2.15	<q.l.	-	<q.l.
2592	Chun You Yuan Bao	*unk.*	SouthernSong	1241-52 AD	*unknown*	24.5	1.1	3	49.7	2.58	<q.l.	45.5	1.93	0.10	-	<q.l.
2598	Chun You Yuan Bao	*unk.*	SouthernSong	1241-52 AD	*unknown*	24.5	1.5	4	64.8	3.01	<q.l.	29.8	2.16	<q.l.	-	0.12
2593	Huang Song Tong Bao	*unk.*	SouthernSong	1253 AD	*unknown*	24.1	1	4	71.6	8.83	<q.l.	18.7	0.53	0.12	-	0.13
2591	Huang Song Yuan Bao	*unk.*	SouthernSong	1253 AD	*unknown*	24.5	1	4	49.5	4.20	<q.l.	43.8	2.16	<q.l.	-	0.14
2594	Huang Song Yuan Bao	*unk.*	SouthernSong	1253 AD	*unknown*	24.5	2.1	2	65.4	3.25	0.36	29.1	1.56	0.25	-	<q.l.
2597	Huang Song Yuan Bao	*unk.*	SouthernSong	1253 AD	*unknown*	25	0.7	3	54.0	3.68	<q.l.	39.7	2.43	<q.l.	-	<q.l.
2599	Huang Song Yuan Bao	*unk.*	SouthernSong	1253 AD	*unknown*	24.5	1	3	59.7	4.09	<q.l.	34.2	1.66	0.10	-	0.11
2600	Huang Song Yuan Bao	*unk.*	SouthernSong	1253 AD	*unknown*	23.5	0.8	3	74.3	3.70	<q.l.	21.5	0.12	0.12	-	0.18
2601	Huang Song Yuan Bao	*unk.*	SouthernSong	1253 AD	*unknown*	24	1	3	57.4	4.11	<q.l.	36.8	1.40	<q.l.	-	<q.l.
2602	Huang Song Yuan Bao	2	SouthernSong	1253 AD	*unknown*	28	1	6	57.0	3.35	<q.l.	37.7	1.62	0.13	-	<q.l.
2605	Huang Song Yuan Bao	2	SouthernSong	1253 AD	*unknown*	29	1	4	61.5	2.96	<q.l.	34.3	0.83	<q.l.	-	0.13
2607	Huang Song Yuan Bao	2	SouthernSong	1253 AD	*unknown*	29.5	1.5	8	69.0	2.82	<q.l.	26.7	1.13	0.14	-	<q.l.
2608	Huang Song Yuan Bao	2	SouthernSong	1253 AD	*unknown*	28.5	1	6	56.1	2.51	<q.l.	39.9	1.14	0.11	-	0.14
2616	Jing Ding Yuan Bao	2	SouthernSong	1260 AD	*unknown*	28.5	1.2	5	49.1	3.25	<q.l.	45.7	1.73	<q.l.	-	<q.l.
2614	Xian Chun Yuan Bao	*unk.*	SouthernSong	1265 AD	*unknown*	28.5	1	3	51.2	6.16	<q.l.	40.5	1.85	<q.l.	-	0.10
2615	Xian Chun Yuan Bao	*unk.*	SouthernSong	1265 AD	*unknown*	28.5	1	2	62.7	2.60	<q.l.	30.2	3.48	0.10	-	0.79
2617	Xian Chun Yuan Bao	*unk.*	SouthernSong	1265 AD	*unknown*	23.5	0.8	2	44.1	3.99	<q.l.	48.2	3.47	<q.l.	-	<q.l.
2619	Xian Chun Yuan Bao	*unk.*	SouthernSong	1265 AD	*unknown*	24	0.8	3	63.7	5.11	<q.l.	29.4	1.45	0.10	-	0.10
2621	Xian Chun Yuan Bao	2	SouthernSong	1265 AD	*unknown*	28.5	1.5	6	35.9	1.55	<q.l.	60.2	2.11	<q.l.	-	<q.l.
2623	Xian Chun Yuan Bao	*unk.*	SouthernSong	1265 AD	*unknown*	23.5	0.9	3	38.0	5.61	<q.l.	53.9	2.19	<q.l.	-	0.15
2624	Xian Chun Yuan Bao	2	SouthernSong	1265 AD	*unknown*	27.5	1.2	6	47.1	5.34	0.22	44.7	2.42	0.11	-	<q.l.
2625	Xian Chun Yuan Bao	2	SouthernSong	1265 AD	*unknown*	27.5	1.4	5	59.9	0.98	<q.l.	37.9	1.00	0.10	-	<q.l.
2626	Xian Chun Yuan Bao	2	SouthernSong	1265 AD	*unknown*	27.5	1	5	20.4	0.45	<q.l.	78.4	0.65	<q.l.	-	<q.l.
2631	Xian Chun Yuan Bao	2	SouthernSong	1265 AD	*unknown*	27.5	0.95	5	42.0	3.63	<q.l.	52.5	1.56	0.11	-	<q.l.
2629	Da Yuan Tong Bao	*unk.*	Yuan?	1271-1368 AD	*unknown*	41	3.5	22	61.0	8.20	<q.l.	28.9	1.55	0.11	-	0.13
2720/3293	Zhi Da Tong Bao	*unk.*	Yuan	1310 AD	*unknown*	23.5	1	4	56.7	6.67	<q.l.	35.6	0.78	<q.l.	-	0.11
2627	Zhi Zheng Tong Bao	2	Yuan	1350 AD	*unknown*	29	1.1	5	46.9	17.9	0.21	33.5	1.17	<q.l.	-	0.22
2630	Zhi Zheng Tong Bao	3	Yuan	1350 AD	*unknown*	32	1.8	9	72.7	16.9	0.22	8.12	1.51	0.13	0.23	0.22
2637	Zhi Zheng Tong Bao	10	Yuan	1350 AD	*unknown*	44	3	19	53.1	14.5	0.35	28.3	3.34	0.12	-	0.24
2632	Tian Qi Tong Bao	*unk.*	Ming	1621 AD	*unknown*	24.5	0.7	2	64.8	1.01	30.5	2.52	0.75	0.10	0.18	0.12
2635	Tian Qi Tong Bao	*unk.*	Ming	1621 AD	*unknown*	23.5	1.5	5	50.8	0.43	46.5	1.57	0.53	<q.l.	-	0.14
2636	Tian Qi Tong Bao	10	Ming	1621 AD	*unknown*	46.5	3	38	64.5	<q.l.	33.6	1.37	0.43	<q.l.	-	<q.l.
2639	Tian Qi Tong Bao	*unk.*	Ming?	1621 AD	*unknown*	23.5	1.1	4	84.9	<q.l.	8.74	4.50	0.60	0.21	0.37	0.67
2642	Tian Qi Tong Bao	*unk.*	Ming	1621 AD	*unknown*	26	0.95	4	56.6	3.59	29.8	9.16	0.65	0.10	-	<q.l.
2645	Tian Qi Tong Bao	*unk.*	Ming?	1621 AD	*unknown*	26	1	4	55.6	2.37	26.5	14.5	0.85	<q.l.	-	<q.l.
2640	Da Zhong Tong Bao	*unk.*	Ming?	1361 AD	*unknown*	24	0.95	3	59.7	13.6	<q.l.	25.5	0.88	<q.l.	-	0.22
2646	Da Zhong Tong Bao	10	Ming?	1361 AD	*unknown*	44.5	3	18	60.9	7.09	0.38	31.1	0.32	0.15	-	<q.l.
2638	Hong Wu Tong Bao	*unk.*	Ming	1368 AD	*unknown*	22.5	1.2	4	49.6	11.0	0.35	36.7	2.09	<q.l.	-	0.18
2641	Hong Wu Tong Bao	*unk.*	Ming	1368 AD	*unknown*	23.5	1.5	4	80.9	6.20	0.29	11.8	0.56	0.11	-	0.13
2651	Hong Wu Tong Bao	10	Ming	1368 AD	*unknown*	45.5	4	35	61.6	7.86	<q.l.	28.1	2.08	<q.l.	-	0.13
2657	Hong Wu Tong Bao	5	Ming	1368 AD	*unknown*	39.5	2.5	17	45.6	6.08	<q.l.	46.0	1.97	<q.l.	-	0.17
2655	Hong Zhi Tong Bao	*unk.*	Ming	1503 AD	*unknown*	24.5	1.2	4	77.8	11.5	0.66	8.9	1.01	0.14	-	<q.l.
2650	Wan Li Tong Bao	*unk.*	Ming	1576 AD	*unknown*	25	1.2	5	60.9	0.40	37.5	1.03	0.14	0.11	-	<q.l.
2653	Wan Li Tong Bao	2	Ming	1576 AD	*unknown*	28.5	1.2	5	63.1	6.68	10.9	17.9	1.23	0.12	-	<q.l.
2659	Tai Chang Tong Bao	*unk.*	Ming	1620 AD	*unknown*	25.5	0.95	3	66.5	<q.l.	31.2	1.2	0.66	0.11	0.16	0.22
2661	Chong Zhen Tong Bao	*unk.*	Ming	1628 AD	*unknown*	23.2	1	4	67.8	<q.l.	29.1	1.0	1.80	0.17	-	<q.l.
2662	Chong Zhen Tong Bao	*unk.*	Ming	1628 AD	*unknown*	34	1.2	10	63.3	0.94	31.6	2.6	0.57	0.11	0.32	0.56
2663	Chong Zhen Tong Bao	*unk.*	Ming	1628 AD	*unknown*	24.5	0.95	4	58.8	<q.l.	38.9	1.6	0.32	<q.l.	0.22	<q.l.
2664	Chong Zhen Tong Bao	*unk.*	Ming	1628 AD	*unknown*	23.5	0.9	2	30.7	1.05	60.5	5.8	1.00	<q.l.	-	0.94
2666	Chong Zhen Tong Bao	*unk.*	Ming	1628 AD	*unknown*	23	0.8	3	47.5	0.50	42.8	4.4	0.88	0.10	-	3.78
2667	Chong Zhen Tong Bao	5	Ming	1628 AD	*unknown*	33.5	1.7	11	64.5	1.24	28.2	3.7	1.89	0.11	-	0.34
2670	Chong Zhen Tong Bao	2	Ming	1628 AD	*unknown*	26.5	1.2	5	63.8	2.18	20.3	11.7	1.75	0.14	-	0.15
3271	Chong Zhen Tong Bao	*unk.*	Ming	1628 AD	*unknown*	23.3	1	2	52.3	0.25	34.4	6.9	1.38	0.15	-	4.65
3272	Chong Zhen Tong Bao	*unk.*	Ming	1628 AD	*unknown*	22.4	0.7	2	54.2	0.14	35.4	6.4	1.29	0.10	-	2.52
3273	Chong Zhen Tong Bao	*unk.*	Ming	1628 AD	*unknown*	24.8	1	3	41.6	0.14	47.7	7.3	1.08	<q.l.	-	2.14
3274	Chong Zhen Tong Bao	*unk.*	Ming	1628 AD	*unknown*	22.4	0.9	3	53.0	0.67	37.5	3.0	1.62	0.12	0.36	3.67

Cu bronze brass unk. - unknown <q.l. - below quantification limit

Table VII.1 Coin attributed data, physical measurements and EDXRF (continued)

Ref.	Name	Cash #	Dynasty	Minting start-end date	Mint name, province	Ø (mm)	Maximum Thickness (mm)	weight (g)	Macro-EDXRF averages [obverse & reverse] (wt%) Cu ave.	Sn ave.	Zn ave.	Pb ave.	Fe ave.	Ni ave.	As ave.	Sb ave.
3275	Chong Zhen Tong Bao	*unk.*	Ming	1628 AD	*unknown*	25.1	1.1	3	41.0	<q.l.	52.6	4.85	1.08	<q.l.	-	0.39
3276	Chong Zhen Tong Bao	*unk.*	Ming	1628 AD	*unknown*	24.7	1.2	3	47.2	<q.l.	46.0	5.42	0.63	0.13	-	0.65
3277	Chong Zhen Tong Bao	*unk.*	Ming	1628 AD	*unknown*	23.2	0.9	3	51.7	<q.l.	39.2	5.68	1.13	<q.l.	-	2.15
3278	Chong Zhen Tong Bao	*unk.*	Ming	1628 AD	*unknown*	23.8	0.8	3	52.9	0.41	38.4	5.70	0.98	0.11	-	1.50
x	Chong Zhen Tong Bao	*unk.*	Ming	1628 AD	*unknown*	22.7	0.9	2	58.7	<q.l.	35.9	3.40	1.37	0.10	-	0.48
2671	Chong Zhen Tong Bao	*unk.*	Ming	1628 AD	*unknown*	23.5	0.7	2	35.9	3.37	40.7	16.96	1.93	<q.l.	-	1.06
2678	Hong Guang Tong Bao	*unk.*	Ming	1644 AD	*unknown*	25	1	4	84.9	<q.l.	8.6	6.06	0.31	0.13	-	<q.l.
2683	Shun Zhi Tong Bao	*unk.*	Qing	1644 AD	Kiang Su	27	0.9	5	63.5	2.14	27.4	5.50	0.67	0.15	-	0.64
2687	Shun Zhi Tong Bao	*unk.*	Qing	1644 AD	Shansi	25.5	0.9	4	70.2	3.07	17.0	8.09	0.99	0.14	-	0.49
2688	Shun Zhi Tong Bao	*unk.*	Qing	1644 AD	Shansi	28.2	0.9	5	78.2	3.31	10.9	6.40	0.47	0.16	-	0.62
2689	Shun Zhi Tong Bao	*unk.*	Qing	1644 AD	*unknown*	25.5	0.9	4	75.1	0.25	17.7	5.29	1.01	0.12	-	0.51
2690	Shun Zhi Tong Bao	*unk.*	Qing	1644 AD	*unknown*	25.5	0.9	3	67.9	2.40	18.3	10.22	0.77	0.16	-	0.18
2691	Shun Zhi Tong Bao	*unk.*	Qing	1644 AD	Kiang Si	27.5	0.9	4	61.5	1.80	27.4	6.78	0.97	0.13	-	1.47
2692	Shun Zhi Tong Bao	*unk.*	Qing	1644 AD	*unknown*	23.1	0.7	2	77.9	1.15	18.2	1.98	0.32	0.15	-	0.36
2693	Shun Zhi Tong Bao	*unk.*	Qing	1644 AD	Shensi	25.5	0.9	4	74.0	3.04	11.5	9.51	1.05	0.17	-	0.76
2694	Shun Zhi Tong Bao	*unk.*	Qing	1644 AD	Shantung	26.5	0.9	5	65.9	2.37	21.2	8.49	1.27	0.11	-	0.66
2696	Shun Zhi Tong Bao	*unk.*	Qing	1644 AD	*unknown*	25.5	0.9	4	67.9	2.66	20.6	7.23	0.84	0.15	-	0.65
2697	Shun Zhi Tong Bao	*unk.*	Qing	1644 AD	*unknown*	25.5	0.8	3	65.6	0.94	29.4	3.23	0.50	0.14	-	0.21
2700	Shun Zhi Tong Bao	*unk.*	Qing	1644 AD	*unknown*	26	1	4	62.6	2.93	19.7	13.27	0.82	<q.l.	-	0.63
2702	Shun Zhi Tong Bao	*unk.*	Qing	1644 AD	*unknown*	25.5	1	4	45.0	0.25	47.8	3.68	1.64	<q.l.	-	1.61
2703	Shun Zhi Tong Bao	*unk.*	Qing	1644 AD	*unknown*	25.5	1	4	66.8	1.76	20.7	9.09	1.14	0.10	-	0.45
2704	Shun Zhi Tong Bao	*unk.*	Qing	1644 AD	Yanghe	24	1	3	53.7	12.8	3.63	27.04	1.98	0.13	-	0.75
2705	Shun Zhi Tong Bao	*unk.*	Qing	1644 AD	*unknown*	24.5	1	4	61.8	0.85	30.9	5.10	0.65	0.10	-	0.61
2706	Shun Zhi Tong Bao	*unk.*	Qing	1644 AD	*unknown*	27.5	1	4	61.4	2.08	27.8	6.66	0.80	0.11	-	1.09
2676	Yong Chang Tong Bao	5	Qing	1644 AD	*unknown*	37.5	1.5	15	62.7	3.26	12.2	20.44	1.08	0.12	-	0.22
2711	Long Wu Tong Bao	2	Qing	1645 AD	*unknown*	26.5	1	4	80.2	<q.l.	18.0	0.49	0.79	0.11	0.31	<q.l.
2709	Yong Li Tong Bao	10	Qing	1647 AD	*unknown*	36.5	1.2	10	80.8	0.28	13.2	3.65	0.86	0.14	0.22	0.83
2714	Yong Li Tong Bao	*unk.*	Qing	1647 AD	*unknown*	24.5	1.5	5	71.9	0.94	21.1	3.98	1.45	<q.l.	-	0.50
2717	Yong Li Tong Bao	*unk.*	Qing	1647 AD	*unknown*	25	1.5	4	63.7	0.31	20.1	9.12	1.94	<q.l.	3.10	1.69
2712	Xing Chao Tong Bao	*unk.*	Qing	1649 AD	*unknown*	28.5	0.7	4	85.9	0.36	8.3	3.71	1.05	0.11	-	0.54
2718	Xing Chao Tong Bao	*unk.*	Qing	1649 AD	*unknown*	46.5	1.5	19	84.3	0.32	10.1	3.58	0.96	0.17	-	0.60
2710	Kang Xi Tong Bao	*unk.*	Qing	1662 AD	*unknown*	27.5	0.7	4	65.7	3.44	15.6	13.1	1.19	<q.l.	-	0.89
2723	Kang Xi Tong Bao	*unk.*	Qing	1662 AD	Hunan ?	24.5	0.8	3	54.0	<q.l.	43.1	1.54	1.27	<q.l.	-	<q.l.
2728	Kang Xi Tong Bao	*unk.*	Qing	1662 AD	Chihli ?	27	0.8	5	67.2	1.98	23.0	6.01	0.76	0.13	-	1.00
2733	Kang Xi Tong Bao	*unk.*	Qing	1662 AD	Chekiang	26.2	0.8	4	64.6	2.19	23.9	6.43	0.76	0.13	-	1.95
2736	Kang Xi Tong Bao	*unk.*	Qing	1662 AD	Taiwan	26	0.8	4	63.2	0.72	32.4	2.32	0.82	0.14	-	0.39
2737	Kang Xi Tong Bao	*unk.*	Qing	1662 AD	Fukien	27	0.7	4	79.2	1.80	4.3	14.0	0.57	0.13	-	<q.l.
2738	Li Yong Tong Bao	5	Qing	1674 AD	*unknown*	31.5	1.2	7	78.4	0.20	11.2	6.51	3.54	0.10	-	0.14
2741	Li Yong Tong Bao	10	Qing	1674 AD	*unknown*	38.2	1.9	16	75.7	0.42	11.1	8.77	3.24	<q.l.	-	0.66
2748	Zhao Wu Tong Bao	*unk.*	Qing	1678 AD	*unknown*	23	1	3	52.3	2.46	25.7	14.33	4.12	0.10	0.96	<q.l.
2751	Zhao Wu Tong Bao	*unk.*	Qing	1678 AD	*unknown*	34.5	1.5	10	81.8	1.58	9.7	4.17	2.47	0.11	-	0.19
2745	Hong Hua Tong Bao	*unk.*	Qing	1678-81 AD	*unknown*	23.5	1	3	73.1	3.18	8.97	13.47	1.15	0.10	-	<q.l.
2750	Yong Zheng Tong Bao	*unk.*	Qing	1723 AD	Shansi	26.5	0.9	4	62.9	1.89	24.4	8.87	1.63	0.15	-	0.18
2752	Yong Zhong Tong Bao	*unk.*	Qing	1723 AD	Fengtien	26.5	1	5	72.5	1.45	19.7	4.73	1.29	<q.l.	-	0.27
2746	Yong Zhong Tong Bao	*unk.*	Qing	1723 AD	*unknown*	25.5	0.9	4	67.7	<q.l.	31.5	0.42	0.30	<q.l.	-	<q.l.
2757	Yong Zhong Tong Bao	*unk.*	Qing	1723 AD	Yunnan	27	1	5	61.8	0.19	28.8	7.94	1.19	0.12	-	<q.l.
2760	Yong Zhong Tong Bao	*unk.*	Qing	1723 AD	Anhwei	27.5	0.9	4	68.6	2.67	22.8	4.06	1.25	0.20	-	0.34
2758	Qian Long Tong Bao	*unk.*	Qing	1736 AD	*unknown*	24.5	1	4	53.8	2.79	34.3	8.01	0.94	<q.l.	-	0.14
2761	Qian Long Tong Bao	*unk.*	Qing	1736 AD	Hangchow , Chekiang	23.5	1	4	50.7	1.27	36.1	10.86	0.92	<q.l.	-	<q.l.
2762	Qian Long Tong Bao	*unk.*	Qing	1736 AD	Wuchang; Hupeh	25	1	5	42.8	0.19	45.6	10.54	0.93	<q.l.	-	0.13
2763	Qian Long Tong Bao	*unk.*	Qing	1736 AD	Beijing	27.2	1.2	7	68.7	<q.l.	28.6	1.29	1.01	<q.l.	-	0.32
2764	Qian Long Tong Bao	*unk.*	Qing	1736 AD	Paoting; Chihli	24.5	1	4	51.6	1.56	39.7	6.20	0.84	<q.l.	-	0.10
2766	Qian Long Tong Bao	*unk.*	Qing	1736 AD	Beijing	26.5	1.1	6	66.2	<q.l.	31.4	1.02	0.44	<q.l.	0.40	0.47
2767	Qian Long Tong Bao	*unk.*	Qing	1736 AD	Fuchou; Fukien	24.5	0.95	4	45.9	2.54	42.5	7.28	1.66	0.10	-	<q.l.
2770	Qian Long Tong Bao	*unk.*	Qing	1736 AD	Shensi	25.2	0.95	4	56.0	2.40	33.2	7.83	0.53	<q.l.	-	<q.l.
2771	Qian Long Tong Bao	*unk.*	Qing	1736 AD	Sinkiang	24.5	1.2	5	99.3	<q.l.	<q.l.	<q.l.	0.30	0.13	-	<q.l.
2772	Qian Long Tong Bao	*unk.*	Qing	1736 AD	Kuelin, Kwangsi	24	1.1	5	53.9	<q.l.	39.2	5.24	1.57	<q.l.	-	<q.l.
2773	Qian Long Tong Bao	*unk.*	Qing	1736 AD	Taiyuan, Shansi	23.1	1.2	4	49.8	1.05	37.5	10.75	0.78	<q.l.	-	<q.l.
2774	Qian Long Tong Bao	*unk.*	Qing	1736 AD	Yunnan	24.5	1	4	45.9	0.35	47.6	4.50	1.52	0.10	-	<q.l.
2775	Qian Long Tong Bao	*unk.*	Qing	1736 AD	Kwangtung	24	1	3	53.4	<q.l.	41.6	3.87	0.87	<q.l.	-	0.11
2776	Qian Long Tong Bao	*unk.*	Qing	1736 AD	Chengtu, Szechuan	25	0.95	4	60.1	<q.l.	31.3	7.42	0.78	<q.l.	-	0.26
2779	Qian Long Tong Bao	10	Qing	1736 AD	Sinkiang	25	1	3	99.4	<q.l.	<q.l.	<q.l.	0.26	0.12	-	<q.l.
2777	Jia Qing Tong Bao	*unk.*	Qing	1796 AD	Beijing	25	0.9	4	59.3	<q.l.	33.7	2.65	1.61	0.15	0.39	2.19
2782	Jia Qing Tong Bao	*unk.*	Qing	1796 AD	Shensi	23	1.2	5	49.3	0.28	34.2	11.57	2.58	<q.l.	0.87	1.14
2783	Jia Qing Tong Bao	*unk.*	Qing	1796 AD	Kiangsi	24	1.2	4	46.8	0.25	43.9	6.83	1.89	<q.l.	-	<q.l.
2785	Jia Qing Tong Bao	*unk.*	Qing	1796 AD	Yunnan	25	0.95	4	54.1	<q.l.	31.8	7.64	2.05	0.21	0.55	3.64
2786	Jia Qing Tong Bao	*unk.*	Qing	1796 AD	Paoting; Chihli	24	1.2	5	54.0	0.13	42.8	1.68	1.33	<q.l.	-	<q.l.
2787	Jia Qing Tong Bao	*unk.*	Qing	1796 AD	Fuchou, Fukien	24.2	1.2	4	67.1	0.47	17.0	11.57	3.34	0.12	0.28	0.20
2788	Jia Qing Tong Bao	*unk.*	Qing	1796 AD	Dong Chuan, Yunnan	25.5	0.9	4	54.5	<q.l.	34.9	8.81	1.64	0.10	-	0.12
2789	Jia Qing Tong Bao	*unk.*	Qing	1796 AD	Hangchow ; Chekiang	24.5	1	4	49.6	0.79	39.0	8.57	1.92	<q.l.	-	<q.l.
2790	Jia Qing Tong Bao	*unk.*	Qing	1796 AD	*unknown*	25	1	4	52.4	<q.l.	37.3	8.64	0.77	0.10	-	0.76
2791	Jia Qing Tong Bao	*unk.*	Qing	1796 AD	*unknown*	23.5	1	4	44.0	<q.l.	49.7	4.65	1.58	<q.l.	-	<q.l.
2792	Jia Qing Tong Bao	*unk.*	Qing	1796 AD	Suchow ; Kiangsu	24.5	1.2	5	51.2	<q.l.	36.9	8.53	1.51	<q.l.	1.30	0.46
2793	Jia Qing Tong Bao	*unk.*	Qing	1796 AD	Kuelin, Kwangsi	25	1	5	49.9	<q.l.	30.3	14.94	0.74	<q.l.	-	4.07
2794	Jia Qing Tong Bao	*unk.*	Qing	1796 AD	Canton, Kwangtung	25.5	1.1	4	59.5	0.16	33.6	4.93	1.04	0.15	0.47	0.15
2796	Jia Qing Tong Bao	*unk.*	Qing	1796 AD	Kweiyang; Kweichow	25.1	1.1	4	47.8	<q.l.	48.4	1.85	1.91	<q.l.	-	<q.l.
2797	Jia Qing Tong Bao	*unk.*	Qing	1796 AD	Hocheng; Sinkiang	25.1	1	4	99.4	n.d.	0.16	<q.l.	0.28	0.13	-	<q.l.
2799	Jia Qing Tong Bao	*unk.*	Qing	1796 AD	Wuch'ang, Hupeh	24	1	4	30.0	<q.l.	62.9	5.16	1.60	<q.l.	-	0.21
2802	Jia Qing Tong Bao	*unk.*	Qing	1796 AD	Talyuan, shansi	23.5	1.1	4	62.5	<q.l.	33.1	3.43	0.74	0.11	-	<q.l.

Cu | bronze | brass | unk. - unknown | <q.l. - below quantification limit

Table VII.1 Coin attributed data, physical measurements and EDXRF (continued)

Ref.	Name	Cash #	Dynasty	Minting start-end date	Mint name, province	Ø (mm)	Maximum Thickness (mm)	weight (g)	Macro-EDXRF averages [obverse & reverse] (wt%)							
									Cu ave.	Sn ave.	Zn ave.	Pb ave.	Fe ave.	Ni ave.	As ave.	Sb ave.
2795	Dao Guang Tong Bao	*unk.*	Qing	1821 AD	Beijing	27	1.1	6	66.0	<q.l.	31.3	1.52	0.66	0.10	-	0.47
2798	Dao Guang Tong Bao	*unk.*	Qing	1821 AD	Beijing	27	1.5	6	71.9	<q.l.	24.8	1.09	1.83	<q.l.	-	0.28
2803	Dao Guang Tong Bao	*unk.*	Qing	1821 AD	Beijing	24	1.2	5	55.5	<q.l.	35.9	5.48	1.81	0.10	-	1.16
2804	Dao Guang Tong Bao	*unk.*	Qing	1821 AD	Hu Mint, Anhwei	23.5	1.5	5	52.8	<q.l.	40.5	5.36	1.19	0.17	-	<q.l.
2805	Dao Guang Tong Bao	*unk.*	Qing	1821 AD	Paoting, Chihli	22.5	1.1	4	49.5	<q.l.	46.3	3.35	0.81	<q.l.	-	<q.l.
2806	Dao Guang Tong Bao	*unk.*	Qing	1821 AD	Wuch'ang, Hupen	23.5	1.1	4	48.1	<q.l.	44.5	5.21	1.92	<q.l.	-	0.15
2807	Dao Guang Tong Bao	*unk.*	Qing	1821 AD	Kwelyang?, kweichow	23	0.7	3	57.1	<q.l.	38.9	2.38	1.49	0.12	-	<q.l.
2812	Dao Guang Tong Bao	*unk.*	Qing	1821 AD	Soohow; Kiangsu	23.5	1.5	5	40.8	0.19	49.0	7.64	2.39	<q.l.	-	<q.l.
2813	Dao Guang Tong Bao	*unk.*	Qing	1821 AD	Kwelyang?, kweichow	24	0.6	3	52.3	<q.l.	43.2	1.42	2.12	0.18	0.51	0.26
2814	Dao Guang Tong Bao	*unk.*	Qing	1821 AD	Ch'ang-sha, Hunan	23.5	1.1	4	55.4	0.10	34.2	7.82	2.20	<q.l.	-	0.23
2815	Dao Guang Tong Bao	*unk.*	Qing	1821 AD	Kuelin, Kwangsi	24.5	1	4	64.5	0.10	18.9	9.09	3.59	0.22	3.00	0.62
2816	Dao Guang Tong Bao	*unk.*	Qing	1821 AD	Kwelyang?, Kweichow	24	1.1	4	60.7	<q.l.	35.1	1.09	2.93	0.14	-	<q.l.
2817	Dao Guang Tong Bao	*unk.*	Qing	1821 AD	Shan Mint, Sian, Shensi	22	1	3	51.7	0.18	35.7	9.87	2.32	0.04	-	0.22
2818	Dao Guang Tong Bao	*unk.*	Qing	1821 AD	Kuche, Sinkiang	25	1.1	5	99.0	<q.l.	0.19	<q.l.	0.60	0.14	-	<q.l.
2819	Dao Guang Tong Bao	*unk.*	Qing	1821 AD	Chengtu; Szechuan	22.1	1	3	51.1	<q.l.	42.5	4.42	1.81	<q.l.	-	<q.l.
2820	Dao Guang Tong Bao	*unk.*	Qing	1821 AD	Sinkiang	24.5	1	4	99.3	n.d.	<q.l.	<q.l.	0.39	0.14	-	<q.l.
2824	Dao Guang Tong Bao	*unk.*	Qing	1821 AD	Dong Chuan, Yunnan	24.5	1	3	53.2	<q.l.	31.7	12.91	1.98	<q.l.	-	<q.l.
2826	Dao Guang Tong Bao	10	Qing	1821 AD	Sinkiang	25.5	1.5	4	96.2	<q.l.	0.22	0.28	3.08	<q.l.	<q.l.	<q.l.
2827	Dao Guang Tong Bao	*unk.*	Qing	1821 AD	Yunnantu; Yunnan	25	1	3	60.1	<q.l.	25.6	10.76	1.88	0.15	-	1.42
3263	Dao Guang Tong Bao	*unk.*	Qing	1821 AD	Kweichow	24.8	1.2	4	54.1	<q.l.	42.9	0.82	1.87	0.15	-	0.11
3264	Dao Guang Tong Bao	*unk.*	Qing	1821 AD	Kweichow	25.2	1.3	5	50.1	<q.l.	46.4	1.30	1.87	0.17	-	0.18
3228	Da Hua Qian	*unk.*	Qing	1840 AD	*unknown*	53	2.5	49	65.7	0.77	27.3	4.41	1.50	0.12	-	0.18
3229	Da Hua Qian	*unk.*	Qing	1840 AD	*unknown*	43.5	2.1	23	56.8	1.71	35.7	3.77	1.49	0.36	-	0.11
3230	Da Hua Qian	*unk.*	Qing	1840 AD	*unknown*	44.5	2	23	60.3	1.01	32.8	3.80	1.24	0.31	-	0.53
3231	Da Hua Qian	*unk.*	Qing	1840 AD	*unknown*	45.5	2.5	31	59.0	1.87	30.1	7.13	1.31	0.11	-	0.46
2822	Tai Pin Tian Guo (xiao)	*unk.*	Qing	1851-64 AD	*unknown*	22	0.7	2	60.6	3.29	27.0	7.65	1.11	0.16	-	0.22
3237	Tai Pin Tian Guo	*unk.*	Qing	1853 AD	*unknown*	23.5	1.5	4	56.4	3.46	25.3	12.58	1.81	0.15	-	0.30
3254	Xian Feng Yuan Bao	100	Qing	1853 AD	unknown	48.9	3.7	44	46.3	1.03	34.8	14.41	2.75	<q.l.	-	0.62
2825	Xian Feng Tong Bao	*unk.*	Qing	1854 AD	Peking	25	1.5	7	61.0	0.44	29.6	5.30	1.74	0.16	0.54	1.17
2829	Xian Feng Tong Bao	*unk.*	Qing	1854 AD	Peking	23.1	1.2	4	62.0	<q.l.	30.0	3.98	1.24	0.18	1.13	1.45
2831	Xian Feng Tong Bao	*unk.*	Qing	1854 AD	Ch'ang-sha; Hunan	21.5	1	3	68.6	2.39	19.9	5.77	1.31	0.21	0.57	1.31
2832	Xian Feng Tong Bao	*unk.*	Qing	1854 AD	Fuchou; Fukien	25.5	1.5	4	57.6	2.18	36.0	2.81	0.99	0.12	-	0.32
2833	Xian Feng Tong Bao	*unk.*	Qing	1854 AD	Kwelyang; Kweichow	23	0.9	2	51.2	0.19	41.2	5.31	1.91	0.19	-	<q.l.
2834	Xian Feng Tong Bao	*unk.*	Qing	1854 AD	Kuelin, Kwangsi	22	0.95	3	48.7	1.80	26.8	15.54	3.92	<q.l.	2.31	0.80
2837	Xian Feng Tong Bao	*unk.*	Qing	1854 AD	Sian; Shensi	22.5	1.5	4	60.3	0.66	26.1	3.93	2.69	0.16	4.31	1.86
2839	Xian Feng Tong Bao	*unk.*	Qing	1854 AD	Nanchang; Kiangsi	21.5	1	3	68.7	3.73	21.0	4.92	1.08	0.21	-	0.38
2840	Xian Feng Tong Bao	*unk.*	Qing	1854 AD	Soohow, Kiangsu	25	1.5	5	62.1	0.30	27.5	4.64	3.07	<q.l.	2.35	<q.l.
2917	Xian Feng Tong Bao	*unk.*	Qing	1854 AD	Talyuan; Shansi	22.1	1.5	3	58.7	<q.l.	33.9	6.85	0.33	0.15	-	0.12
2920	Xian Feng Tong Bao	*unk.*	Qing	1854 AD	Tung Ch'uan, Yunnan	23.5	1.1	5	51.6	<q.l.	30.4	15.74	2.06	<q.l.	-	0.13
2924	Xian Feng Tong Bao	5	Qing	1854 AD	Sinkiang	24	1	3	99.2	n.d.	<q.l.	0.23	0.34	<q.l.	-	<q.l.
2948	Xian Feng Yuan Bao	100	Qing	1854 AD	K'aifeng, Honan	48	4	47	57.4	0.86	33.6	5.46	1.76	0.13	-	0.80
2953	Xian Feng Yuan Bao	100	Qing	1854 AD	Hweiyuan, Sinkiang	47.5	2	22	64.5	1.83	24.3	7.67	1.56	<q.l.	-	0.11
2959	Xian Feng Yuan Bao	*unk.*	Qing	1854 AD	Beijing	48.5	3.1	43	54.7	<q.l.	35.8	6.67	2.35	0.15	-	0.27
2962	Xian Feng Yuan Bao	*unk.*	Qing	1854 AD	Beijing	48.5	4	41	59.5	0.96	30.6	6.03	2.17	0.13	-	0.67
3240	Xian Feng Yuan Bao	100	Qing	1854 AD	Sian, Shensi	50.1	4.5	54	60.7	0.95	30.9	5.29	1.52	0.13	-	0.58
3242	Xian Feng Yuan Bao	100	Qing	1854 AD	Suchow, Kiangsu	60	3.5	68	57.6	1.26	33.6	4.81	1.81	0.13	-	0.73
3243	Xian Feng Yuan Bao	100	Qing	1854 AD	Beijing	52.8	2.9	39	51.7	0.80	38.9	5.58	2.54	0.10	-	0.45
3244	Xian Feng Yuan Bao	100	Qing	1854 AD	Beijing	49.7	4.3	50	58.4	3.13	24.4	10.19	2.50	0.28	-	1.18
3245	Xian Feng Yuan Bao	100	Qing	1854 AD	Wuch'ang, Hupeh	53.8	3.3	54	68.2	6.57	20.8	2.33	0.75	0.19	-	1.22
3246	Xian Feng Yuan Bao	500	Qing	1854 AD	Beijing	57.3	3.5	57	72.8	<q.l.	25.6	0.59	0.79	<q.l.	-	<q.l.
3247	Xian Feng Yuan Bao	500	Qing	1854 AD	Beijing	52.7	3.5	50	58.6	0.84	31.6	5.75	2.25	0.13	-	0.81
2925	Xian Feng Zhong Bao	10	Qing	1854 AD	Tung Ch'uan, Yunnan	37	2	16	54.3	<q.l.	31.4	12.25	1.74	0.11	-	0.17
2927	Xian Feng Zhong Bao	10	Qing	1854 AD	Fuchou; Fukin	36	2.1	16	71.8	0.51	1.2	14.81	6.79	0.15	1.53	3.24
2929	Xian Feng Zhong Bao	10	Qing	1854 AD	Yunnantu; Yunnan	38	1.6	15	49.7	0.15	16.1	17.01	3.43	0.13	3.89	9.62
2931	Xian Feng Zhong Bao	10	Qing	1854 AD	Difi, sinkiang	26	1.2	6	52.7	<q.l.	18.6	27.23	1.30	<q.l.	-	<q.l.
2932	Xian Feng Zhong Bao	10	Qing	1854 AD	Peking	33	1.6	12	58.2	0.28	31.1	5.55	1.91	0.18	0.93	1.81
2933	Xian Feng Zhong Bao	10	Qing	1854 AD	Soohow, Kiangsu	36	1.9	13	53.4	1.41	36.6	4.73	2.51	0.14	0.53	0.72
2936	Xian Feng Zhong Bao	10	Qing	1854 AD	Nanchang; Kiangsi	37	2	15	44.7	3.71	41.7	6.74	2.74	0.16	-	0.33
2938	Xian Feng Zhong Bao	10	Qing	1854 AD	Hangchow, Chekiang	37	2	16	53.4	1.03	35.5	7.13	1.87	<q.l.	0.27	0.69
2941	Xian Feng Zhong Bao	10	Qing	1854 AD	Nanchang; Kiangsi	36	2.1	14	59.6	3.36	26.4	8.48	1.65	0.16	-	0.45
2943	Xian Feng Zhong Bao	50	Qing	1854 AD	Beijing	40.5	3.5	32	60.1	0.26	28.7	6.05	2.76	0.13	0.67	1.38
2944	Xian Feng Zhong Bao	10	Qing	1854 AD	Wuchang; Hupeh	35	2	16	71.0	<q.l.	22.7	0.47	1.82	0.21	1.20	2.48
2945	Xian Feng Zhong Bao	50	Qing	1854 AD	Peking	44	35	35	53.0	<q.l.	40.7	3.82	2.25	<q.l.	-	0.16
2946	Xian Feng Zhong Bao	50	Qing	1854 AD	Kaileng, Honan	44	4.1	41	68.4	0.86	18.0	7.76	3.27	0.11	0.53	1.04
2947	Xian Feng Zhong Bao	10	Qing	1854 AD	Wuchang; Hupeh	34.5	2	14	51.3	<q.l.	39.2	5.22	1.87	0.14	0.39	1.86
2949	Xian Feng Zhong Bao	20	Qing	1854 AD	Fu mint, fuchou,fukien	45.5	2.5	34	76.0	0.53	1.26	17.22	1.84	0.19	1.64	1.36
2950	Xian Feng Zhong Bao	50	Qing	1854 AD	Yarkand?, Sinkiang	38	1.1	14	98.4	<q.l.	0.41	0.76	0.29	0.13	-	0.01
2951	Xian Feng Zhong Bao	50	Qing	1854 AD	Beijing	41.5	4	40	57.1	0.56	34.8	3.50	1.94	0.31	0.55	1.19
2952	Xian Feng Zhong Bao	20	Qing	1854 AD	Fuchou, Fukien	47	3	38	74.4	0.46	0.8	12.79	4.50	0.19	2.11	4.78
2956	Xian Feng Zhong Bao	50	Qing	1854 AD	Beijing	47	2.6	36	44.2	0.44	45.0	5.20	2.04	0.10	0.44	2.62
3128	Xian Feng Zhong Bao	10	Qing	1854 AD	Kuelin, Kwangsi	39.5	1.7	18	61.9	0.35	27.8	3.56	1.52	0.15	1.51	3.23
3241	Xian Feng Zhong Bao	50	Qing	1854 AD	Suchow, Kiangsu	53.1	3.2	38	57.2	0.56	34.5	5.19	1.79	0.12	-	0.74
3248	Xian Feng Zhong Bao	50	Qing	1854 AD	Beijing	53.8	3.9	50	55.6	3.21	29.9	7.91	2.08	0.26	-	1.03
3249	Xian Feng Zhong Bao	50	Qing	1854 AD	Nanchang, Kiangsi	49.7	3	36	54.5	0.90	36.1	6.32	1.67	0.10	-	0.47
3250	Xian Feng Zhong Bao	50?	Qing	1854 AD	Beijing	54.7	3.4	56	53.6	<q.l.	37.7	6.61	1.80	0.11	-	0.15
3251	Xian Feng Zhong Bao	50	Qing	1854 AD	Kungchang, Kansu	49	3.2	37	64.9	1.54	26.0	4.95	2.02	0.11	-	0.48
3252	Xian Feng Zhong Bao	50	Qing	1854 AD	Chengtu; Szechuan	50.4	3.4	44	51.3	1.33	23.2	21.58	2.18	0.11	-	0.34
y	Xian Feng Zhong Bao	50	Qing	1854 AD	Sinkiang	37.6	1.8	13	99.1	n.d.	<q.l.	0.22	0.37	0.11	-	<q.l.
w	Xian Feng Zhong Bao	10	Qing	1854 AD	Chengtu, Szechuan	35.9	2	14	62.0	<q.l.	31.3	4.26	2.29	0.10	-	0.10

Cu bronze brass unk. - unknown <q.l. - below quantification limit

Table VII.1 Coin attributed data, physical measurements and EDXRF (continued)

Ref.	Name	Cash #	Dynasty	Minting start-end date	Mint name, province	Ø (mm)	Maximum Thickness (mm)	weight (g)	Macro-EDXRF averages [obverse & reverse] (wt%) Cu ave.	Sn ave.	Zn ave.	Pb ave.	Fe ave.	Ni ave.	As ave.	Sb ave.
2954	Tong Zhi Tong Bao	*unk.*	Qing	1862 AD	Beijing	21.5	0.6	2	59.5	2.26	35.0	2.32	0.70	0.12	-	<q.l.
2955	Tong Zhi Tong Bao	*unk.*	Qing	1862 AD	Kuelin, Kwangsi	23.5	1.1	4	58.7	1.13	31.2	6.35	1.97	0.10	-	0.62
2958	Tong Zhi Tong Bao	*unk.*	Qing	1862 AD	Yunnan	24.5	1.2	5	44.8	<q.l.	46.1	7.10	1.96	<q.l.	-	<q.l.
2960	Tong Zhi Tong Bao	10	Qing	1862 AD	Beijing	21.5	0.7	2	60.4	0.67	30.7	5.58	1.65	0.13	-	0.92
2961	Tong Zhi Tong Bao	*unk.*	Qing	1862 AD	Nanchang, Kiangsi	24	1.1	5	54.6	3.12	26.9	13.59	1.25	0.16	-	0.36
2963	Tong Zhi Tong Bao	*unk.*	Qing	1862 AD	Fuchou, Fukien	23	1	4	31.3	0.70	42.4	15.59	2.88	<q.l.	1.11	5.97
2964	Tong Zhi Tong Bao	*unk.*	Qing	1862 AD	Kuelin, Kwangsi	24	1	4	59.9	1.20	29.8	6.38	2.03	0.10	-	0.66
2965	Tong Zhi Tong Bao	*unk.*	Qing	1862 AD	Hangchow, Chekiang	23	1	4	60.0	3.79	28.4	6.12	1.22	0.16	-	0.38
2966	Tong Zhi Tong Bao	*unk.*	Qing	1862 AD	Ch'ang-sha, Hunan	21	1	3	52.0	2.54	36.7	6.02	2.32	<q.l.	-	0.39
2968	Tong Zhi Tong Bao	*unk.*	Qing	1862 AD	Chengtu, Szechuan	23	1	4	44.0	<q.l.	49.2	4.68	1.51	<q.l.	-	0.53
2969	Tong Zhi Tong Bao	*unk.*	Qing	1862 AD	Tai mint, taiwan	18	0.8	1	53.8	1.11	38.0	5.01	1.27	0.10	-	0.70
2970	Tong Zhi Tong Bao	10	Qing	1862 AD	Kuche, Sinkiang	25.5	1.2	5	99.3	<q.l.	0.19	0.03	0.35	0.10	-	<q.l.
2971	Tong Zhi Tong Bao	*unk.*	Qing	1862 AD	Soochow, Kiangsu	22.7	1.1	4	59.2	<q.l.	33.0	1.87	2.02	0.17	1.55	2.06
2974	Tong Zhi Tong Bao	*unk.*	Qing	1862 AD	Tundch'uan, Yunnan	20	0.5	0*	49.1	0.17	24.3	22.44	3.47	0.15	-	0.40
2957	Tong Zhi Zhong Bao	10	Qing	1862 AD	Beijing	26.5	1	5	57.9	0.67	30.3	7.22	2.12	0.18	0.31	1.35
2977	Tong Zhi Zhong Bao	10	Qing	1862 AD	Yunnan	37	1.1	9	64.4	18.55	0.65	11.11	3.20	0.18	1.67	0.24
2981	Guang Xu Tong Bao	*unk.*	Qing	1875 AD	Beijing	22.5	1	2	62.8	0.29	34.1	1.66	0.68	<q.l.	0.36	<q.l.
2984	Guang Xu Tong Bao	*unk.*	Qing	1875 AD	Beijing	22.5	1.2	2	47.1	0.10	46.0	5.59	1.14	<q.l.	-	<q.l.
2989	Guang Xu Tong Bao	10	Qing	1875 AD	Kucha, Sinkiang	25	1	2	98.4	<q.l.	<q.l.	0.49	0.71	0.10	<q.l.	<q.l.
2990	Guang Xu Tong Bao	*unk.*	Qing	1875 AD	Canton, Kwangtung	23.5	1	2	67.3	<q.l.	31.3	0.99	0.20	<q.l.	0.21	<q.l.
2991	Guang Xu Tong Bao	*unk.*	Qing	1875 AD	Ching	19	0.9	2	61.6	0.80	29.3	5.55	1.76	0.11	-	0.95
2992	Guang Xu Tong Bao	*unk.*	Qing	1875 AD	Paoting, Chihli	23.5	1.1	3	58.2	1.02	35.3	3.42	1.16	<q.l.	0.51	0.24
2993	Guang Xu Tong Bao	*unk.*	Qing	1875 AD	Yunnanfu, Yunnan	24	0.95	3	99.1	<q.l.	0.20	<q.l.	0.49	0.11	-	<q.l.
2995	Guang Xu Tong Bao	*unk.*	Qing	1875 AD	Wuch'ang, Hupeh	22.5	1	3	51.8	0.55	44.6	2.58	0.38	<q.l.	-	<q.l.
2998	Guang Xu Tong Bao	*unk.*	Qing	1875 AD	Paoting, Chihli	23.5	1.1	4	62.2	0.23	35.1	1.76	0.60	<q.l.	-	<q.l.
3003	Guang Xu Tong Bao	*unk.*	Qing	1875 AD	K'aifeng, Honan	21.5	1.1	3	53.2	2.10	35.8	7.37	1.06	0.18	-	0.39
3006	Guang Xu Tong Bao	*unk.*	Qing	1875 AD	Soohow, Kiangsu	20.5	1	2	63.2	1.18	23.8	9.36	1.58	0.11	-	0.85
3008	Guang Xu Tong Bao	*unk.*	Qing	1875 AD	Beijing	21	1.1	3	53.0	0.13	40.0	5.08	1.60	<q.l.	-	0.12
3009	Guang Xu Tong Bao	*unk.*	Qing	1875 AD	K'aifeng, Honan	21.5	1	3	55.3	0.98	39.2	3.45	0.75	0.10	-	0.22
3010	Guang Xu Tong Bao	10	Qing	1875 AD	Kashgar, Sinkiang	25	1	4	99.3	<q.l.	0.20	<q.l.	0.36	<q.l.	-	<q.l.
3011	Guang Xu Tong Bao	*unk.*	Qing	1875 AD	K'aifeng, Honan	21.5	1	3	61.3	1.90	16.7	15.75	4.04	0.11	-	0.28
3012	Guang Xu Tong Bao	*unk.*	Qing	1875 AD	Tientsin, Chihli	20.5	1	2	59.4	0.71	30.9	6.15	1.96	0.11	-	0.79
3013	Guang Xu Tong Bao	*unk.*	Qing	1875 AD	Tientsin, Chihli	22	1	3	57.4	0.28	38.9	1.66	1.61	0.10	-	<q.l.
3018	Guang Xu Tong Bao	*unk.*	Qing	1875 AD	K'aifeng, Honan	21	1	2	46.5	2.43	46.8	2.90	1.26	0.10	-	<q.l.
3019	Guang Xu Tong Bao	*unk.*	Qing	1875 AD	Tientsin, Chihli	20.5	0.7	2	56.8	0.84	29.9	8.95	2.27	<q.l.	-	1.14
3020	Guang Xu Tong Bao	*unk.*	Qing	1875 AD	Fuchou, Fukien	23	1	4	50.0	0.58	47.2	1.68	0.49	<q.l.	-	<q.l.
3021	Guang Xu Tong Bao	*unk.*	Qing	1875 AD	Fengtien	20	1	2	54.3	0.37	27.2	12.93	3.49	<q.l.	1.57	0.20
3022	Guang Xu Tong Bao	*unk.*	Qing	1875 AD	K'aifeng, Honan	21	1	3	60.2	1.64	28.9	7.20	1.46	0.30	-	0.33
3023	Guang Xu Tong Bao	*unk.*	Qing	1875 AD	Fuchou, Fukien	21.5	1.1	4	55.9	0.10	40.1	2.77	1.07	<q.l.	-	<q.l.
3025	Guang Xu Tong Bao	*unk.*	Qing	1875 AD	Yunnantu, Yunnan	19.5	1	2	56.7	<q.l.	32.2	8.77	1.81	0.13	-	0.30
3026	Guang Xu Tong Bao	*unk.*	Qing	1875 AD	K'aifeng, Honan	21.5	0.95	2	55.5	1.11	37.9	3.82	1.40	0.13	-	0.16
3027	Guang Xu Tong Bao	*unk.*	Qing	1875 AD	Kwelyang, Kweichow	20.5	0.95	2	46.4	<q.l.	46.9	4.83	1.81	<q.l.	-	<q.l.
3029	Guang Xu Tong Bao	*unk.*	Qing	1875 AD	K'aifeng, Honan	21.5	0.95	2	50.8	1.04	40.2	6.50	1.17	0.17	-	0.21
3030	Guang Xu Tong Bao	10	Qing	1875 AD	Beijing	20.5	0.9	2	55.1	0.62	35.4	5.34	2.24	0.15	0.57	0.61
3031	Guang Xu Tong Bao	*unk.*	Qing	1875 AD	K'aifeng, Honan	21.5	1	3	61.2	1.32	29.9	5.54	1.52	0.18	-	0.34
3032	Guang Xu Tong Bao	*unk.*	Qing	1875 AD	Chi mint, Kirin	21	1.1	3	59.4	0.18	37.1	1.24	1.99	<q.l.	-	<q.l.
3034	Guang Xu Tong Bao	*unk.*	Qing	1875 AD	K'aifeng, Honan	21	0.8	2	61.4	1.27	29.6	5.75	1.61	0.18	-	0.24
3035	Guang Xu Tong Bao	*unk.*	Qing	1875 AD	Tientsin, Chihli	22	0.9	2	61.1	0.50	36.7	0.82	0.26	<q.l.	0.59	<q.l.
3236	Guang Xu Tong Bao	*unk.*	Qing	1875 AD	*unknown*	25	1.2	5	55.7	0.64	37.1	4.47	1.22	<q.l.	-	0.76
3262	Guang Xu Tong Bao	*unk.*	Qing	1875 AD	Kweichow	22.7	1.2	3	49.4	n.d.	44.8	4.82	0.89	<q.l.	-	<q.l.
2994	Guang Xu Zhong Bao	10	Qing	1875 AD	Beijing	30	1.5	8	52.9	0.18	39.3	5.24	2.20	0.11	-	0.14
2997	Guang Xu Zhong Bao	10	Qing	1875 AD	Beijing	27	1.7	7	47.7	<q.l.	44.2	5.45	2.16	<q.l.	-	0.33
3454	*unknown*	*unk.*	*unknown*	*unknown*	*unknown*	20	1	2	72.7	1.17	13.8	7.51	3.96	0.14	-	0.75
3455	*unknown*	*unk.*	*unknown*	*unknown*	*unknown*	22.5	1.3	2	63.6	0.78	22.0	8.47	4.00	<q.l.	-	1.12
3457	*unknown*	*unk.*	*unknown*	*unknown*	*unknown*	26.4	1.4	3	38.8	2.29	8.3	46.14	4.39	<q.l.	-	<q.l.
3458	*unknown*	*unk.*	*unknown*	*unknown*	*unknown*	23.3	0.8	1	83.0	<q.l.	10.8	3.87	2.13	<q.l.	-	<q.l.
3459	*unknown*	*unk.*	*unknown*	*unknown*	*unknown*	20.2	0.8	1	55.3	0.93	25.3	12.62	4.97	<q.l.	-	0.86
3460	*unknown*	*unk.*	*unknown*	*unknown*	*unknown*	26.6	1.9	5	58.5	<q.l.	25.4	7.67	7.35	<q.l.	-	0.95
3461	*unknown*	*unk.*	*unknown*	*unknown*	*unknown*	24.6	2	2	39.6	<q.l.	55.2	2.65	2.44	<q.l.	-	<q.l.
3462	*unknown*	*unk.*	*unknown*	*unknown*	*unknown*	23.9	1.6	3	39.8	0.64	47.7	8.79	2.93	<q.l.	-	<q.l.
3463	*unknown*	*unk.*	*unknown*	*unknown*	*unknown*	20.6	0.8	2	59.3	6.05	15.6	16.69	1.72	0.13	-	0.50
m106-1968	*unknown*	*unk.*	*unknown*	*unknown*	*unknown*	25	1.4	3	46.7	0.23	49.4	1.02	2.63	0.04	-	<q.l.
m112-1990	*unknown*	*unk.*	*unknown*	*unknown*	*unknown*	24.9	3	4	29.6	0.16	58.3	6.08	5.83	<q.l.	-	<q.l.
m114-1990	*unknown*	*unk.*	*unknown*	*unknown*	*unknown*	21.2	1	2	65.4	0.68	21.8	8.25	3.55	<q.l.	-	0.19
m115-1992	*unknown*	*unk.*	*unknown*	*unknown*	*unknown*	23.3	1.4	3	67.6	<q.l.	23.0	5.24	3.14	<q.l.	-	0.99
m117-1992	*unknown*	*unk.*	*unknown*	*unknown*	*unknown*	18	2	<1	57.0	0.93	32.0	6.71	2.76	<q.l.	-	0.55

Cu bronze brass unk. - unknown <q.l. - below quantification limit

Table VII.2 Macro-EDXRF (surface) and micro-EDXRF (cleaned sections) of 109 selected coins

		Macro-EDXRF								Micro-EDXRF								
Mint date	**Ref.**	**Fe**	**Ni**	**Cu**	**Zn**	**As**	**Sn**	**Sb**	**Pb**	**Fe**	**Ni**	**Cu**	**Zn**	**As**	**Sn**	**Sb**	**Pb**	**Bi**	**Ref.**
40 AD	**2209**	5.46	0.10	82.51	0.19	-	5.70	0.06	6.00	3.90	0.23	89.00	-	0.30	4.23	0.35	1.97	-	**2209**
621 AD	**2242**	1.75	0.53	71.75	0.10	0.19	16.58	0.01	9.09	3.07	0.68	70.40	-	0.69	15.20	-	9.90	-	**2242**
1174-89 AD	**2416**	1.84	0.10	44.95	0.10	-	6.17	0.10	46.76	1.18	-	60.54	-	-	3.70	-	34.60	-	**2416**
1174-89 AD	**2419**	1.32	0.14	66.02	0.30	-	2.54	0.04	29.66	2.16	-	59.18	-	0.67	2.76	-	35.40	-	**2419**
1174-89 AD	**2421**	3.23	0.10	62.42	0.11	-	3.34	0.13	30.69	1.03	-	57.93	-	0.16	2.00	-	38.67	-	**2421**
1174-89 AD	**2427**	1.72	0.11	60.33	0.10	-	4.75	0.05	32.97	1.86	-	63.32	-	0.42	5.14	-	29.00	-	**2427**
1174-89 AD	**2433**	2.53	0.11	56.08	0.11	-	2.56	0.03	38.60	1.80	-	61.64	-	0.33	2.36	-	33.60	-	**2433**
1195-1200 AD	**2471**	1.81	0.09	50.35	0.10	-	2.35	0.26	45.06	1.40	-	62.62	-	0.76	2.38	-	32.60	-	**2471**
1195-1200 AD	**2479**	6.29	0.09	42.48	0.12	-	4.04	0.13	46.87	1.94	-	60.46	-	0,36	2.92	-	34.40	-	**2479**
1195-1200 AD	**2495**	2.26	0.10	62.06	0.08	-	2.89	0.13	32.50	1.28	-	60.98	-	0.30	1.80	-	35.80	-	**2495**
1195-1200 AD	**2498**	1.86	0.13	64.64	0.13	-	3.68	0.03	29.54	1.36	-	61.32	-	-	2.68	-	34.60	-	**2498**
1195-1200 AD	**2500**	2.34	0.09	62.20	0.10	-	4.41	0.04	30.83	0.78	-	64.64	-	-	3.62	-	31.00	-	**2500**
1195-1200 AD	**2501**	1.19	0.12	72.22	1.04	-	3.17	0.09	22.19	1.42	-	59.80	-	0.81	2.76	-	35.20	-	**2501**
1195-1200 AD	**2503**	2.51	0.09	43.13	0.18	-	5.59	0.42	48.11	1.26	-	69.62	-	0.92	3.62	-	24.60	-	**2503**
1195-1200 AD	**2504**	0.85	0.13	70.35	0.11	-	2.91	0.10	25.57	1.56	-	72.76	-	0.51	2.60	-	22.02	-	**2504**
1208-24 AD	**2519**	1.02	0.16	84.94	0.28	0.77	1.10	0.05	11.70	0.64	-	90.00	-	5.97	0.99	-	2.27	-	**2519**
1208-24 AD	**2522**	2.07	0.10	76.99	0.14	-	0.46	0.15	20.11	0.96	-	63.06	-	0.26	3.70	-	32.20	-	**2522**
1208-24 AD	**2525**	2.34	0.18	49.58	0.51	-	5.03	0.04	42.33	2.07	-	60.07	-	0.40	2.03	-	35.33	-	**2525**
1208-24 AD	**2528**	2.35	0.10	72.16	0.11	-	4.07	0.09	21.14	0.91	-	67.14	-	0.43	2.98	-	28.40	-	**2528**
1208-24 AD	**2534**	1.32	0.08	32.51	0.17	-	0.15	0.15	65.65	1.66	-	64.88	-	1.56	0.00	0.20	31.60	-	**2534**
1208-24 AD	**2544**	2.61	0.08	26.12	0.07	-	0.75	0.03	70.36	1.96	0.19	41.10	-	0.67	1.86	-	54.80	-	**2544**
1228-33 AD	**2558**	1.60	0.11	64.26	0.35	-	3.39	0.04	30.26	4.96	-	61.70	-	0.20	2.70	-	30.20	-	**2558**
1228-33 AD	**2563**	1.27	0.11	61.25	0.09	-	3.49	0.09	33.73	2.40	0.19	69.76	-	0.37	3.16	-	24.00	-	**2563**
1228-33 AD	**2564**	2.82	0.07	39.22	0.19	-	8.00	0.09	49.62	1.07	-	72.40	-	0.36	5.10	-	21.20	-	**2564**
1228-33 AD	**2568**	1.43	0.09	46.61	0.11	-	2.11	0.09	49.58	2.32	-	56.74	-	0.25	1.80	-	39.00	-	**2568**
1228-33 AD	**2571**	1.85	0.08	34.06	0.08	-	1.10	0.04	62.80	2.44	-	65.60	-	0.39	1.75	-	30.00	-	**2571**
1241-52 AD	**2578**	2.17	0.07	45.66	0.08	-	3.91	0.16	47.98	3.18	-	59.44	-	0.38	2.78	-	34.20	-	**2578**
1241-52 AD	**2581**	1.27	0.11	64.88	0.10	-	1.88	0.05	31.73	2.48	-	61.43	-	0.26	1.90	-	34.25	-	**2581**
1241-52 AD	**2582**	2.41	0.07	48.25	0.12	-	1.82	0.07	47.27	1.04	-	62.16	-	0.44	2.38	-	34.00	-	**2582**
1241-52 AD	**2585**	1.21	0.06	35.69	0.17	-	2.02	0.08	60.80	2.12	-	51.14	-	0.48	2.17	-	44.00	-	**2585**
1241-52 AD	**2588**	2.15	0.09	48.17	0.08	-	2.16	0.09	47.28	2.32	0.20	69.66	-	0.55	3.12	-	24.00	-	**2588**
1265-74 AD	**2614**	1.85	0.06	51.21	0.09	-	6.16	0.10	40.55	2.04	-	61.76	-	0.29	4.96	-	31.00	-	**2614**
1265-74 AD	**2615**	3.48	0.10	62.70	0.17	-	2.60	0.79	30.19	2.50	-	60.84	-	0.55	2.50	0.68	33.00	-	**2615**
1260-64 AD	**2616**	1.73	0.08	49.08	0.18	-	3.25	0.04	45.66	1.90	0.19	59.92	0.23	0.36	3.12	-	34.20	-	**2616**
1265-74 AD	**2617**	3.47	0.09	44.08	0.12	-	3.99	0.05	48.21	2.73	-	58.44	-	0.35	3.19	-	34.90	-	**2617**
1265-74 AD	**2619**	1.45	0.10	63.74	0.10	-	5.11	0.10	29.40	1.84	-	73.18	-	0.45	4.10	-	20.00	-	**2619**
1265-74 AD	**2621**	2.11	0.09	35.88	0.12	-	1.55	0.05	60.22	7.22	-	55.88	-	0.34	1.64	-	35.00	-	**2621**
1265-74 AD	**2623**	2.19	0.08	38.04	0.09	-	5.61	0.15	53.87	2.36	-	55.28	-	0.39	3.50	-	38.20	-	**2623**
1265-74 AD	**2624**	2.42	0.11	47.12	0.22	-	5.34	0.06	44.74	2.56	-	53.84	-	0.36	4.20	-	39.20	-	**2624**
1265-74 AD	**2625**	1.00	0.10	59.89	0.13	-	0.98	0.06	37.87	1.04	0.16	52.28	-	0.31	1.36	-	45.00	-	**2625**
1265-74 AD	**2626**	0.65	0.06	20.36	0.06	-	0.45	0.04	78.41	2.56	-	62.74	-	0.50	3.64	-	30.40	-	**2626**
1265-74 AD	**2631**	1.56	0.11	42.05	0.13	-	3.63	0.04	52.51	1.32	-	63.70	-	0.44	4.50	-	30.20	-	**2631**
1576 AD	**2650**	0.14	0.11	60.86	37.46	-	0.40	0.01	1.03	0.10	-	61.87	37.03	-	0.00	-	0.83	0.18	**2650**
1576 AD	**2653**	1.23	0.12	63.13	10.93	-	6.68	0.07	17.86	0.40	-	70.10	11.03	-	4.90	-	13.67	-	**2653**
1620 AD	**2659**	0.66	0.11	66.53	31.16	0.16	0.02	0.22	1.18	0.48	0.13	72.73	24.70	0.50	0.00	-	1.30	0,38	**2659**
1621-27 AD	**2632**	0.75	0.10	64.83	30.50	0.18	1.01	0.12	2.52	0.66	-	54.26	41.44	-	1.28	-	2.35	-	**2632**
1621-27 AD	**2635**	0.53	0.07	50.78	46.49	-	0.43	0.14	1.57	0.34	-	60.23	37.37	0.32	0.46	-	0.97	0.31	**2635**
1621-27 AD	**2636**	0.43	0.08	64.52	33.58	-	0.02	0.02	1.37	0.32	-	65.87	32.30	-	0.00	-	1.30	0.20	**2636**
1621-27 AD	**2639**	0.60	0.21	84.85	8.74	0.37	0.08	0.67	4.50	0.36	0.32	80.37	12.53	0.95	0.24	0.39	5.00	-	**2639**
1621-27 AD	**2642**	0.65	0.10	56.60	29.83	-	3.59	0.08	9.16	0.43	-	61.93	24.63	-	3.47	-	9.67	-	**2642**
1621-27 AD	**2645**	0.85	0.08	55.64	26.52	-	2.37	0.07	14.50	0.31	0.11	63.93	28.23	0.17	1.17	-	6.00	0,42	**2645**
1628-44 AD	**2661**	1.80	0.17	67.80	29.14	-	0.03	0.06	1.01	1.65	0.23	71.47	25.63	-	0.00	-	1.00	-	**2661**
1628-44 AD	**2662**	0.57	0.11	63.32	31.61	0.32	0.94	0.56	2.60	0.36	0.12	63.47	32.20	0.40	0.67	0.44	2.13	0.24	**2662**
1628-44 AD	**2663**	0.32	0.08	58.84	38.90	0.22	0.02	0.04	1.60	0.13	-	62.13	36.00	0.43	0.00	-	0.37	0.97	**2663**
1628-44 AD	**2664**	1.00	0.07	30.69	60.50	-	1.05	0.94	5.75	0.61	0.09	53.30	38.23	-	0.83	0.38	6.67	-	**2664**
1628-44 AD	**2666**	0.88	0.10	47.54	42.85	-	0.50	3.78	4.38	0.49	0.11	52.27	37.97	0.45	0.00	3.13	5.33	-	**2666**
1628-44 AD	**2667**	1.89	0.11	64.51	28.19	-	1.24	0.34	3.73	0.52	0.12	67.57	26.03	0.41	1.00	-	4.17	0.21	**2667**
1628-44 AD	**2670**	1.75	0.14	63.79	20.30	-	2.18	0.15	11.72	0.39	0.21	57.30	25.77	0.30	1.70	-	14.33	0.30	**2670**
1628-44 AD	**2671**	1.93	0.07	35.90	40.72	-	3.37	1.06	16.96	0.59	0.16	57.10	26.67	0.43	3.77	1.57	9.67	0.08	**2671**
1628-44 AD	**3271**	1.38	0.15	52.28	34.45	-	0.25	4.65	6.87	1.12	0.17	55.97	29.87	0.98	0.00	3.67	8.00	-	**3271**
1628-44 AD	**3272**	1.29	0.10	54.16	35.40	-	0.14	2.52	6.42	0.86	-	54.67	33.50	-	0.00	2.30	8.67	-	**3272**
1628-44 AD	**3273**	1.08	0.09	41.57	47.70	-	0.14	2.14	7.30	0.79	-	52.17	34.63	0.32	0.00	1.93	10.00	-	**3273**
1628-44 AD	**3274**	1.62	0.12	53.04	37.48	0.36	0.67	3.67	3.05	0.91	0.13	50.33	39.53	0.49	0.00	2.73	6.00	-	**3274**
1628-44 AD	**3275**	1.08	0.08	40.96	52.63	-	0.03	0.39	4.85	0.70	0.10	54.67	40.30	0.08	0.00	-	4.20	-	**3275**
1628-44 AD	**3276**	0.63	0.13	47.17	46.00	-	0.02	0.65	5.42	0.32	0.12	54.30	38.77	0.26	0.00	0.56	5.67	-	**3276**
1628-44 AD	**3277**	1.13	0.09	51.69	39.17	-	0.06	2.15	5.68	0.42	0.05	56.23	37.13	-	0.00	1.60	4.67	-	**3277**
1628-44 AD	**3278**	0.98	0.11	52.86	38.44	-	0.41	1.50	5.70	0.58	0.10	54.27	39.10	0.74	0.00	1.10	4.10	-	**3278**
1628-44 AD	**X**	1.37	0.10	58.69	35.92	-	0.06	0.48	3.40	0.52	0.09	51.33	46.10	0.10	0.00	0.20	1.63	-	**X**
1644-61 AD	**2704**	1.98	0.13	53.70	3.60	-	12.80	0.75	27.00	0.34	0.16	68.33	10.33	0.34	5.03	0.31	15.33	-	**2704**

Table VII.2 Macro-EDXRF (surface) and micro-EDXRF (cleaned sections) of 109 selected coins (continued)

		Macro-EDXRF								Micro-EDXRF									
Mint date	**Ref.**	**Fe**	**Ni**	**Cu**	**Zn**	**As**	**Sn**	**Sb**	**Pb**	**Fe**	**Ni**	**Cu**	**Zn**	**As**	**Sn**	**Sb**	**Pb**	**Bi**	**Ref.**
1662-1722 AD	**2710**	1.19	0.09	65.70	15.57	-	3.44	0.89	13.15	0.55	0.13	56.57	29.17	0.16	2.53	0.78	10.23	-	**2710**
1662-1722 AD	**2723**	1.27	0.07	54.04	43.06	-	0.02	0.01	1.54	1.00	-	46.90	51.60	-	0.00	-	0.40	-	**2723**
1662-1722 AD	**2728**	0.76	0.13	67.15	22.99	-	1.98	1.00	6.01	0.57	0.13	65.13	23.97	0.24	1.83	0.93	7.17	-	**2728**
1662-1722 AD	**2733**	0.76	0.13	64.61	23.94	-	2.19	1.95	6.43	0.55	0.14	65.33	23.43	0.21	1.66	1.36	7.03	-	**2733**
1662-1722 AD	**2736**	0.82	0.14	63.24	32.41	-	0.72	0.39	2.32	0.80	-	61.50	32.70	0.60	0.70	0.30	3.30	-	**2736**
1662-1722 AD	**2737**	0.57	0.13	79.16	4.27	-	1.80	0.06	14.02	0.44	-	78.57	3.51	1.03	2.13	-	14.33	-	**2737**
1736-95 AD	**2758**	0.94	0.05	53.80	34.29	-	2.79	0.14	8.01	0.34	-	53.13	35.00	-	2.90	0.30	8.33	-	**2758**
1736-95 AD	**2761**	0.92	0.05	50.74	36.14	-	1.27	0.04	10.86	0.56	0.05	49.80	36.80	-	0.96	0.15	12.00	-	**2761**
1736-95 AD	**2762**	0.93	0.06	42.78	45.64	-	0.19	0.13	10.54	0.64	0.07	54.60	39.05	-	0.22	0.14	5.50	-	**2762**
1736-95 AD	**2763**	1.01	0.08	68.68	28.58	-	0.06	0.32	1.29	0.48	-	68.23	29.97	0.48	0.00	-	0.83	-	**2763**
1736-95 AD	**2764**	0.84	0.07	51.58	39.66	-	1.56	0.10	6.20	0.25	-	53.87	38.30	-	1.30	0.14	6.13	-	**2764**
1736-95 AD	**2766**	0.44	0.09	66.16	31.43	0.40	0.00	0.47	1.02	0.36	0.06	65.50	32.63	0.42	0.00	0.34	0.70	-	**2766**
1736-95 AD	**2767**	1.66	0.10	45.88	42.53	-	2.54	0.04	7.28	1.82	-	46.93	41.27	1.20	2.10	0.19	6.60	-	**2767**
1736-95 AD	**2770**	0.53	0.06	55.98	33.20	-	2.40	0.01	7.83	0.27	-	55.27	35.03	-	2.07	0.15	7.00	-	**2770**
1736-95 AD	**2771**	0.30	0.13	99.32	0.17	-	0.02	0.02	0.06	0.09	[0,27]	99.53	0.00	-	0.00	-	0.15	-	**2771**
1736-95 AD	**2772**	1.57	0.06	53.85	39.24	-	0.03	0.02	5.24	1.28	-	46.70	47.87	-	0.00	-	4.17	-	**2772**
1736-95 AD	**2773**	0.78	0.06	49.78	37.50	-	1.05	0.01	10.75	0.30	0.06	53.70	38.13	-	0.93	0.14	6.60	-	**2773**
1736-95 AD	**2774**	1.52	0.10	45.90	47.62	-	0.35	0.03	4.50	0.92	-	48.05	46.70	0.06	0.42	-	4.13	-	**2774**
1736-95 AD	**2775**	0.87	0.06	53.41	41.62	-	0.08	0.11	3.87	0.54	-	49.57	45.03	0.17	0.00	-	4.70	-	**2775**
1736-95 AD	**2776**	0.78	0.08	60.09	31.35	-	0.04	0.26	7.42	0.23	-	58.80	32.53	0.08	0.23	0.23	8.00	-	**2776**
1736-95 AD	**2779**	0.26	0.12	99.39	0.16	-	0.00	0.02	0.05	0.11	[0,27]	99.50	0.00	0.09	0.00	-	0.00	-	**2779**
1796-1820 AD	**2777**	1.61	0.15	59.28	33.68	0.39	0.07	2.19	2.65	0.99	0.16	64.37	30.13	0.65	0.00	1.26	2.43	-	**2777**
1796-1820 AD	**2782**	2.58	0.08	49.29	34.20	0.87	0.28	1.14	11.57	1.52	-	52.90	35.37	2.70	0.00	1.06	6.60	-	**2782**
1796-1820 AD	**2783**	1.89	0.06	46.78	43.87	-	0.25	0.03	6.83	1.83	-	46.77	42.90	1.56	0.00	-	6.97	-	**2783**
1796-1820 AD	**2785**	2.05	0.21	54.07	31.77	0.55	0.08	3.64	7.64	2.28	0.25	52.33	30.83	1.57	0.00	3.30	9.67	-	**2785**
1796-1820 AD	**2786**	1.33	0.08	54.00	42.75	-	0.13	0.05	1.68	0.49	-	59.00	39.13	-	0.00	-	1.37	-	**2786**
1796-1820 AD	**2787**	3.34	0.12	67.07	16.99	0.28	0.47	0.20	11.57	1.58	0.18	55.20	34.40	1.01	0.49	-	7.13	-	**2787**
1796-1820 AD	**2788**	1.64	0.10	54.47	34.85	-	0.02	0.12	8.81	1.37	0.09	55.07	35.80	0.20	0.00	-	7.60	-	**2788**
1796-1820 AD	**2789**	1.92	0.07	49.58	39.04	-	0.79	0.04	8.57	1.65	0.06	51.30	36.93	0.55	0.75	-	8.83	-	**2789**
1796-1820 AD	**2790**	0.77	0.10	52.41	37.26	-	0.06	0.76	8.64	0.09	0.09	53.83	38.00	0.59	0.00	0.55	6.83	-	**2790**
1796-1820 AD	**2791**	1.58	0.04	43.96	49.70	-	0.02	0.07	4.65	1.15	-	43.73	50.77	-	0.00	-	4.37	-	**2791**
1796-1820 AD	**2792**	1.51	0.07	51.23	36.86	1.30	0.05	0.46	8.53	0.77	0.09	53.60	34.13	4.05	0.00	0.42	6.60	-	**2792**
1796-1820 AD	**2793**	0.74	0.08	49.86	30.26	-	0.07	4.07	14.94	0.26	-	53.23	31.40	1.70	0.00	3.37	10.00	-	**2793**
1796-1820 AD	**2794**	1.04	0.15	59.49	33.63	0.47	0.16	0.15	4.93	0.82	0.13	56.13	34.67	1.14	0.00	-	7.03	-	**2794**
1796-1820 AD	**2796**	1.91	0.07	47.76	48.36	-	0.02	0.03	1.85	1.46	-	45.57	52.03	0.13	0.00	0.13	0.67	-	**2796**
1796-1820 AD	**2797**	0.28	0.13	99.38	0.16	-	0.00	0.01	0.04	0.01	-	99.63	0.00	0.05	0.00	0.21	0.06	-	**2797**
1796-1820 AD	**2799**	1.60	0.05	30.04	62.94	-	0.02	0.21	5.16	1.38	0.06	43.23	49.53	0.18	0.00	0.27	5.30	-	**2799**
1796-1820 AD	**2802**	0.74	0.11	62.50	33.15	-	0.02	0.07	3.43	0.38	-	61.83	32.73	0.01	0.26	-	4.83	-	**2802**
1862-74 AD	**2977**	3.20	0.18	64.40	0.65	1.67	18.60	0.24	11.10	0.69	0.18	73.33	0.27	1.90	10.10	0.32	13.33		**2977**
unknown	**M117**	2.76	0.08	56.99	31.99	-	0.93	0.55	6.71	0.94	0.09	60.03	30.10	0.83	0.92	0.46	6.60	-	**M117**

Table VII.3 Micro-EDXRF results and OM images of the cleaned sections

	Micro-EDXRF (wt.%)								Qin Dynasty		
Ref.	Fe	Ni	Cu	Zn	As	Sn	Sb	Pb	Date	Designation	Alloy
2209	3.63	0.19	82.37	-	0.39	4.23	0.34	1.87	40AD	Xiao Wu Zhu	Bronze

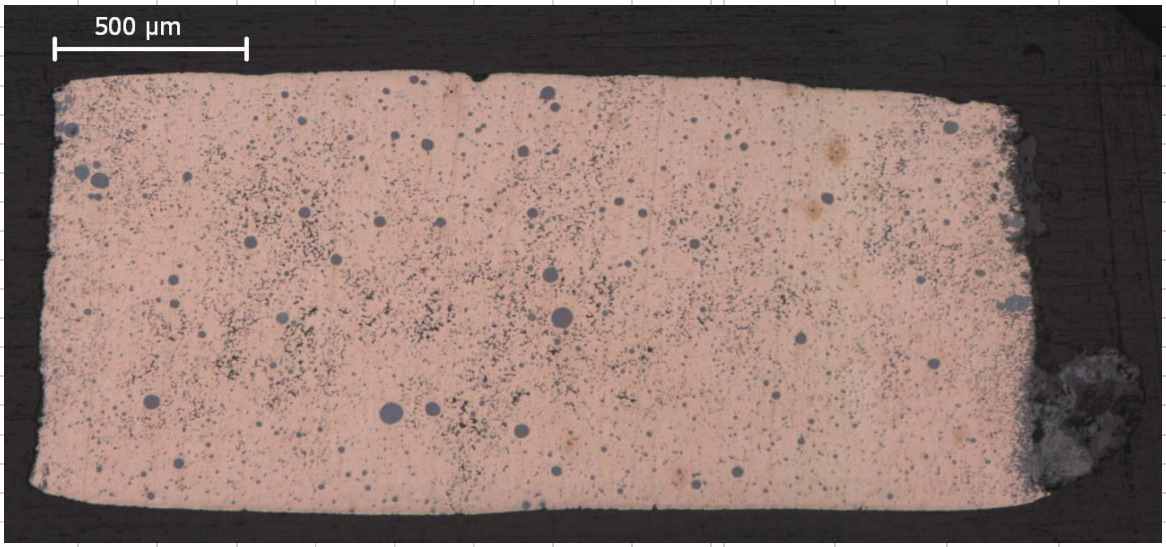

	Micro-EDXRF (wt.%)								Qin Dynasty		
Ref.	Fe	Ni	Cu	Zn	As	Sn	Sb	Pb	Date	Designation	Alloy
2242	3.07	0.68	70.4	-	0.69	15.2	-	9.9	621AD	Kai Yuan Tong Bao	Bronze

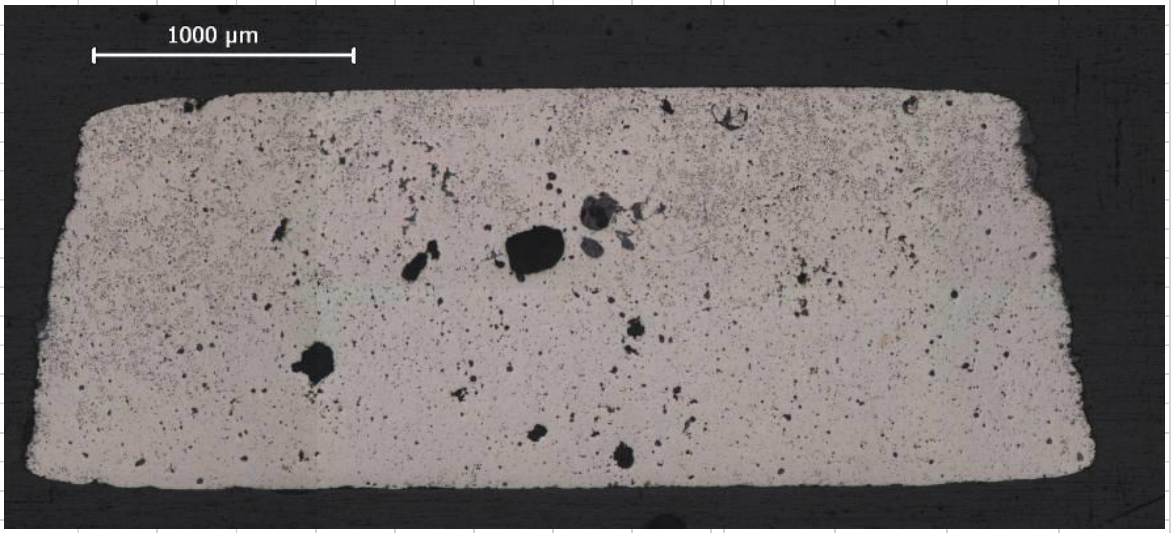

	Micro-EDXRF (wt.%)								Song Dynasty		
Ref.	Fe	Ni	Cu	Zn	As	Sn	Sb	Pb	Date	Designation	Alloy
2416	1.18	-	60.54	-	-	3.7	-	34.6	1174AD	Chun Xi Yuan Bao	Bronze

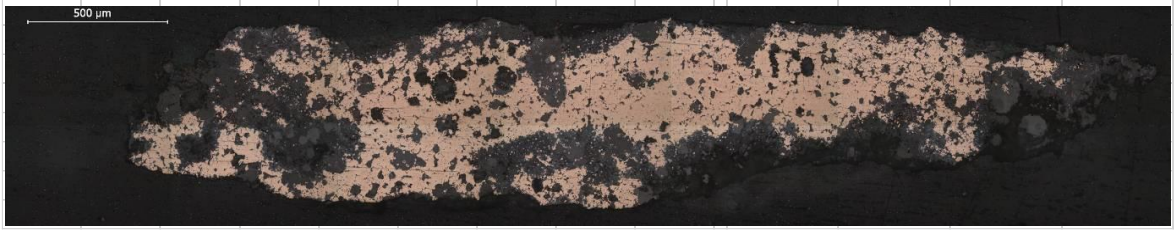

Table VII.3 Micro-EDXRF results and OM images of the cleaned sections (continued)

	Micro-EDXRF (wt.%)								Song Dynasty			
Ref.	**Fe**	**Ni**	**Cu**	**Zn**	**As**	**Sn**	**Sb**	**Pb**	**Date**	**Designation**		**Alloy**
2419	2.16	-	59.18	-	0.67	2.76	-	35.4	1174AD	Chun Xi Yuan Bao		Bronze

	Micro-EDXRF (wt.%)								Song Dynasty			
Ref.	**Fe**	**Ni**	**Cu**	**Zn**	**As**	**Sn**	**Sb**	**Pb**	**Date**	**Designation**		**Alloy**
2421	1.03	-	57.93	-	0.16	2,00	-	38.67	1174AD	Chun Xi Yuan Bao		Bronze

	Micro-EDXRF (wt.%)								Song Dynasty			
Ref.	**Fe**	**Ni**	**Cu**	**Zn**	**As**	**Sn**	**Sb**	**Pb**	**Date**	**Designation**		**Alloy**
2427	1.86	-	63.32	-	0.42	5.14	-	29,00	1174AD	Chun Xi Yuan Bao		Bronze

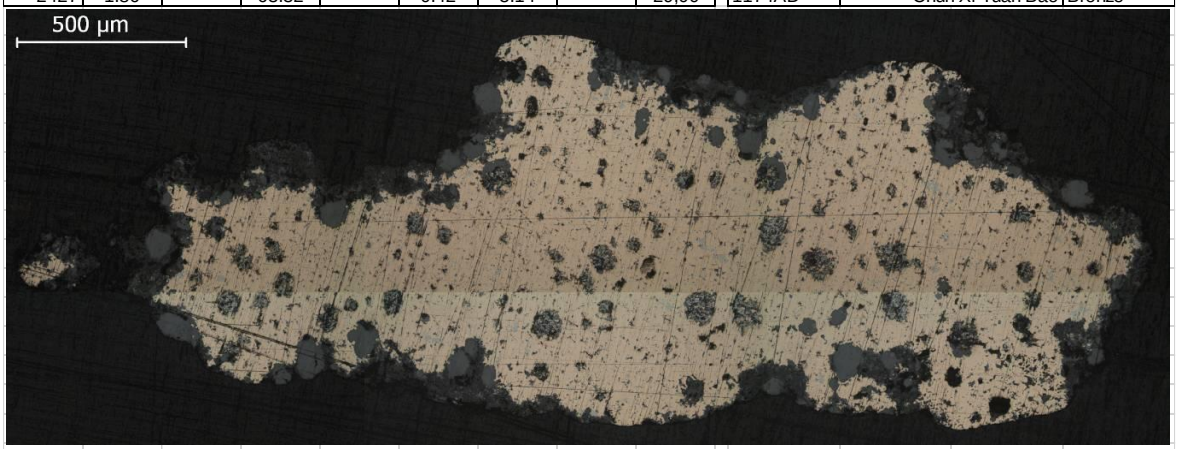

	Micro-EDXRF (wt.%)								Song Dynasty			
Ref.	**Fe**	**Ni**	**Cu**	**Zn**	**As**	**Sn**	**Sb**	**Pb**	**Date**	**Designation**		**Alloy**
2433	1.8	-	61.64	-	0.33	2.36	-	33.6	1174AD	Chun Xi Yuan Bao		Bronze

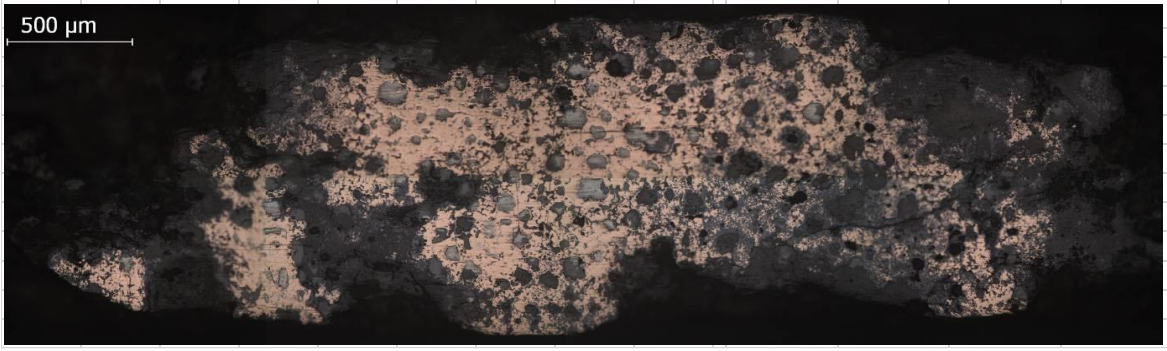

Table VII.3 Micro-EDXRF results and OM images of the cleaned sections (continued)

	Micro-EDXRF (wt.%)								Song Dynasty			
Ref.	Fe	Ni	Cu	Zn	As	Sn	Sb	Pb	Date	Designation		Alloy
2471	1.4	-	62.62	-	0.76	2.38	-	32.6	1195AD	Qing Yuan Tong Bao		Bronze

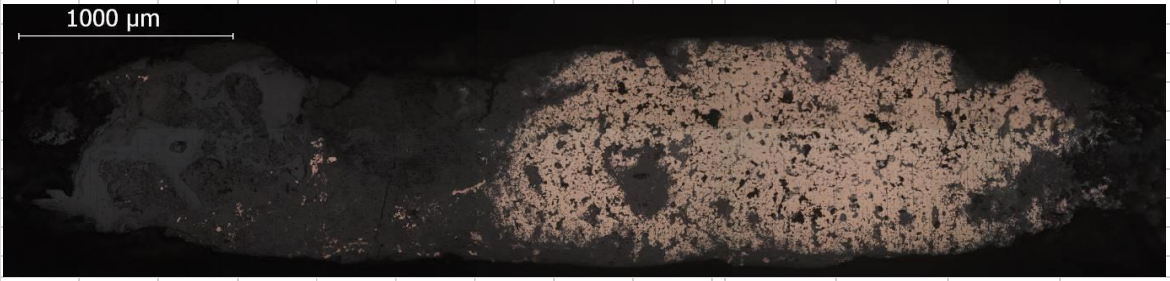

	Micro-EDXRF (wt.%)								Song Dynasty			
Ref.	Fe	Ni	Cu	Zn	As	Sn	Sb	Pb	Date	Designation		Alloy
2479	1.94	-	60.46	-	[0.36]	2.92	-	34.4	1195AD	Qing Yuan Tong Bao		Bronze

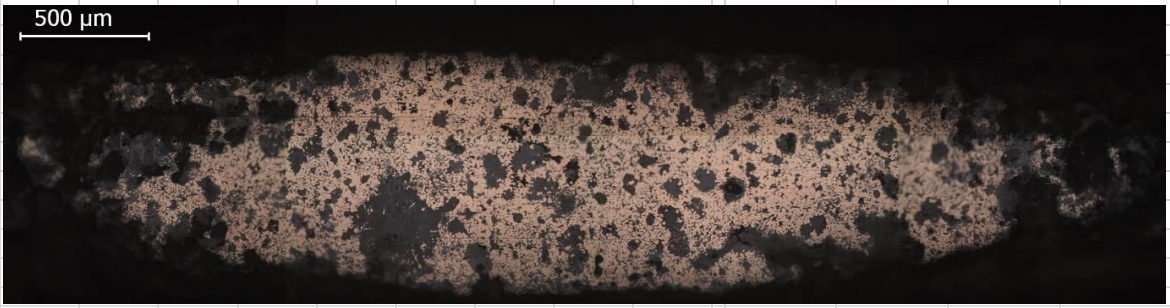

	Micro-EDXRF (wt.%)								Song Dynasty			
Ref.	Fe	Ni	Cu	Zn	As	Sn	Sb	Pb	Date	Designation		Alloy
2495	1.28	-	60.98	-	0.3	1.8	-	35.8	1195AD	Qing Yuan Tong Bao		Bronze

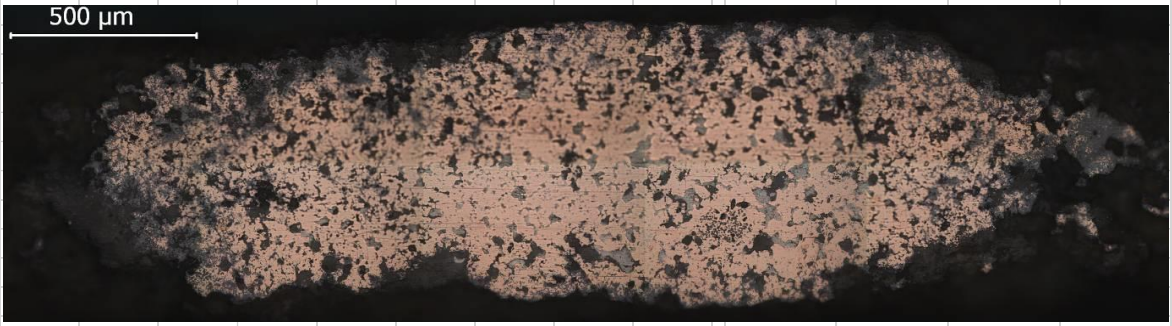

	Micro-EDXRF (wt.%)								Song Dynasty			
Ref.	Fe	Ni	Cu	Zn	As	Sn	Sb	Pb	Date	Designation		Alloy
2498	1.36	-	61.32	-	-	2.68	-	34.6	1195AD	Qing Yuan Tong Bao		Bronze

Table VII.3 Micro-EDXRF results and OM images of the cleaned sections (continued)

	Micro-EDXRF (wt.%)								Song Dynasty			
Ref.	Fe	Ni	Cu	Zn	As	Sn	Sb	Pb	Date	Designation		Alloy
2500	0.78	-	64.64	-	-	3.62	-	31,00	1195AD	Qing Yuan Tong Bao		Bronze

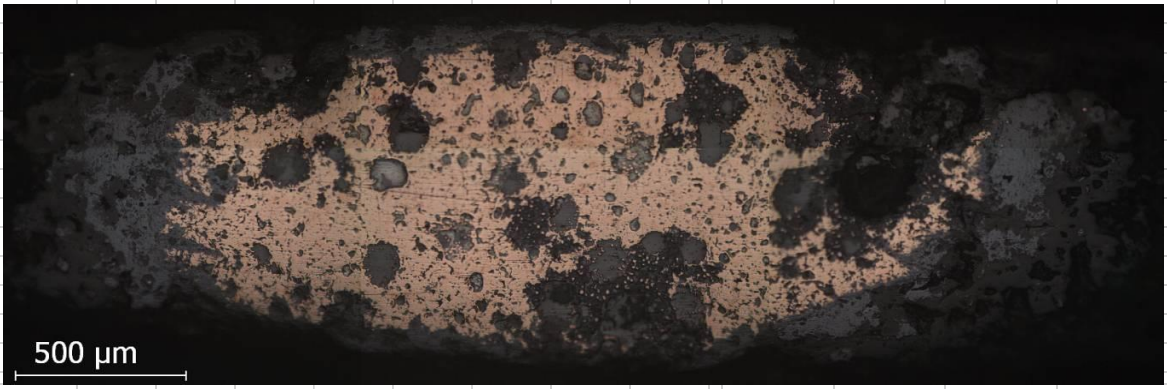

	Micro-EDXRF (wt.%)								Song Dynasty			
Ref.	Fe	Ni	Cu	Zn	As	Sn	Sb	Pb	Date	Designation		Alloy
2501	1.42	-	59.8	-	0.81	2.76	-	35.2	1195AD	Qing Yuan Tong Bao		Bronze

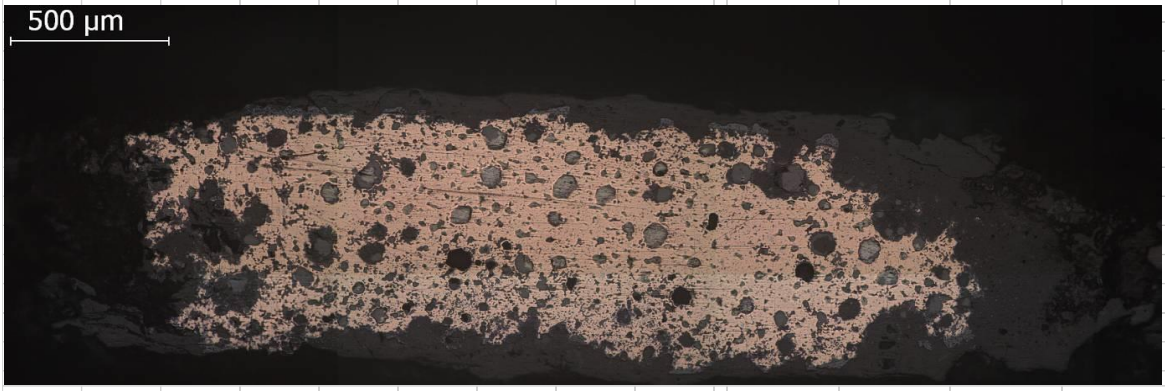

	Micro-EDXRF (wt.%)								Song Dynasty			
Ref.	Fe	Ni	Cu	Zn	As	Sn	Sb	Pb	Date	Designation		Alloy
2503	1.26	-	69.62	-	0.92	3.62	-	24.6	1195AD	Qing Yuan Tong Bao		Bronze

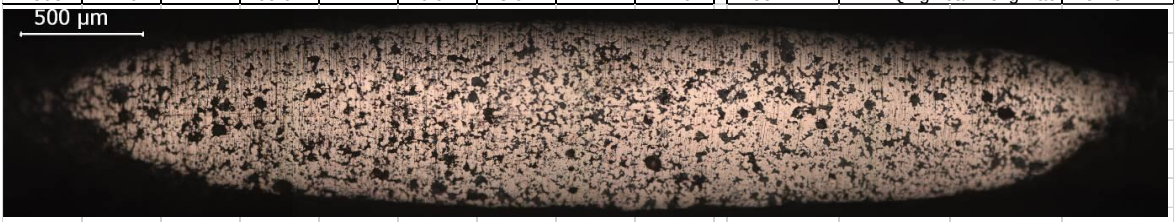

	Micro-EDXRF (wt.%)								Song Dynasty			
Ref.	Fe	Ni	Cu	Zn	As	Sn	Sb	Pb	Date	Designation		Alloy
2504	1.56	-	72.76	-	0.51	2.6	-	22.02	1195AD	Qing Yuan Tong Bao		Bronze

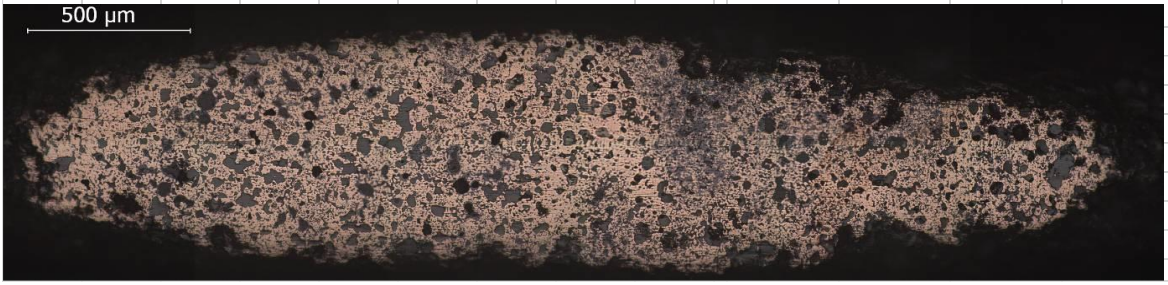

Table VII.3 Micro-EDXRF results and OM images of the cleaned sections (continued)

	Micro-EDXRF (wt.%)								Song Dynasty			
Ref.	**Fe**	**Ni**	**Cu**	**Zn**	**As**	**Sn**	**Sb**	**Pb**	**Date**	**Designation**		**Alloy**
2519	0.64	-	90,00	-	5.97	0.99	-	2.27	1208-24AD	Jia Ding Tong Bao		Bronze

	Micro-EDXRF (wt.%)								Song Dynasty			
Ref.	**Fe**	**Ni**	**Cu**	**Zn**	**As**	**Sn**	**Sb**	**Pb**	**Date**	**Designation**		**Alloy**
2522	0.96	-	63.06	-	0.26	3.7	-	32.2	1208-24AD	Jia Ding Tong Bao		Bronze

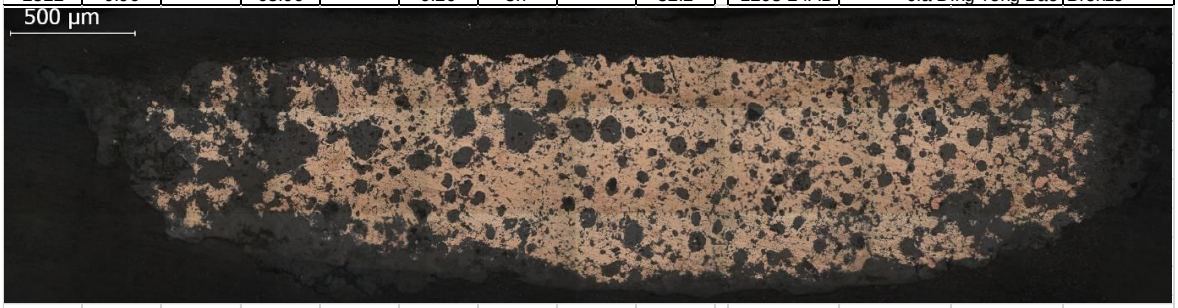

	Micro-EDXRF (wt.%)								Song Dynasty			
Ref.	**Fe**	**Ni**	**Cu**	**Zn**	**As**	**Sn**	**Sb**	**Pb**	**Date**	**Designation**		**Alloy**
2525	2.07	-	60.07	-	0.4	2.03	-	35.33	1208-24AD	Jia Ding Tong Bao		Bronze

	Micro-EDXRF (wt.%)								Song Dynasty			
Ref.	**Fe**	**Ni**	**Cu**	**Zn**	**As**	**Sn**	**Sb**	**Pb**	**Date**	**Designation**		**Alloy**
2528	0.91	-	67.14	-	0.43	2.98	-	28.4	1208-24AD	Jia Ding Tong Bao		Bronze

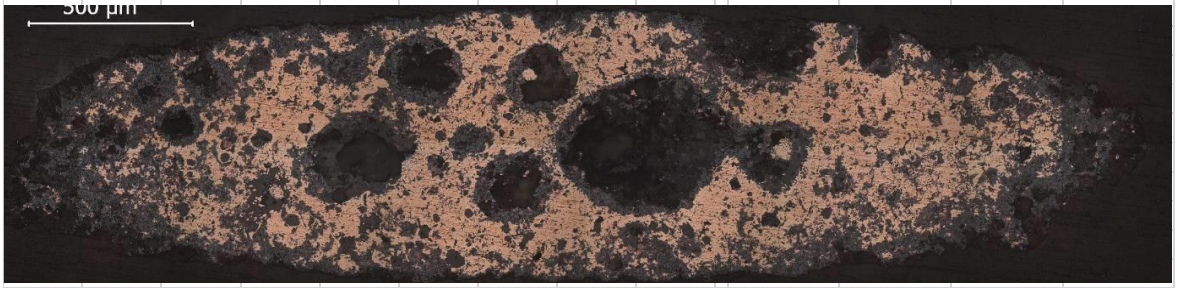

Table VII.3 Micro-EDXRF results and OM images of the cleaned sections (continued)

	Micro-EDXRF (wt.%)								Song Dynasty			
Ref.	Fe	Ni	Cu	Zn	As	Sn	Sb	Pb	Date	Designation		Alloy
2534	1.66	-	64.88	-	1.56	-	0.2	31.6	1208-24AD	Jia Ding Tong Bao		Bronze

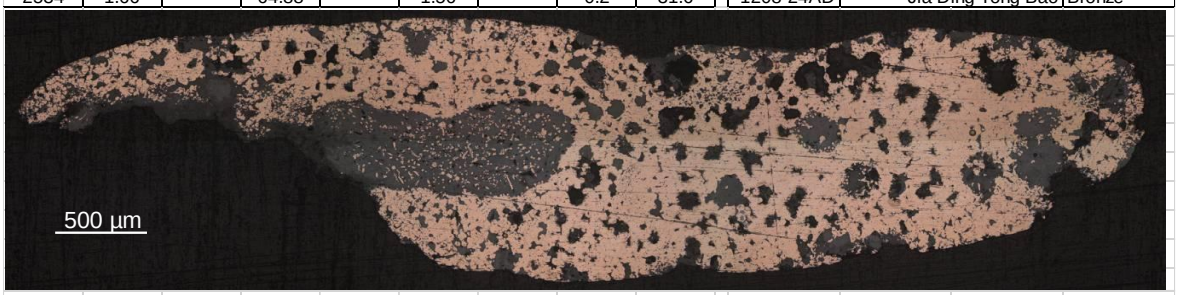

	Micro-EDXRF (wt.%)								Song Dynasty			
Ref.	Fe	Ni	Cu	Zn	As	Sn	Sb	Pb	Date	Designation		Alloy
2544	1.96	0.19	41.1	-	0.67	1.86	-	54.8	1208-24AD	Jia Ding Tong Bao		Bronze

	Micro-EDXRF (wt.%)								Song Dynasty			
Ref.	Fe	Ni	Cu	Zn	As	Sn	Sb	Pb	Date	Designation		Alloy
2558	4.96	-	61.7	-	0.2	2.7	-	30.2	1228-33AD	Shao Ding Tong Bao		Bronze

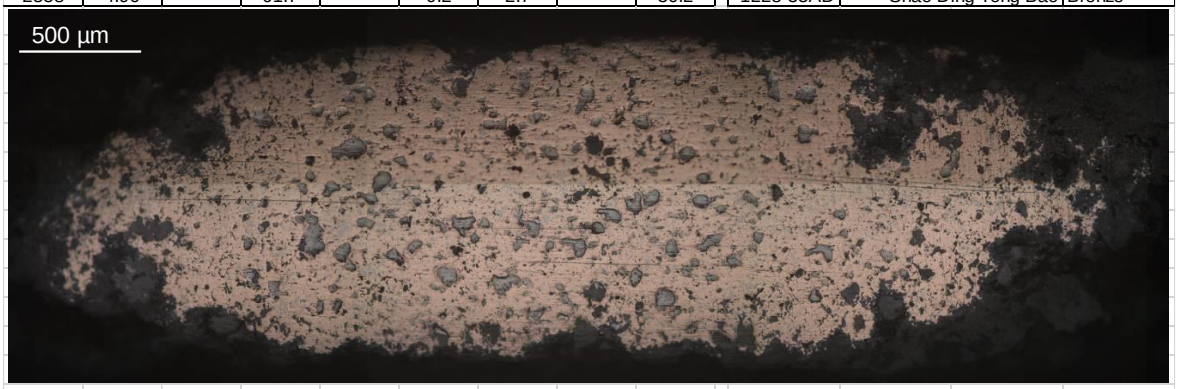

	Micro-EDXRF (wt.%)								Song Dynasty			
Ref.	Fe	Ni	Cu	Zn	As	Sn	Sb	Pb	Date	Designation		Alloy
2563	2.4	0.19	69.76	-	0.37	3.16	-	24,00	1228-33AD	Shao Ding Tong Bao		Bronze

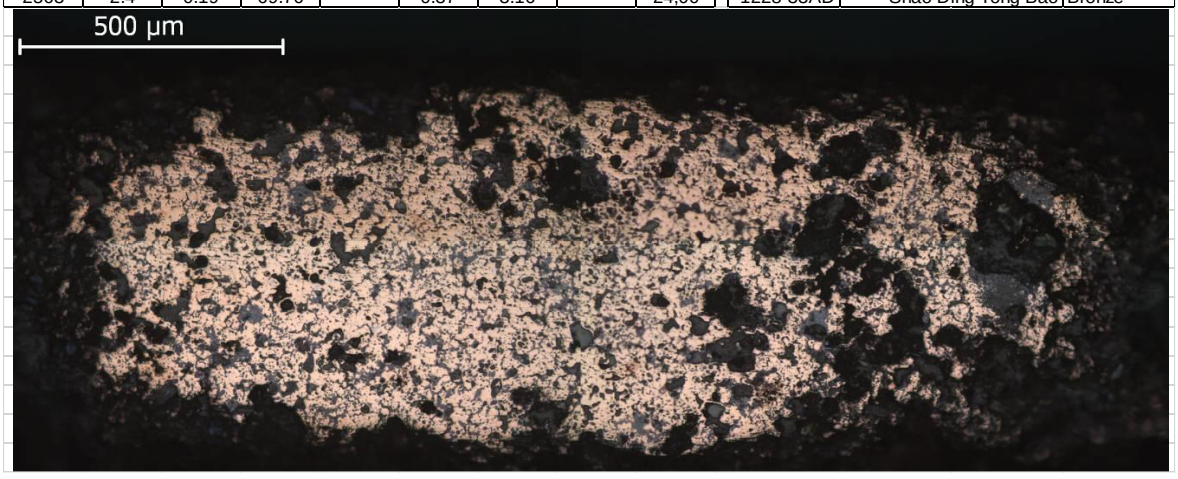

Table VII.3 Micro-EDXRF results and OM images leaned sections (continued)

	Micro-EDXRF (wt.%)								Song Dynasty			
Ref.	**Fe**	**Ni**	**Cu**	**Zn**	**As**	**Sn**	**Sb**	**Pb**	**Date**	**Designation**		**Alloy**
2564	1.07	-	72.4	-	0.36	5.1	-	21.2	1228-33AD	Shao Ding Tong Bao		Bronze

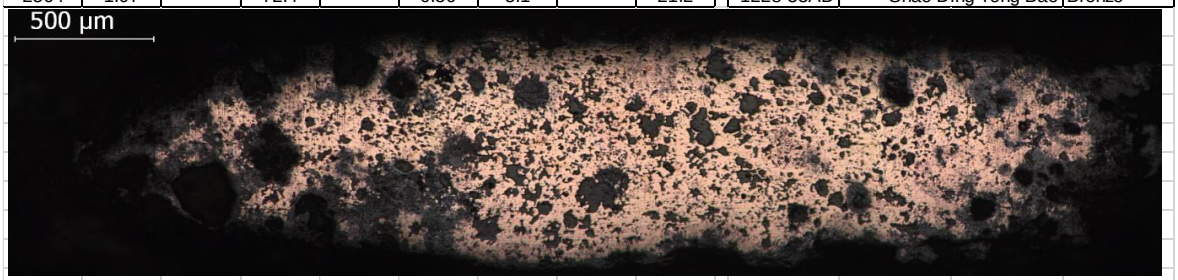

	Micro-EDXRF (wt.%)								Song Dynasty			
Ref.	**Fe**	**Ni**	**Cu**	**Zn**	**As**	**Sn**	**Sb**	**Pb**	**Date**	**Designation**		**Alloy**
2568	2.32	-	56.74	-	0.25	1.8	-	39,00	1228-33AD	Shao Ding Tong Bao		Bronze

	Micro-EDXRF (wt.%)								Song Dynasty			
Ref.	**Fe**	**Ni**	**Cu**	**Zn**	**As**	**Sn**	**Sb**	**Pb**	**Date**	**Designation**		**Alloy**
2571	2.44	-	65.6	-	0.39	1.75	-	30,00	1228-33AD	Shao Ding Tong Bao		

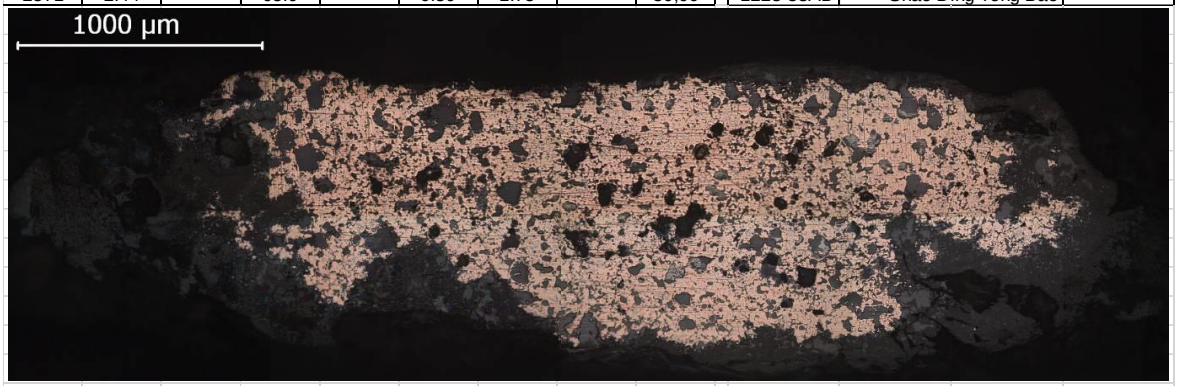

	Micro-EDXRF (wt.%)								Song Dynasty			
Ref.	**Fe**	**Ni**	**Cu**	**Zn**	**As**	**Sn**	**Sb**	**Pb**	**Date**	**Designation**		**Alloy**
2578	3.18	-	59.44	-	0.38	2.78	-	34.2	1241-52AD	Chun You Yuan Bao		Bronze

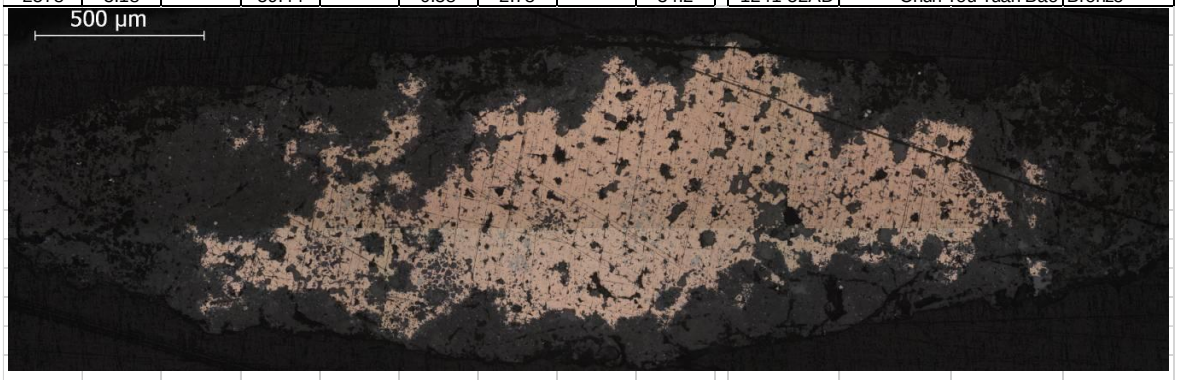

Table VII.3 Micro-EDXRF results and OM images of the cleaned sections (continued)

	Micro-EDXRF (wt.%)								Song Dynasty			
Ref.	Fe	Ni	Cu	Zn	As	Sn	Sb	Pb	Date	Designation		Alloy
2581	2.48	-	61.43	-	0.26	1.9	-	34.25	1241-52AD	Chun You Yuan Bao		Bronze

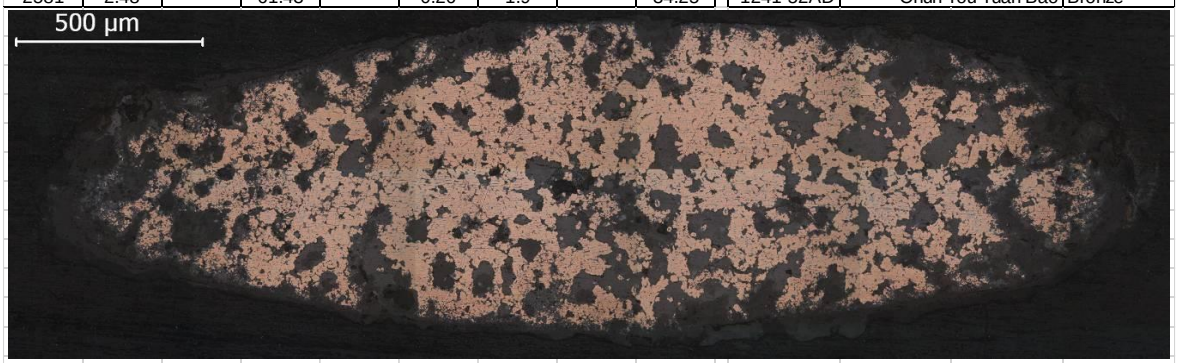

	Micro-EDXRF (wt.%)								Song Dynasty			
Ref.	Fe	Ni	Cu	Zn	As	Sn	Sb	Pb	Date	Designation		Alloy
2582	1.04	-	62.16	-	0.44	2.38	-	34,00	1241-52AD	Chun You Yuan Bao		Bronze

	Micro-EDXRF (wt.%)								Song Dynasty			
Ref.	Fe	Ni	Cu	Zn	As	Sn	Sb	Pb	Date	Designation		Alloy
2585	2.12	-	51.14	-	0.48	2.17	-	44,00	1241-52AD	Chun You Yuan Bao		Bronze

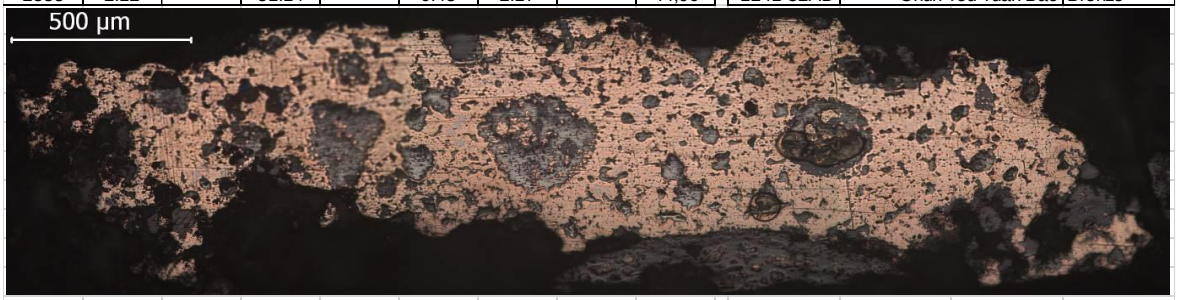

	Micro-EDXRF (wt.%)								Song Dynasty			
Ref.	Fe	Ni	Cu	Zn	As	Sn	Sb	Pb	Date	Designation		Alloy
2588	2.32	0.2	69.66	-	0.55	3.12	-	24,00	1241-52AD	Chun You Yuan Bao		Bronze

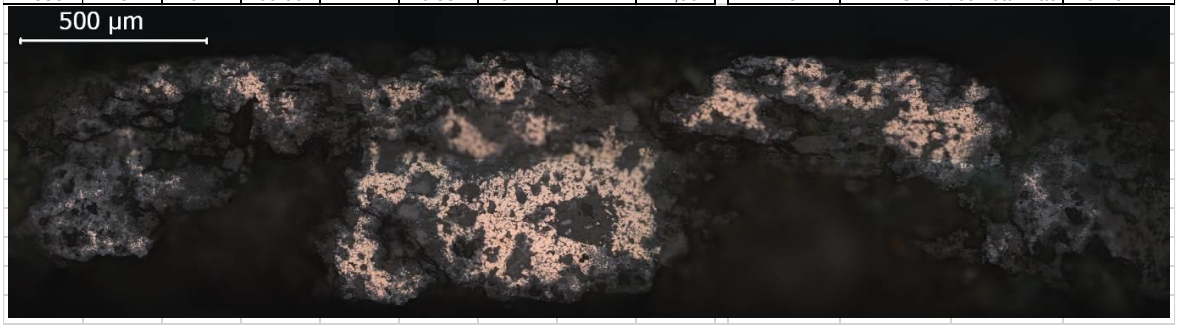

Table VII.3 Micro-EDXRF results and OM images of the cleaned sections (continued)

	Micro-EDXRF (wt.%)								Song Dynasty			
Ref.	Fe	Ni	Cu	Zn	As	Sn	Sb	Pb	Date	Designation		Alloy
2614	2.04	-	61.76	-	0.29	4.96	-	31,00	1265AD	Xian Chun Yuan Bao		Bronze

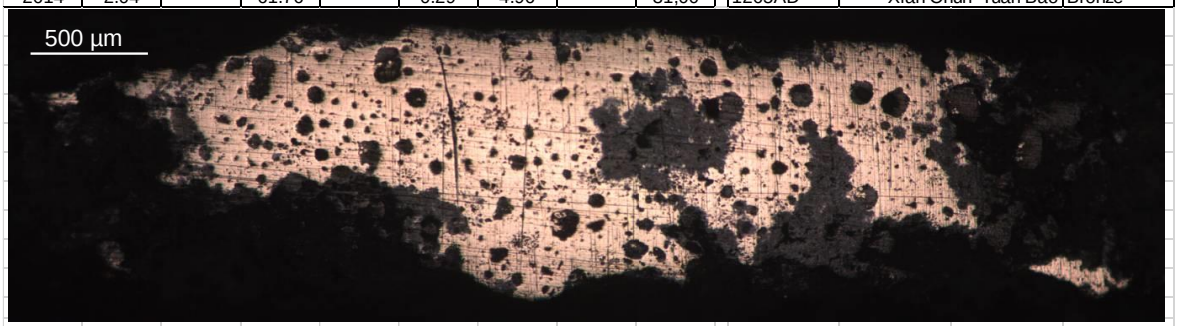

	Micro-EDXRF (wt.%)								Song Dynasty			
Ref.	Fe	Ni	Cu	Zn	As	Sn	Sb	Pb	Date	Designation		Alloy
2615	2.5	-	60.84	-	0.55	2.5	0.68	33,00	1265AD	Xian Chun Yuan Bao		Bronze

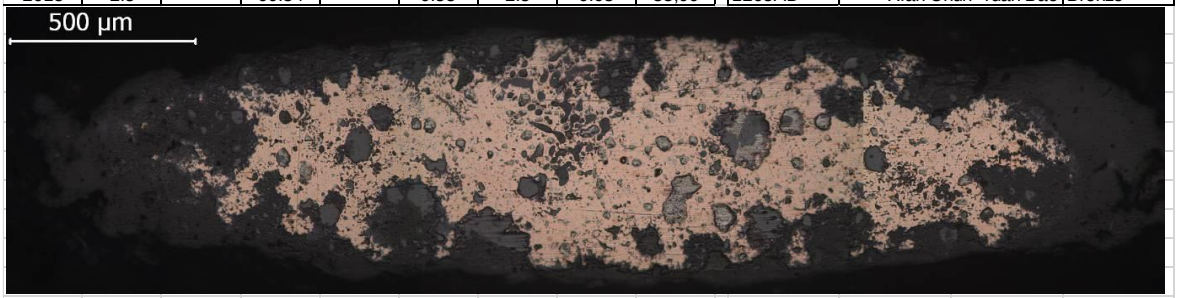

	Micro-EDXRF (wt.%)								Song Dynasty			
Ref.	Fe	Ni	Cu	Zn	As	Sn	Sb	Pb	Date	Designation		Alloy
2616	1.9	0.19	59.92	0.23	0.36	3.12	-	34.2	1260AD	Jing Ding Yuan Bao		Bronze

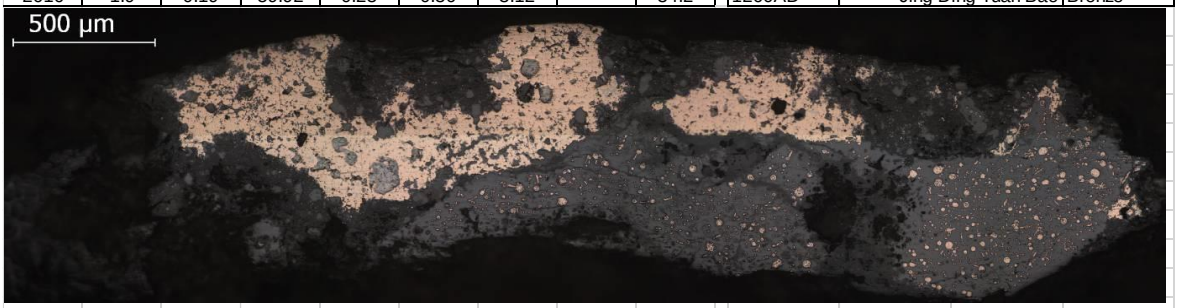

	Micro-EDXRF (wt.%)								Song Dynasty			
Ref.	Fe	Ni	Cu	Zn	As	Sn	Sb	Pb	Date	Designation		Alloy
2617	2.54	-	58.58	-	0.29	3.12	-	34.4	1265AD	Xian Chun Yuan Bao		Bronze

Table VII.3 Micro-EDXRF results and OM images of the cleaned sections (continued)

	Micro-EDXRF (wt.%)								Song Dynasty			
Ref.	**Fe**	**Ni**	**Cu**	**Zn**	**As**	**Sn**	**Sb**	**Pb**	**Date**	**Designation**		**Alloy**
2619	1.84	-	72.58	-	0.44	4.06	-	19.8	1265AD	Xian Chun Yuan Bao		Bronze

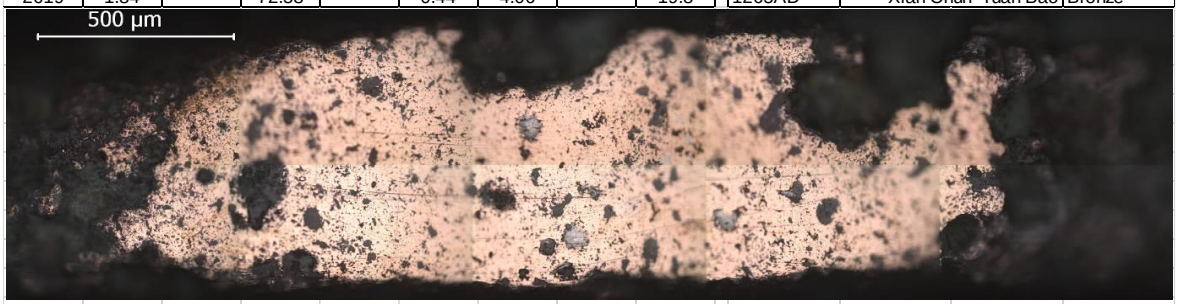

	Micro-EDXRF (wt.%)								Song Dynasty			
Ref.	**Fe**	**Ni**	**Cu**	**Zn**	**As**	**Sn**	**Sb**	**Pb**	**Date**	**Designation**		**Alloy**
2621	7.22	-	55.88	-	0.34	1.64	-	35,00	1265AD	Xian Chun Yuan Bao		Bronze

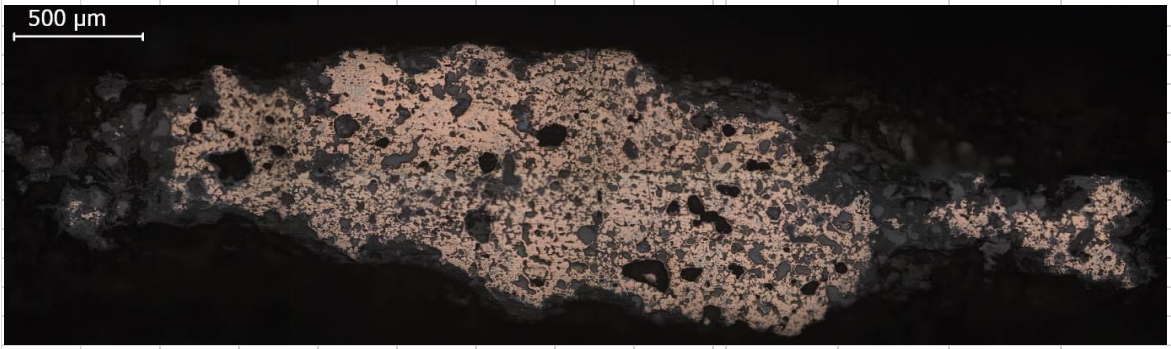

	Micro-EDXRF (wt.%)								Song Dynasty			
Ref.	**Fe**	**Ni**	**Cu**	**Zn**	**As**	**Sn**	**Sb**	**Pb**	**Date**	**Designation**		**Alloy**
2623	2.36	-	55.28	-	0.39	3.5	-	38.2	1265AD	Xian Chun Yuan Bao		Bronze

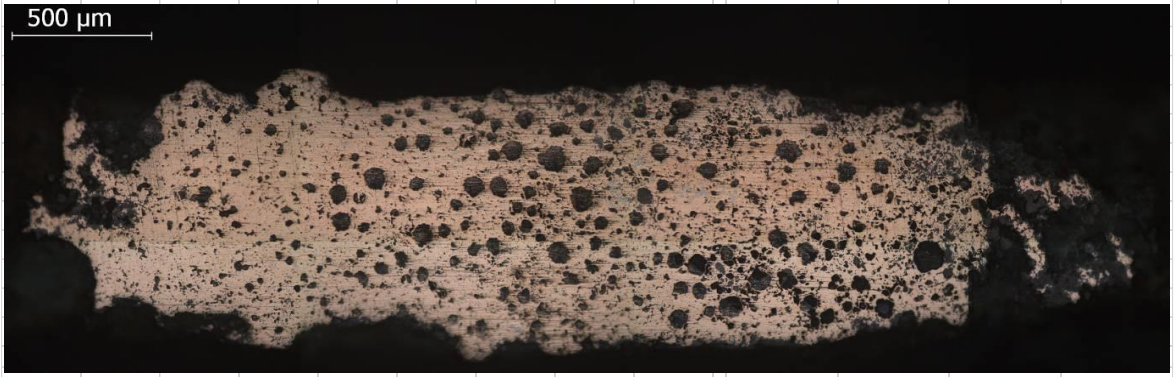

	Micro-EDXRF (wt.%)								Song Dynasty			
Ref.	**Fe**	**Ni**	**Cu**	**Zn**	**As**	**Sn**	**Sb**	**Pb**	**Date**	**Designation**		**Alloy**
2624	2.56	-	53.84	-	0.36	4.2	-	39.2	1265AD	Xian Chun Yuan Bao		Bronze

Table VII.3 Micro-EDXRF results and OM images of the cleaned sections (continued)

	Micro-EDXRF (wt.%)								Song Dynasty		
Ref.	Fe	Ni	Cu	Zn	As	Sn	Sb	Pb	Date	Designation	Alloy
2625	1.04	0.16	52.28	-	0.31	1.36	-	45,00	1265AD	Xian Chun Yuan Bao	Bronze

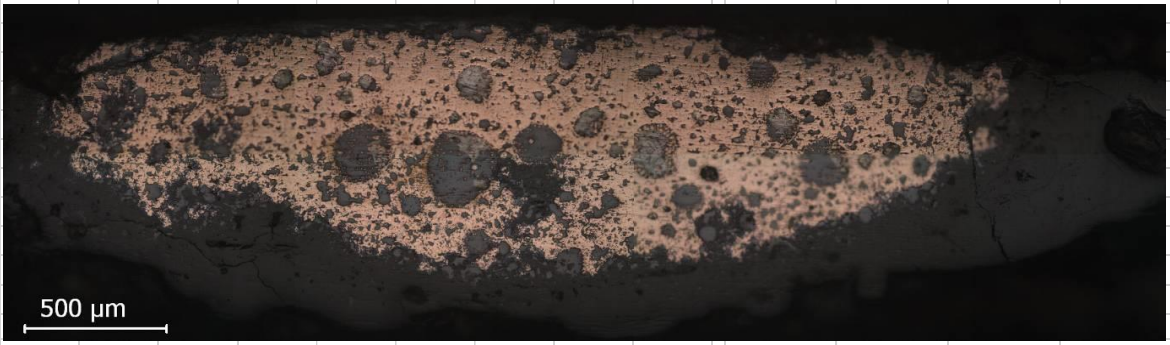

	Micro-EDXRF (wt.%)								Song Dynasty		
Ref.	Fe	Ni	Cu	Zn	As	Sn	Sb	Pb	Date	Designation	Alloy
2626	2.56	-	62.74	-	0.5	3.64	-	30.4	1265AD	Xian Chun Yuan Bao	Bronze

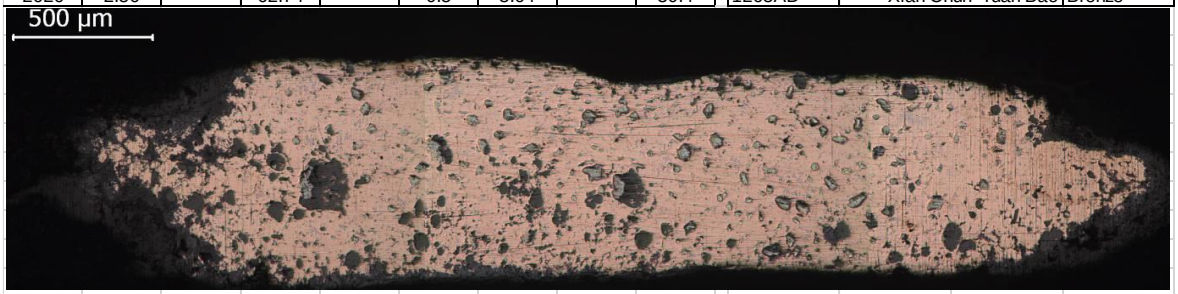

	Micro-EDXRF (wt.%)								Song Dynasty		
Ref.	Fe	Ni	Cu	Zn	As	Sn	Sb	Pb	Date	Designation	Alloy
2631	1.32	-	63.7	-	0.44	4.5	-	30.2	1265AD	Xian Chun Yuan Bao	Bronze

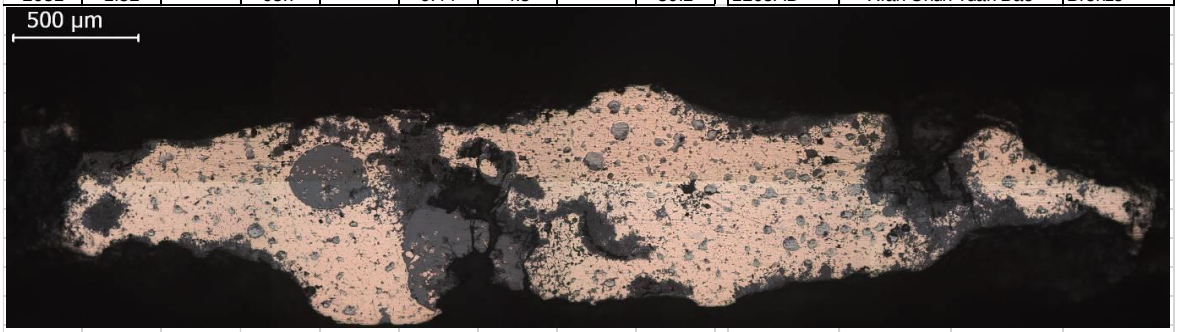

	Micro-EDXRF (wt.%)								Qing Dynasty		
Ref.	Fe	Ni	Cu	Zn	As	Sn	Sb	Pb	Date	Designation	Alloy
2704	0.34	0.16	68.3	10.3	0.34	5.03	0.31	15.33	1644-61 AD	Shun Zhi Tong Bao	Bronze

	Micro-EDXRF (wt.%)								Qing Dynasty		
Ref.	Fe	Ni	Cu	Zn	As	Sn	Sb	Pb	Date	Designation	Alloy
2977	0.69	0.18	73.3	0.27	1.9	10.1	0.32	13.33	1862 AD	Guang Xu Zhong Bao	Bronze

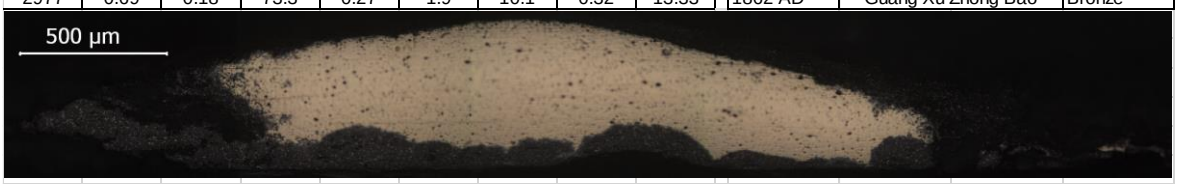

Table VII.3 Micro-EDXRF results and OM images of the cleaned sections (continued)

	Micro-EDXRF (wt.%)							
Ref.	Fe	Ni	Cu	Zn	As	Sn	Sb	Pb
2632	0.66	-	54.26	41.44	-	1.28	-	2.35
Observed Phase(s)	β+α							

Ming Dynasty		
Date	Designation	Alloy
1621 AD	Tian Qi Tong Bao	Brass

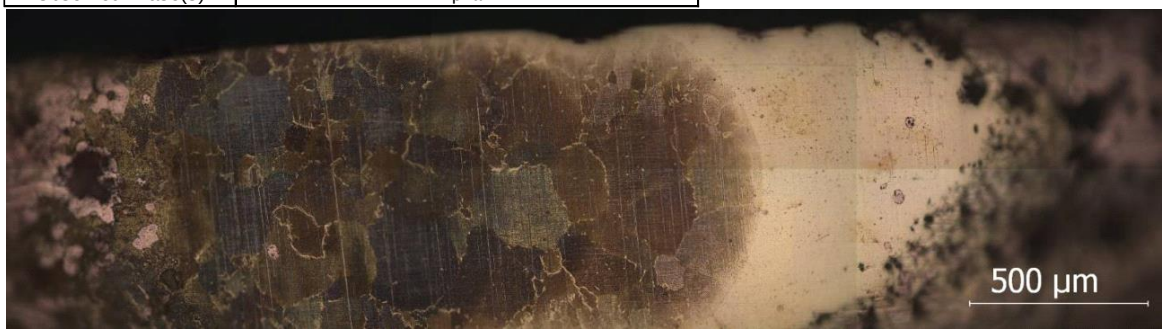

	Micro-EDXRF (wt.%)							
Ref.	Fe	Ni	Cu	Zn	As	Sn	Sb	Pb
2635	0.34	-	60.23	37.37	0.32	0.46	-	0.97
Observed Phase(s)	α+β							

Ming Dynasty		
Date	Designation	Alloy
1621 AD	Tian Qi Tong Bao	Brass

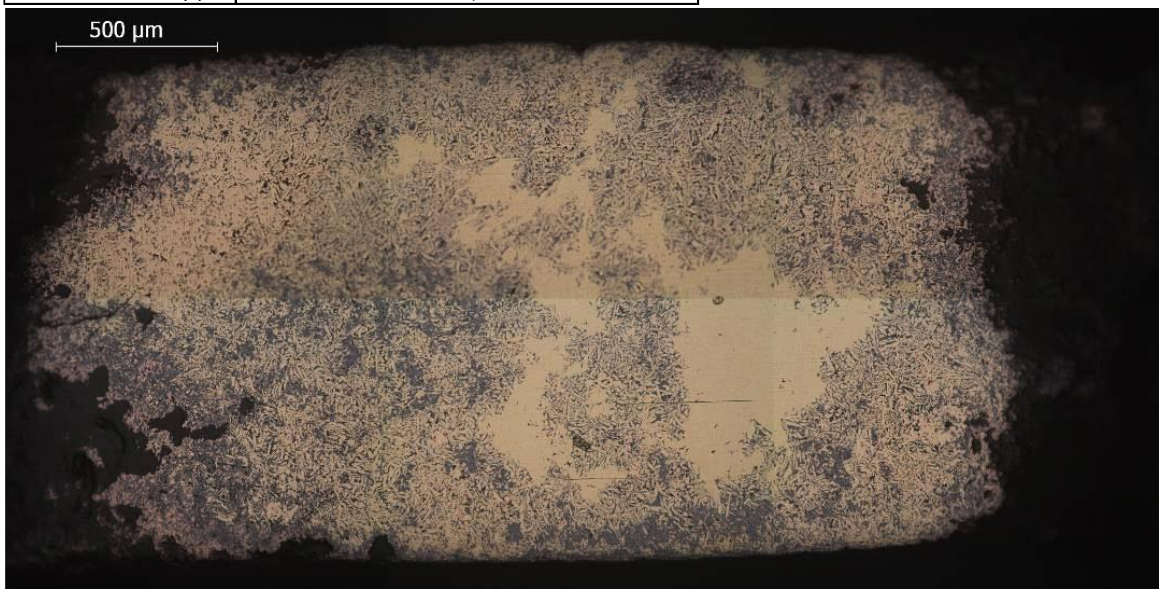

	Micro-EDXRF (wt.%)							
Ref.	Fe	Ni	Cu	Zn	As	Sn	Sb	Pb
2636	0.32	-	65.87	32.3	-	-	-	1.3
Observed Phase(s)	α							

Ming Dynasty		
Date	Designation	Alloy
1621 AD	Tian Qi Tong Bao	Brass

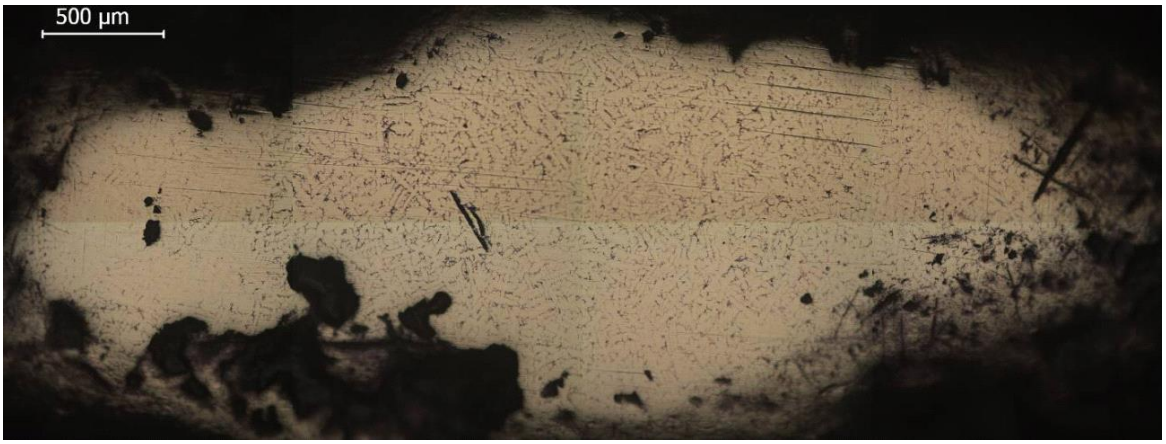

Table VII.3 Micro-EDXRF results and OM images of the cleaned sections (continued)

	Micro-EDXRF (wt.%)							
Ref.	Fe	Ni	Cu	Zn	As	Sn	Sb	Pb
2639	0.36	0.32	80.37	12.53	0.95	0.24	0.39	5.00
Observed Phase(s)	α+γ+(Pb)							

Ming Dynasty		
Date	Designation	Alloy
1621 AD	Tian Qi Tong Bao	Brass

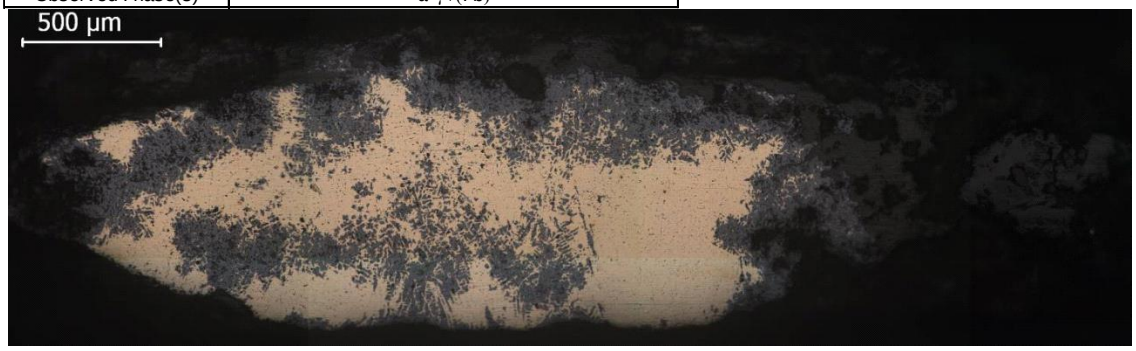

	Micro-EDXRF (wt.%)							
Ref.	Fe	Ni	Cu	Zn	As	Sn	Sb	Pb
2642	0.43	-	61.93	24.63	-	3.47	-	9.67
Observed Phase(s)	α+γ+(Pb)							

Ming Dynasty		
Date	Designation	Alloy
1621 AD	Tian Qi Tong Bao	Brass

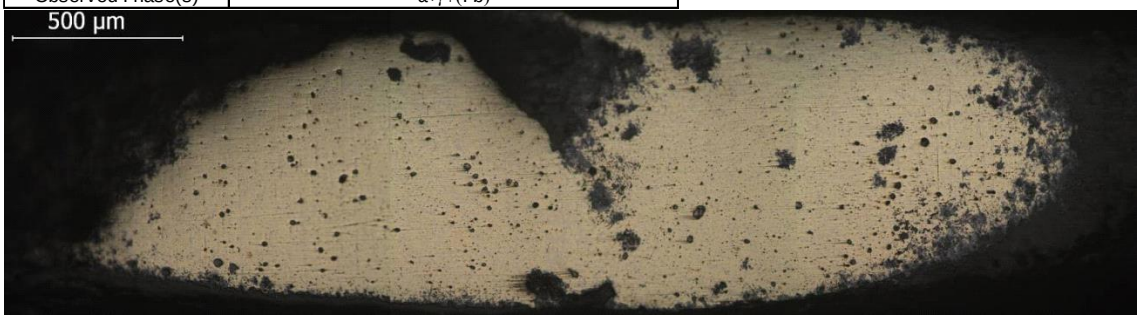

	Micro-EDXRF (wt.%)							
Ref.	Fe	Ni	Cu	Zn	As	Sn	Sb	Pb
2645	0.31	0.11	63.93	28.23	0.17	1.17	-	6.00
Observed Phase(s)	α+γ+(Pb)							

Ming Dynasty		
Date	Designation	Alloy
1621 AD	Tian Qi Tong Bao	Brass

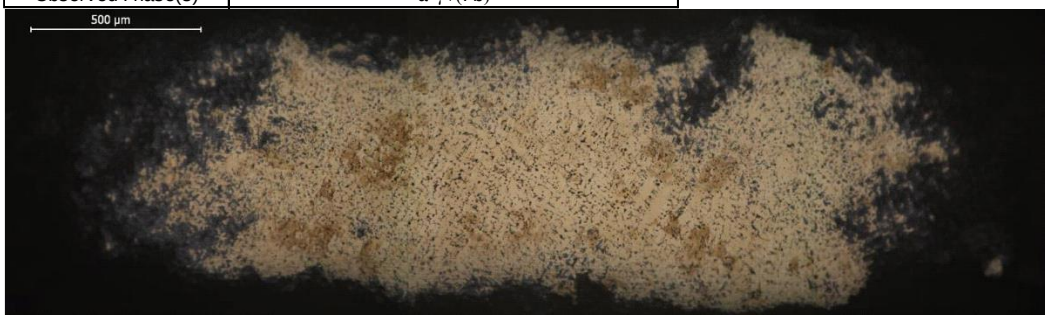

	Micro-EDXRF (wt.%)							
Ref.	Fe	Ni	Cu	Zn	As	Sn	Sb	Pb
2650	0.1	-	61.87	37.03	-	-	-	0.83
Observed Phase(s)	α+β							

Ming Dynasty		
Date	Designation	Alloy
1576 AD	Wan Li Tong Bao	Brass

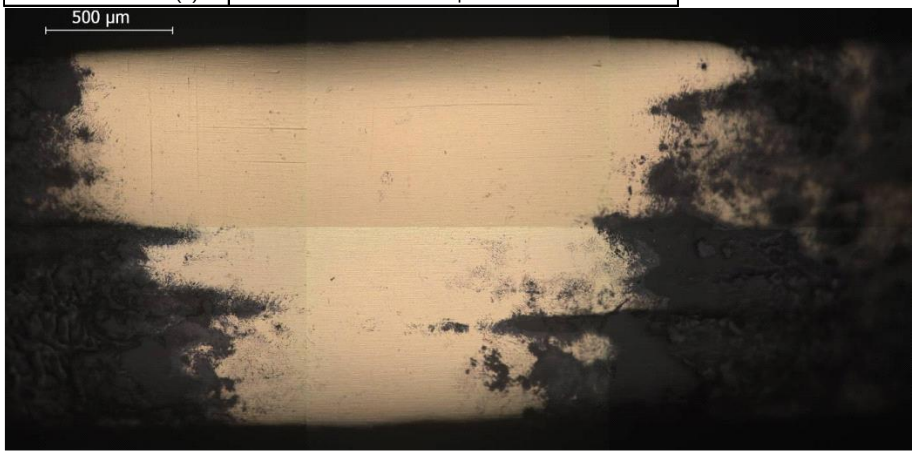

Table VII.3 Micro-EDXRF results and OM images of the cleaned sections (continued)

	Micro-EDXRF (wt.%)							
Ref.	Fe	Ni	Cu	Zn	As	Sn	Sb	Pb
2653	0.4	-	70.1	11.03	-	4.9	-	13.67
Observed Phase(s)	α+γ+(Pb)							

Ming Dynasty		
Date	Designation	Alloy
1576 AD	Wan Li Tong Bao	Brass

	Micro-EDXRF (wt.%)							
Ref.	Fe	Ni	Cu	Zn	As	Sn	Sb	Pb
2659	0.48	0.13	72.73	24.7	0.5	-	-	1.3
Observed Phase(s)	α							

Ming Dynasty		
Date	Designation	Alloy
1620 AD	Tai Chang Tong Bao	Brass

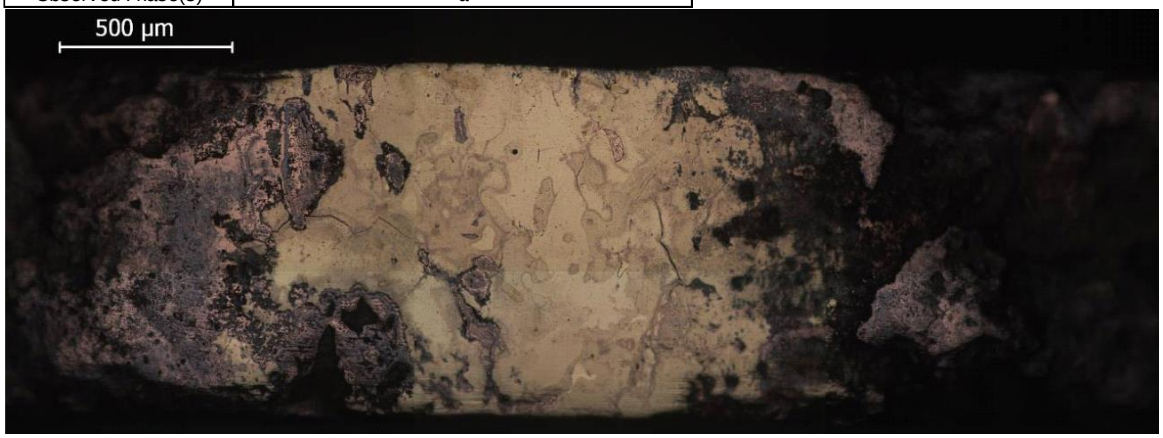

	Micro-EDXRF (wt.%)							
Ref.	Fe	Ni	Cu	Zn	As	Sn	Sb	Pb
2661	1.65	0.23	71.47	25.63	-	-	-	1.00
Observed Phase(s)	α+(α-Fe)							

Ming Dynasty		
Date	Designation	Alloy
1628 AD	Chong Zhen Tong Bao	Brass

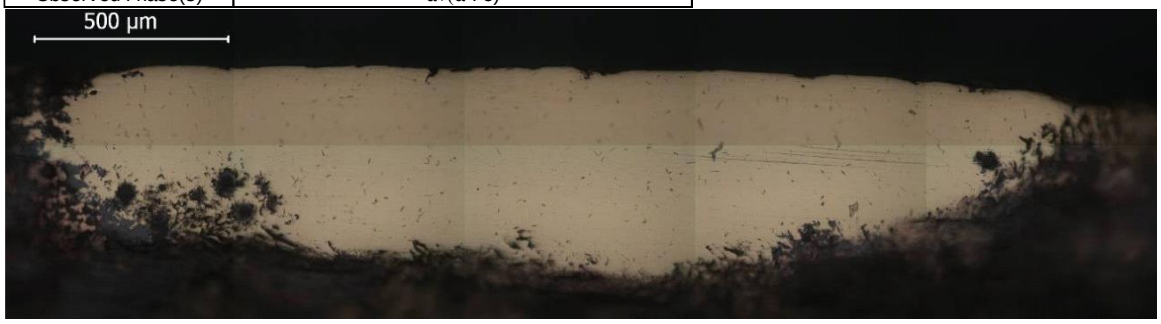

	Micro-EDXRF (wt.%)							
Ref.	Fe	Ni	Cu	Zn	As	Sn	Sb	Pb
2662	0.36	0.12	63.47	32.2	0.4	0.67	0.44	2.13
Observed Phase(s)	α							

Ming Dynasty		
Date	Designation	Alloy
1628 AD	Chong Zhen Tong Bao	Brass

Table VII.3 Micro-EDXRF results and OM images of the cleaned sections (continued)

	Micro-EDXRF (wt.%)							
Ref.	Fe	Ni	Cu	Zn	As	Sn	Sb	Pb
2663	0.13	-	62.13	36.00	0.43	-	-	0.37
Observed Phase(s)	α+β							

Ming Dynasty		
Date	Designation	Alloy
1628 AD	Chong Zhen Tong Bao	Brass

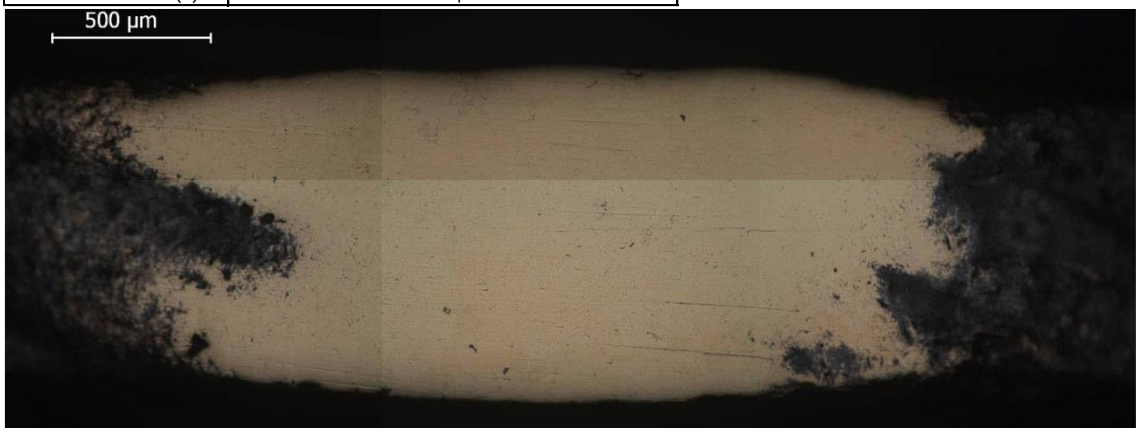

	Micro-EDXRF (wt.%)							
Ref.	Fe	Ni	Cu	Zn	As	Sn	Sb	Pb
2664	0.61	0.09	53.3	38.23	-	0.83	0.38	6.67
Observed Phase(s)	α+β							

Ming Dynasty		
Date	Designation	Alloy
1628 AD	Chong Zhen Tong Bao	Brass

	Micro-EDXRF (wt.%)							
Ref.	Fe	Ni	Cu	Zn	As	Sn	Sb	Pb
2666	0.49	0.11	52.27	37.97	0.45	-	3.13	5.33
Observed Phase(s)	β+γ							

Ming Dynasty		
Date	Designation	Alloy
1628 AD	Chong Zhen Tong Bao	Brass

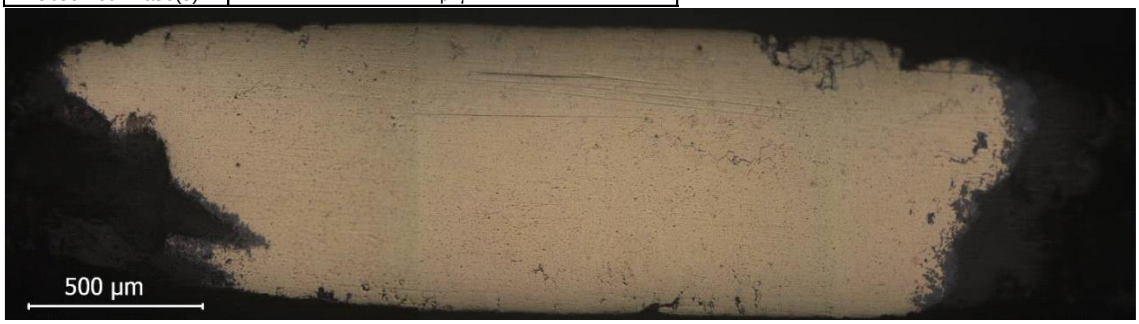

	Micro-EDXRF (wt.%)							
Ref.	Fe	Ni	Cu	Zn	As	Sn	Sb	Pb
2667	0.52	0.12	67.57	26.03	0.41	1.00	-	4.17
Observed Phase(s)	α+γ							

Ming Dynasty		
Date	Designation	Alloy
1628 AD	Chong Zhen Tong Bao	Brass

Table VII.3 Micro-EDXRF results and OM images of the cleaned sections (continued)

	Micro-EDXRF (wt.%)							
Ref.	Fe	Ni	Cu	Zn	As	Sn	Sb	Pb
2670	0.39	0.21	57.3	25.77	0.3	1.7	-	14.33
Observed Phase(s)	α+γ+(Pb)							

Ming Dynasty		
Date	Designation	Alloy
1628 AD	Chong Zhen Tong Bao	Brass

	Micro-EDXRF (wt.%)							
Ref.	Fe	Ni	Cu	Zn	As	Sn	Sb	Pb
2671	0.59	0.16	57.1	26.67	0.43	3.77	1.57	9.67
Observed Phase(s)	α+γ+(Pb)							

Ming Dynasty		
Date	Designation	Alloy
1628 AD	Chong Zhen Tong Bao	Brass

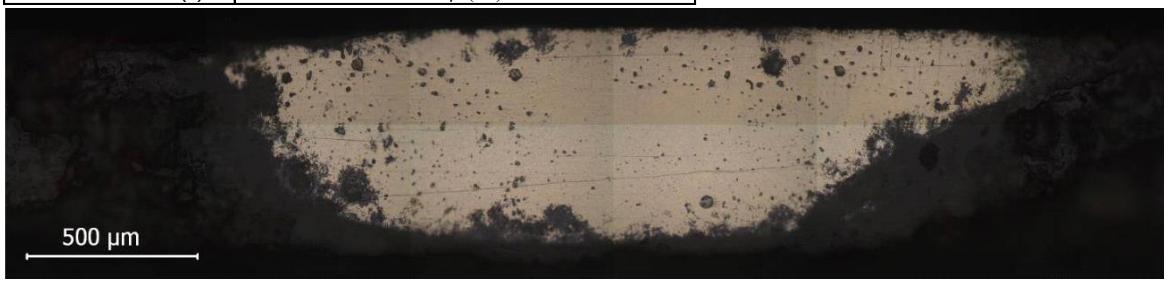

	Micro-EDXRF (wt.%)							
Ref.	Fe	Ni	Cu	Zn	As	Sn	Sb	Pb
3271	1.12	0.17	55.97	29.87	0.98	-	3.67	8.00
Observed Phase(s)	α+γ+(Pb)							

Ming Dynasty		
Date	Designation	Alloy
1628 AD	Chong Zhen Tong Bao	Brass

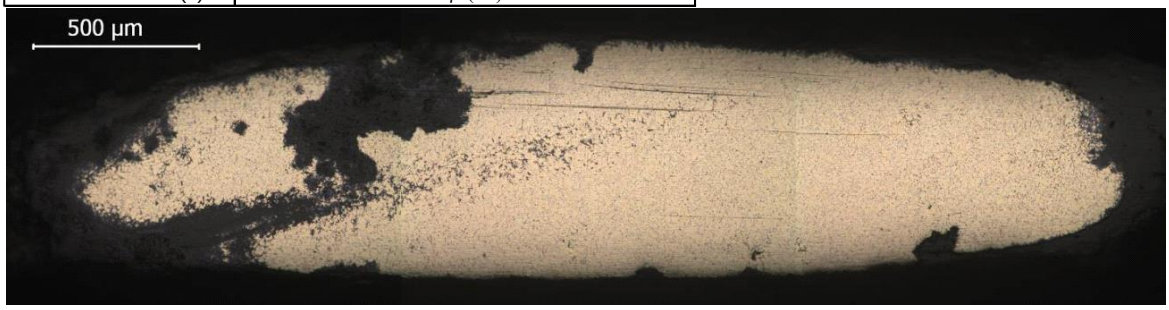

	Micro-EDXRF (wt.%)							
Ref.	Fe	Ni	Cu	Zn	As	Sn	Sb	Pb
3272	0.86	-	54.67	33.5	-	-	2.3	8.67
Observed Phase(s)	α+γ+(Pb)							

Ming Dynasty		
Date	Designation	Alloy
1628 AD	Chong Zhen Tong Bao	Brass

Table VII.3 Micro-EDXRF results and OM images of the cleaned sections (continued)

	Micro-EDXRF (wt.%)							
Ref.	Fe	Ni	Cu	Zn	As	Sn	Sb	Pb
3273	0.79	-	52.17	34.63	0.32	-	1.93	10.00
Observed Phase(s)	α+β+γ+(Pb)							

Ming Dynasty		
Date	Designation	Alloy
1628 AD	Chong Zhen Tong Bao	Brass

	Micro-EDXRF (wt.%)							
Ref.	Fe	Ni	Cu	Zn	As	Sn	Sb	Pb
3274	0.91	0.13	50.33	39.53	0.49	-	2.73	6.00
Observed Phase(s)	β+γ							

Ming Dynasty		
Date	Designation	Alloy
1628 AD	Chong Zhen Tong Bao	Brass

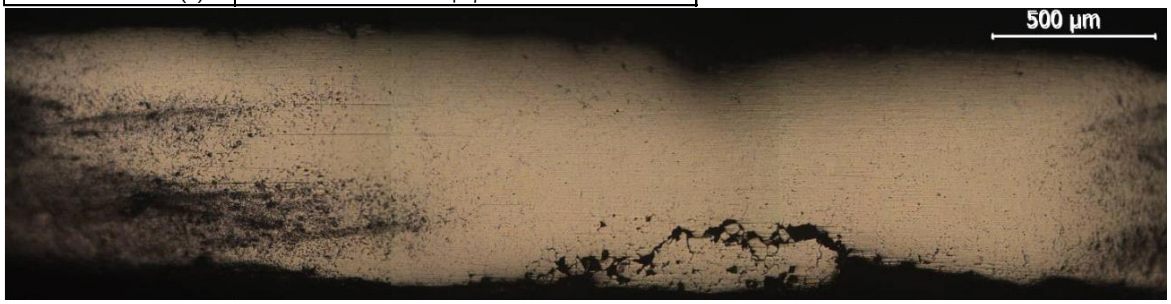

	Micro-EDXRF (wt.%)							
Ref.	Fe	Ni	Cu	Zn	As	Sn	Sb	Pb
3275	0.7	0.1	54.67	40.3	0.08	-	-	4.2
Observed Phase(s)	α+β							

Ming Dynasty		
Date	Designation	Alloy
1628 AD	Chong Zhen Tong Bao	Brass

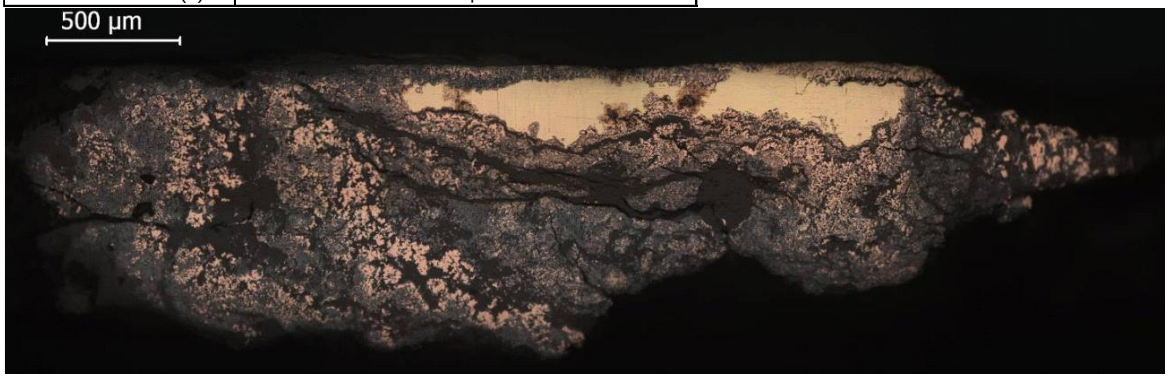

	Micro-EDXRF (wt.%)							
Ref.	Fe	Ni	Cu	Zn	As	Sn	Sb	Pb
3276	0.32	0.12	54.3	38.77	0.26	-	0.56	5.67
Observed Phase(s)	α+β							

Ming Dynasty		
Date	Designation	Alloy
1628 AD	Chong Zhen Tong Bao	Brass

Table VII.3 Micro-EDXRF results and OM images of the cleaned sections (continued)

	Micro-EDXRF (wt.%)							
Ref.	Fe	Ni	Cu	Zn	As	Sn	Sb	Pb
3277	0.42	0.05	56.23	37.13	-	-	1.6	4.67
Observed Phase(s)	α+β							

Ming Dynasty		
Date	Designation	Alloy
1628 AD	Chong Zhen Tong Bao	Brass

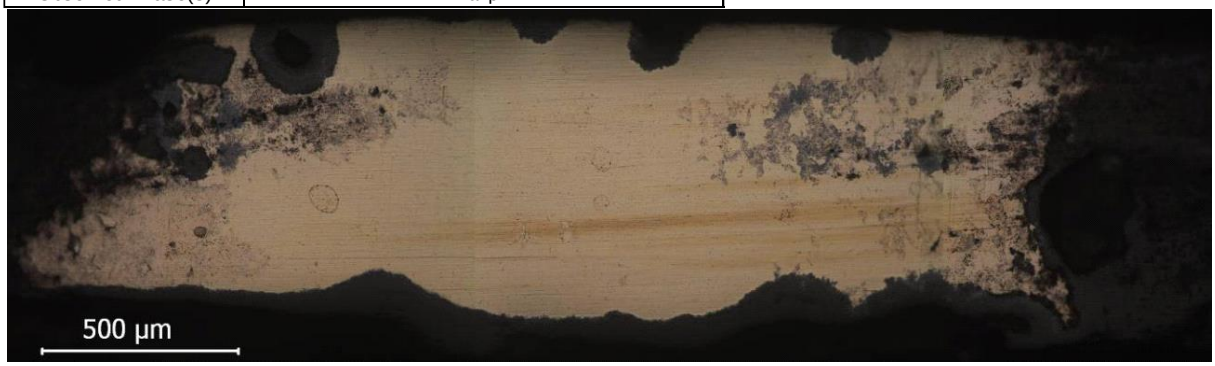

	Micro-EDXRF (wt.%)							
Ref.	Fe	Ni	Cu	Zn	As	Sn	Sb	Pb
3278	0.58	0.1	54.27	39.1	0.74	-	1.1	4.1
Observed Phase(s)	α+β+γ							

Ming Dynasty		
Date	Designation	Alloy
1628 AD	Chong Zhen Tong Bao	Brass

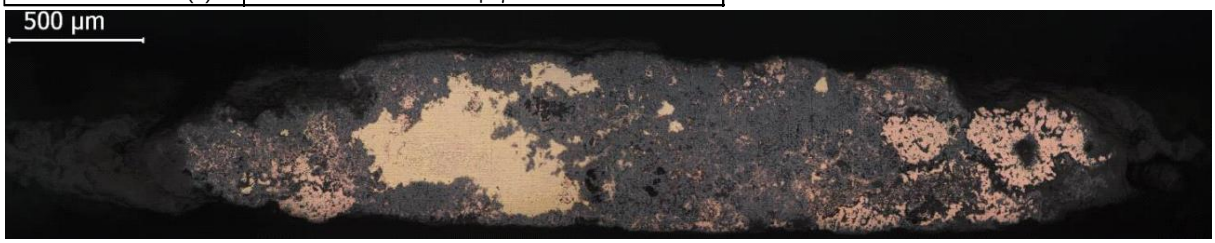

	Micro-EDXRF (wt.%)							
Ref.	Fe	Ni	Cu	Zn	As	Sn	Sb	Pb
X	0.52	0.09	51.33	46.1	0.1	-	0.2	1.63
Observed Phase(s)	β							

Ming Dynasty		
Date	Designation	Alloy
1628 AD	Chong Zhen Tong Bao	Brass

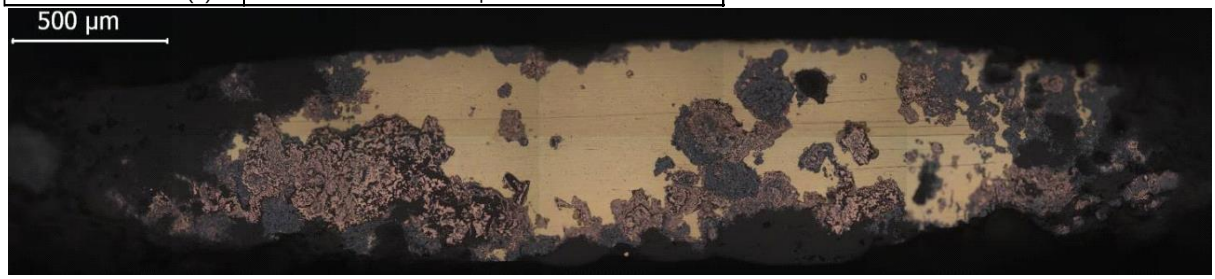

	Micro-EDXRF (wt.%)							
Ref.	Fe	Ni	Cu	Zn	As	Sn	Sb	Pb
M117	0.94	0.09	60.03	30.1	0.83	0.92	0.46	6.6
Observed Phase(s)	α+β+γ							

Unknown dynasty		
Date	Designation	Alloy
unkown	unknown	Brass

	Micro-EDXRF (wt.%)							
Ref.	Fe	Ni	Cu	Zn	As	Sn	Sb	Pb
2710	0.55	0.13	56.57	29.17	0.16	2.53	0.78	10.23
Observed Phase(s)	α+γ+(Pb)							

Qing Dynasty		
Date	Designation	Alloy
1662 AD	Kang Xi Tong Bao	Brass

Table VII.3 Micro-EDXRF results and OM images of the cleaned sections (continued)

	Micro-EDXRF (wt.%)							
Ref.	Fe	Ni	Cu	Zn	As	Sn	Sb	Pb
2723	1.0	-	46.9	51.6	-	-	-	0.4
Observed Phase(s)	β+γ							

Qing Dynasty		
Date	Designation	Alloy
1662 AD	Kang Xi Tong Bao	Brass

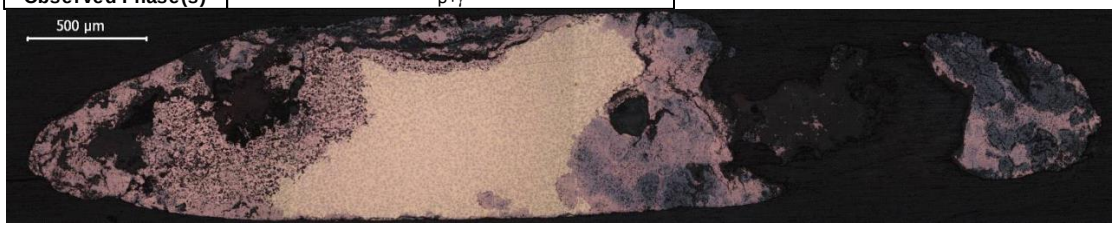

	Micro-EDXRF (wt.%)							
Ref.	Fe	Ni	Cu	Zn	As	Sn	Sb	Pb
2728	0.57	0.13	65.13	23.97	0.24	1.83	0.93	7.17
Observed Phase(s)	α+γ+(Pb)							

Qing Dynasty		
Date	Designation	Alloy
1662 AD	Kang Xi Tong Bao	Brass

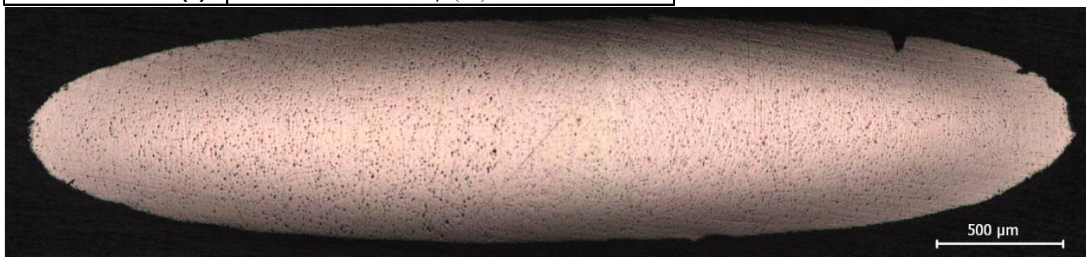

	Micro-EDXRF (wt.%)							
Ref.	Fe	Ni	Cu	Zn	As	Sn	Sb	Pb
2733	0.55	0.14	65.33	23.43	0.21	1.66	1.36	7.03
Observed Phase(s)	α+γ+(Pb)							

Qing Dynasty		
Date	Designation	Alloy
1662 AD	Kang Xi Tong Bao	Brass

	Micro-EDXRF (wt.%)							
Ref.	Fe	Ni	Cu	Zn	As	Sn	Sb	Pb
2736	0.8	-	61.5	32.7	0.6	0.7	0.3	3.3
Observed Phase(s)	α+γ+(α-Fe)+(Pb)							

Qing Dynasty		
Date	Designation	Alloy
1662 AD	Kang Xi Tong Bao	Brass

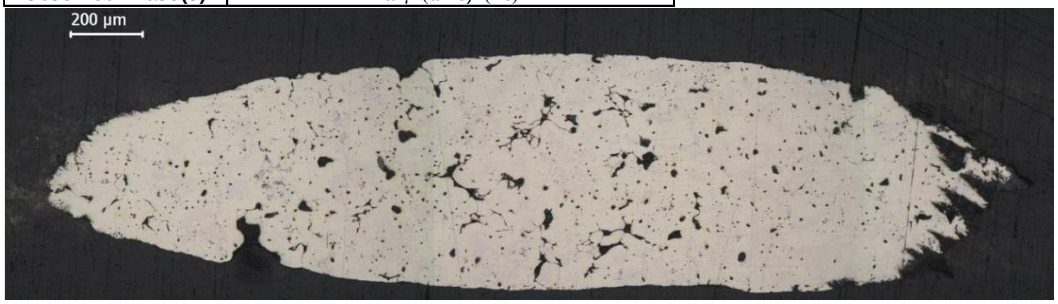

	Micro-EDXRF (wt.%)							
Ref.	Fe	Ni	Cu	Zn	As	Sn	Sb	Pb
2737	0.44	-	78.57	3.51	1.03	2.13	-	14.33
Observed Phase(s)	α+γ+(Pb)							

Qing Dynasty		
Date	Designation	Alloy
1662 AD	Kang Xi Tong Bao	Brass

Table VII.3 Micro-EDXRF results and OM images of the cleaned sections (continued)

	Micro-EDXRF (wt.%)							
Ref.	Fe	Ni	Cu	Zn	As	Sn	Sb	Pb
2758	0.34	-	53.13	35.00	-	2.9	0.3	8.33
Observed Phase(s)	α+β+γ+(Pb)							

Qing Dynasty		
Date	Designation	Alloy
1736 AD	Qian Long Tong Bao	Brass

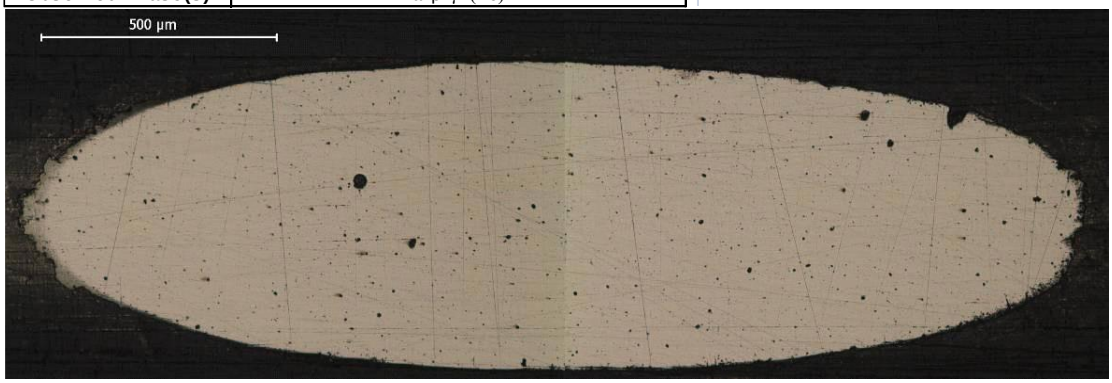

	Micro-EDXRF (wt.%)							
Ref.	Fe	Ni	Cu	Zn	As	Sn	Sb	Pb
2761	0.56	0.08	64.27	25.75	-	1.22	0.18	8.03
Observed Phase(s)	α+β+(Pb)							

Qing Dynasty		
Date	Designation	Alloy
1736 AD	Qian Long Tong Bao	Brass

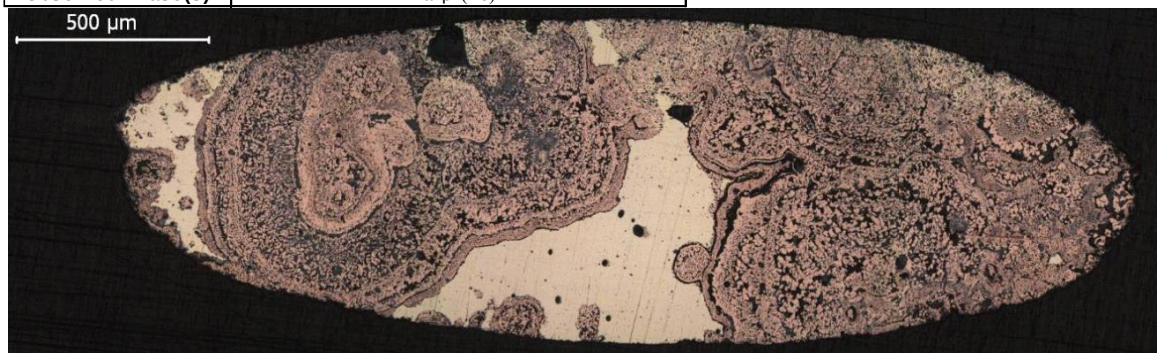

	Micro-EDXRF (wt.%)							
Ref.	Fe	Ni	Cu	Zn	As	Sn	Sb	Pb
2762	0.64	0.07	54.6	39.05	-	0.22	0.14	5.5
Observed Phase(s)	α+β+(Pb)							

Qing Dynasty		
Date	Designation	Alloy
1736 AD	Qian Long Tong Bao	Brass

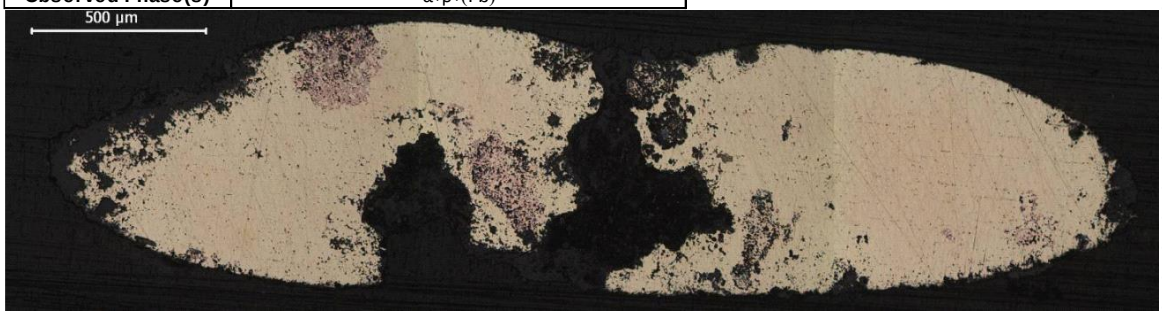

	Micro-EDXRF (wt.%)							
Ref.	Fe	Ni	Cu	Zn	As	Sn	Sb	Pb
2763	0.48	-	68.23	29.97	0.48	-	-	0.83
Observed Phase(s)	α							

Qing Dynasty		
Date	Designation	Alloy
1736 AD	Qian Long Tong Bao	Brass

Table VII.3 Micro-EDXRF results and OM images of the cleaned sections (continued)

	Micro-EDXRF (wt.%)							
Ref.	**Fe**	**Ni**	**Cu**	**Zn**	**As**	**Sn**	**Sb**	**Pb**
2764	0.25	-	53.87	38.3	-	1.3	0.14	6.13
Observed Phase(s)	α+β+(Pb)							

Qing Dynasty		
Date	**Designation**	**Alloy**
1736 AD	Qian Long Tong Bao	Brass

	Micro-EDXRF (wt.%)							
Ref.	**Fe**	**Ni**	**Cu**	**Zn**	**As**	**Sn**	**Sb**	**Pb**
2766	0.36	0.06	65.5	32.63	0.42	-	0.34	0.7
Observed Phase(s)	α							

Qing Dynasty		
Date	**Designation**	**Alloy**
1736 AD	Qian Long Tong Bao	Brass

	Micro-EDXRF (wt.%)							
Ref.	**Fe**	**Ni**	**Cu**	**Zn**	**As**	**Sn**	**Sb**	**Pb**
2767	1.82	-	46.93	41.27	1.2	2.1	0.19	6.6
Observed Phase(s)	β+γ+Fe_2As+(Pb)							

Qing Dynasty		
Date	**Designation**	**Alloy**
1736 AD	Qian Long Tong Bao	Brass

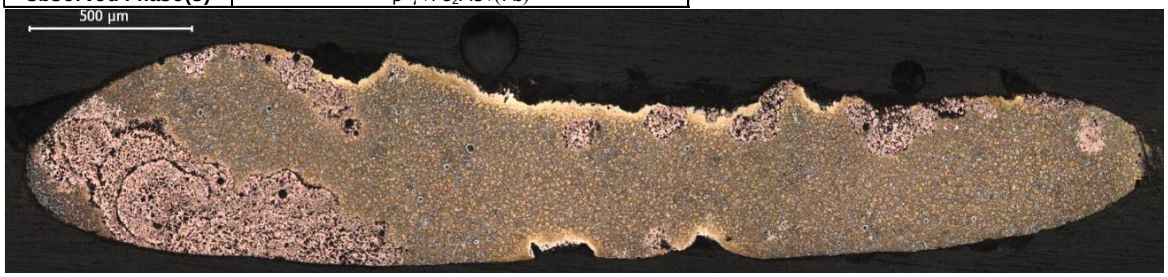

	Micro-EDXRF (wt.%)							
Ref.	**Fe**	**Ni**	**Cu**	**Zn**	**As**	**Sn**	**Sb**	**Pb**
2770	0.27	-	55.27	35.03	-	2.07	0.148	7.00
Observed Phase(s)	α+β+γ+(Pb)							

Qing Dynasty		
Date	**Designation**	**Alloy**
1736 AD	Qian Long Tong Bao	Brass

Table VII.3 Micro-EDXRF results and OM images of the cleaned sections (continued)

	Micro-EDXRF (wt.%)							
Ref.	**Fe**	**Ni**	**Cu**	**Zn**	**As**	**Sn**	**Sb**	**Pb**
2771	0.089	[0.28]	98.77	-	-	-	-	0.11
Observed Phase(s)	α							

Qing Dynasty		
Date	**Designation**	**Alloy**
1736 AD	Qian Long Tong Bao	Copper

	Micro-EDXRF (wt.%)							
Ref.	**Fe**	**Ni**	**Cu**	**Zn**	**As**	**Sn**	**Sb**	**Pb**
2772	1.28	-	46.7	47.87	-	-	-	4.17
Observed Phase(s)	β+γ+(Pb)							

Qing Dynasty		
Date	**Designation**	**Alloy**
1736 AD	Qian Long Tong Bao	Brass

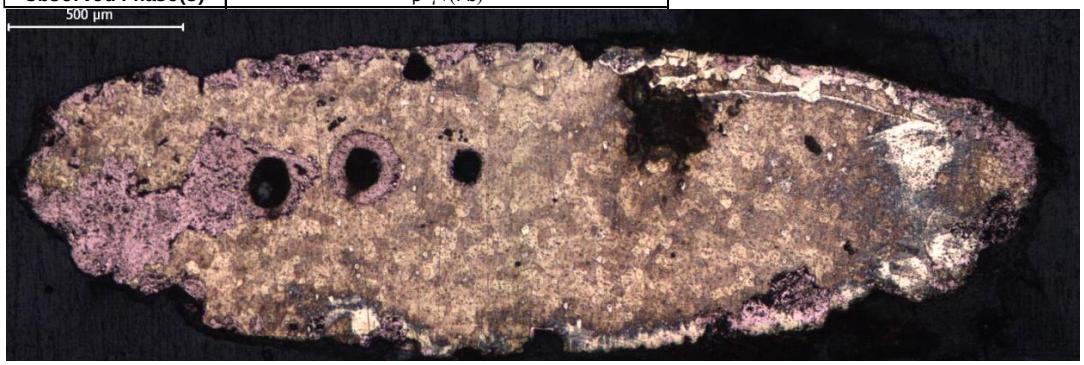

	Micro-EDXRF (wt.%)							
Ref.	**Fe**	**Ni**	**Cu**	**Zn**	**As**	**Sn**	**Sb**	**Pb**
2773	0.3	0.06	53.7	38.13	-	0.93	0.14	6.6
Observed Phase(s)	α+β+(Pb)							

Qing Dynasty		
Date	**Designation**	**Alloy**
1736 AD	Qian Long Tong Bao	Brass

	Micro-EDXRF (wt.%)							
Ref.	**Fe**	**Ni**	**Cu**	**Zn**	**As**	**Sn**	**Sb**	**Pb**
2774	0.92	-	48.05	46.7	0.06	[0.42]	-	4.13
Observed Phase(s)	β+γ+(α-Fe)+(Pb)							

Qing Dynasty		
Date	**Designation**	**Alloy**
1736 AD	Qian Long Tong Bao	Brass

Table VII.3 Micro-EDXRF results and OM images of the cleaned sections (continued)

	Micro-EDXRF (wt.%)							
Ref.	Fe	Ni	Cu	Zn	As	Sn	Sb	Pb
2775	0.54	-	49.57	45.03	0.165	-	-	4.7
Observed Phase(s)	β+(Pb)							

Qing Dynasty		
Date	Designation	Alloy
1736 AD	Qian Long Tong Bao	Brass

	Micro-EDXRF (wt.%)							
Ref.	Fe	Ni	Cu	Zn	As	Sn	Sb	Pb
2776	0.23		58.93	33.6	0.14		0.21	7.00
Observed Phase(s)	α+β+(Pb)							

Qing Dynasty		
Date	Designation	Alloy
1736 AD	Qian Long Tong Bao	Brass

	Micro-EDXRF (wt.%)							
Ref.	Fe	Ni	Cu	Zn	As	Sn	Sb	Pb
2777	0.99	0.16	64.37	30.13	0.65	-	1.26	2.43
Observed Phase(s)	α+γ+(Pb)							

Qing Dynasty		
Date	Designation	Alloy
1796 AD	Jia Qing	Brass

	Micro-EDXRF (wt.%)							
Ref.	Fe	Ni	Cu	Zn	As	Sn	Sb	Pb
2779	0.11	[0.27]	99.5	-	0.09	-	-	-
Observed Phase(s)	α+Cu_2S							

Qing Dynasty		
Date	Designation	Alloy
1736 AD	Qian Long Tong Bao	Copper

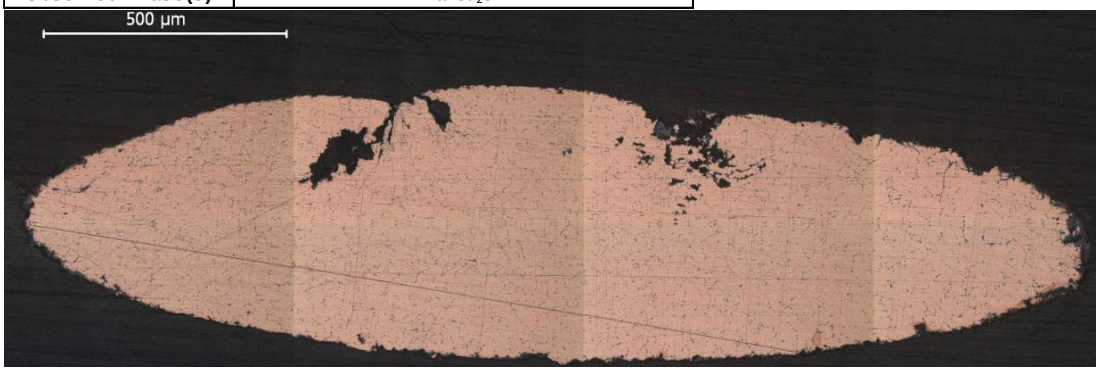

Table VII.3 Micro-EDXRF results and OM images of the cleaned sections (continued)

	Micro-EDXRF (wt.%)							
Ref.	Fe	Ni	Cu	Zn	As	Sn	Sb	Pb
2782	1.52	-	52.9	35.37	2.7	-	1.06	6.6
Observed Phase(s)	α+γ+(α-Fe)+Fe_2As+(Pb)							

Qing Dynasty		
Date	Designation	Alloy
1796 AD	Jia Qing	Brass

	Micro-EDXRF (wt.%)							
Ref.	Fe	Ni	Cu	Zn	As	Sn	Sb	Pb
2783	1.83	-	46.77	42.9	1.56	-	-	6.97
Observed Phase(s)	β+Fe_2As+(Pb)							

Qing Dynasty		
Date	Designation	Alloy
1796 AD	Jia Qing	Brass

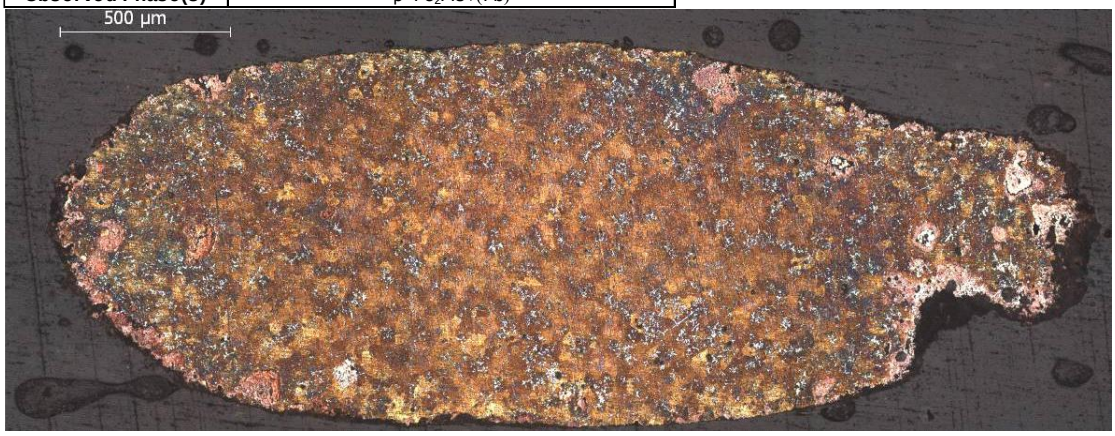

	Micro-EDXRF (wt.%)							
Ref.	Fe	Ni	Cu	Zn	As	Sn	Sb	Pb
2785	2.28	0.25	52.33	30.83	1.57	-	3.3	9.67
Observed Phase(s)	α+γ+(α-Fe)+Fe_2As+(Pb)							

Qing Dynasty		
Date	Designation	Alloy
1796 AD	Jia Qing	Brass

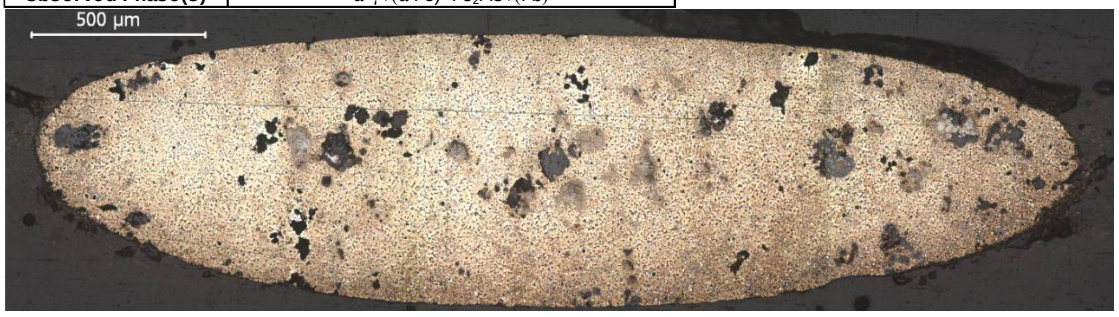

	Micro-EDXRF (wt.%)							
Ref.	Fe	Ni	Cu	Zn	As	Sn	Sb	Pb
2786	0.49	-	59.00	39.13	-	-	-	1.37
Observed Phase(s)	α+β+(Pb)							

Qing Dynasty		
Date	Designation	Alloy
1796 AD	Jia Qing	Brass

Table VII.3 Micro-EDXRF results and OM images of the cleaned sections (continued)

	Micro-EDXRF (wt.%)							
Ref.	**Fe**	**Ni**	**Cu**	**Zn**	**As**	**Sn**	**Sb**	**Pb**
2787	1.58	0.18	55.2	34.4	1.01	0.49	-	7.13
Observed Phase(s)	$\alpha+\beta+(\alpha\text{-Fe})+Fe_2As+(Pb)$							

Qing Dynasty		
Date	**Designation**	**Alloy**
1796 AD	Jia Qing	Brass

	Micro-EDXRF (wt.%)							
Ref.	**Fe**	**Ni**	**Cu**	**Zn**	**As**	**Sn**	**Sb**	**Pb**
2788	1.37	0.09	55.07	35.8	0.2	-	-	7.6
Observed Phase(s)	$\alpha+\beta+(Pb)$							

Qing Dynasty		
Date	**Designation**	**Alloy**
1796 AD	Jia Qing	Brass

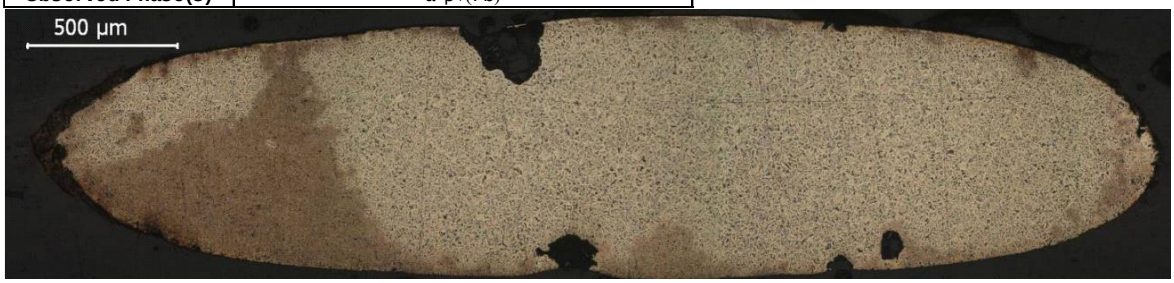

	Micro-EDXRF (wt.%)							
Ref.	**Fe**	**Ni**	**Cu**	**Zn**	**As**	**Sn**	**Sb**	**Pb**
2789	1.65	0.06	51.3	36.93	0.55	0.75	-	8.83
Observed Phase(s)	$\alpha+\beta+(\alpha\text{-Fe})+(Pb)$							

Qing Dynasty		
Date	**Designation**	**Alloy**
1796 AD	Jia Qing	Brass

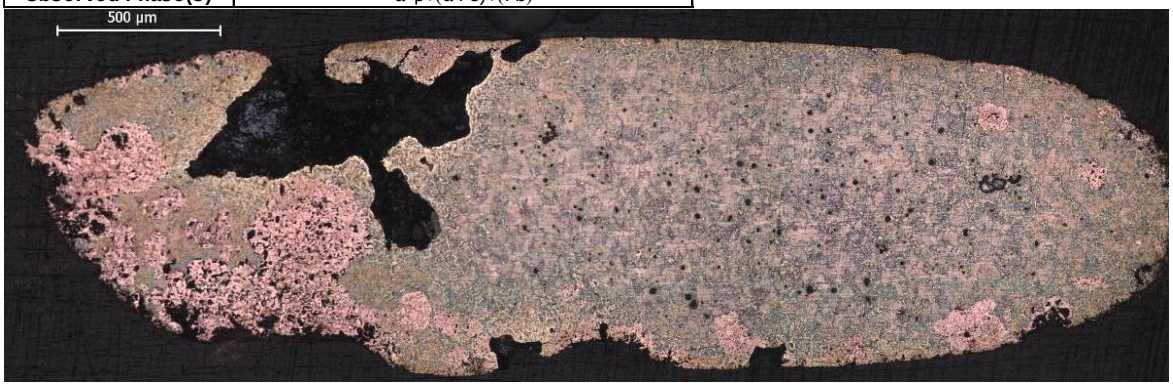

	Micro-EDXRF (wt.%)							
Ref.	**Fe**	**Ni**	**Cu**	**Zn**	**As**	**Sn**	**Sb**	**Pb**
2790	0.09	0.09	53.83	38.00	0.59	-	0.55	6.83
Observed Phase(s)	$\alpha+\beta+\gamma+(Pb)$							

Qing Dynasty		
Date	**Designation**	**Alloy**
1796 AD	Jia Qing	Brass

Table VII.3 Micro-EDXRF results and OM images of the cleaned sections (continued)

	Micro-EDXRF (wt.%)							
Ref.	**Fe**	**Ni**	**Cu**	**Zn**	**As**	**Sn**	**Sb**	**Pb**
2791	1.15	-	43.73	50.77	-	-	-	4.37
Observed Phase(s)	β+γ+(Pb)							

Qing Dynasty		
Date	**Designation**	**Alloy**
1796 AD	Jia Qing	Brass

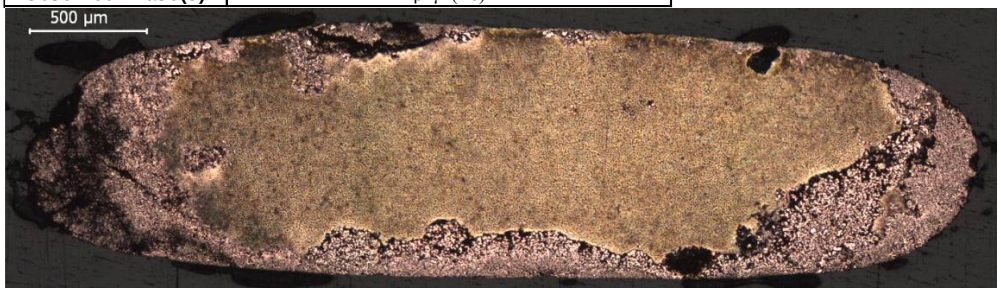

	Micro-EDXRF (wt.%)							
Ref.	**Fe**	**Ni**	**Cu**	**Zn**	**As**	**Sn**	**Sb**	**Pb**
2792	0.77	0.09	53.6	34.13	4.05	-	0.42	6.6
Observed Phase(s)	α+β+γ+Fe_2As+(γ-As)+(Pb)							

Qing Dynasty		
Date	**Designation**	**Alloy**
1796 AD	Jia Qing	Brass

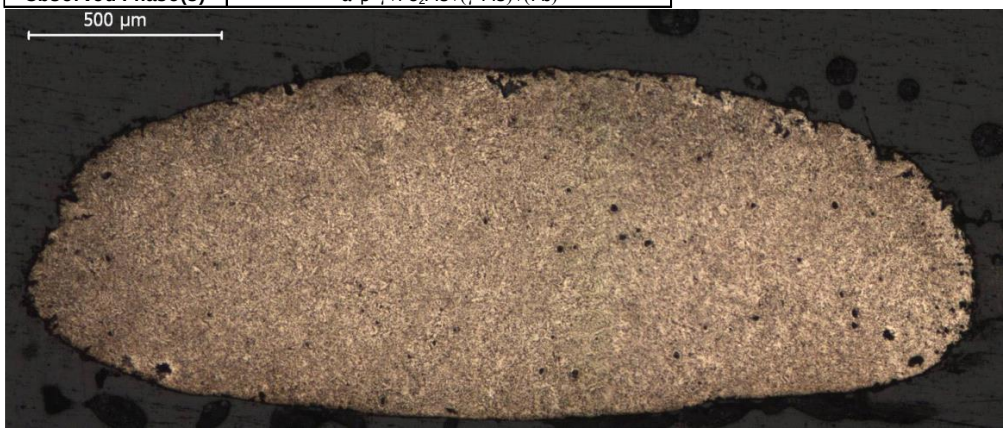

	Micro-EDXRF (wt.%)							
Ref.	**Fe**	**Ni**	**Cu**	**Zn**	**As**	**Sn**	**Sb**	**Pb**
2793	0.26	-	53.23	31.4	1.7	-	3.37	10.00
Observed Phase(s)	α+γ+(γ-As)+(Pb)							

Qing Dynasty		
Date	**Designation**	**Alloy**
1796 AD	Jia Qing	Brass

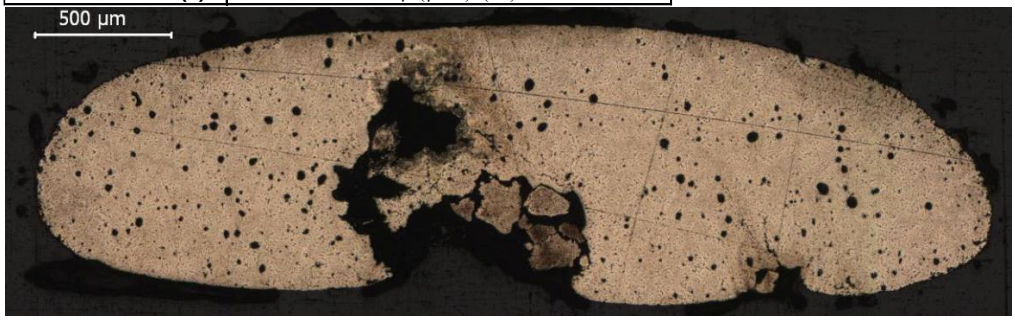

	Micro-EDXRF (wt.%)							
Ref.	**Fe**	**Ni**	**Cu**	**Zn**	**As**	**Sn**	**Sb**	**Pb**
2794	0.82	0.13	56.13	34.67	1.14	-	-	7.03
Observed Phase(s)	α+β+Fe_2As+(Pb)							

Qing Dynasty		
Date	**Designation**	**Alloy**
1796 AD	Jia Qing	Brass

Table VII.3 Micro-EDXRF results and OM images of the cleaned sections (continued)

	Micro-EDXRF (wt.%)							
Ref.	Fe	Ni	Cu	Zn	As	Sn	Sb	Pb
2796	1.46	-	45.57	52.03	0.13	-	0.13	0.67
Observed Phase(s)	β+γ							

Qing Dynasty		
Date	Designation	Alloy
1796 AD	Jia Qing	Brass

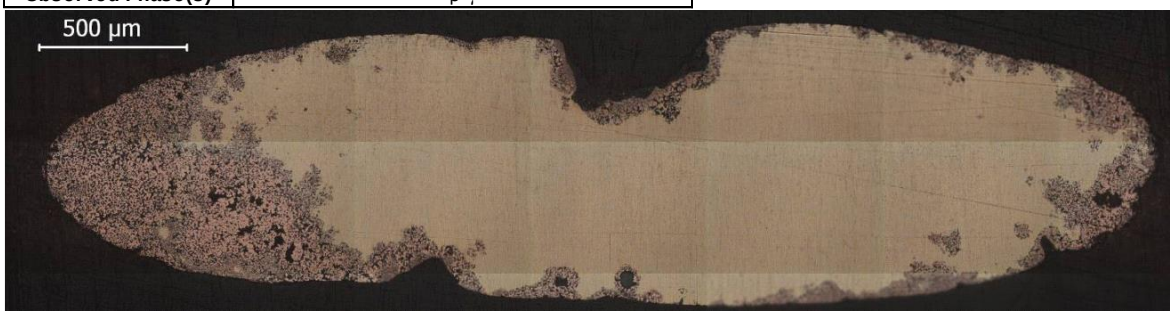

	Micro-EDXRF (wt.%)							
Ref.	Fe	Ni	Cu	Zn	As	Sn	Sb	Pb
2797	0.01	-	99.63	-	0.05	-	0.21	0.06
Observed Phase(s)	α+Cu_2S							

Qing Dynasty		
Date	Designation	Alloy
1796 AD	Jia Qing	Copper

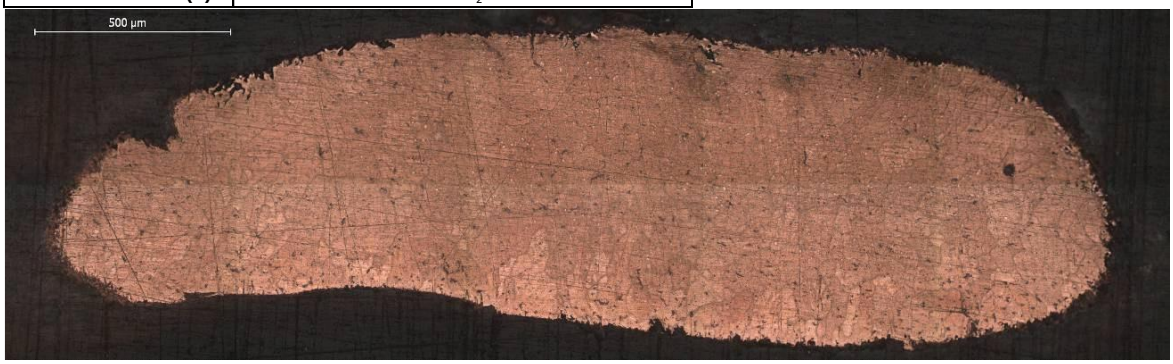

	Micro-EDXRF (wt.%)							
Ref.	Fe	Ni	Cu	Zn	As	Sn	Sb	Pb
2799	1.36	0.01	42.57	48.73	0.18	-	0.27	5.2
Observed Phase(s)	β+γ+(Pb)							

Qing Dynasty		
Date	Designation	Alloy
1796 AD	Jia Qing	Brass

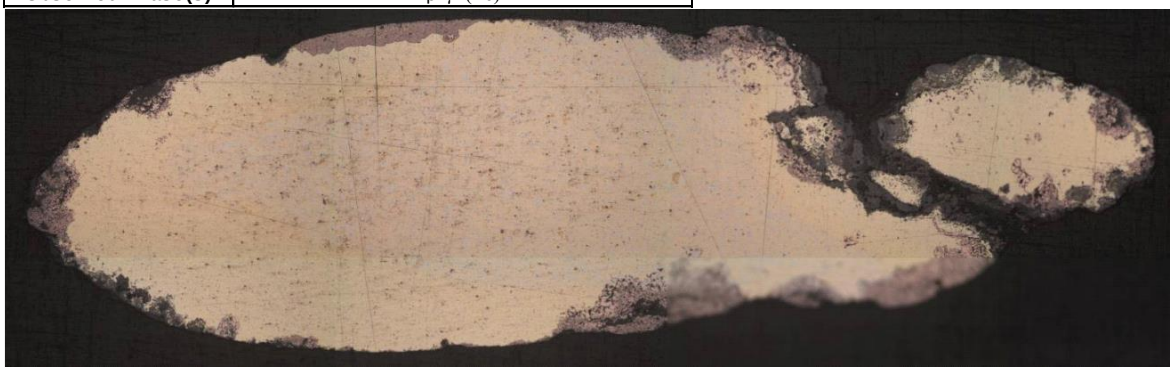

	Micro-EDXRF (wt.%)							
Ref.	Fe	Ni	Cu	Zn	As	Sn	Sb	Pb
2802	0.38	-	61.83	32.73	0.01	0.26	-	4.83
Observed Phase(s)	α+β+(Pb)							

Qing Dynasty		
Date	Designation	Alloy
1796 AD	Jia Qing	Brass

Appendix VIII - Digital X-Radiography of selected coins and Pb content (macro-EDXRF)

Batch #1

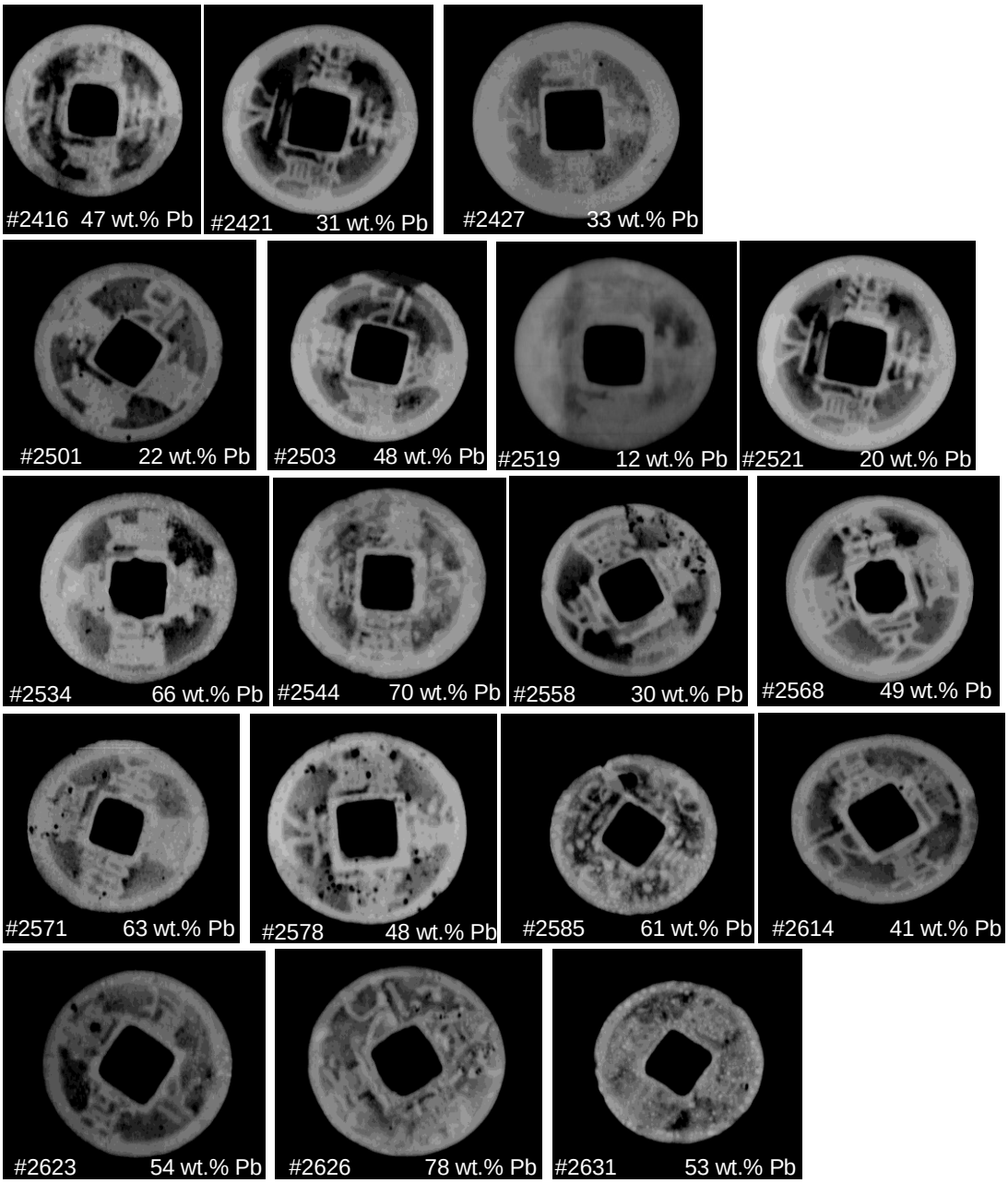

Batch #2

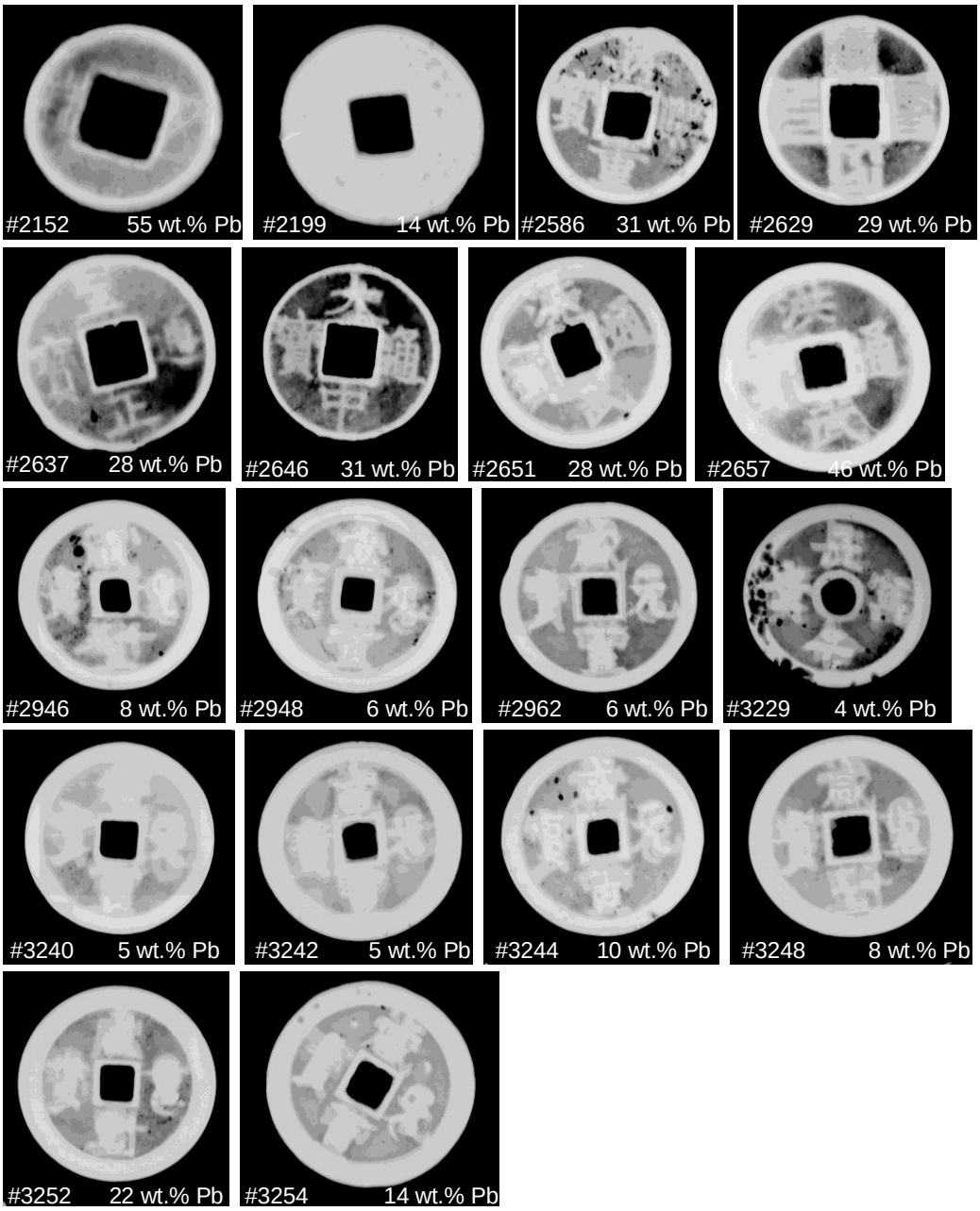
#2152 55 wt.% Pb
#2199 14 wt.% Pb
#2586 31 wt.% Pb
#2629 29 wt.% Pb
#2637 28 wt.% Pb
#2646 31 wt.% Pb
#2651 28 wt.% Pb
#2657 46 wt.% Pb
#2946 8 wt.% Pb
#2948 6 wt.% Pb
#2962 6 wt.% Pb
#3229 4 wt.% Pb
#3240 5 wt.% Pb
#3242 5 wt.% Pb
#3244 10 wt.% Pb
#3248 8 wt.% Pb
#3252 22 wt.% Pb
#3254 14 wt.% Pb